



## Durham E-Theses

---

### *A study of the molecular dynamics of compounds containing rotor groups of $c(3)$ symmetry*

Ratcliffe, C. I.

#### How to cite:

---

Ratcliffe, C. I. (1975) *A study of the molecular dynamics of compounds containing rotor groups of  $c(3)$  symmetry*, Durham theses, Durham University. Available at Durham E-Theses Online:  
<http://etheses.dur.ac.uk/8184/>

#### Use policy

---

The full-text may be used and/or reproduced, and given to third parties in any format or medium, without prior permission or charge, for personal research or study, educational, or not-for-profit purposes provided that:

- a full bibliographic reference is made to the original source
- a [link](#) is made to the metadata record in Durham E-Theses
- the full-text is not changed in any way

The full-text must not be sold in any format or medium without the formal permission of the copyright holders.

Please consult the [full Durham E-Theses policy](#) for further details.

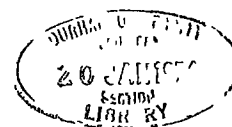
---

Academic Support Office, Durham University, University Office, Old Elvet, Durham DH1 3HP  
e-mail: [e-theses.admin@dur.ac.uk](mailto:e-theses.admin@dur.ac.uk) Tel: +44 0191 334 6107  
<http://etheses.dur.ac.uk>

A STUDY OF THE MOLECULAR DYNAMICS OF COMPOUNDS  
CONTAINING ROTOR GROUPS OF  $C_3$  SYMMETRY.

by

C.I. RATCLIFFE B.Sc. (DUNELM)



A thesis submitted in part fulfilment of the requirements for the degree of Doctor of Philosophy in the University of Durham.

September 1975.

## PREFACE

The work described in this thesis is original except where specifically stated to the contrary. It has not previously been submitted either wholly, or in part, for a degree at this or at any other university.

## ACKNOWLEDGEMENTS

I should like to express my thanks to Professor T.C.Waddington under whose guidance this research was undertaken, for much advice and discussion. I would also like to thank Dr C.J. Ludman and his technical assistants for preparing, and assisting in handling, many of the compounds studied.

At Harwell the cooperation and assistance of the whole university support section was appreciated, especially Mr D.H.C. Harris and Mr G. Haines. A special word of thanks in general goes to my colleagues in the neutron scattering group at Durham.

In conclusion I gratefully acknowledge the award of a Science Research Council Studentship.

## ABSTRACT

Models for calculation of barriers to rotation from torsional mode frequencies were reviewed, and a new simple harmonic quantum mechanical treatment of two coaxial rotors with both internal and external barriers was developed.

Torsional and librational mode frequencies of several sets of compounds containing hydrogenous  $C_3$  rotor groups were obtained principally by incoherent inelastic neutron scattering, with reference to both new and old infrared and Raman studies.

The internal and external potentials in the  $N_2H_6^{+2}$  halide salts were calculated using the new model. The external barriers were used to calculate the appreciable hydrogen bond strengths, and the internal barrier was found to be less than in ethane.

The different phases of the monomethylammonium halide and  $PF_6^-$  salts were studied, including selective deuteration studies, and the new model again applied to obtain barriers. The model worked well for the chloride  $\beta$ -phase but began to break down for the bromide, indicating loss of simple harmonic behaviour. The other phases all displayed non-harmonic behaviour. The internal barrier was found to be intermediate between that of  $N_2H_6^{+2}$  and  $C_2H_6$ .

In the  $C_6H_5NH_3^+Cl^-$  and  $Br^-$  salts the internal barrier was found to be very small, and the external  $-NH_3^+$  torsional barrier for the chloride was in good agreement with that in  $N_2H_6^{+2}Cl_2^-$ .

A large number of methyl-halogeno compounds of the group IV elements were studied. Multiple top torsional mode frequency splittings were observed and their neutron scattering intensities related

to their mode degeneracies. Several previous I.R. determinations were shown to be in error.

The di-, tri- and tetra-methylammonium halide salts were studied and torsional mode splittings were again observed. Barriers to methyl rotation were found to be relatively high, and steric effects due to the short C-N bond length, and external influences, were found to be quite important.

## CONTENTS

	<u>Page</u>
<u>CHAPTER 1.</u> BARRIERS TO MOLECULAR ROTATION	1
<u>Section 1.</u> The Internal Barrier.	1
<u>Section 2.</u> Interaction with External Modes.	15
<u>Section 3.</u> A simple harmonic treatment of a system with two coaxial rotors involving external and internal barriers.	18
<u>Section 4.</u> Multiple Top Rotors.	31
<u>Section 5.</u> Methods of Barrier Determination.	40
<u>Section 6.</u> Barrier Origins.	47
<u>References.</u>	50
<u>CHAPTER 2.</u> TECHNIQUES AND INSTRUMENTATION	53
<u>Section 1.</u> Optical Spectra.	53
<u>Section 2.</u> I.N.S. Spectra.	55
<u>Section 2.1</u> Theoretical Aspects.	55
<u>Section 2.2</u> Instrumentation.	62
<u>Section 2.3</u> Sample Containment.	80
<u>Section 2.4</u> Artificial Curve Resolution of Beryllium Filter Spectra.	83
<u>References.</u>	85
<u>CHAPTER 3.</u> THE HYDRAZINIUM $N_2H_6^{+2}$ SALTS	87
<u>Section 1.</u> Previous Studies.	87
<u>Section 2.</u> Factor Groups.	93
<u>Section 3.</u> Experimental.	95
<u>Section 4.</u> X-ray Powder Data.	97
<u>Section 5.</u> Spectroscopic Data.	101
<u>Section 6.</u> Calculations.	116
<u>Section 7.</u> Discussion.	122
<u>References.</u>	126



	<u>Page</u>
<u>CHAPTER 4.</u> MONOMETHYLAMMONIUM SALTS	128
<u>Section 1.</u> Previous Studies.	128
<u>Section 2.</u> Experimental.	141
<u>Section 3.</u> Assignment of Spectra.	144
<u>Section 4.</u> Barrier Calculations and Related Discussion.	185
<u>References.</u>	213
<u>CHAPTER 5.</u> ANILINE HYDROCHLORIDE AND HYDROBROMIDE.	215
<u>Section 1.</u> Previous Studies.	216
<u>Section 2.</u> Experimental.	220
<u>Section 3.</u> Assignment of torsional bands.	221
<u>Section 4.</u> Discussion and Calculation of Barriers.	227
<u>References.</u>	233
<u>CHAPTER 6.</u> METHYL HALOGENO COMPOUNDS OF GROUP IV ELEMENTS	234
<u>PART A:</u> THE CARBON SERIES	
<u>Section A1.</u> Previous Work.	236
A2.    Experimental.	238
A3.    Assignment and Discussion of Spectra.	241
A4.    Barrier Calculations.	273
<u>PART B:</u> THE SILICON SERIES	
<u>Section B1.</u> Previous Work.	280
B2.    Experimental.	281
B3.    Assignment and Discussion of Spectra.	282
B4.    Barrier Calculations.	293

	<u>Page</u>
<u>PART C:</u> GERMANIUM SPECIES	
<u>Section C1.</u> Previous Work.	296
C2. Experimental.	296
C3. Assignment and Discussion of Spectra.	298
C4. Barrier Calculations.	301
<u>PART D:</u> TIN SPECIES	
<u>Section D1.</u> Previous Work.	302
D2. Experimental.	303
D3. Assignment and Discussion of Spectra.	304
D4. Barrier Calculations.	308
<u>PART E:</u> GENERAL DISCUSSION OF BARRIER CALCULATIONS	310
<u>References.</u>	318
<u>CHAPTER 7.</u> THE MULTI-METHYLAMMONIUM HALIDE SALTS	324
<u>Section 1.</u> Previous Studies.	324
<u>Section 2.</u> Experimental.	331
<u>Section 3.</u> Assignment of Spectra.	332
<u>Section 4.</u> Barrier Calculations.	355
<u>Section 5.</u> Discussion.	363
<u>References.</u>	371
<u>CHAPTER 8.</u> CONCLUSION	373
<u>References.</u>	381

CHAPTER 1BARRIERS TO MOLECULAR ROTATIONSection 1. The Internal Barrier.

For a long time it was thought that molecules such as ethane were examples of free internal rotation, until it was realised that certain discrepancies observed in the thermodynamics of such systems could be explained by invoking a rotational barrier (1). From this the idea and theory of potential barriers to molecular rotation has progressed to quite a complicated stage.

The actual nature of the hindering interaction and quantum mechanical treatments of their origins are discussed later, as the theoretical area of immediate interest is that which develops models relating the potential barriers to experimentally observed parameters.

A number of preliminary but reasonably valid assumptions have to be made:-

- a) The potential is time independent.
- b) Related to this; the intramolecular vibrational modes are fast enough to produce an averaged potential.
- c) The hamiltonian for the motion can be separated from the total hamiltonian, and solved independently.

Choice of Potential Function.

The potential is described for the most general case as a Fourier series in terms of the angle of rotation ( $\theta$ ) of one group relative

$$V(\theta) = \sum_m a_m \cos m\theta + b_m \sin m\theta \quad (1.1.1)$$

to the other, where  $a_m, b_m$  are coefficients. For each individual case the terms which make a relevant contribution have to be selected. For symmetrical cases where the potential form is repeated  $n$  times on rotation through  $2\pi$  the expression usually taken is

$$V(\theta) = \sum_m \frac{V_{mn}}{2} (1 - \cos mn\theta) \quad (1.1.2)$$

$V_{mn}$  = barrier parameters

where the sine terms disappear on account of the symmetry.

This simplifies even further to

$$V(\theta) = \frac{V_n}{2} (1 - \cos n\theta) \quad (1.1.3)$$

$V_n$  = barrier height

if the higher order terms are assumed to be very small.

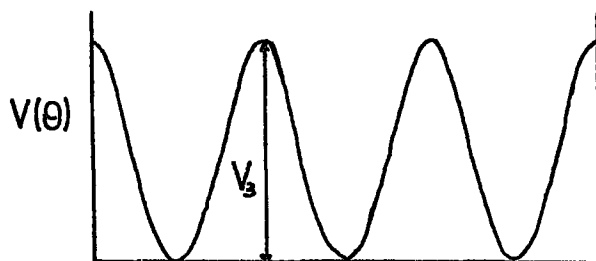


Fig (1.1). Potential generated by  $V(\theta)$  for  $n = 3$ .

The effect of the second term  $\frac{V_{2n}}{2} (1 - \cos 2n\theta)$  has been discussed by several workers (2-5) and for symmetrical cases  $V_{2n}$  is usually

found to be quite small (two orders of magnitude less than  $V_n$ ). The effect of this is shown exaggerated in figure (1.2). If  $V_{2n} \ll V_n$  the barrier height is still  $V_n$  but the shape of the well is affected.

However, cases have been found for external rotation barriers where it is useful to introduce a larger term with  $V_{2n} < V_n$  but not very small (6). Situations such as this produce a meta-stable well and the effective barrier height is increased (fig. 1.3).

For some unsymmetrical cases e.g.  $\text{CH}_2\text{ClCH}_2\text{Cl}$  where the barriers are not all equivalent as the rotor turns through  $2\pi$ , several terms have to be taken e.g. for a 3-well case

$$V(\theta) = \frac{V_1}{2}(1-\cos \theta) + \frac{V_2}{2}(1-\cos 2\theta) + \frac{V_3}{2}(1-\cos 3\theta) \quad (1.1.4)$$

but it is difficult to evaluate all three parameters from available observed data (7).

A very important feature of rotational potentials is that the barrier height depends strongly on the symmetry of the situation. This can be illustrated quite neatly:-

Consider a symmetric 3-fold rotor rotating against a fixed symmetric 3-fold environment. Each atom of the rotor on turning through  $2\pi$  experiences a 3 well potential. Considering the interactions on all 3 atoms at any one time we find they are identical and hence add up constructively to give an overall 3-fold potential. If, however, the environment is 4-fold symmetric the 3 atoms have interactions  $2\pi/3$  out of phase at any one time and hence

Fig (1.2). Effects of small  $V_6$  terms.

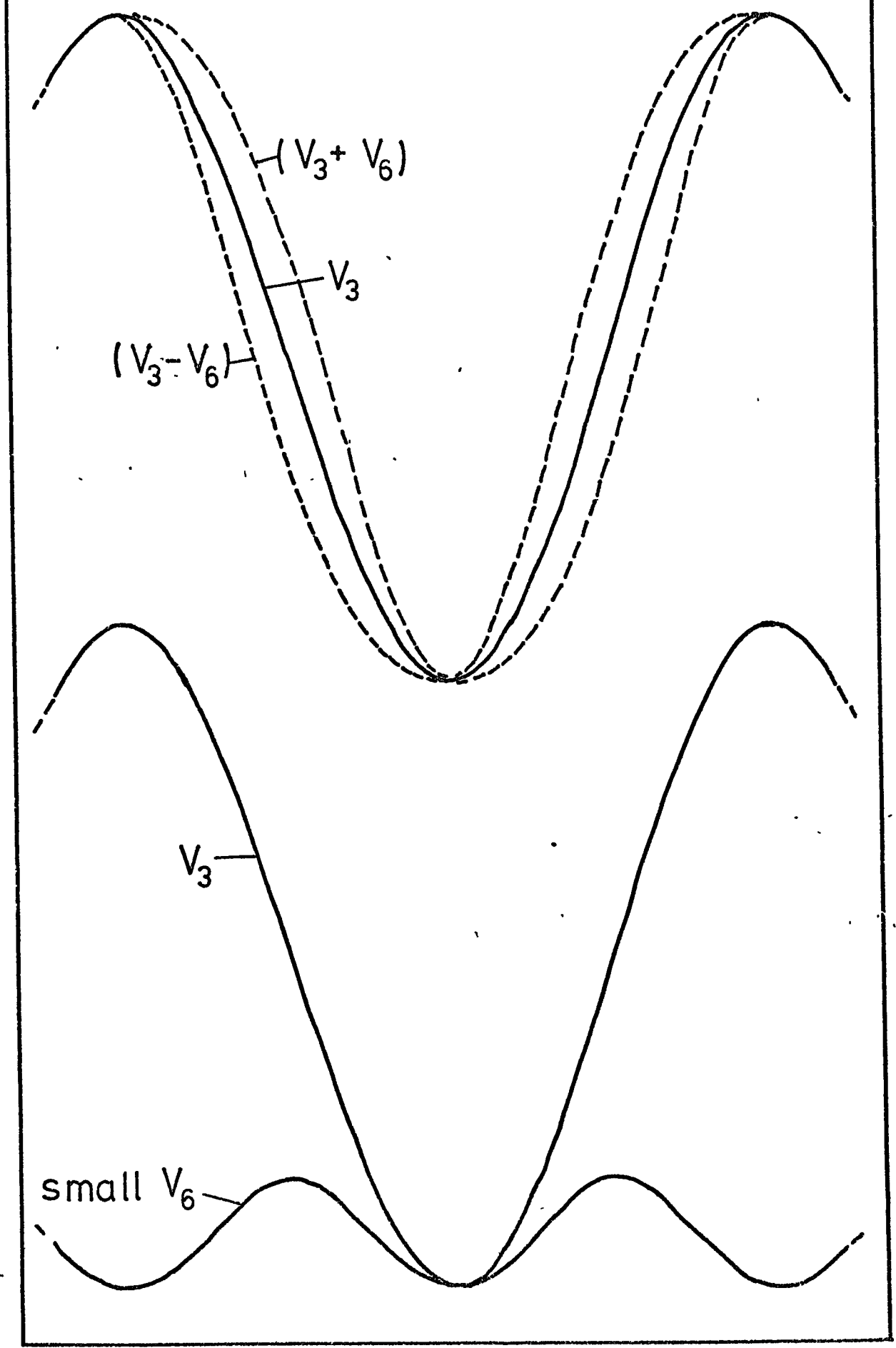


Fig (1.3). Effects of large  $V_6$  term.

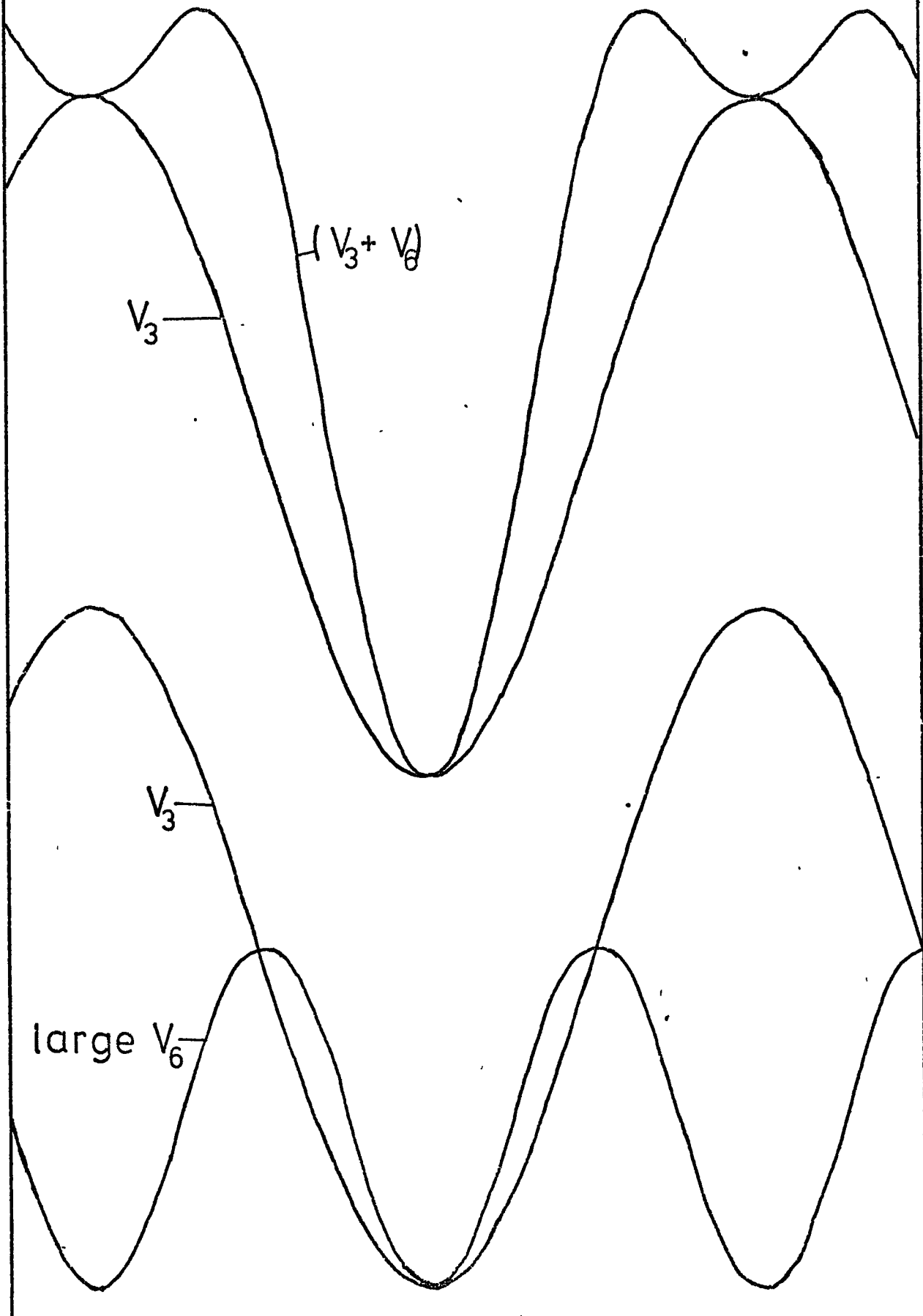
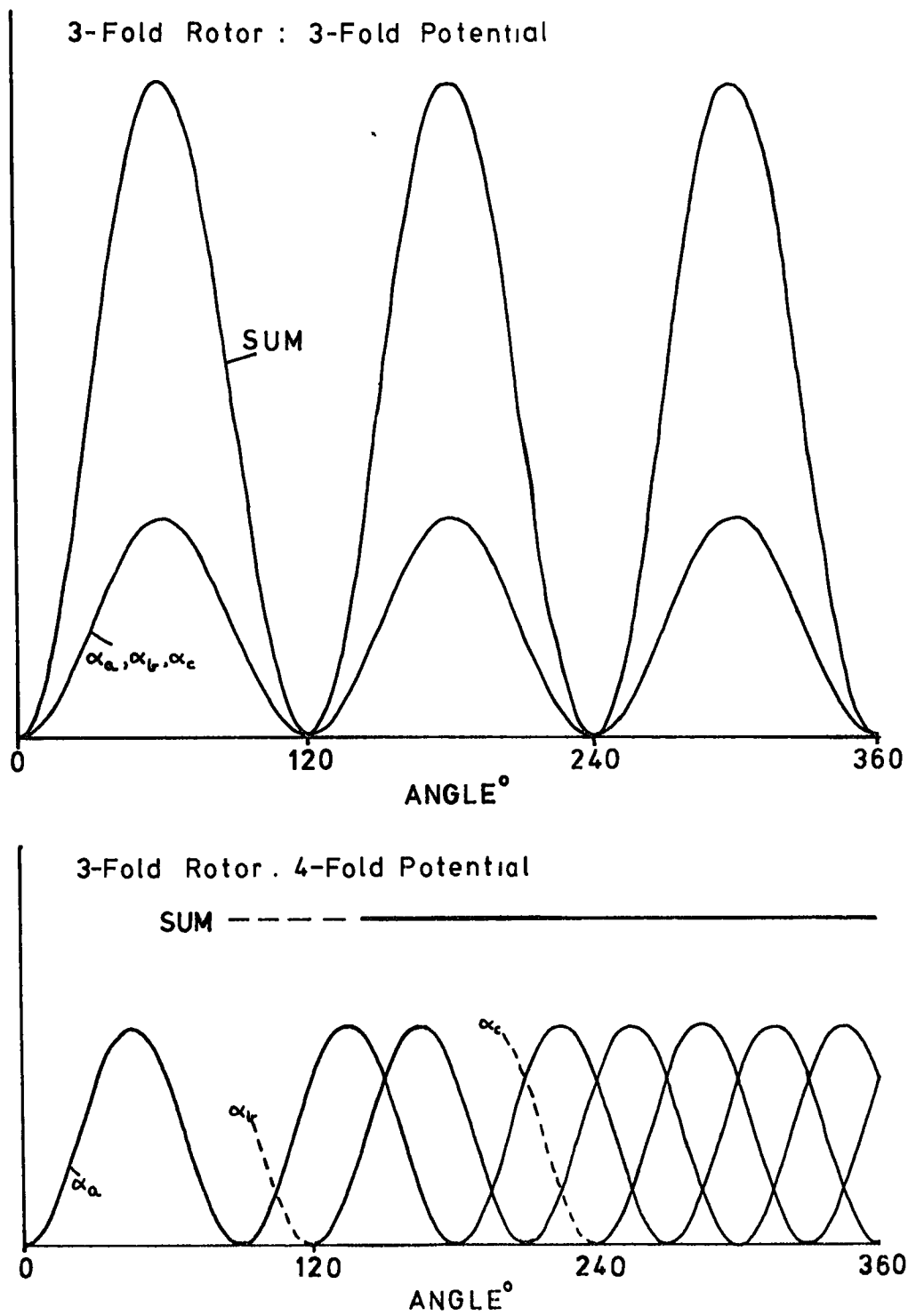


Fig. (1.4)





add up destructively to give a completely level potential (see figure (1.4)). This applies for the first and second cosine terms  $\text{Cos } 4\theta$ ,  $\text{Cos } 8\theta$  but the  $\text{Cos } 12\theta$  would introduce a small 12-fold ripple on the potential if its coefficient was large enough. The two points emerging from this are:

- (1) The deepest wells occur when the potentials experienced by individual atoms of the rotor are in phase.
- (2) When the periodicity of the field ( $j$ ) does not match that of the rotor ( $n$ ) any potential variation, if any is observed, is described by the term in  $\text{Cos } nj\theta$  in the cosine series.

#### Solution of the Equations of Motion.

Having determined the form of the potential it remains to solve the resulting Schrodinger equation. For the simplest case:-

$$\frac{1}{I_{\text{red}}} \frac{d^2 \psi(\theta)}{d\theta^2} + \frac{8\pi^2}{h^2} \left[ E - \frac{V_n}{2} (1 - \text{Cos } n\theta) \right] \psi(\theta) = 0 \quad (1.1.5)$$

(where  $I_{\text{red}}$  = reduced moment of inertia for the motion).

This is directly related to Mathieu's equation:

$$\frac{d^2 y}{dx^2} + (b - s \text{Cos}^2 x)y = 0 \quad (1.1.6)$$

$b$  = an eigenvalue                       $s$  = a dimensionless parameter

which has different sets of solutions for different angular periods.

The evaluation of  $s$  and  $b$  is a laborious process but several tabulations,

over several ranges of values, for different periodicities have been produced (8-13).

For the case  $n = 3$  the condition of invariance  $\psi(\theta) = \psi(\theta + 2\pi/3)$  and the boundary condition  $\psi(\theta) = \psi(\theta + 2\pi)$  means that there are two sets of solutions. Each energy level, ground state included is split into an A and an E level, one being a solution periodic in  $\frac{2\pi}{3}$  and two degenerate ones being  $2\pi$  periodic. This splitting can be regarded in physical terms as the result of quantum mechanical tunnelling through the barrier, and it increases towards the top of the barrier. If the barrier became infinite, however, no such splitting should occur.

By comparing the two equations above

$$s = \frac{V_n \cdot 4}{F \cdot n^2} \qquad b_{v\sigma} = \frac{E_{v\sigma} \cdot 4}{F \cdot n^2} \qquad (1.1.7)$$

where

$$F = \frac{h^2}{8\pi^2 I_{\text{red}}} \qquad v = \text{principal torsional quantum no.}$$

$$\sigma = \text{sublevel designation.}$$

and

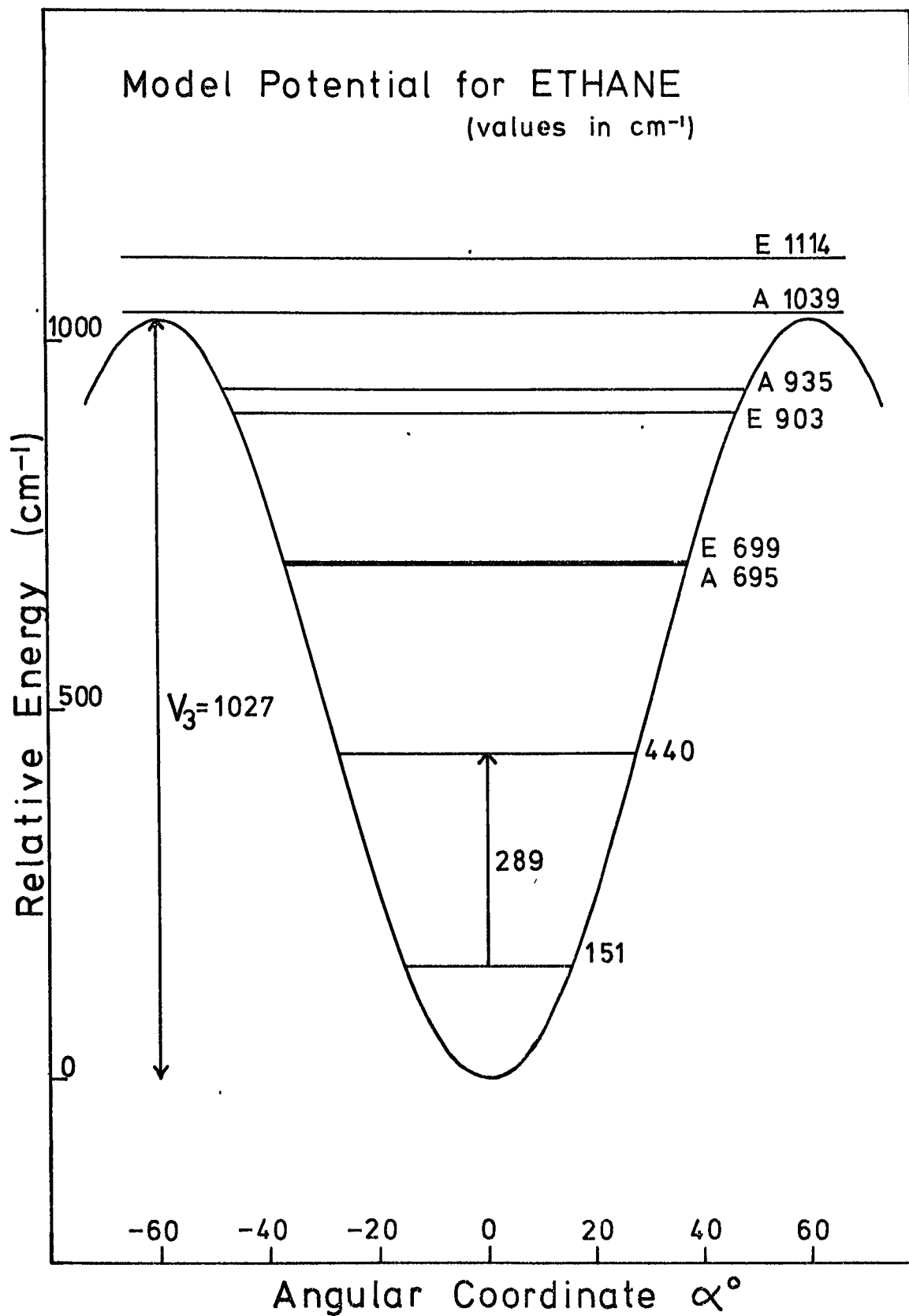
$$E_{v\sigma} = \left( E - \frac{V_n}{2} \right)_{v\sigma}$$

Hence if a transition frequency  $\Delta E_{v\sigma}$  from  $v = 0 \rightarrow 1$  is observed and  $I_{\text{red}}$  is known,  $\Delta b_{v\sigma}$  can be found. Thus  $\Delta b_{v\sigma}$  can then be correlated with a value of  $s$  from the appropriate table and  $V_n$  calculated.

(Fig. 1.5) shows the potential and levels for ethane.

Approaching the two extreme cases of this model further

Fig. (1.5)



simplifications can be made

a) Low barrier approximation.

If  $V_n \rightarrow 0$   $b_{v\sigma} \gg s$

$$\text{So } \frac{d^2 y}{dx^2} + b_{v\sigma} y = 0 \quad (1.1.8)$$

which has solutions  $y = e^{\pm irx}$   $r = 0, 1, 2, 3 \dots$  but the condition  $\psi(\theta) = \psi(\theta + \frac{2\pi}{n})$  requires only  $r = 0, 2, 4, 6 \dots$  Substituting back we find  $b_{v\sigma} = r^2$  and hence obtain

$$E_r - \frac{V_n}{2} = \frac{n^2 h^2 r^2}{32\pi^2 I_{red}} \quad (1.1.9)$$

which is similar to the expression for a free rotor.

b) High barrier approximation.

The term  $\cos n\theta$  can be expanded as a series

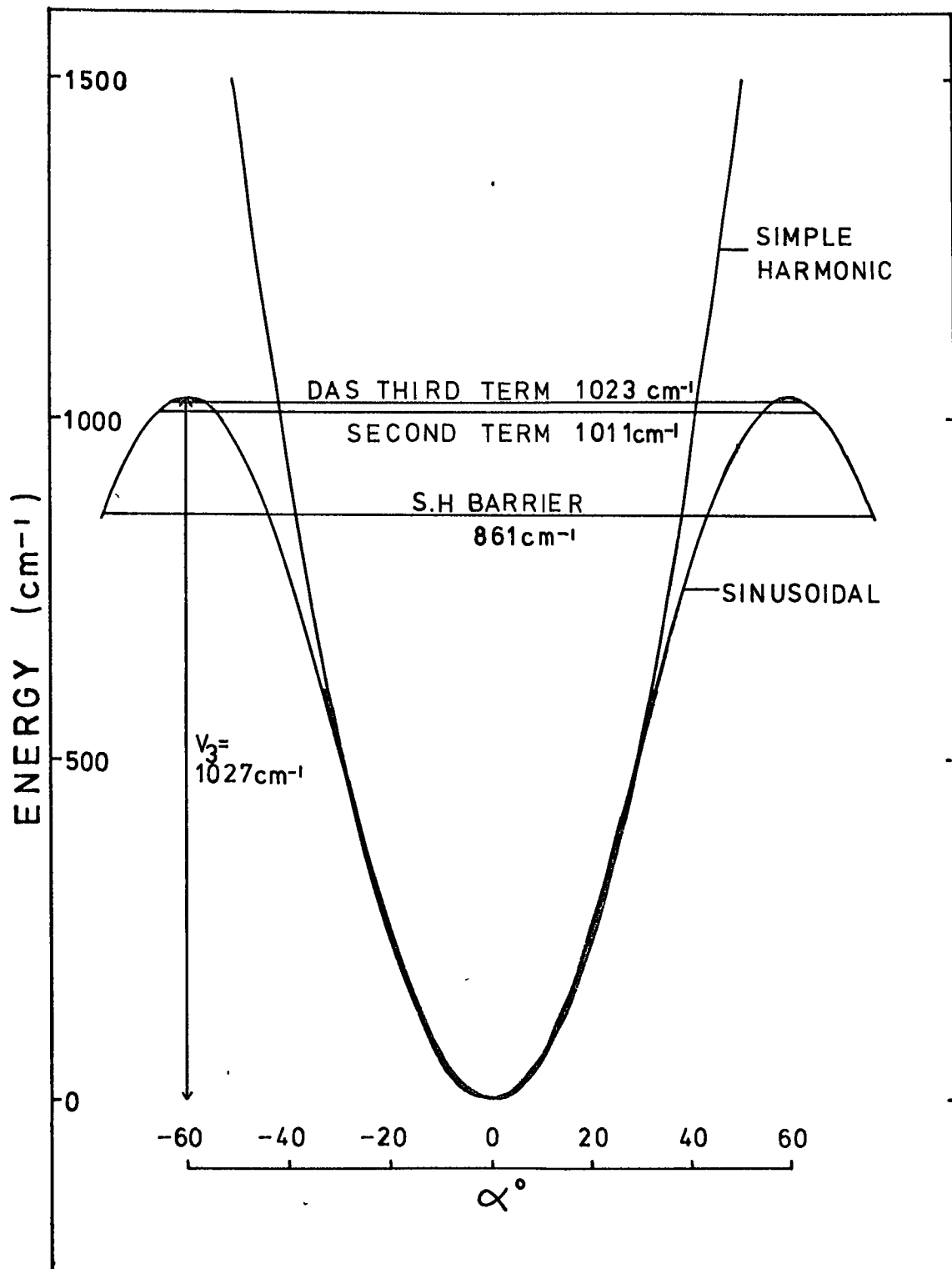
$$\cos n\theta = 1 - \frac{n^2 \theta^2}{2!} + \frac{n^4 \theta^4}{4!} - \frac{n^6 \theta^6}{6!} \dots \quad (1.1.10)$$

If the barrier is relatively high and the rotor is confined to small oscillations in levels near the bottom of the wells variation of  $\theta$  will be small and terms above the square can be ignored. This gives

$$\frac{d^2 \psi(\theta)}{d\theta^2} + \left( \frac{8\pi^2 I_{red}}{h^2} \right) \left[ E_p - \frac{V_n \cdot n^2}{4} \theta^2 \right] \psi(\theta) = 0 \quad (1.1.11)$$

which is the equation of a simple harmonic oscillator, with eigenvalues

Fig. (1.6) Comparison of Models.



given by

$$E_p = \left( p + \frac{1}{2} \right) \left[ \frac{n^2 h^2 \bar{v}_n}{8\pi^2 I_{\text{red}}} \right]^{\frac{1}{2}} \quad (1.1.12)$$

$p$  = quantum no.

= 0, 1, 2 ....

Considering the  $0 \rightarrow 1$  transition

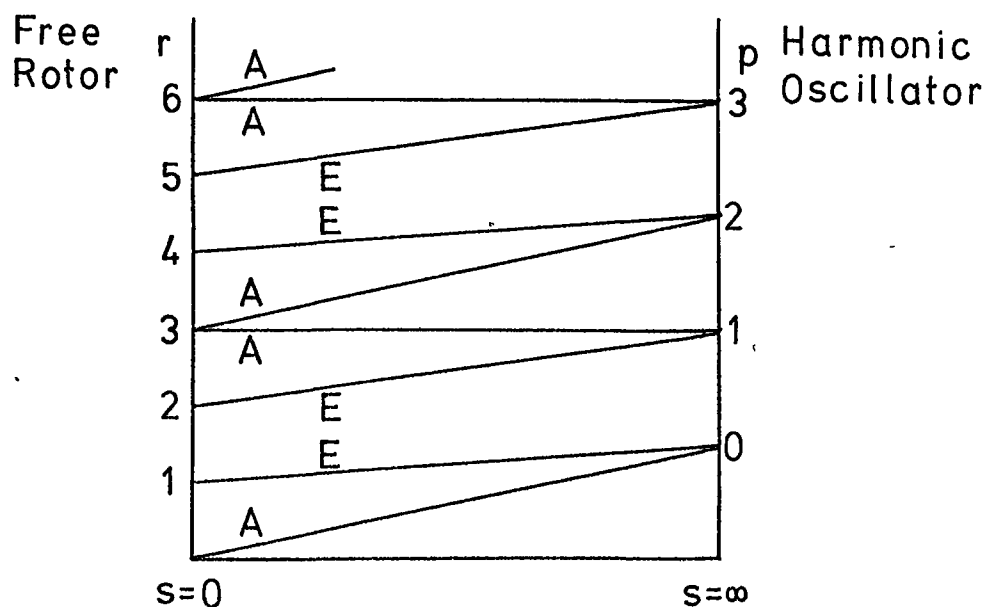
$$\bar{v}_n = \frac{8\pi^2 c I_{\text{red}} \cdot \bar{v}^2}{n^2 h} \quad (1.1.13)$$

$\bar{v}_n$  = barrier in  $\text{cm}^{-1}$

$\bar{v}$  = frequency in  $\text{cm}^{-1}$

It is generally accepted that this gives a useful estimate of the barrier if  $> 2.5$  kcal/mole ( $\approx 874 \text{ cm}^{-1}$ ) (14), but it does give consistently lower values. See figure (1.6) for comparison in the case of ethane.

Figure (1.7) shows diagrammatically the relationship between these two extremes and the intermediate cases, (after Herschbach (13)).



The Das approximation.

Das (15) has developed a method of obtaining approximate solutions to the Mathieu equation which for high and intermediate barriers proves to be quite good, and further he obtains an expression for the level splittings.

He expands the Mathieu eigenfunction as a series which converges for  $V_n$  moderately large and goes on to show that the corresponding eigenvalues can also be obtained as a series:-

$$E_p = \frac{V_n}{k^2} \left[ k(2p+1) - \frac{1}{4}(p^2 + (p+1)^2) - \frac{k^{-1}}{16}(p^3 + (p+1)^3) - \frac{k^{-2}}{128}(5p^4 + 5(p+1)^4 + p^2 + (p+1)^2) \dots \right] \quad (1.1.14)$$

$$\text{where } k = \left( \frac{32\pi^2 I_{\text{red}} V_n}{n^2 h^2} \right)^{\frac{1}{2}} \quad p = \text{torsional quantum no.}$$

(Taking only the first term returns to the simple harmonic expression).

Considering the  $0 \rightarrow 1$  transition and working out the expression for the barrier height taking into account successive terms obtains:-

$$\begin{aligned} (1) \quad \bar{V}_n &= \bar{v}^2 / K \\ (2) \quad \bar{V}_n &= (\bar{v} + K/4)^2 / K \\ (3) \quad \bar{V}_n^2 - (\bar{v}^2 + 3K^2/16 + \bar{v}K/2)\bar{V}_n / K + (K/16)^2 &= 0 \end{aligned} \quad (1.1.15)$$

$$\text{(where } K = \frac{n^2 h^2}{8\pi^2 c I_{\text{red}}}).$$

To illustrate these the barriers calculated from successively more complicated expressions for  $\text{CH}_3\text{CH}_3$  and  $\text{CH}_3\text{CCl}_3$  are given in table (1.1) and compared with the values obtained using Mathieu

eigenvalue tables. The ethane case is also illustrated in fig. (1.6).

Table (1.1) Comparison of different approximations.

	$\text{CH}_3\text{CCl}_3$	$\text{CH}_3\text{CH}_3$
$I_{\text{red}}$ (a.m.u. $\text{\AA}^2$ )	3.1798	1.5625
$\bar{\nu}$ ( $\text{cm}^{-1}$ )	290	289
Simple harmonic $\bar{V}_3$ ( $\text{cm}^{-1}$ )	1763	861
Das 2nd term $\bar{V}_3$ ( $\text{cm}^{-1}$ )	1911	1011
Das 3rd term $\bar{V}_3$ ( $\text{cm}^{-1}$ )	1917	1023
Mathieu $\bar{V}_3$ ( $\text{cm}^{-1}$ )	1920	1027

Quite clearly the third term very nearly gives the true barrier.

Hence Das's formula should be very useful for cases where the Mathieu tables are not of the correct period or do not extend far enough.

Das gives the sublevels due to tunnelling as an expression to

$$\left. \begin{array}{l} \text{be added to } E_p: \quad A_p \cdot 2 \cos \left( \frac{2\pi\sigma}{n} \right) \\ \text{where} \quad A_p = 2^{3p} \times \frac{n^2}{p!} \cdot k^{(p+1)} \cdot e^{-2k} \cdot \left( \frac{k}{\pi} \right)^{\frac{1}{2}} \end{array} \right\} \quad (1.1.16)$$

and  $k$  was defined at equation (1.1.14)  $\sigma = 0, 1, 2$  for the



threefold case so

$$\sigma = 0 \rightarrow 2A_p$$

$$1 \rightarrow -A_p$$

$$2 \rightarrow -A_p$$

and hence the splitting of each level is given by  $3A_p$ . For the ground level for ethane  $3A_p = 5.7 \times 10^{-4} \text{ cm}^{-1}$  compared with  $2.5 \times 10^{-4} \text{ cm}^{-1}$  calculated from Herschbach's Mathieu eigenvalues.

## Section 2. Interaction with external modes.

The discussion so far has dealt with pure torsional motion, but the true physical picture for the 'free' molecule involves interaction with the overall rotations. Most of the theoretical papers mentioned earlier (Mathieu eigenfunction tabulators) discuss the problem in terms of this. The different modes can be separated and hence the problem solved exactly for coaxial symmetric tops; the case of ethane was first looked at by Nielsen in 1932 (16).

For less symmetrical cases the external and internal rotations can be essentially separated but a small interaction term remains which requires a perturbation treatment.

The net observed effect of this is that the rotational bands in the microwave spectrum show considerable structure; and the torsional band itself may show rotational fine structure if the barrier is low and the molecule light. Another point to note is that the full reduced moment of inertia for the internal rotation should include terms concerning the principal moments of inertia of the whole molecule:-

$$I_{\text{red}} = I_A \left[ 1 - I_A \sum_g \lambda_g^2 / I_g \right] \quad (1.2.1)$$

$I_A$  = internal top moment of inertia about its own axis

$\lambda_g$  = Cosine of angle between internal top axis and the  $g^{\text{th}}$  principal axis of entire molecule

$I_g$  =  $g^{\text{th}}$  principal moment of inertia.

For cases such as  $\text{CH}_3\text{CH}_3$ ,  $\text{CH}_3\text{CCl}_3$  two of the principal axes are at  $90^\circ$  to the internal rotor axis and the third is coaxial so

$$I_{\text{red}}(\text{C}_2\text{H}_6) = \frac{I_{\text{CH}_3} \cdot I_{\text{CH}_3}}{I_{\text{CH}_3} + I_{\text{CH}_3}} = \frac{I_{\text{CH}_3}}{2}, \quad I_{\text{red}}(\text{CH}_3\text{CCl}_3) = \frac{I_{\text{CH}_3} I_{\text{CCl}_3}}{I_{\text{CH}_3} + I_{\text{CCl}_3}} \approx I_{\text{CH}_3}$$

#### Barriers to rotational motion in solids.

A molecule placed in a crystal lattice still has modes corresponding to the three external rotations of the free species, but due to lattice interactions of various kinds (discussed later) these motions are restricted by potential barriers, which necessarily produce an increase in the mode frequency. In some cases it may still be possible to "rotate" relatively easily, this is the phenomenon of 'rotational diffusion' observed for the solid phases of so called 'globular' compounds such as  $\text{CCl}_4$  and  $(\text{CH}_3)_4\text{C}$ . Where the motion is restricted enough so that the molecule just oscillates about an equilibrium position, the rotation has been reduced to a libration.

Clearly a knowledge of the molecule's crystal environment is very helpful. Even then, unless the crystal field barriers are high enough to fix the rotation axes with respect to the lattice, the problem of finding a suitable coordinate description for the potential in space becomes quite involved. However, once a suitable description

has been found solution of the equation of motion can proceed along similar lines as for internal rotation.

It should also be pointed out that the lattice modes are of low frequency and hence cause slower oscillations of the potential, which may affect the rotor motion. A recent paper by Larrison (17) on the gross features of some I.N.S. spectra of solids attempts to take this into account, but generally speaking this is very difficult to accomplish and so for simplicity the fields have to be approximated as static.

Studies of molecular or ionic rotations (or librations) in crystal fields have mainly been of whole body motions, for instance the ammonium halides (18), alkali metal borohydrides and incorporated ammonium ions (19), where a  $T_d$  spherical top ion (with all three moments of inertia the same) sits in a lattice site which has cubic or octahedral symmetry.

Not much attention has so far been paid to compounds which have both internal and external barriers of appreciable size. The solid phases of many molecular compounds have been studied to obtain internal barriers, making the assumption that the external barriers are small, even though it is found that the torsional frequency quite often increases on going from the gas to the solid (20) [it may well be that the extent of this shift can give some idea of the strength of the external interaction but no one has quantified this yet]. However, there do exist a number of compounds which have strong interactions between the lattice and an ionic group which also has internal torsion. The examples studied in the present work have generally been species with hydrogen bonds producing the barriers.

The models chosen to describe the motions are again very dependent on the particular case, unsymmetrical cases being too difficult to formulate let alone solve without making gross assumptions. For a few special symmetric cases moderately simple treatments have been found. There is the advantage with these hydrogen bonded systems that the principal axes of the ionic group take up specific orientations in the lattice and the barriers are high enough to permit use of the simple harmonic approximation.

A particularly useful model was developed for the hydrazinium and methylammonium salts which have two coaxial torsioning  $C_3$  rotor groups librating in external 3 fold potentials. This treatment is developed in full in the following section:-

Section 3. A simple harmonic treatment of a system with two coaxial rotors involving external and internal barriers.

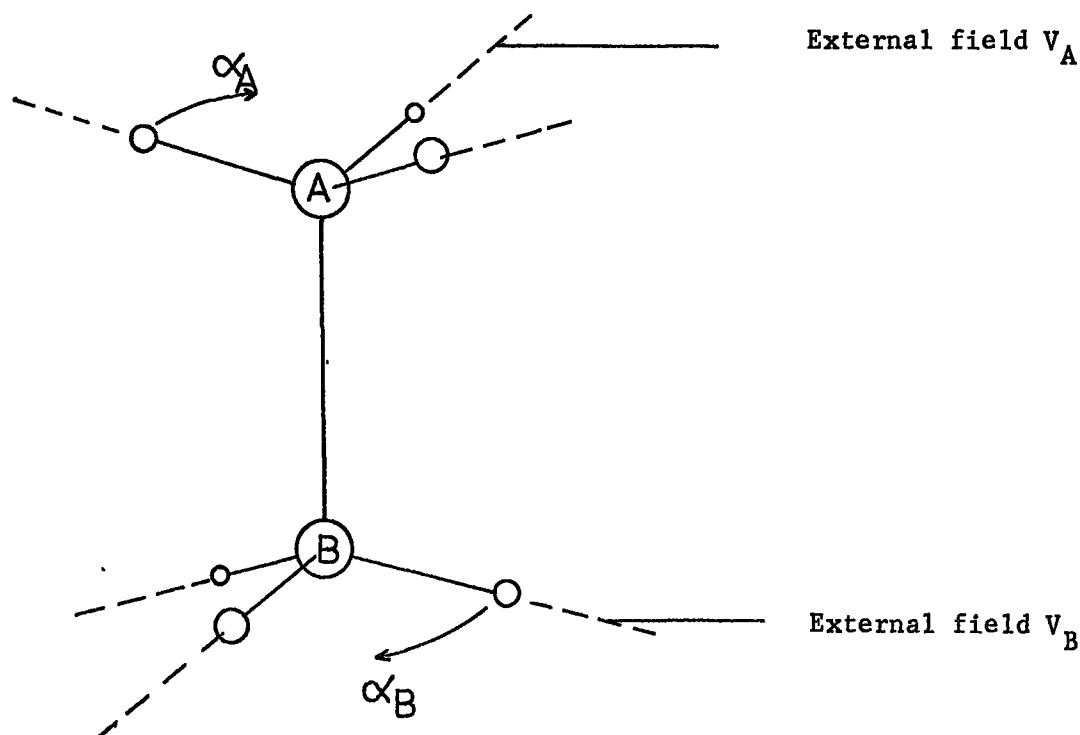


Fig (1.8).

### 3a. Quantum-mechanical treatment.

The energy operators can be written as follows:-

$$\text{Kinetic Energy } T = -\frac{\hbar^2}{8\pi^2} \left[ \frac{1}{I_A} \frac{\partial^2}{\partial \alpha_A^2} + \frac{1}{I_B} \frac{\partial^2}{\partial \alpha_B^2} \right] \quad (1.3.1)$$

Potential Energy, consisting of three sinusoidal potentials

$$\begin{aligned} V = & + \frac{V_A}{2} (1 - \cos n_A \alpha_A) \quad \text{external field at A} \\ & + \frac{V_B}{2} (1 - \cos n_B \alpha_B) \quad \text{external field at B} \\ & + \frac{V_I}{2} (1 - \cos n_I (\alpha_A - \alpha_B)) \quad \text{internal field} \end{aligned} \quad (1.3.2)$$

where  $\hbar$  = Planck's constant

$I_{A,B}$  = moments of inertia of the two ends of the molecule about the principle axis

$\alpha_A, \alpha_B$  = rotational angular coordinates

$V_{A,B,I}$  = barriers to rotation

$n_{A,B,I}$  = multiplicity of barrier over  $2\pi$

Note that the potentials are described here so as to give an equilibrium position at the minimum of all three wells. One might possibly envisage a crystal system where two of the fields are much larger than the third and strong enough to hold the molecule in a configuration which is not at the minimum potential of the weak field. Without making simplifications solution of the Schrodinger equation would be virtually impossible. However assuming that the parts of the molecule execute small oscillations in deep wells (the simple

harmonic oscillator approximation described earlier), terms higher than the square can be ignored in the cosine expansion series. Note that this would require at least two of the three barriers to be high. This obtains:-

$$\begin{aligned}
 V &= \frac{V_A}{2} \cdot \frac{n^2 \alpha_A^2}{2} + \frac{V_B}{2} \cdot \frac{n^2 \alpha_B^2}{2} + \frac{V_I}{2} \left[ \frac{n^2 \alpha_A^2}{2} + \frac{n^2 \alpha_B^2}{2} - n^2 \alpha_A \alpha_B \right] \\
 &= \left[ \frac{V_A n^2 + V_I n^2}{4} \right] \alpha_A^2 + \left[ \frac{V_B n^2 + V_I n^2}{4} \right] \alpha_B^2 - \left[ \frac{V_I n^2}{2} \right] \alpha_A \alpha_B \quad (1.3.3)
 \end{aligned}$$

$$\begin{aligned}
 \text{Put } d_A &= \frac{1}{I_A} \left[ \frac{V_A n^2 + V_I n^2}{4} \right] \quad d_B = \frac{1}{I_B} \left[ \frac{V_B n^2 + V_I n^2}{4} \right] \\
 d_I &= \frac{1}{I_A I_B} \left[ -\frac{V_I n^2}{2} \right] \quad (1.3.4)
 \end{aligned}$$

So

$$V = d_A (\sqrt{I_A} \alpha_A)^2 + d_B (\sqrt{I_B} \alpha_B)^2 + d_I (\sqrt{I_A} \alpha_A) (\sqrt{I_B} \alpha_B) \quad (1.3.5)$$

Now substitute

$$x = \alpha_A \sqrt{I_A} \quad y = \alpha_B \sqrt{I_B}$$

then the Schrodinger equation for the system is:-

$$\frac{\partial^2 \psi}{\partial x^2} + \frac{\partial^2 \psi}{\partial y^2} + \frac{8\pi^2}{h^2} [E - (d_A x^2 + d_B y^2 + d_I xy)] \psi = 0 \quad (1.3.6)$$

This can be made separable by making the new substitutions

$$\begin{aligned}
 x &= a \cos \theta + b \sin \theta \\
 y &= a \sin \theta - b \cos \theta \quad (1.3.7)
 \end{aligned}$$

Because of orthogonality the Laplacian transforms as

$$\frac{\partial^2}{\partial x^2} + \frac{\partial^2}{\partial y^2} \rightarrow \frac{\partial^2}{\partial a^2} + \frac{\partial^2}{\partial b^2}$$

$$\begin{aligned} \text{and } d_A x^2 + d_B y^2 + d_I xy &= d_A(a^2 \cos^2 \theta + b^2 \sin^2 \theta + 2ab \sin \theta \cos \theta) \\ &+ d_B(a^2 \sin^2 \theta + b^2 \cos^2 \theta - 2ab \sin \theta \cos \theta) \\ &+ d_I((a^2 - b^2) \sin \theta \cos \theta + ab(\sin^2 \theta - \cos^2 \theta)) \\ &= a^2(d_A \cos^2 \theta + d_B \sin^2 \theta + d_I \sin \theta \cos \theta) \\ &+ b^2(d_A \sin^2 \theta + d_B \cos^2 \theta - d_I \sin \theta \cos \theta) \\ &+ ab(2(d_A - d_B) \sin \theta \cos \theta + d_I(\sin^2 \theta - \cos^2 \theta)) \\ &= \lambda_1 a^2 + \lambda_2 b^2 \quad \dots \quad (1.3.8) \end{aligned}$$

where  $\lambda_1, \lambda_2$  are the coefficients of  $a^2, b^2$  respectively and the cross term  $ab$  has been removed by making its coefficient zero, (see equations 1.3.(13-19)).

The equation is now separable:-

$$\frac{\partial^2 \psi_1}{\partial a^2} + \frac{8\pi^2}{h^2} [E_1 - \lambda_1 a^2] \psi_1 = 0 \quad (1.3.9)$$

$$\text{and } \frac{\partial^2 \psi_2}{\partial b^2} + \frac{8\pi^2}{h^2} [E_2 - \lambda_2 b^2] \psi_2 = 0$$

$$\text{Put } k = \frac{8\pi^2}{h^2}, \epsilon_1 = kE_1, K_1^2 = \lambda_1 k$$

and this gives

$$\frac{\partial^2 \psi_1}{\partial a^2} + (\epsilon_1 - K_1^2 a^2) \psi_1 = 0 \quad (1.3.10)$$

which has solutions  $\epsilon_1 = (2p + 1)K_1$   $p = 0, 1, 2, \dots$

Similarly the second equation gives

$$\epsilon_2 = (2q + 1)K_2$$

And hence the transition energies are given by:

$$\Delta E_{1(0 \rightarrow 1)} = \frac{2K_1}{k} = hc \bar{\nu}_{1(0 \rightarrow 1)} \quad (1.3.11)$$

$$\Delta E_{2(0 \rightarrow 1)} = \frac{2K_2}{k} = hc \bar{\nu}_{2(0 \rightarrow 1)}$$

$$\text{So } \bar{\nu}_{1(0 \rightarrow 1)} = \left( \frac{\lambda_1}{2\pi^2 c} \right)^{\frac{1}{2}} \quad \bar{\nu}_{2(0 \rightarrow 1)} = \left( \frac{\lambda_2}{2\pi^2 c} \right)^{\frac{1}{2}} \quad (1.3.12)$$

where  $\bar{\nu}$  are spectroscopic frequencies.

Removing the cross term (at equation 1.3.8) generates specific values for the terms in  $\theta$  as follows:-

Putting the coefficient of  $\underline{ab}$  equal to zero

$$2(d_A - d_B) \sin \theta \cos \theta + d_I (\sin^2 \theta - \cos^2 \theta) = 0 \quad (1.3.13)$$

$$\left( \frac{d_A - d_B}{d_I} \right) = \frac{\cos^2 \theta - \sin^2 \theta}{2 \sin \theta \cos \theta} = \frac{\cos 2\theta}{\sin 2\theta}$$

$$\text{putting } A = \frac{d_A - d_B}{d_I}, \text{ then } \tan 2\theta = \frac{1}{A} \quad (1.3.14)$$

Using this expression terms in  $\theta$  can be eliminated from  $\lambda_1$  and  $\lambda_2$ . Attempts at direct substitution would be difficult, however a simpler mathematical approach is to consider the combinations

$$\lambda_1 + \lambda_2 \quad \text{and} \quad \lambda_1 - \lambda_2$$

$$\text{We immediately see that } \lambda_1 + \lambda_2 = d_A + d_B \quad (1.3.15)$$

$$\lambda_1 - \lambda_2 = (d_A - d_B)(\cos^2 \theta - \sin^2 \theta) + 2d_I \sin \theta \cos \theta \quad (1.3.16)$$

$$\left( \frac{\lambda_1 - \lambda_2}{d_I} \right) = A \cos 2\theta + \sin 2\theta$$



$$\text{Put } \varphi = \left( \frac{\lambda_1 - \lambda_2}{d_I} \right) \quad \text{so} \quad \frac{\varphi}{\sin 2\theta} = (\Lambda^2 + 1)$$

$$\text{Squaring } \varphi^2 = (\Lambda^2 + 1)^2 \sin^2 2\theta$$

$$\text{However } \frac{\sin 2\theta}{\cos 2\theta} = \frac{1}{\Lambda} \quad \frac{\sin^2 2\theta}{\cos^2 2\theta} = \frac{1}{\Lambda^2}$$

$$\sin^2 2\theta \Lambda^2 = 1 - \sin^2 2\theta$$

$$\text{so } \sin^2 2\theta = \frac{1}{(\Lambda^2 + 1)}$$

$$\therefore \varphi^2 = \Lambda^2 + 1$$

$$\text{and } \lambda_1 - \lambda_2 = \pm \left( (d_A - d_B)^2 + d_I^2 \right)^{\frac{1}{2}} \quad (1.3.17)$$

$$(\lambda_1 + \lambda_2) + (\lambda_1 - \lambda_2) = 2\lambda_1 = \frac{(d_A + d_B) + \left( (d_A - d_B)^2 + d_I^2 \right)^{\frac{1}{2}}}{1} \quad (1.3.18)$$

$$(\lambda_1 + \lambda_2) - (\lambda_1 - \lambda_2) = 2\lambda_2 = \frac{(d_A + d_B) - \left( (d_A - d_B)^2 + d_I^2 \right)^{\frac{1}{2}}}{1} \quad (1.3.19)$$

Taking the - ve root for  $(\lambda_1 - \lambda_2)$  we see that the values of  $\lambda_1, \lambda_2$  interchange.

Returning to the solution for  $\theta$ :-  $\tan 2\theta$  will give a series of possible  $2\theta$  values since  $\tan 2\theta = \tan (2\theta + n\pi)$  which in turn gives rise to two series of  $\theta$  values separated from each other by  $\pi/2$

$$\theta' = \theta_0 + n\pi/2 \quad n = \text{even}$$

$$\theta'' = \theta_0 + n\pi/2 \quad n = \text{odd}$$

It is very easily shown that  $\tan \theta' = - \frac{1}{\tan \theta''}$

$$\begin{array}{l}
 \text{and } \left. \begin{array}{l} \sin \theta' = -\sin \theta_0 \\ \cos \theta' = -\cos \theta_0 \end{array} \right\} n = 2, 6, \dots \quad \text{or} \quad \left. \begin{array}{l} \sin \theta_0 \\ \cos \theta_0 \end{array} \right\} n = 0, 4, \dots \\
 \left. \begin{array}{l} \sin \theta'' = \cos \theta_0 \\ \cos \theta'' = -\sin \theta_0 \end{array} \right\} n = 1, 5, \dots \quad \text{or} \quad \left. \begin{array}{l} -\cos \theta_0 \\ \sin \theta_0 \end{array} \right\} n = 3, 7, \dots
 \end{array}$$

so clearly

$$\begin{array}{l}
 \sin \theta' = \pm \cos \theta'' \\
 \cos \theta' = \mp \sin \theta''
 \end{array}$$

i.e. absolute values are interchangeable as long as the signs are the same for  $\theta'$  and opposite for  $\theta''$

Returning to the substitution made for X, Y and rearranging gives

$$\begin{array}{l}
 a = X \cos \theta + Y \sin \theta \\
 b = X \sin \theta - Y \cos \theta
 \end{array} \quad (1.3.20)$$

where

$$\begin{array}{l}
 X = \sqrt{I_A} \alpha_A \\
 Y = \sqrt{I_B} \alpha_B
 \end{array}$$

a and b must be the normal coordinates of the system as they allow separation of the equations, and by substituting for  $\theta$  we can find the contributions of  $\alpha_A, \alpha_B$  to these. If we use  $\theta'$  then  $\theta''$  and substitute their values of  $\theta_0$  we see that

$$\begin{array}{l}
 a' = \pm b'' \\
 b' = \mp a''
 \end{array}$$

i.e. again interchangeable subject to sign restrictions.

However the values involved in the Schrodinger equation are  $a^2, b^2$  so there the restrictions are no longer necessary, and  $(a')^2 = (b'')^2$ ,  $(b')^2 = (a'')^2$ . We have also seen that  $\lambda_1, \lambda_2$  interchange when

we change the root. So clearly both roots give the same answer and each value of  $\lambda$  is associated with a particular normal coordinate mixture of  $\alpha_A, \alpha_B$ .

$$\begin{aligned} a &= (\sqrt{I_A} \cos \theta) \alpha_A + (\sqrt{I_B} \sin \theta) \alpha_B \\ b &= (\sqrt{I_A} \sin \theta) \alpha_A - (\sqrt{I_B} \cos \theta) \alpha_B \end{aligned} \quad 1.3.21$$

These coefficients will be the equivalent of the  $L^{-1}$  matrix in a normal coordinate type analysis.

Eigenfunctions: These will be the same as for the S.H. oscillator and so for the equation

$$\frac{\partial^2 \psi_1}{\partial a^2} + \frac{8\pi^2}{h^2} [E_1 - \lambda_1 a^2] \psi_1 = 0$$

the normalised eigenfunctions are

$$\begin{aligned} \psi_0(y) &= \frac{1}{\pi^{\frac{1}{4}}} e^{-(y^2/2)} \\ \psi_1(y) &= \frac{1}{(4\pi)^{\frac{1}{4}}} 2y \cdot e^{-(y^2/2)} \end{aligned}$$

where

$$y = \left( \frac{8\pi^2 \lambda_1}{h^2} \right)^{\frac{1}{4}} \cdot a$$

### 3b. Special Simplifications.

Obviously for a number of special cases the equations can be much simplified.

a) D<sub>3d</sub> symmetric field. Both rotors and their external fields are identical e.g. the hydrazinium dihalides N<sub>2</sub>H<sub>6</sub>X<sub>2</sub> (Chapter 3)

$$V_A = V_B \quad I_A = I_B \quad n_A = n_I = 3$$

So  $d_A = d_B$  and the solutions become

$$2\pi^2 c^2 \bar{v}_1^{-2} = \lambda_1 = d_A + d_{I/2} = 9V_A/4I_A$$

$$2\pi^2 c^2 \bar{v}_2^{-2} = \lambda_2 = d_A - d_{I/2} = 9V_A/4I_A + \frac{9V_I}{2I_A}$$

$$\text{From } \lambda_1 \quad \bar{V}_A = \frac{8\pi^2 c I_A}{9h} \bar{v}_1^{-2} \quad (1.3.22)$$

$$\text{from } \lambda_2 - \lambda_1 \quad \bar{V}_I = \frac{4\pi^2 c I_A}{9h} (\bar{v}_2^{-2} - \bar{v}_1^{-2}) \quad (1.3.23)$$

$$\text{For the normal coordinates } \tan 2\theta = \frac{d_I}{d_A - d_A} = \infty$$

$$2\theta = 90^\circ \quad \theta = 45^\circ \quad \sin \theta = \cos \theta = \frac{1}{\sqrt{2}}$$

So  $a = \frac{1}{\sqrt{2}} (\alpha_1 + \alpha_2)$  where  $I_A$  has been removed

$b = \frac{1}{\sqrt{2}} (\alpha_1 - \alpha_2)$  as a common factor.

Here we effectively see separation of a whole rigid body libration where the two NH<sub>3</sub> groups rotate together against external fields, and a mode where the two groups contra-rotate involving the internal and external fields.

b) External barriers  $\rightarrow 0$  e.g.  $\text{CH}_3\text{NH}_3\text{PF}_6$  (Chapter 4)

$$V_A, V_B \rightarrow 0 \quad d_A \rightarrow \frac{n_I^2 V_I}{4I_A} \quad d_B \rightarrow \frac{n_I^2 V_I}{4I_A}$$

$$\lambda_1 \rightarrow \frac{n_I^2 V_I}{4} \left( \frac{I_A + I_B}{I_A I_B} \right) \quad \text{and} \quad \lambda_2 \rightarrow 0, (\nu_2 \rightarrow 0)$$

$$\text{So} \quad \bar{V}_I = \frac{8\pi^2 c I_{\text{red}}}{n_I^2 h} \bar{\nu}_1^2 \quad I_{\text{red}} = \frac{I_A I_B}{I_A + I_B}$$

For the normal coordinates:-

$$\tan 2\theta \rightarrow \infty \quad \theta \rightarrow 45^\circ$$

Again we are seeing separation of internal and overall rotors, but in this case the overall rotor is practically free and the torsional mode frequency is almost that which would be obtained for the 'free' molecule or ion.

c) Internal barrier  $\rightarrow 0$  e.g. Aniline salts (Chapter 5)

$$V_I \rightarrow 0 \quad \text{so} \quad d_I \rightarrow 0$$

$$\lambda_1 \rightarrow \frac{1}{2} (d_A + d_B + \sqrt{(d_A - d_B)^2}) \rightarrow d_A$$

$$\lambda_2 \rightarrow d_B$$

$$\bar{V}_A = \frac{8\pi^2 c I_A}{n_A^2 h} \bar{\nu}_1^2 \quad \text{similarly} \quad \bar{V}_B = \frac{8\pi^2 c I_B}{n_B^2 h} \bar{\nu}_2^2$$

For the normal coordinates

$$\tan 2\theta = 0 \quad \theta = 0 \quad \sin \theta = 0 \quad \cos \theta = 1$$

$$\text{hence} \quad a = \alpha_1 \quad b = \alpha_2$$

As expected we now see two independent rotors.

### 3c. Classical-Mechanical Treatment.

The problem can also be solved classically and a normal coordinate treatment applied to the frequencies. See also ref (21).

#### Theory.

$$\text{K.E.} \quad 2T = I_A \dot{\alpha}_A^2 + I_B \dot{\alpha}_B^2 \quad (1.3.24)$$

$$\begin{aligned} \text{P.E.} \quad 2V &= k_A \alpha_A^2 + k_B \alpha_B^2 + k_I (\alpha_A - \alpha_B)^2 \\ &= (k_A + k_I) \alpha_A^2 + (k_B + k_I) \alpha_B^2 - 2k_I \alpha_A \alpha_B \end{aligned} \quad (1.3.25)$$

where we have made the S.H.O. approximation and

$$k_A = \frac{V_A n_A^2}{2}, \quad k_B = \frac{V_B n_B^2}{2}, \quad k_I = \frac{V_I n_I^2}{2}$$

$$\text{Applying Lagrange's Equation} \quad \left( \frac{d}{dt} \left( \frac{\partial T}{\partial \dot{\alpha}_i} \right) + \frac{\partial V}{\partial \alpha_i} = 0 \right)$$

$$\left. \begin{aligned} I_A \ddot{\alpha}_A + (k_A + k_I) \alpha_A - k_I \alpha_B &= 0 \\ I_B \ddot{\alpha}_B + (k_B + k_I) \alpha_B - k_I \alpha_A &= 0 \end{aligned} \right\} (1.3.26)$$

$$\text{Substitute } \alpha_A = A e^{i\omega t}, \quad \alpha_B = B e^{i\omega t} \quad \text{where } \omega = 2\pi\nu$$

$$(-I_A \omega^2 + k_A + k_I) A \cancel{e^{i\omega t}} - k_I B \cancel{e^{i\omega t}} = 0$$

$$(-I_B \omega^2 + k_B + k_I) B \cancel{e^{i\omega t}} - k_I A \cancel{e^{i\omega t}} = 0$$

Hence the secular determinantal equation for non-trivial solutions:-

$$\begin{vmatrix} (k_A + k_I - I_A \omega^2) & -k_I \\ -k_I & (k_B + k_I - I_B \omega^2) \end{vmatrix} = 0 \quad (1.3.27)$$

which is a quadratic in  $\omega^2$

$$\text{So } \omega^2 = \frac{1}{2} \left[ \frac{k_A + k_I}{I_A} + \frac{k_B + k_I}{I_B} \pm \sqrt{\left( \frac{k_A + k_I}{I_A} - \frac{k_B + k_I}{I_B} \right)^2 + \frac{4k_I^2}{I_B I_A}} \right]$$

If we change to the substitutions used in the Q.M. treatment

$$\omega^2 = [d_A + d_B \pm \sqrt{(d_A - d_B)^2 + d_I^2}] = 2\lambda \quad (1.3.28)$$

$$\text{since } \omega^2 = 4\pi^2 \nu^2 \quad \text{and} \quad \lambda = 2\pi^2 \nu^2$$

i.e. Exactly the same two values for the frequencies.

Note this is basically the normal coordinate treatment

Since  $\alpha_A, \alpha_B$  are already symmetry coordinates, with a unit U matrix

we can write down F, G immediately

$$F = \begin{bmatrix} (k_A + k_I) & -k_I \\ -k_I & (k_B + k_I) \end{bmatrix} \dots (1.3.29) \quad G = \begin{bmatrix} \frac{1}{I_A} & 0 \\ 0 & \frac{1}{I_B} \end{bmatrix} \dots (1.3.30)$$

$$GF = \begin{bmatrix} \frac{(k_A + k_I)}{I_A} & -\frac{k_I}{I_A} \\ -\frac{k_I}{I_B} & \frac{(k_B + k_I)}{I_B} \end{bmatrix} \dots (1.3.31)$$

Using the secular determinantal equation  $[GF - \lambda] L = 0$  the secular determinant is the same as above and gives the values of  $\lambda$ . We can now write the equations:

$$\begin{aligned}
 & \left[ \frac{k_A + k_I}{I_A} - \lambda_H \right] L_{11} - \left[ \frac{k_I}{I_A} \right] L_{21} = 0 \\
 & - \left[ \frac{k_I}{I_B} \right] L_{12} + \left[ \frac{k_B + k_I}{I_B} - \lambda_L \right] L_{22} = 0
 \end{aligned} \tag{1.3.32}$$

and obtain ratios of L values. By normalising the L, L' matrices and using  $LL' = G$  we can calculate all the values of the full L matrix. Then finding  $L^{-1}$  we find the contributions of  $\alpha_A$ ,  $\alpha_B$  to each normal coordinate Q

$$\begin{aligned}
 Q_1 &= L_{11}^{-1} \alpha_A + L_{12}^{-1} \alpha_B = a \\
 Q_2 &= L_{21}^{-1} \alpha_A + L_{22}^{-1} \alpha_B = b
 \end{aligned} \tag{1.3.33}$$

which are the same as the coordinates a, b in the Q.M. treatment.



#### Section 4. Multiple Top Rotors.

In the cases of molecules containing more than one rotor group attached to the same atom the potential is modified due to interaction of the tops, and more energy levels are obtained. The complexity of the full theoretical treatment is great even without considering full external rotation interactions, although the simpler cases of identical threefold symmetric rotors have been studied. 2, 3 and 4 tops attached to a common atom have been treated by many authors (22-31), resulting in different notations, and arguments about which terms to include and which ones cancel.

The potential interaction terms can be obtained by taking the terms in an N-dimensional Fourier expansion which correspond with molecular symmetry (N = no. of interacting tops). This means that there is an increased number of parameters to find and these are often lumped together into just two as usually there is insufficient data available for complete evaluation.

The kinetic energy expressions also become more complicated, through interaction of the tops with overall rotation. The full energy is given by:

$$\begin{aligned}
 2T = & \sum_{g=x,y,z} I_g \dot{\omega}_g^2 && \text{..... overall rotation} \\
 & + \sum_{i=1}^3 I_\alpha \dot{\alpha}_i^2 && \text{..... internal rotors} \\
 & + 2 \sum_{i=1}^3 I_\alpha \dot{\alpha}_i \left[ \sum_{g=x,y,z} \lambda_{ig} \omega_g \right] && \text{..... interactions} \quad (1.4.1)
 \end{aligned}$$

as given by Pitzer and Gwinn (23) and Crawford (22).

Where  $I_g$  = principal moments of inertia for overall rotation.  
 $I_\alpha$  = moment of inertia of internal top  
 $\omega_g$  = angular velocity about the  $g^{\text{th}}$  principal axis  
 $\dot{\alpha}_i$  = angular velocity of  $i^{\text{th}}$  top about its axis  
 $\lambda_{ig}$  = cosine of the angle between the top axis  $i$  and the principal axis  $g$ .

The case of the two top system is developed below in order to show where some of the terms arise.

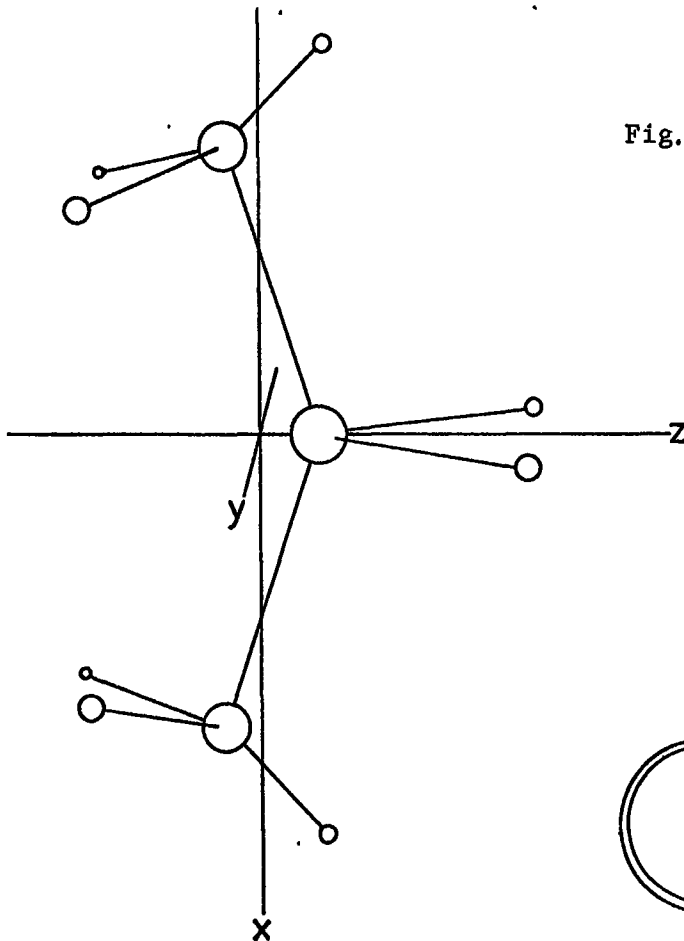
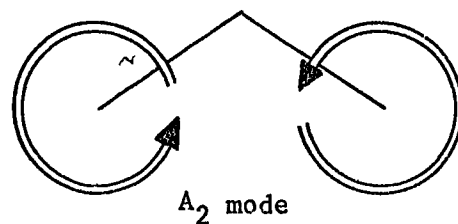
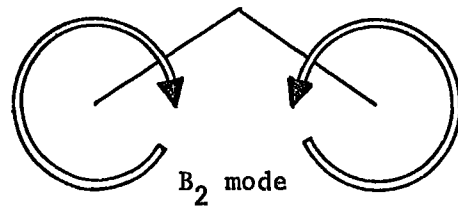


Fig. 1.9 Choice of axes and symmetry of torsional modes.



Kinetic energy:-

$$\begin{aligned}
 T = & \frac{1}{2} I_x \omega_x^2 + \frac{1}{2} I_y \omega_y^2 + \frac{1}{2} I_z \omega_z^2 \\
 & + \frac{1}{2} I_\alpha \dot{\alpha}_1^2 + \frac{1}{2} I_\alpha \dot{\alpha}_2^2 \\
 & + I_\alpha \lambda_x \omega_x (\dot{\alpha}_1 - \dot{\alpha}_2) + I_\alpha \lambda_z \omega_z (\dot{\alpha}_1 + \dot{\alpha}_2)
 \end{aligned} \tag{1.4.2}$$

From this the conjugate momenta  $P_g, p_i$  are found using  $P_g = \frac{\partial T}{\partial \omega_g}$  and  $p_i = \frac{\partial T}{\partial \dot{\alpha}_i}$  and the energy then re-expressed in terms of these as

$$\begin{aligned}
 T = & B P_x^2 + C P_y^2 + A P_z^2 \dots \text{overall rotations} \\
 & F(p_1^2 + p_2^2) + F'(p_1 p_2 + p_2 p_1) \dots \text{internal rotations} \\
 & -2Q_x P_x (p_1 - p_2) - 2Q_z P_z (p_1 + p_2) \dots \text{external/internal} \\
 & \hspace{15em} \text{interactions} \tag{1.4.3}
 \end{aligned}$$

the coefficients are given by Swalen and Costain (25), except that their x, z coordinates have been interchanged.

Potential energy:-

$$\begin{aligned}
 2V(\alpha_1, \alpha_2) = & V_0 - V_3(\cos 3\alpha_1 + \cos 3\alpha_2) \\
 & - V_a \cos 3\alpha_1 \cos 3\alpha_2 + V_b \sin 3\alpha_1 \sin 3\alpha_2 \\
 & + V_6 (\cos 6\alpha_1 + \cos 6\alpha_2) \dots \dots \dots \tag{1.4.4}
 \end{aligned}$$

where

$$\begin{aligned}
 V_0 & = \text{gathered constants} \\
 V_3 & = \text{3-fold potential barrier} \\
 \left. \begin{array}{l} V_a \\ V_b \end{array} \right\} & = \text{interactions constants} \\
 V_6 & = \text{6-fold potential constant}
 \end{aligned}$$

The  $V_6$  + higher order terms are usually omitted as before, and the kinetic external/internal interactions are again regarded as small enough to ignore, although effects of this coupling are retained in the torsional kinetic energy terms.

The Hamiltonian can now be separated into overall rotational and internal torsional Hamiltonians.. ( $H_R + H_T$ )

So

$$H_T = V_0 + F(p_1^2 + p_2^2) - \frac{V_3}{2} (\cos 3\alpha_1 + \cos 3\alpha_2) \\ + F'(p_1 p_2 + p_2 p_1) - \frac{V_a}{2} \cos 3\alpha_1 \cos 3\alpha_2 + \frac{V_b}{2} \sin 3\alpha_1 \sin 3\alpha_2 \\ \dots(1.4.5)$$

It can be seen that this consists of two sets of terms as for two non-interacting rotors and cross terms involving the interactions.

#### a) Perturbation treatment solutions

Some mention should be made here of treatments for 2 and 3 top cases by Möller and Andresen (28) which treat the cross terms as a perturbation after solving the non-interacting terms using the ordinary Mathieu solutions. The resulting expressions are extremely complicated although for cases where the Mathieu parameter  $S \geq 45$  (i.e. moderately high barrier) some simplification can be done. Even so these expressions are comparatively complex and in order to evaluate all the parameters of interest several assigned transitions must be known, and hence very few people appear to have actually used the formulas, preferring the much simpler S.H. treatments (described

shortly). The treatment has not been extended to the even more complex 4-rotor case. Interesting points which do however arise from the treatment are that perturbations due to the  $V_a$  and  $V_6$  terms shift all the levels in the same direction, and that perturbations due to the  $V_b$  term and the kinetic term  $F'(p_1^2 + p_2^2)$  cause the levels above the ground level to split.

#### b) S.H. Multiple rotor treatments

Fortunately the simple harmonic approximation can be usefully applied to obtain solutions for high barrier cases. This has been done for 2, 3, 4 rotors again by the various authors, but fortunately Weiss and Leroi (31) have sorted out the notations to give a comprehensive picture as we proceed from 2 to 4 rotors. They just give the necessary formulas and results so the two top case will again be developed in full and 3 and 4 in brief:

2 tops. The full expression for the Hamiltonian was given above eq. (1.4.5) and after making the approximation ignoring terms greater than the square in the cosine and sine expansions the Schrödinger equation can be written:-

$$F\left(\frac{\partial^2 \psi}{\partial \alpha_1^2} + \frac{\partial^2 \psi}{\partial \alpha_2^2}\right) + F'\left(\frac{\partial}{\partial \alpha_1} \cdot \frac{\partial \psi}{\partial \alpha_2} + \frac{\partial}{\partial \alpha_2} \cdot \frac{\partial \psi}{\partial \alpha_1}\right) + \left[E - \frac{K}{2}(\alpha_1^2 + \alpha_2^2) - L\alpha_1\alpha_2\right] \psi = 0 \quad (1.4.6)$$

where

$$K = \frac{9}{2}(V_3 + V_a) \quad L = \frac{9}{2}(V_b) \quad (1.4.7)$$

The coordinates are now transformed to

$$\begin{aligned}\alpha_+ &= \frac{1}{\sqrt{2}} (\alpha_1 + \alpha_2) \\ \alpha_- &= \frac{1}{\sqrt{2}} (\alpha_1 - \alpha_2)\end{aligned}\quad (1.4.8)$$

This is very similar to the treatment developed earlier for the external-internal barriers of hydrazinium salts except that no kinetic cross term was needed there. The equation is now separable:-

$$\left. \begin{aligned}F_A \frac{\partial^2 \psi_+}{\partial \alpha_+^2} + \left[ E_+ - \frac{(K+L)}{2} \alpha_+^2 \right] \psi_+ &= 0 \\ F_B \frac{\partial^2 \psi_-}{\partial \alpha_-^2} + \left[ E_- - \frac{(K-L)}{2} \alpha_-^2 \right] \psi_- &= 0\end{aligned} \right\} (1.4.9)$$

$$\text{where } F_A = F + F' \quad \text{and} \quad F_B = F - F' \quad (1.4.10)$$

Hence for the  $0 \rightarrow 1$  ( $\pm$ ) transitions

$$\begin{aligned}h\nu_+ &= [2F_A (K+L)]^{\frac{1}{2}} \\ h\nu_- &= [2F_B (K-L)]^{\frac{1}{2}}\end{aligned}\quad (1.4.11)$$

Taking the values of  $F$  and  $F'$  referred to earlier (25)

$$\begin{aligned}F_A &= \frac{h^2}{2I_\alpha} \left[ \frac{1}{1 - (2\lambda_z^2 I_\alpha / I_z)} \right] = \frac{h^2}{2} \cdot \frac{1}{r_z} \\ F_B &= \frac{h^2}{2I_\alpha} \left[ \frac{1}{1 - (2\lambda_x^2 I_\alpha / I_x)} \right] = \frac{h^2}{2} \cdot \frac{1}{r_x}\end{aligned}\quad (1.4.12)$$

where  $I_x, I_z$  = moments of inertia about principal axes  $x, z$   
 $I_\alpha$  = moment of inertia of internal top

$$\text{Hence } \bar{v}_+ = \left[ \frac{9h}{8\pi^2 cr_z} \cdot (\bar{V}_3 + \bar{V}_a + \bar{V}_b) \right]^{\frac{1}{2}}$$

$$\bar{v}_- = \left[ \frac{9h}{8\pi^2 cr_x} \cdot (\bar{V}_3 + \bar{V}_a - \bar{V}_b) \right]^{\frac{1}{2}} \quad (1.4.13)$$

remembering that the z axis corresponds with the  $C_2$  axis.

3 tops. Note that this applies only for  $C_{3V}$  molecules. The z axis is chosen to coincide with the  $C_3$  axis, and the x and y axes pass through the centre of mass.

Fourier expansion:-

$$2V = V_0 - V_3 \sum_{i=1}^3 \cos 3\alpha_i - V_a \sum_{i>j} \cos 3\alpha_i \cos 3\alpha_j$$

$$+ V_b \sum_{i>j} \sin 3\alpha_i \sin 3\alpha_j - V_c \cos 3\alpha_1 \cos 3\alpha_2 \cos 3\alpha_3$$

$$+ V_d \sum_{i \neq j \neq k} \cos 3\alpha_i \sin 3\alpha_j \sin 3\alpha_k \quad (1.4.14)$$

Making S.H. approximation

$$V = \frac{K}{2} (\alpha_1^2 + \alpha_2^2 + \alpha_3^2) + L(\alpha_1\alpha_2 + \alpha_2\alpha_3 + \alpha_3\alpha_1) \quad (1.4.15)$$

where now

$$K = \frac{9}{2}(V_3 + 2V_b + V_c) \quad L = \frac{9}{2}(V_b + V_d) \quad (1.4.16)$$

The coordinate transformation now required is

$$x_1 = \frac{1}{\sqrt{3}} (\alpha_1 + \alpha_2 + \alpha_3)$$

$$x_2 = \frac{1}{\sqrt{6}} (\alpha_1 + \alpha_2 - 2\alpha_3) \quad (1.4.17)$$

$$x_3 = \frac{1}{\sqrt{2}} (\alpha_1 - \alpha_2)$$

which leads to three separate equations, two of which give the same solution. Hence  $0 \rightarrow 1$  transitions are given by

$$\begin{aligned} h\nu_A &= [2F_A (K + 2L)]^{\frac{1}{2}} \\ h\nu_E &= [2F_E (K - L)]^{\frac{1}{2}} \end{aligned} \quad (1.4.18)$$

where

$$F_A = \frac{h^2}{2r_z} \quad F_E = \frac{h^2}{2r_x}$$

and

$$r_z = (1 - 3\lambda_z^2 I_\alpha / I_z) I_\alpha$$

$$r_x = (1 - 3\lambda_x^2 I_\alpha / I_x) I_\alpha$$

It happens for the  $C_{3v}$  case that  $\lambda_x^2 = 1 - \lambda_z^2$ .

4 tops. Note this applies only for Td molecules.

The Fourier series now contains even more terms see Weiss and Leroi (31) but making the S.H. approximation we again obtain

$$V = \frac{K}{2} \sum_{i=1}^4 \alpha_i^2 + L \sum_{i>j} \alpha_i \alpha_j \quad (1.4.19)$$

where now

$$\begin{aligned} K &= \frac{9}{2} (V_3 + 3V_a + 3V_c + V_e) \\ L &= \frac{9}{2} (V_b + 3V_d + V_f) \end{aligned} \quad (1.4.20)$$

The coordinate transformation

$$\begin{aligned} X_1 &= \frac{1}{2} (\alpha_1 + \alpha_2 + \alpha_3 + \alpha_4) \\ X_2 &= \frac{1}{2\sqrt{3}} (3\alpha_1 - \alpha_2 - \alpha_3 - \alpha_4) \\ X_3 &= \frac{1}{\sqrt{6}} (-2\alpha_2 + \alpha_3 + \alpha_4) \\ X_4 &= \frac{1}{\sqrt{2}} (\alpha_3 - \alpha_4) \end{aligned} \quad (1.4.21)$$



leads to 4 separate equations three of which give the same solution and for  $0 \rightarrow 1$

$$\begin{aligned} h\nu_A &= [2F(K + 3L)]^{\frac{1}{2}} \\ h\nu_F &= [2F(K - 1)]^{\frac{1}{2}} \end{aligned} \quad (1.4.22)$$

$$\text{where } F = \frac{h^2}{2I_{\text{red}}} \quad I_{\text{red}} = I_{\alpha} (1 - 4I_{\alpha} \cos^2(\theta_d/2)/I)$$

$$I = I_x = I_y = I_z$$

For all three cases if the two frequencies predicted can be obtained the parameters K, L can be evaluated. It should also be noted that if the terms involved in L other than  $V_b$  are assumed to be small enough to ignore, and the effects of the reduced moments of inertia are small, the values of the splitting parameter  $(\nu_2^2 - \nu_1^2)$  for a series of related compounds such as  $(\text{CH}_3)_x \text{CY}_{(4-x)}$  ( $x = 2, 3, 4$ ) ought to have the approximate ratio 2:3:4 for 2,3,4 tops respectively. ( $\nu_2$  and  $\nu_1$  are the two observed frequencies). This should not hold so well if the angle between the tops is able to distort to different angles, depending on the other substituent on the carbon.

## Section 5. Methods of Barrier Determination.

In theory any physical property of a substance which shows internal rotation could be utilised to find potential barriers and in fact a number of different methods have been used.

### 1) Thermodynamic Properties.

Smith and Vaughan (32) were the first to ascertain that discrepancies between calculated and observed thermodynamic functions of ethane arose in connection with the internal motion, hitherto regarded as free, but Kemp and Pitzer (1) were the first to invoke a sinusoidal barrier and estimated the  $C_2H_6$  barrier as  $\sim 3.15$  kcal/mole. From here the idea was rapidly extended to other molecules.

The method consists of calculating such parameters as heat capacity, entropy, and free energy by the statistical method using all the usual vibrational and rotational etc. partition functions (p.f.) and relating the difference between these and the observed values to an internal rotation p.f. from which the barrier can be found.

In theory this could be applied to any system, but the main drawback, apart from experimental inaccuracies, is that the p.f.'s for all the other types of motion must be obtained accurately, which requires definite assignments of all the vibrational frequencies etc. It has been found by comparison with other techniques that barriers obtained from thermal data of solids are more reliable than gas phase determinations.

Several reviews have appeared (33-35) and a recent example of the use of the method is given by ref (36).

## 2) Microwave Studies of torsion-rotation interaction.

Two principal methods have been adopted.

### a) Intensity

This method utilises the fact that for excited torsional states the molecular configuration is slightly different (due to centrifugal distortions etc.) and hence the rotational spectrum of this state will be different from the ground state. As a result the microwave spectrum shows strong ground torsional state rotational lines with weaker excited state satellites. The relative intensities are governed by the Boltzmann populations of the torsional levels and from this the barrier can be deduced.

### b) Splitting due to interactions

This method consists of a rigorous analysis of the complicated splittings in the rotation bands caused by interaction with the internal mode, for which the relevant theory has been worked out as mentioned earlier. However, this method is restricted to rotors attached to an asymmetric frame e.g.  $\text{CH}_3\text{CHCl}_2$ , since for symmetric types such as  $\text{CH}_3\text{SiF}_3$  the rotational coupling terms for the A and E torsional levels are the same and hence give no splitting. Also in the case of very high barriers splittings due to the ground torsional state may be too small to observe, although the satellites due to higher torsional states may show them.

The intensity method leads to less reliable results due to problems of assignment, inaccurate intensity measurement and complications due to splitting, but the splitting method has been

applied with a great deal of success. Refer to the following (37, 38, 14). However, microwave studies are generally limited to molecules in the vapour phase and cannot be used to find external barriers in solids, and the molecules must also have a permanent dipole in order to produce a spectrum.

### 3) Torsion-Vibration-Rotation Interaction.

Extending the idea of interactions even further, studies of vibration-torsion combination bands under very high resolution are now being undertaken to observe fine structure arising from torsion-rotation interaction. Again, after careful assignment and using relevant theory a barrier can be determined, however this effectively looks at the barrier for an excited vibrational state.

Susskind (39) has obtained a barrier of 3.33kcal/mole for ethane using the band ( $\nu_{11} + \nu_4$ ) and 3.02 kcal/mole using ( $\nu_{12} + \nu_4$ ). We immediately see that these are higher than the ground state value of 2.93kcal/mole obtained by direct observation of the  $0 \rightarrow 1$  torsion transition. (40)

### 4) Direct Observation of Torsional Frequencies.

All the theory described earlier was directed at calculation of barriers from observed transitions between torsional levels. These frequencies are obtained using spectroscopic I.R., Raman and I.N.S. techniques.

a) I.R./Raman

Strictly speaking, a pure torsional frequency can only be obtained in the gas phase and since observation of an I.R. or Raman band depends on whether it is allowed by the selection rules symmetric molecules such as  $\text{CH}_3\text{CCl}_3$  cannot be studied (as the vapour) by these methods. Even for some species with allowed transitions the band is very weak. However, hot bands and overtones may be allowed and quite often combination bands are observed, which can be used to obtain a reasonable estimate of the torsional frequency and hence the barrier.

There are fortunately ways of breaking the selection rules for the symmetric cases, such as using high pressures and long path lengths (Weiss and Leroi used this for ethane (40)) and measurements on the liquid or solid phases (Durig (14) gives numerous examples). This latter method depends on slight distortions from the pure symmetry caused by the crystal environment, and also usually assumes that interaction with the external modes is still not very relevant, even though shifts in frequency (20) are often observed, as mentioned earlier.

In all these methods however the bands are usually weak and dubious assignments have sometimes been made. Isotopic substitution helps to minimise this possibility.

Reviews have appeared (14, 41, 42).

b) I.N.S.

Using incoherent I.N.S. spectroscopy, because the cross-section of hydrogen is at least an order of magnitude greater than for any other element (see later) the selection rule for observation of a

transition is simply that the mode involves hydrogen motion. For torsional motions there is the added advantage that the amplitude of the H-motion is large and hence the band observed is usually the most intense in the spectrum, and so makes assignment much more definite.

Since chlorine has an appreciable cross section (3.5 barns) it may be possible to obtain incoherent I.N.S. frequencies for such as  $C_2Cl_6$ . Other elements present possibilities when we turn to coherent I.N.S. due to higher cross sections.

Rotational diffusion in solids can also be very conveniently measured using I.N.S., since this kind of motion produces a broadening of the elastic peak.

The main disadvantage of I.N.S. at present apart from cost is that resolution is not nearly so good as for I.R./Raman.

It should be pointed out here that all three techniques can be applied to obtaining external barriers from the location of librational mode bands. This is again subject to crystal factor group selection rules for I.R. and Raman.

#### 5) Nuclear Magnetic Resonance.

Many N.M.R. studies of the solid phases of compounds with protonated librating or torsioning groups have been undertaken. The rotor motion is found to have a pronounced effect on the line width and on relaxation times, and by measuring these properties as a function of temperature an activation energy for the motion can usually be obtained (Refs. 43-47).

a) Line width measurement

In an N.M.R. experiment the magnetic nuclei are aligned by the applied magnetic field according to their nuclear spin quantum no. and transitions between these spin levels are induced by a radiofrequency field. However, the nuclei themselves produce local magnetic fields and so the field at any one fixed nucleus is modified by the fields of its neighbours. Consequently in a solid the resonance (transition) frequencies are spread out more giving a broader line signal. If the nuclei are in motion, such as a rotation around some axis, this causes fluctuations in the local fields due to changes in the orientations of the internuclear vectors. If then these motions are random and of the right speed the local fields are averaged out and the line is narrowed. (For liquids the line becomes very sharp). Clearly the amount of motion will increase as the temperature rises giving a decreasing line width. This temperature dependence can then be related to the barrier to motion.

b) Spin-lattice relaxation times ( $T_1$ ,  $T_{1p}$ )

These properties are the rates at which an excited (hot) nuclear spin system exchanges energy with the lattice to re-attain thermal equilibrium. This relaxation is a result of the oscillating local magnetic fields generated by the magnetic nuclei as they ride on the various lattice motions. Clearly large motions such as group rotations will produce much greater fluctuations and hence be expected to dominate in the relaxation process. This property will again be a function of temperature.

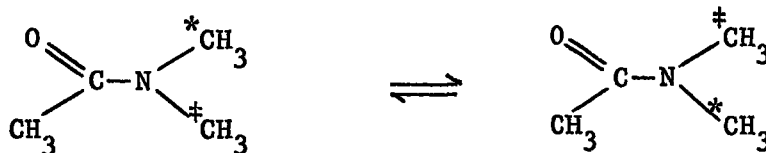
The theory relating these phenomena to barrier heights is rather complex but it can be shown that the effects observed in N.M.R.

relaxation of molecules with rotor groups are due to movements from one trough of the potential to another either by quantum tunnelling (A  $\leftrightarrow$  E transitions), or classical rotation above the barrier. These motions have time scales of the same order as the resonance frequency. Tunnelling is found to be more important at low temperatures and applies mainly to protons, and the classical motion takes over as the temperature increases.

More recently interest has been developing in the use of ENDOR techniques for determining tunnelling frequencies in solids (48).

c) N.M.R. line shapes in liquids

Some mention should also be made here of techniques for determining barrier heights from the N.M.R. of liquids, again by line shape analysis. A simple earlier example showing the principle of the technique was studied by Gutowsky and Holm (57) in



where rotation of the  $(\text{CH}_3)_2\text{N}$  group about the N-C axis was studied. (Though species more related to the present work such as substituted ethanes have also been studied). At low temperatures the rotation process is slow compared to the N.M.R. time scale and the two methyls \* and # having different environments give rise to a doublet signal. As the temperature is raised these broaden and finally coalesce due to the increasing rate of rotation. Increasing the temperature even further so that reorientation becomes very rapid narrows the N.M.R. signal even more. An analysis of the temperature dependence of these



changes in line shape can be successfully applied to obtain barrier activation energies. E.g. refs. (57-59). However, an important point is that this method can only be applied to asymmetric molecules.

#### 6) Other Methods.

Brief mention should be made of techniques which have been used much less extensively. These include sound absorption, electron diffraction (49), E.S.R. and N.Q.R. (Reviews 38, 50).

#### Section 6. Barrier Origins.

Since the realisation of the existence of internal barriers a great deal of work has been carried out attempting to calculate them directly from physical interactions of various kinds, also hoping that this would indicate their origin. It is not intended to give here more than a very brief survey of what is now quite an expansive field, but some of the conclusions about the nature of the barrier are important.

Some methods have used classical electrostatic polar interactions and steric repulsive potential models (51-53) but it is also clear that both methods on their own could be fitted to the experimental potential. Another simple model (54) suggested putting point charges on the rotating bond segments, and also correlating these with the electronegativities of the atoms involved. However, these all build in considerable empirical data and do not really lead to an understanding of the exact source of the interaction.

Direct quantum mechanical calculations have been produced in large numbers, using many kinds of treatments from simple semi-empirical and valence-bond to full ab initio, and often giving considerable ranges of barrier values for the same molecule. However the answers are of the correct order and some of the more recent calculations do seem to be falling nearer the mark (see ref. (60) for a short tabulation of ab initio results). The problem is that the energy differences involved are quite small and hence the wavefunctions used really need to be very precise. The commonly used method is to take the difference of the calculated total electronic and nuclear energies of the staggered and eclipsed configurations. Refinements such as allowing the bond lengths and angles to change on going to the eclipsed configuration, are features of more complex treatments.

Many theoreticians have studied only simpler symmetric types such as ethane, whereas it is now becoming clear that more information on non-symmetrical types and series of compounds which differ slightly, lead to a more enlightening view. Up to now no-one seems to be agreed on a general description of the barrier origins though most seem to indicate that the answer lies in the balance of interactions of lone pairs, bonds and the rotor nuclei. It seems, from various discussions in a number of papers, that the prominent interaction terms may depend on the particular electron distribution of the molecule in question, e.g. when one F atom, which is strongly electronegative, is introduced into ethane the charge distribution changes considerably.

A number of comprehensive reviews on this subject have appeared (38, 55, 56).

When we turn to external barriers in solids the picture is somewhat different since we have intermolecular interactions. No one as yet seems to have attempted a quantum mechanical treatment, but a number of treatments using electrostatic interactions extending out into the lattice, and steric repulsions of shorter range have been attempted. Calculations (19) on the  $\text{NH}_4^+$  ion in halide salts and in alkali halide lattices indicate that the steric potential is probably more important than the electrostatic (but H-bonding is even more important). Such calculations as these are also useful in attempting to find the stable configurations of the ion in the lattice when these are not directly obvious.

Clearly in cases where H-bonding occurs, as in the hydrazinium halides discussed later, this bonding force is a drastic interaction with the lattice and it seems that this can be categorically specified as the principal cause of the barrier.

References - Chapter 1

1. J.D. Kemp, K.S. Pitzer, J. Chem. Phys. 4, 749 (1936).
2. R.W. Kilb, C.C. Lin, E.B. Wilson, *ibid* 26, 1695 (1957).
3. R.W. Kilb, L. Pierce, *ibid* 27, 108 (1957).
4. D.R. Herschbach, *ibid* 31, 91 (1959).
5. W.G. Fateley, F.A. Miller, Spectrochim. Acta. 17, 857 (1961);  
*ibid* 19, 611 (1963).
6. R.E. Ghosh, T.C. Waddington, C.J. Wright, J.C.S. Faraday II, 69  
275 (1973).
7. F.A. Miller, W.G. Fateley, R.E. Witkowski, Spectrochim. Acta 23A,  
891 (1967).
8. G. Blanch, I. Rhodes, Wash. Acad. Sci. 45, 166 (1955).
9. R.W. Kilb, 'Tables of Mathieu Eigenvalues and Eigenfunctions for  
Special Boundary Conditions', Dept. Chem., Harvard Univ. (1956).
10. J.C.M. Li, K.S. Pitzer, J. Phys. Chem. 60, 466 (1956).
11. E.D. Stejskal, H.S. Gutowsky, J. Chem. Phys. 28, 388 (1958).
12. 'Tables Relating to Mathieu Functions' Columbia Univ. Press,  
New York, (1951).
13. D.R. Herschbach 'Tables for the Internal Rotation Problem' Dept.  
Chem., Harvard Univ.
14. J.R. Durig, S.M. Craven, W.C. Harris 'Vibrational Spectra and  
Structure 1' p.81 (1972).
15. T.P. Das, J. Chem. Phys. 25, 896 (1956).
16. H.H. Nielsen, Phys. Rev. 40, 445 (1932).
17. K.E. Larsson, J. Chem. Phys. 59, 4612 (1973).
18. G. Venkataraman, J. Phys. Chem. Solids 27, 1103 (1966).
19. J. Tomkinson, Ph.D. Thesis, Durham University (1974).

20. J.R. Durig, C.M. Player Jr., J. Bragin, J. Chem. Phys. 54, 460 (1971).
21. R.D. Waldron, *ibid* 21, 734 (1953).
22. B.L. Crawford, *ibid* 8, 273 (1940).
23. K.S. Pitzer, W.D. Gwinn, *ibid* 10, 428 (1942).
24. D.R. Lide Jr., D.E. Mann *ibid* 28, 572 (1958).
25. J.D. Swalen, C.C. Costain, *ibid* 31, 1562 (1959).
26. K.L. Myers, E.B. Wilson Jr., *ibid* 33, 186 (1960).
27. M.L. Sage, *ibid* 35, 142 (1961).
28. K.D. Möller, H.G. Andresen, *ibid* 37, 1800 (1962); 39, 17 (1963).
29. K.D. Möller, A.R. de Meo, D.R. Smith, L.H. London; *ibid* 47, 2609 (1967).
30. J.R. Hoyland, *ibid* 49, 1908 (1968).
31. S. Weiss, G.E. Leroi, Spectrochim. Acta 25A, 1759 (1969).
32. H.A. Smith, W.E. Vaughan, J. Chem. Phys. 3, 341 (1935).
33. E.B. Wilson Jr., Chem. Revs. 27, 17 (1940).
34. K.S. Pitzer, Disc. Faraday Soc. 10, 66 (1951).
35. J. G. Aston, *ibid* 10, 73 (1951).
36. H.L. Clever, E.F. Westrum Jr., J. Phys. Chem. 74, 1309 (1970).
37. C.C. Lin, J.D. Swalen, Rev. Mod. Phys. 31, 841 (1959).
38. J.P. Lowe, Progress in Physical Organic Chemistry 6, 1 (1968).
39. J. Susskind, J. Mol. Spec. 49, 1-17, 331 (1974).
40. S. Weiss, G.E. Loeroi, J. Chem. Phys. 48, 962 (1968).
41. A. Finch et al., 'Chemical Applications of Far Infra-red Spectroscopy', Academic Press, London-New York p.78 (1970).
42. K.D. Möller, W.G. Rothschild, 'Far Infra-red Spectroscopy' Wiley-Interscience p.256 (1971).

43. J.G. Powles, H.S. Gutowsky, J. Chem. Phys. 21, 1695 (1953);  
    ibid 23, 1692 (1955).
44. H.S. Gutowsky, Disc. Faraday Soc. 19, 187 (1955).
45. T.P. Das, J. Chem. Phys. 27, 763 (1957).
46. E.D. Stejskal, H.S. Gutowsky, ibid 28, 388 (1958).  
    ibid 31, 55 (1959).
47. A. Abragam, 'Principles of Nuclear Magnetism', O.U.P.
48. S. Clough, J.R. Hill, M. Punkkinen, J. Phys. C. Solid State  
    Phys. 7, 3779 (1974).
49. Y. Morino, E. Hirota, J. Chem. Phys. 28, 185 (1958).
50. E.B. Wilson Jr., 'Advances in Chemical Physics' Vol 2,  
    Interscience N.Y. 1959 p.367.
51. E.N. Lasettre, L.B. Dean, J. Chem. Phys. 17, 317 (1949).
52. N.W. Luft, ibid 22, 1814 (1954).
53. M. Karplus, R.G. Parr, ibid 38, 1547 (1963).
54. J.P. Lowe, R.G. Parr, ibid 43, 2565 (1965); ibid 44, 3001 (1966).
55. L.J. Oosterhoff, Pure Appl. Chem. 25, 563 (1971).
56. J.-M. Lehn, 'Conformational Analysis' Academic Press N.Y. (1971)  
    p.129.
57. H.S. Gutowsky, C.H. Holm, J. Chem. Phys. 25, 1228 (1956).
58. L.H. Piette, W.A. Anderson, ibid 30, 899 (1959).
59. M.T. Rogers, J.C. Woodbrey, J. Phys. Chem. 66, 540 (1962).
60. A. Veillard, "Internal Rotation in Molecules", Edited  
    Orville-Thomas, Wiley, London (1974) Chapter 11.

CHAPTER 2TECHNIQUES AND INSTRUMENTATIONIntroduction.

The main object of this second chapter is to give an idea of the techniques used throughout the present work in obtaining torsional mode frequencies, and also to cover the relevant aspects of neutron scattering theory. Information has been gained primarily from the inelastic neutron scattering (I.N.S.) spectra of compounds containing hydrogenous rotor groups. Infra-red (I.R.) and Raman spectroscopy have also been used where necessary to help locate torsional bands: In the I.N.S. spectra these bands are usually very strong whereas in I.R. or Raman spectra they are often not allowed by the selection rules or when they do appear they are usually weak.

Section 1. Optical Spectra.

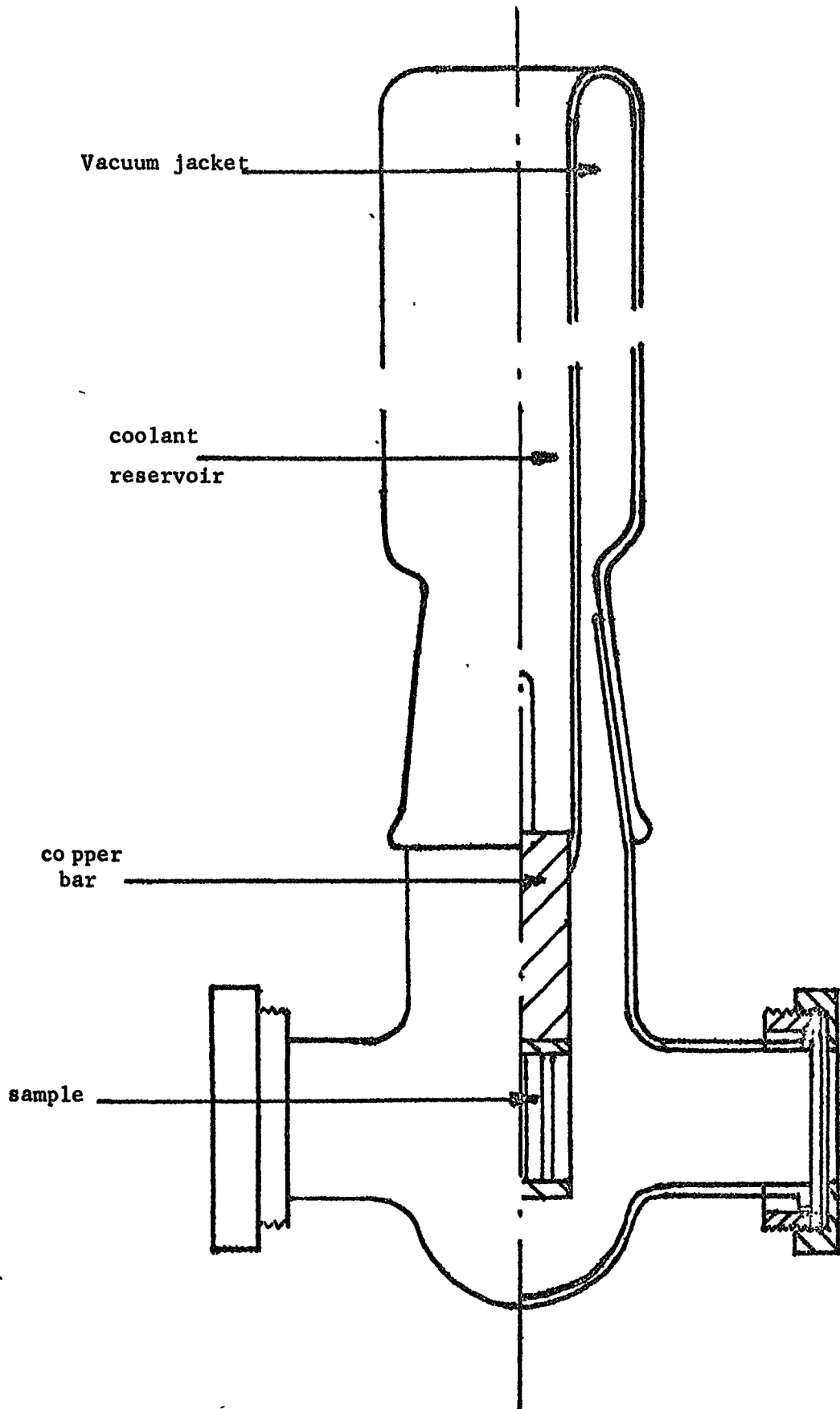
The optical spectrometers used are standard and by now well characterised:-

Near I.R.	Perkin-Elmer	457	grating spectrometers
	" "	577*	
Far I.R.	Beckman-RIIC	FS720	Interferometer
Raman	Cary 82 * using:		
	Spectra-Physics Model 125 He/Ne gas laser at $15,802 \text{ cm}^{-1}$ (red)		
	Model 164 Ar/Kr ion laser at $19436.3 \text{ cm}^{-1}$ (green)		

(The instruments marked \* are more recent acquisitions).

Punched tape data from the F.S.720 was processed on the N.U.M.A.C. computer, an I.B.M. 360-67 using a program developed by Symon (1).

Sample Dewar for I.R. Spectroscopy at liquid nitrogen temperatures





I.R. spectra, both near and far, at temperatures approaching that of liquid nitrogen were obtained using two evacuable glass dewar cells of similar construction, see fig. ( 2.1 ), the only major difference between the two being the material used for the windows. (Polythene for the far I.R. and CsI for the near I.R.). Samples usually as nujol mulls were either smeared onto a polythene disc or pressed between two CsI discs and inserted into their respective cells. After evacuating the systems the dewar was filled with liquid nitrogen.

The near I.R. cold cell also has an attachment which allows liquid or gas samples to be sprayed and frozen onto the CsI sample disc at liquid nitrogen temperatures. Several spectra were obtained in this way.

## Section 2. I.N.S. Spectra.

### 2.1 Theoretical Aspects

Whole books have been devoted to the theory of thermal neutron scattering (2-4) as well as many shorter reviews and articles (e.g. 5-9, 17,18), including a number which give particular attention to molecular spectroscopy. Without entering into the highly mathematical realm of the physicist it is intended here to give some idea of the basic principals of neutron scattering, quoting results of relevance to the current work.

Since we are dealing with the interaction of two particles, the neutron and the nucleus, some potential is required to describe this. The only function which gives satisfactory results is the so-called Fermi pseudo-potential (16).

$$V(r) = \frac{2\pi\hbar^2}{m} \cdot b \cdot \delta(r-R)$$

where  $\delta(\ )$  is a delta function

$m$  is the mass of the neutron

$r$  is the position vector of the neutron

$R$  " " " " nucleus

$\hbar = h/2\pi$   $h = \text{Planck's constant}$

and  $b$  is a quantity known as the scattering length, which varies from one element, or even isotope, to another, and also depends on the nuclear spin. Since the neutron has spin quantum number  $= \frac{1}{2}$  this can obviously interact with its spin parallel or antiparallel to any nuclear spin. ( $b$  has to be determined experimentally).

The total scattering cross-section per atom  $\sigma_{\text{TOTAL}}$  is the effective area presented to an incoming neutron around an atom, within which the neutron would be scattered, and is given by:

$$\sigma_{\text{TOTAL}} = 4\pi \langle |b|^2 \rangle \quad b = \text{scattering length}$$

When a neutron wave encounters an array of nuclei, because of the variation of scattering length due to different isotopes and the spin orientations, it does not see a uniform scattering potential, but one which varies from one point to another. Those scattered waves which interfere strongly form the coherent scattering cross section. Since it is only the mean scattering potential that can give interference effects this is proportional to  $|\langle b \rangle|$  and the coherent scattering cross section is proportional to  $|\langle b \rangle|^2$ . The individual deviations from the mean potential give rise to incoherent scattering, (the random distribution cannot give rise to interference), and its cross section

is proportional to the mean square deviation of scattering lengths  
 $\langle |b - \langle b \rangle|^2 \rangle = \langle |b|^2 \rangle - |\langle b \rangle|^2$ . Elements which have  
 predominantly one isotope and no spin have zero incoherent cross-sections  
 (e.g. C, O) and in general most elements scatter predominantly coherently.  
 The one great exception is the hydrogen atom which has an anomalously  
 high incoherent cross-section of an order of magnitude larger than for  
 any other element. Some cross-section values for elements involved in  
 the present study are given below:-

Table (2.1) Coherent and incoherent scattering cross-sections  
 of several elements.

Element	$\sigma_{\text{COH}}$ (barns)*	$\sigma_{\text{INCOH.}}$ (barns)
H	1.8	79.7
D	5.6	2.0
C	5.6	0.0
N	11.1	0.3
O	4.23	0.0
F	3.98	0.0
Si	2.16	0.0
Cl <sub>Ave.</sub>	11.5	3.5
Ge	8.42	1.0
Br	5.79	0.3
Sn <sub>Ave.</sub>	4.7	0.2
I	3.50	0.4
Al ‡	1.5	0.0

\* 1 barn =  $10^{-28} \text{ m}^2$ . ‡ Material often used as a window and  
 for containers.

It can be seen that the next significant incoherent scatterer after  
 hydrogen is chlorine which is still about twenty times less, and that  
 deuterium is completely different (in the first place it has a different  
 spin quantum number) an aspect which is very useful for isotopic

substitution studies. The fact that incoherent neutron scattering from hydrogenous materials is swamped by the hydrogen contribution is utilised mainly by molecular spectroscopists (and is the centre of the present study).

The quantity of most interest is the double differential scattering cross-section  $\frac{\partial^2 \sigma}{\partial \Omega \partial E}$  which is the probability that an incident neutron will be scattered by a nuclear array into a given solid angle  $\Omega$  with a known energy  $E$  (effectively giving the intensity at these conditions). This again can be separated into coherent and incoherent parts and since from now on only hydrogen is to be considered only the incoherent expression will be retained.

When a neutron is incident on a molecular or ionic system it may be scattered either elastically, with no change in energy, or inelastically where the neutron either gains energy from or loses it to the system, analogous to Raman scattering. However, a uniqueness of particle scattering is that the energy transfer is also accompanied by a momentum change, and so neutrons which may have undergone the same energy change but have scattered into different angles have undergone different momentum changes (since momentum is a vector quantity). Consequently any evaluation of  $\frac{\partial^2 \sigma}{\partial \Omega \partial E}$  must involve both the energy and momentum transfers. Expressions have been developed for various types of molecular motion: translation, rotation and (of most relevance here) for molecular vibrations. The complicated derivations of these expressions take into account the complicated motions of the scattering atoms, and the effects of temperature on the motions and the population

of energy levels. The expression for molecular vibrations is:-

$$\frac{\partial^2 \sigma}{\partial \Omega \partial E} = \frac{N}{2\pi} \left( \frac{k}{k_0} \right) \sum_j (b_j^2) \frac{Q^2 \cdot \langle u_{j,n}^2 \rangle}{M_j w_n} g(w) \exp(-2W_j) P(i)$$

where:

$Q = k - k_0$  the momentum transfer

$k$  = final momentum vector of the neutron

$k_0$  = initial " " " "

$b_j$  = incoherent scattering length of atom  $j$  of mass  $M_j$   
with a mean square vibrational amplitude  $\langle u_{j,n}^2 \rangle$  in the  $n^{\text{th}}$   
normal mode of frequency  $w_n$

$g(w)$  = distribution of frequencies ( $w_n$ )

$\exp(-2W_j)$  = Debye-Waller factor

$P(i)$  = thermal population of initial state

( $N$  = number of atoms in sample)

The Debye-Waller factor exponent is a sum over all the normal modes of the system:-

$$2W_j = \frac{\hbar}{2M_j} \sum_n \frac{Q^2 \cdot \langle u_{j,n}^2 \rangle}{w_n} \coth\left(\frac{\hbar w_n}{2k_B T}\right)$$

$k_B$  = Boltzmann constant       $T$  = temperature

(The Debye-Waller factor itself has the effect of attenuating the cross-section and arises because interference effects between atoms on different sites are smoothed out by thermal vibrations).

The full expression indicates that the vibrational modes of a molecule give rise to a series of  $\delta$ -functions in the I.N.S. spectrum,

with intensities governed by the scattering length of the nuclei which are involved in the modes (principally hydrogen) and their mean square amplitudes of motion. The mode intensity and also its width are dependent on the angle of scatter. The latter effect of momentum transfer broadening is a minimum for low angles (i.e. low  $Q$ ), and so by measuring the neutron spectrum at angles not far from the incident neutron direction this factor is reduced, improving the resolution. (This is the working basis of so-called low  $Q$  spectrometers).

Whereas optical spectroscopy looks at energy transfers with practically zero momentum transfer, I.N.S. also looks at a curious cut through a large range of momentum transfer space. As a consequence, if the energy transfer of a mode varies with momentum transfer (dispersion effect) the frequency of a mode may change from angle to angle. This is particularly relevant to lattice modes, since internal modes do not usually show much dispersion. The dispersion curve of acoustic lattice modes is such that they have zero energy transfer at zero momentum transfer, and consequently are not seen in the optical spectra, but they should be seen in the I.N.S. spectrum for values of  $Q$  greater than zero (provided they satisfy the other conditions for scattering which apply to all types of modes).

When comparing optical and I.N.S. spectra it would therefore be desirable to obtain the equivalent I.N.S. spectrum at zero momentum transfer. This can only be obtained by extrapolating information from several angles of neutron scatter. A method has been described by Egelstaff (5) which can be applied to the data obtained from the time-of-flight spectrometers described next, but not the beryllium filter spectrometer since this only collects data at one

angle . In brief the procedure follows from the following:-

$\frac{\partial^2 \sigma}{\partial \Omega \partial E}$  can be expressed in ways other than the equation given earlier by performing fourier transformations during the derivation. One such expression is

$$\frac{\partial^2 \sigma}{\partial \Omega \partial E} = N \frac{b^2}{\hbar} \frac{k}{k_0} S(Q, w)$$

and  $S(Q, w)$  is the so-called 'scattering law' function.

For neutron energy gain experiments where neutrons are scattered from a sample which has a complicated thermal population of energy levels, this scattering law must be corrected for the Boltzmann distribution. A new scattering law is defined as:-

$$\tilde{S}(Q, w) = \exp(-\hbar w_n / 2k_B T) S(Q, w)$$

By obtaining this new scattering law at several angles of scatter an extrpolation can be performed and the result expressed in terms of the frequency distribution:-

$$g(w) = \frac{4M \cdot w_n}{\hbar} \sinh\left(\frac{\hbar w_n}{2k_B T}\right) \left[ \frac{\tilde{S}(Q, w)}{Q^2} \right]_{Q^2 \rightarrow 0}$$

## 2.2 Instrumentation for I.N.S. spectroscopy

All the I.N.S. spectra presented in this thesis were obtained using machines at the Atomic Energy Research Establishment, Harwell, where the sources of neutrons are the two experimental nuclear reactors DIDO and PLUTO. Fuelled by uranium enriched with  $^{235}\text{U}$  the chain reaction is moderated by  $\text{D}_2\text{O}$  which effectively brings the energetic neutrons which are produced into thermal equilibrium with the reactor. Neutrons for experimental purposes are allowed to pass out of the core, through the heavy shielding walls, along narrow beam holes. At this stage the neutrons have a Boltzmann energy distribution.

### 2.2a The time-of-flight neutron energy gain spectrometers, 6H and 4H5

These spectrometers, mounted on the DIDO reactor are described in detail elsewhere (10,11), but the essential details are described here, with particular reference to the 6H machine. A cross section is shown in fig. ( 2.2 ).

Neutrons passing along the guide tube first encounter a polycrystalline beryllium filter cooled at liquid nitrogen temperature, through which only neutrons with a wavelength greater than  $3.96 \text{ \AA}$  ( $\sim 42 \text{ cm}^{-1}$ ) can pass. Following this,  $\gamma$ -rays are greatly reduced by a bismuth filter. Emerging from the reactor face the beam encounters two phased rotors. Each rotor has curved slots cut into it at the level of the beam and it rotates at a certain speed about its vertical axis. The first rotor chops the neutron beam into pulses. At the same time only the neutrons of a certain narrow band of velocities in the admitted pulse



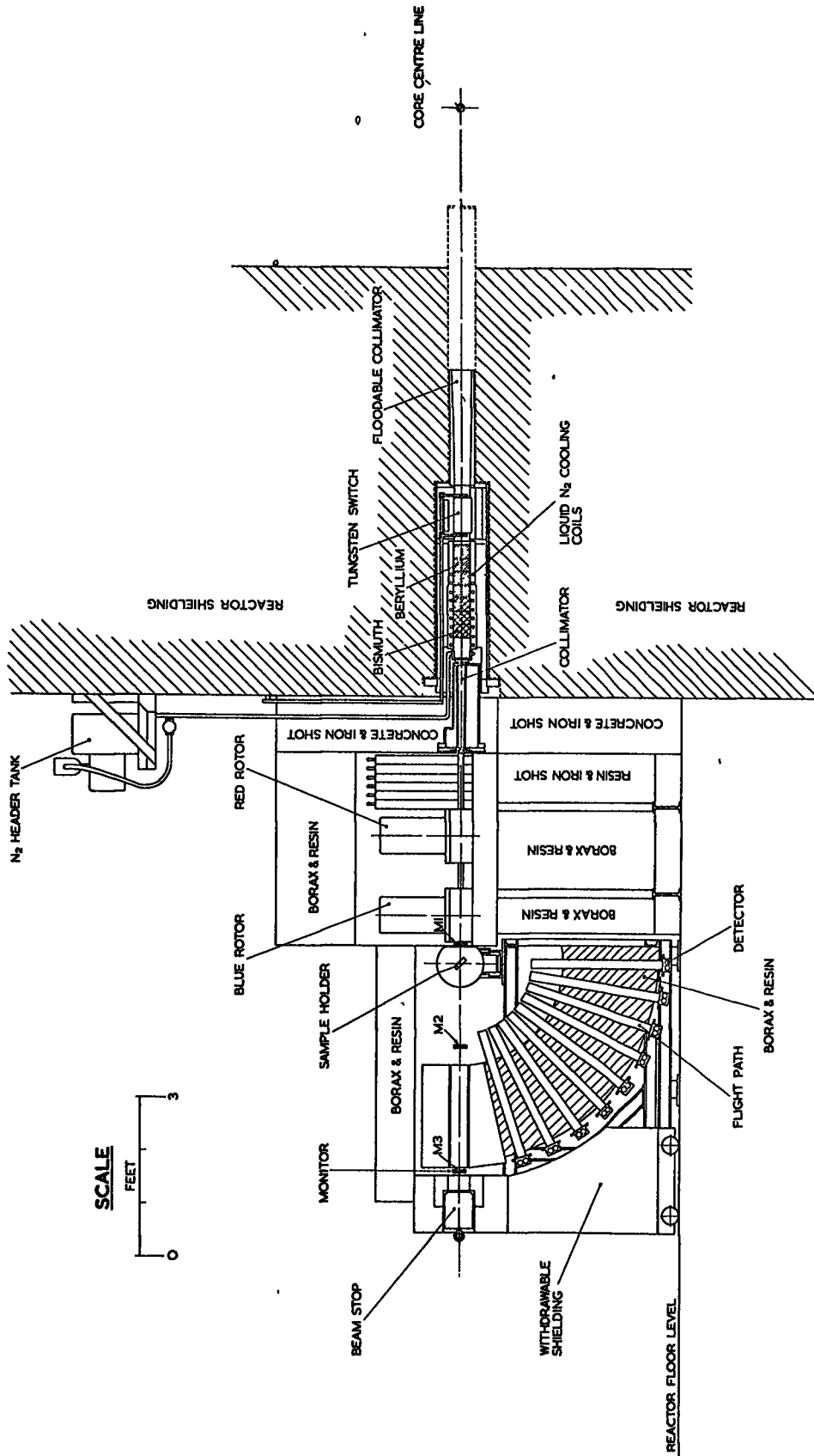


Fig. 2.2 A cross section of the 6H time of flight machine. Ref. (10).

can pass right through. In the space between the first and the second rotor this narrow band spreads out in space on account of the different neutron velocities and by phasing the second rotor relative to the first this chops out an even narrower band within the pulse, effecting reasonable monochromation. This system gives its maximum neutron flux for the 6H machine at neutron energies of  $37 \text{ cm}^{-1}$  (wavelength  $4.2 \text{ \AA}$  or reciprocal velocity  $1062 \text{ \mu sec/metre}$ ), and consequently this energy was used in the present experiments.

In the 4H5 machine the thermal distribution of neutrons is first cooled by a liquid hydrogen moderator in the pile before passing through the filters. This increases the flux of cold neutrons, and peak flux after monochromation occurs for wavelengths of  $\sim 5.3 \text{ \AA}$ .

The pulsing of neutrons is utilised to determine their velocity, by measuring their time-of-flight from the rotor to the detectors. The pulses impinge on the sample (usually a thin layer of the polycrystalline solid, although liquids can also be studied) which is held at  $45^\circ$  to the incident direction. Scattered neutrons in the 6H machine are detected by 9 detector banks at angles to the incident beam of  $90, 81 \dots 18^\circ$  ( $9^\circ$  intervals). All the detectors are placed at 1.35 metres from the sample, at the end of cadmium lined flight tubes which also collimate the scattered neutrons.

The time scale of each pulse is divided into  $6\text{-}\mu\text{sec}$  channels and the number of counts arriving in each channel for each angle are recorded. Counts from the same time channel in the next pulse are added and so on.

This time-of-flight detection enables calculation of the scattered neutron energies. Because of their low incident energy the neutrons are scattered inelastically principally by removing energy from molecules in the sample i.e. the neutrons gain energy and hence arrive at the detectors before the elastically scattered neutrons. The machine therefore looks at energy transitions between thermally populated levels to lower levels in molecules.

Provided the sample is not too thick about 90% of the neutrons are not scattered at all but pass right through. This direct beam is monitored by three fission chambers placed at 13 cm before, and 55 and 118 cm after the sample which also measure the time-of-flight of the pulse. The incident energy of the pulse can therefore be calculated accurately.

The sample is clamped over a hole on a movable metal base, which also has a space for a blank background sample, and a third place which holds a Vanadium standard. This is all enclosed in a chamber which is either filled with helium gas or evacuated. During the course of a run the three samples are consecutively placed in the beam. Usually this cycling lasts about an hour, and the whole run takes  $\sim 24$  hours to obtain sufficient data. The cycling helps to smooth out any changes in flux or the counter efficiencies. A variable cold temperature sample changer is also available in which the sample positions are cooled by coiled tubes carrying a stream of very cold nitrogen. The pre-set temperature is maintained by thermocouples which control a switch on the coolant supply.

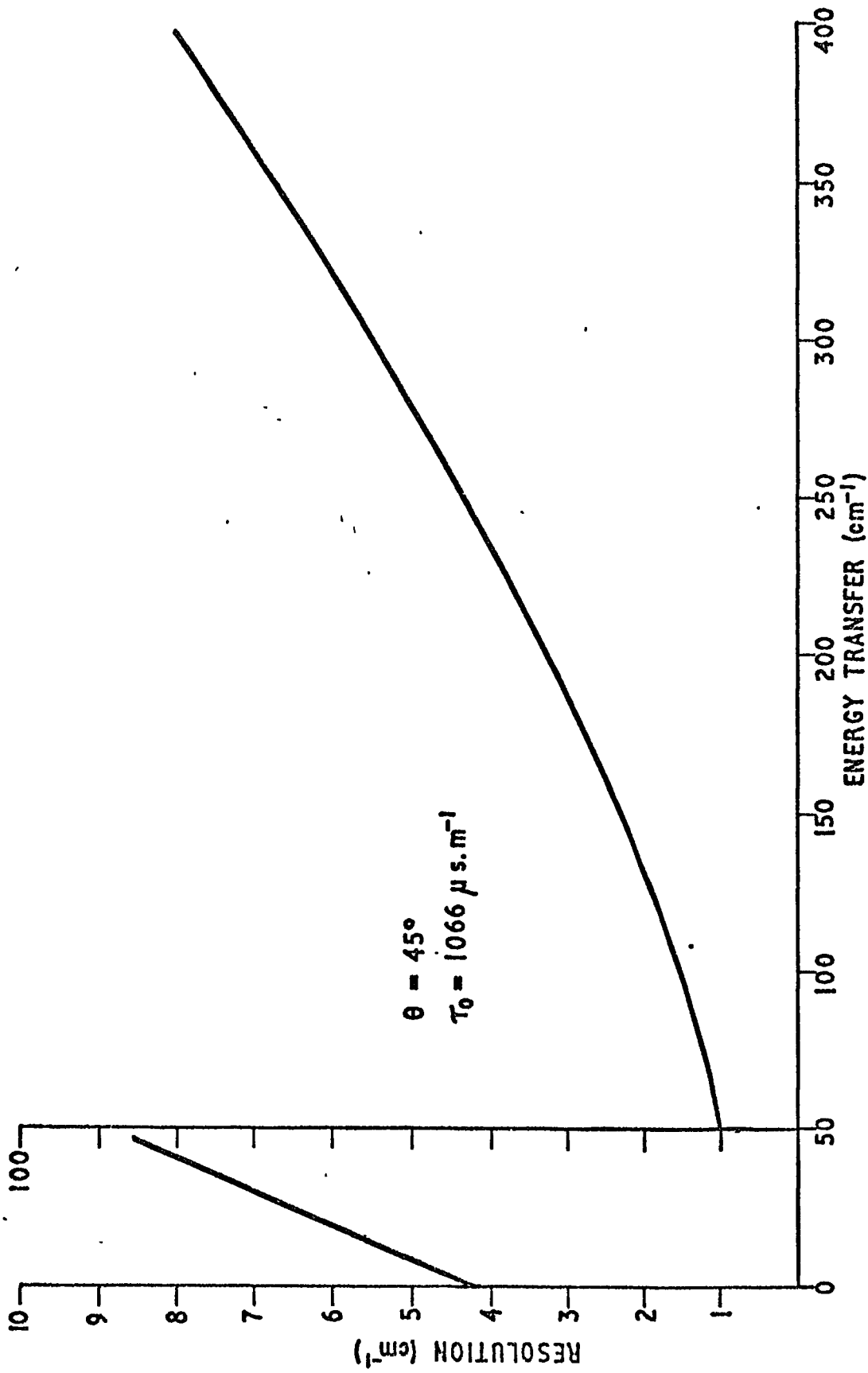
All the counts are accumulated by a small computer, "Cassandra", which also controls the run. When complete the data is read onto magnetic tape and sent for initial processing. This first stage analyses the monitor data and scattering from the Vanadium, and prints out all the raw data in tabular form. This data is then further processed to normalise the scattering from the background blank and the sample against Vanadium. The background is then subtracted to give the 'pure' sample scattering and a correction is made for counter efficiency, which varies with energy. This, which is the effective double differential scattering cross-section, can then be used to calculate the scattering law. The data is processed separately for each angle.

Further calculations can then be done to correct the data at each angle for the Boltzmann factor and then extrapolate the data from several angles to zero momentum transfer. The results which can be presented as a frequency distribution should then enable direct comparison with optical spectra.

All data processing in the present time-of-flight studies was carried out using the IBM 370-195 computer at the S.R.C. Rutherford Laboratory at Harwell, using standard programs (12,13).

The resolution of the time-of-flight machines has been discussed by Harryman (14) and depends principally on three effects;

- a) the rotor monochromation (main problem)
- b) the angle of the sample to the beam
- c) the finite thickness of the detectors.



6H RESOLUTION vs ENERGY TRANSFER: ROTOR DEPENDENCE.

Fig. (2.3) Ref. (14)

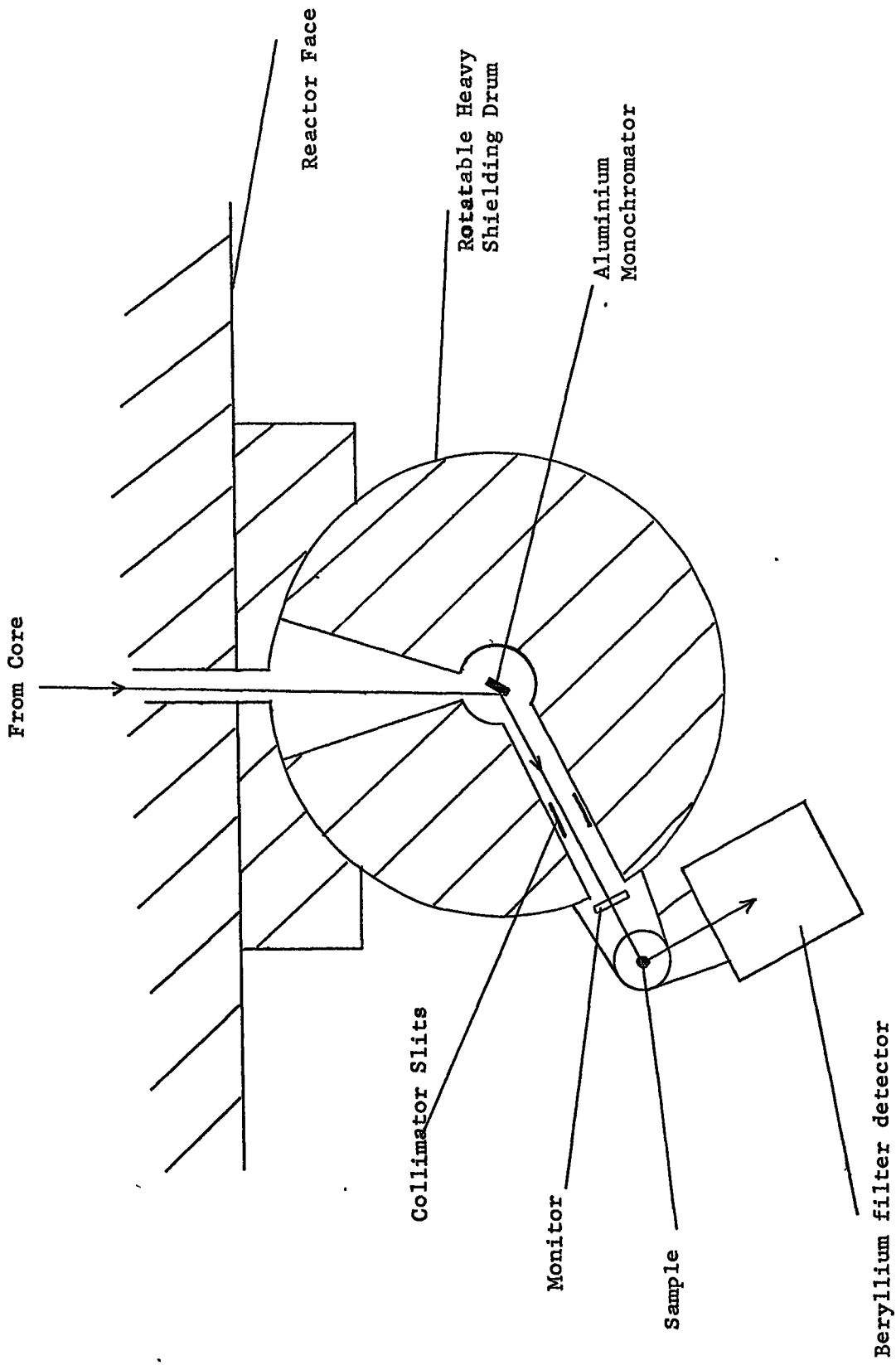
(a) There is a finite energy distribution of neutrons which can pass through the rotor slots and the beam is not perfectly collimated. The effects of wobble in the rotors are also significant to the energy selection. (b) The sample which is normally at  $45^\circ$  to the incident beam (as in all the present experiments) does not present a point scattering source; some neutrons travel further at the incident energy and velocity before encountering the sample. Hence although they may gain as much energy as neutrons which strike the sample nearer the rotor exit, their time of arrival at the detectors is slightly later. (c) The finite thickness of the detectors also creates an uncertainty in the time that the neutron is registered.

All these effects have to be convoluted and the resulting resolution curve is shown in fig. ( 2.3 ). It can be seen that above  $\sim 200 \text{ cm}^{-1}$  resolution becomes increasingly bad. The instrument (and 4H5) is therefore used principally to look at modes in the low frequency region where resolution is quite good in comparison with the beryllium filter machine described next.

#### 2.2b The beryllium filter neutron energy gain spectrometer.

This instrument on the PLUTO reactor is a parasitic part of a much more complicated triple axis spectrometer, making use of its neutron incident energy selection system. (It has proved so successful that a new entirely separate beryllium filter spectrometer has been commissioned). The essential parts of the instrument are shown in fig. ( 2.4 ). A detailed report on the machine has recently appeared (15), but a fairly detailed description will also be given here.

Fig. (2.4) Plan of Beryllium Filter Machine.



The basic principle of the spectrometer is very simple:- Monoenergetic neutrons impinge on the sample and lose energy in inelastic processes to the excitation of molecular modes of lower energy. Some of the total scattered neutrons pass into a liquid nitrogen cooled beryllium filter but only those which have lost sufficient energy so that they have less than  $42 \text{ cm}^{-1}$  are transmitted and detected e.g. neutrons in the incident energy range  $200\text{-}242 \text{ cm}^{-1}$  inelastically scattered by a mode with an excitation of  $200 \text{ cm}^{-1}$  will be detected. The maximum transmission of neutrons within this  $42 \text{ cm}^{-1}$  range depends on several factors discussed shortly, but needless to say a peak of neutrons appears in the spectrum equivalent to the excitation.

A beam of neutrons is taken directly out of the reactor core surrounded by very heavy shielding and impinges on an Aluminium single crystal in the centre of the rotatable shielding drum (see fig. 2.4). The incident neutron energy is then selected by Bragg scattering from one of the crystal planes. Using the first order Bragg equation

$$2d\sin \theta = \lambda$$

$\theta = \text{Bragg angle}$   
 $d = \text{spacing of atomic planes}$   
 $\lambda = \text{wavelength}$

it can be seen that as the angle of incidence is varied (by rotating the aluminium crystal) the wavelength and hence energy of the selected neutrons changes. To permit passage of the reflected beams at different energies the heavy shielding drum, which has a guide tube built in, has also to be rotated. Different planes of the Aluminium



crystal are used to optimise the flux and resolution at particular energies. The useful energy range for some planes is also limited by the physical limits of rotation of the drum. Flux is greatest for the lowest order planes but at the same time their resolution is poorer.

The scanning ranges which until recently have been used are as follows:-

<u>Incident energy scan (<math>\text{cm}^{-1}</math>)</u>	<u>Al plane</u>
80 → 180	111
180 → 700	311
600 → upwards	511

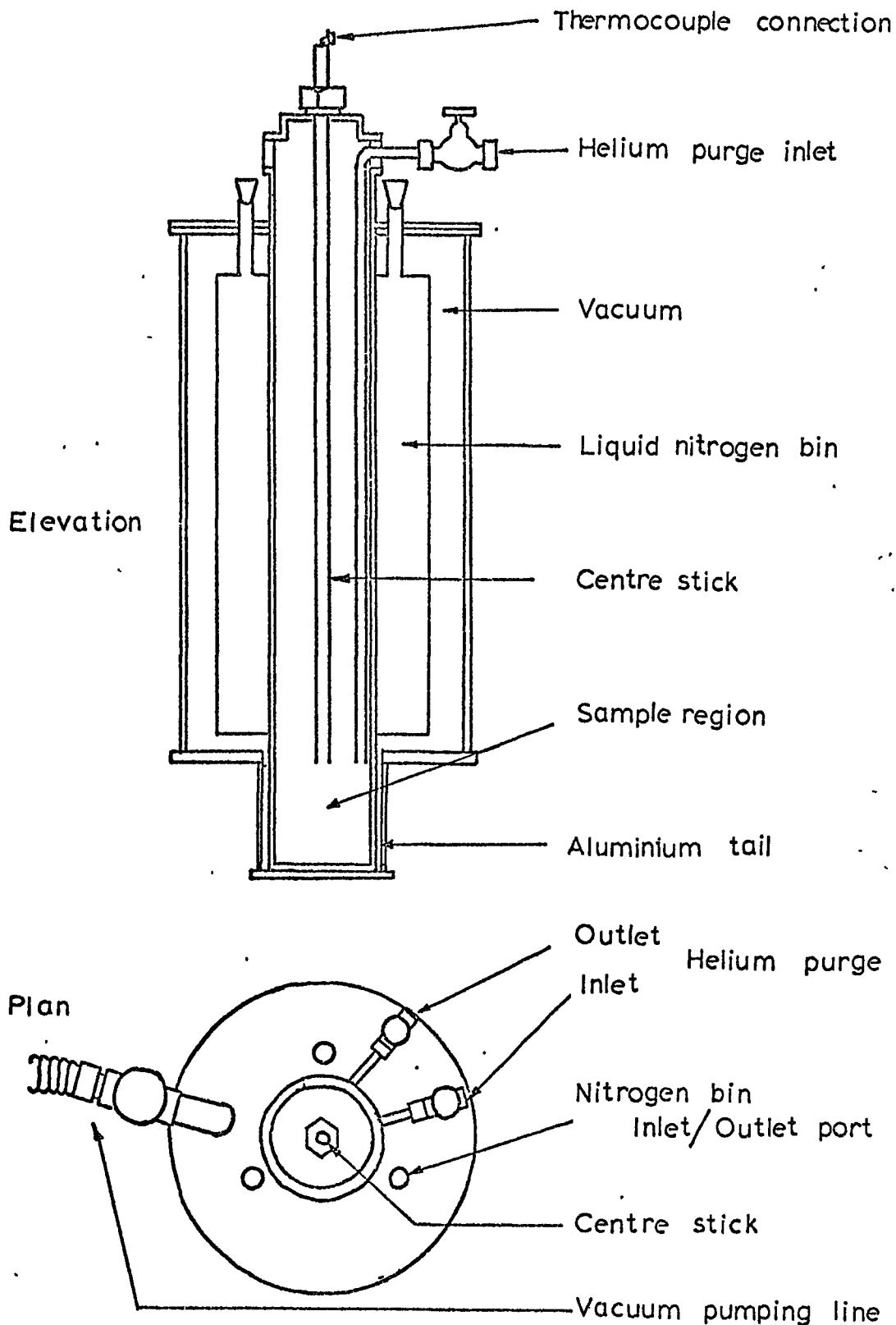
It has recently been determined (15) that the 511 plane gives slightly better resolution than the 311 plane above  $\sim 550 \text{ cm}^{-1}$  (but at the same time flux is reduced considerably, requiring much longer counting times).

As the monochromated beam passes down the guide tube it is collimated by two 6" soller slits. Then since the flux varies with the plane and the energy selected the beam is monitored before reaching the sample. During a scan the collected data at each energy step can be normalised by counting for as long as it takes the monitor to register a fixed pre-set number of counts. The intensity spectrum which this produces is directly proportional to the density of states.

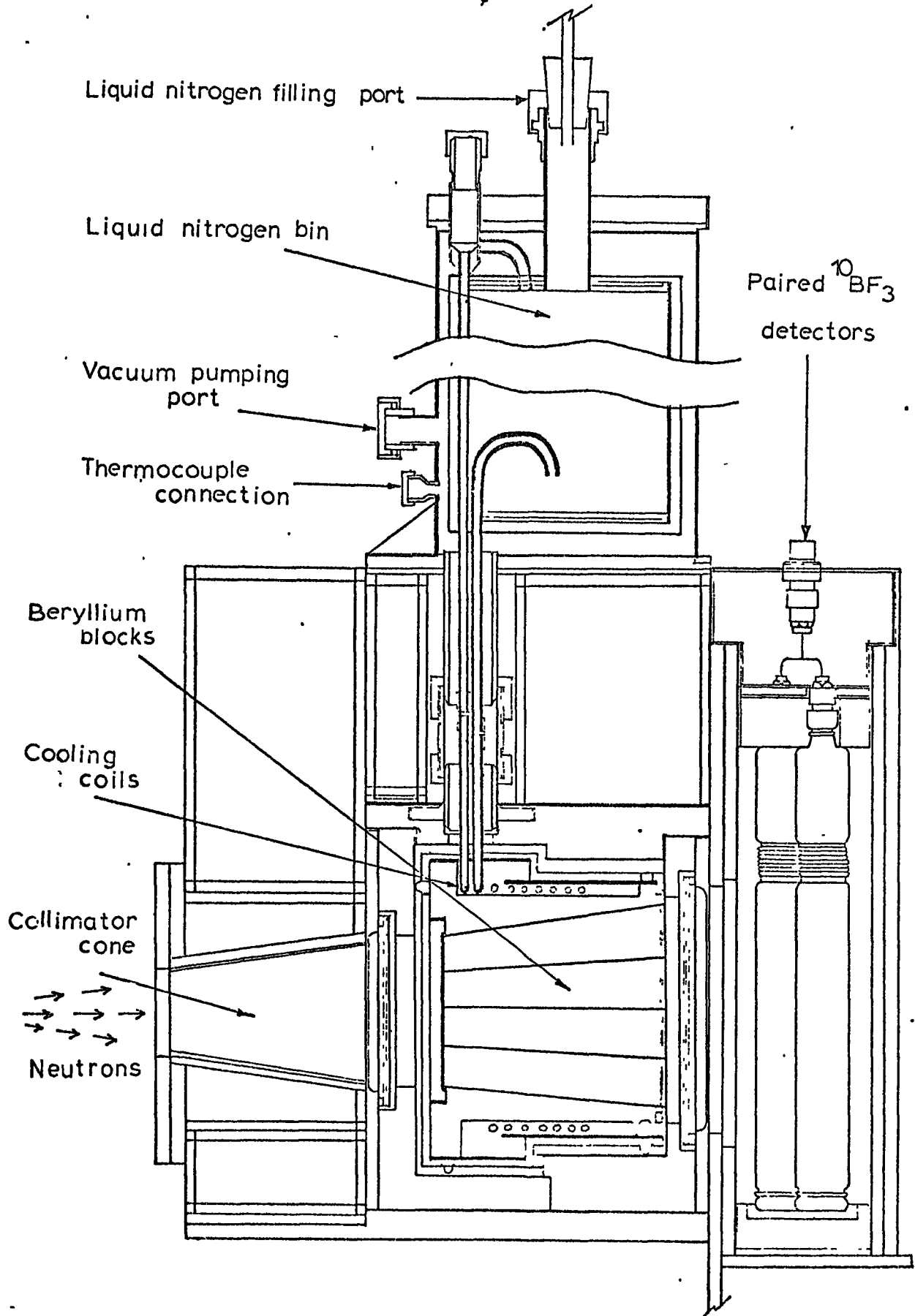
The thin flat sample is held at an angle of  $\sim 45^\circ$  to the incident beam and as in the present experiments is most usually maintained very close to liquid nitrogen temperature in a cryostat, fig. ( 2.5) in a helium atmosphere. This means that most modes will have their

Fig. (2.5) Ref. (15)

### The sample cryostat



### The Beryllium Filter

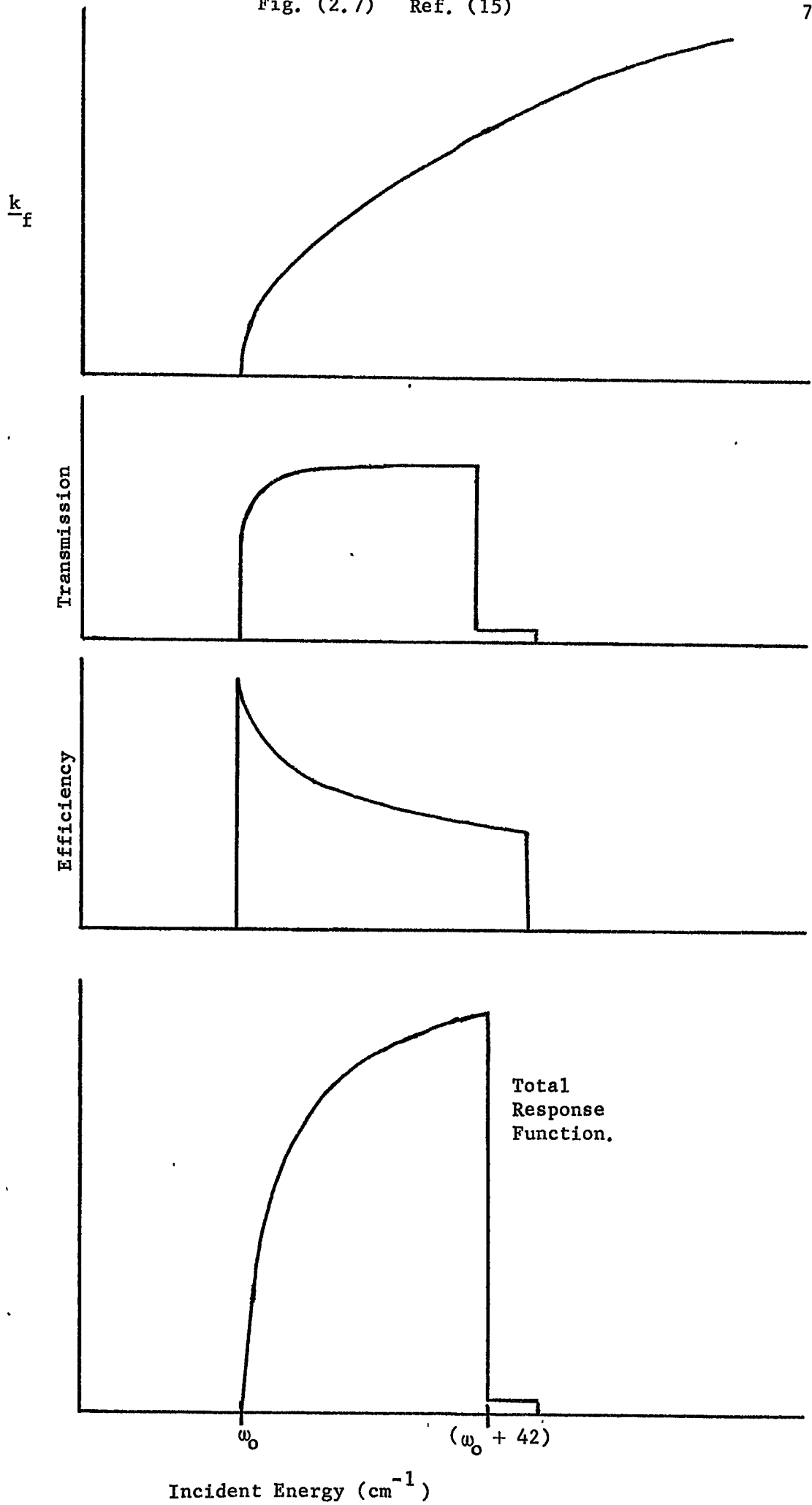


highest population in the ground state, and so the observed transitions are usually  $0 \rightarrow 1$ ,  $0 \rightarrow 2$  etc, a less complicated situation than for room temperature samples. Cooling also helps reduce the Debye-Waller factor; the greater effect of this at room temperature tends to broaden out the spectra.

Neutrons scattered at about  $90^\circ$  to the incident beam pass into the beryllium filter assembly (fig. 2.6 ) which has an acceptance angle of  $17.5^\circ$  which focusses on the sample position. The filter cuts out all neutrons with energy  $> 42 \text{ cm}^{-1}$  and the rest pass on to the detectors. An important feature here is that because the energies accepted are all in the same low range (for all incident energies) the counter efficiency correction is roughly constant. (This contrasts with time-of-flight where the larger range of energies require individual counter corrections).

Control and data collection is by a P.D.P.8 computer via instructions from a Decwriter. The operator selects the aluminium plane to be used and the scan range (this selectivity is very economic of expensive machine time), and also the monitor counts to be obtained at each incident energy step. This energy is usually incremented in  $10 \text{ cm}^{-1}$  steps, although  $5 \text{ cm}^{-1}$  is sometimes useful to clarify shoulders on peaks. When the pre-set monitor counts have been collected the computer prints out all the data collected at that position, changes the configuration of the instrument for the next energy and then proceeds to count.

All the beryllium filter spectra shown in this thesis are presented as the resulting plots of neutron counts vs. incident energy. Much



better counting statistics can be gained using this machine than for the individual angles on the 6H machine, and over a much shorter period of time quite a large energy range can be covered. Typically the strongest peak maximum counts obtained are of the order of 10 → 20 thousand, using pre-set monitor counts of 3 → 5 thousand, although in some cases peaks have been recorded up to 70,000 counts high.

The correction to be subtracted from the incident energy to give the true mode frequency varies according to the incident energy and the Aluminium plane used. The recent report (15) explains this in detail.

If the incident neutrons were totally monochromatic the observed peak maximum position would depend entirely on the response function of the detector system to neutrons in the energy range of the beryllium filter "windows". This depends on three factors:-

- a) the scattered wave vector  $k_f$
- b) the true transmission of the beryllium filter which shows some slight absorption at very low energies. The cut off at  $42 \text{ cm}^{-1}$  stops only 96.5% of the neutrons and the remaining 3.5% are not cut off until  $52 \text{ cm}^{-1}$
- c) the counter efficiencies for different neutron energies.

These functions are all shown in fig. ( 2.7 ) together with the resulting total response function. This indicates that the peak maximum would occur at  $42 \text{ cm}^{-1}$  after the threshold (i.e. for incident energy  $42 \text{ cm}^{-1}$  greater than the mode frequency being observed).

However, in the real system the incident beam is not quite monochromatic, due to a mosaic spread of  $\sim 13'$  caused by the crystallites within the Aluminium crystal and the finite width of the collimator slits which permit an angular divergence of  $\pm 0.6^\circ$  (for 6" slits) in  $2\theta$  ( $\theta$  = Bragg angle).

Consequently this distribution of incident energies has to be convoluted with the response function. In the recent report this energy distribution has been taken as a gaussian function

$$f(E_i) = (2\pi\sigma^2)^{-\frac{1}{2}} \exp(-E_i^2/2\sigma^2)$$

Where  $E_i$  = incident energy and  $\sigma$  is a parameter related to the deviations from  $E_i$  as follows:

The neutron energy determined by the Bragg condition at the crystal can be written as

$$E_i = \frac{h^2}{8md^2} \cdot \frac{1}{\sin^2 \theta}$$

where as usual

- h = Planck's constant
- d = interplanar spacing
- $\theta$  = Bragg angle
- m = neutron mass.

differentiating with respect to  $\theta$  gives

$$dE_i = 2E_i \cot \theta d\theta$$

The error  $dE_i$  can then be calculated using the error  $d\theta$  caused by the angular spread. ( $dE_i$  must vary from plane to plane for the same  $E_i$ )

value since different Bragg angles are required to produce it).

Having found  $dE_i$  this is identified with the full width at half maximum (F.W.H.M.) of the gaussian function where

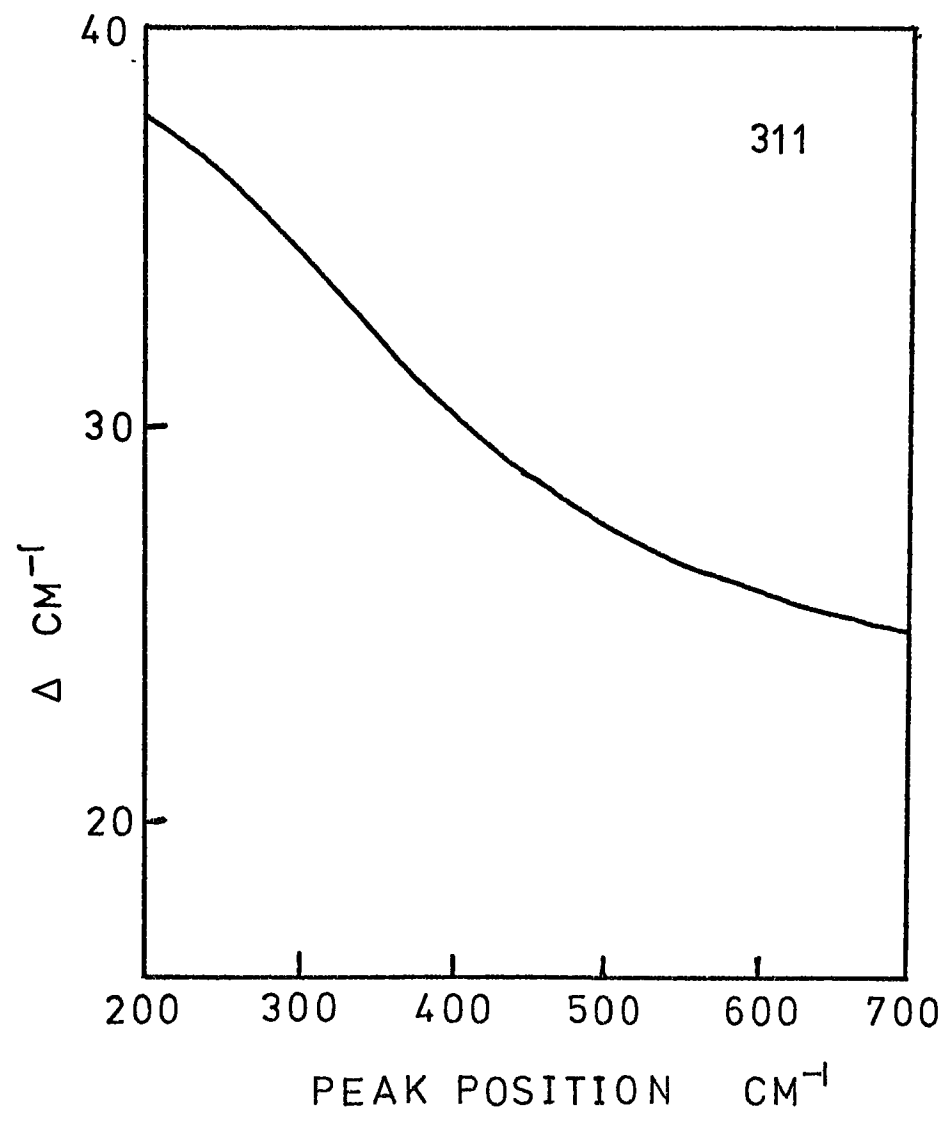
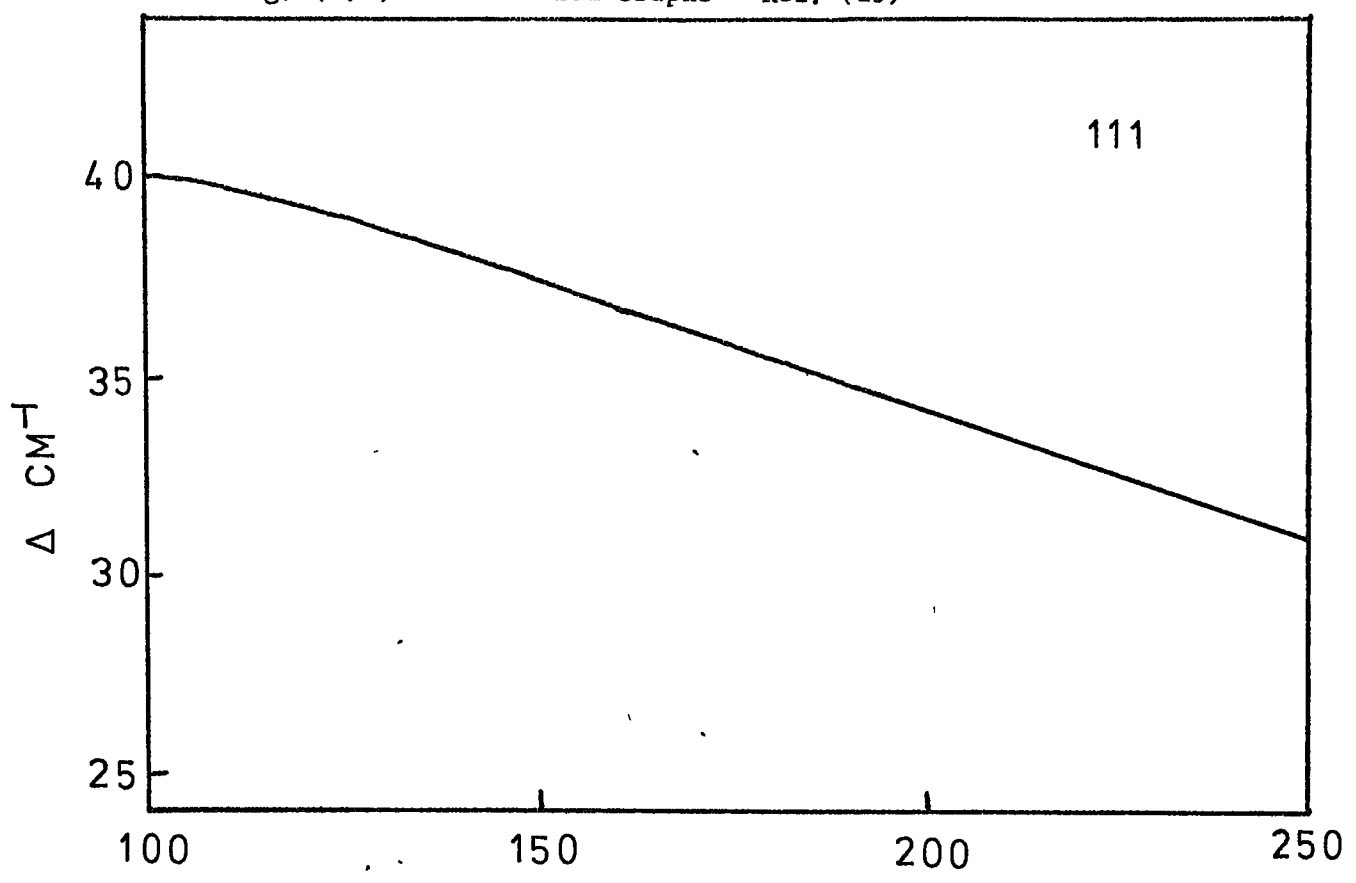
$$\text{F.W.H.M.} = 2.35\sigma$$

This function can be convoluted with the response function to give the peak maximum. It is found that as the spread of the incident energy distribution increases (i.e.  $\sigma$  increases) the convoluted band becomes more symmetric and its maximum moves down from  $42 \text{ cm}^{-1}$  above the threshold value towards an asymptote of  $24.5 \text{ cm}^{-1}$  above the threshold. (The threshold value refers to the true mode frequency i.e. scattered neutron energy of zero).

Graphs of this correction vs. nominal incident energy have been prepared. Fig. ( 2.8) shows these for the 111, and 311 planes, for 6" collimator slits. To obtain the true frequency of the mode the correction is subtracted from the incident energy (in the spectra presented throughout the thesis the true corrected energy of a peak is indicated above it).

Resolution is also determined by the value of  $\sigma$ . A doublet should be clearly distinguished if its separation of peak maxima is greater than the F.W.H.M. value determined by  $\sigma$  at that energy, for the particular Al plane being used. The plane with the lowest  $\sigma$  value at a particular energy should then be used for greatest resolution. In general the F.W.H.M. of a peak observed should not fall below  $\sim 37 \text{ cm}^{-1}$  and for the maximum energies used on the 311 plane in this thesis (for which the  $\sigma$  value is largest) the F.W.H.M. should not exceed  $\sim 44 \text{ cm}^{-1}$ . Consequently the machine has an advantage over the time of flight instruments above  $\sim 200 \text{ cm}^{-1}$ , but it is restricted at present to





collecting data at  $\sim 90^\circ$  to the incident beam. (It should perhaps be mentioned that a  $90^\circ$  counting angle also helps to reduce background noise, which is a bigger problem in this instrument than in 6H or 4H5).

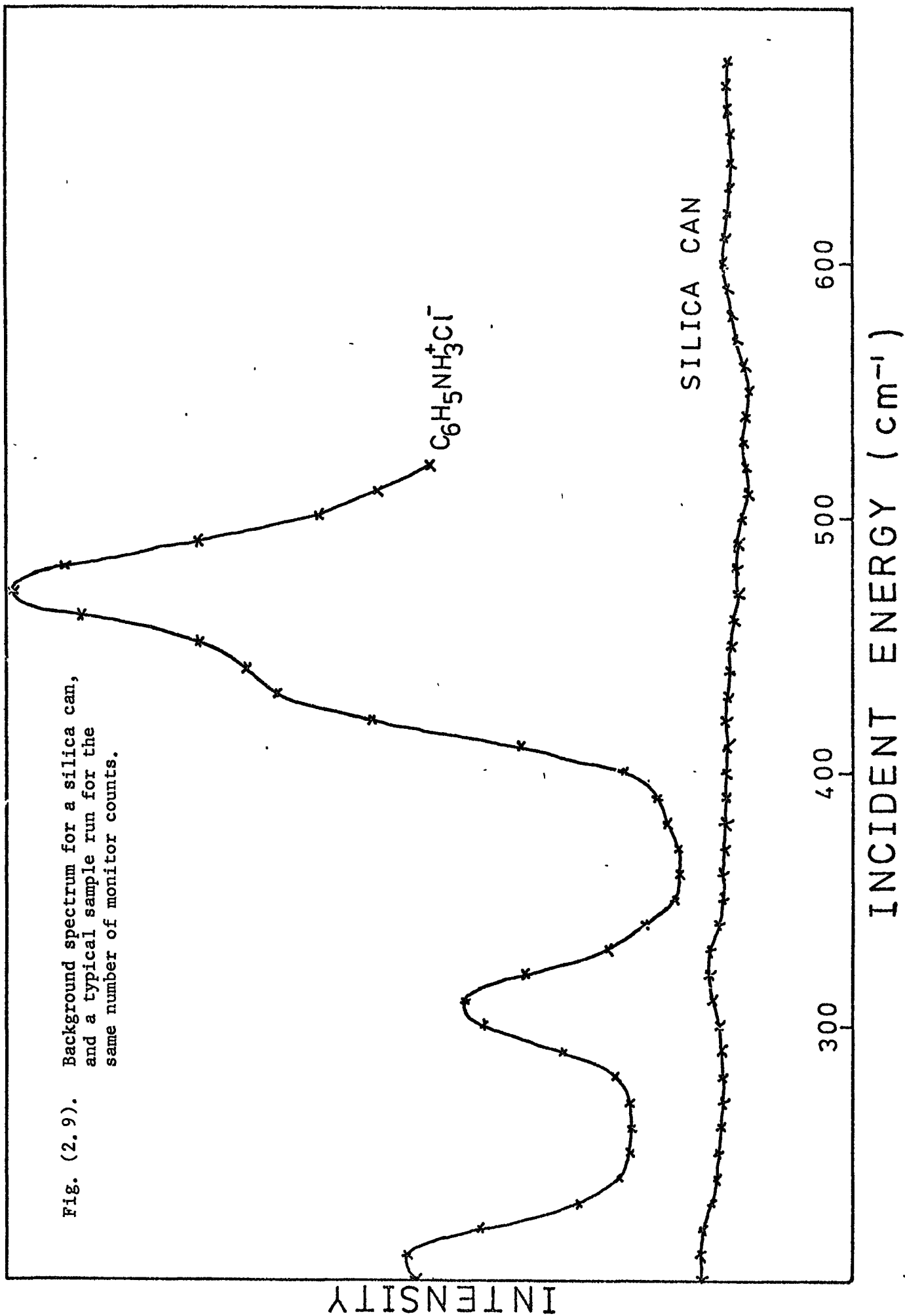
### 2.3 Sample containment for I.N.S. spectroscopy.

Since the scattering from hydrogenous materials is predominantly incoherent (incoherent cross section for hydrogen being an order of magnitude greater than for any other element) polycrystalline samples are used in experiments. Room temperature liquid samples frozen down and run as solids on the beryllium filter machine did not show any large crystal growth when taken out of the cryostat (probably since they froze down very quickly) and so possibilities of coherent scattering from other elements was regarded as very small.

In order to use as many neutrons as possible it is desirable to cover the whole area of the beam with sample. In order to minimise double scattering events the sample should be as thin as possible, but at the same time this has to be weighed against the amount of hydrogen in the sample and the amount of time and neutrons which it is desirable to spend in collecting the data. For the time-of-flight machines the optimum situation is usually taken as a sample thickness which will produce about 10% total scatter (the other 90% passing straight through). This clearly depends to some extent on the density of the sample, and for most of the samples used in the present work the required thickness was between 0.3 and 0.5 mm., and for the more hydrogenous materials such as  $(\text{CH}_3)_4\text{C}$  even less. Because of difficulties in producing sample containers with this spacing some toleration of thickness variation was necessary.

The simplest form of container is an aluminium foil sachet. This can be used generally for air stable solids which will not attack aluminium. An amount of powdered sample is placed in the simple sachet of .002" aluminium foil and rolled out into a thin layer between the sheets. The open end is then sealed off. Although this sounds rather crude it is surprisingly effective in producing a thin, fairly even sheet of sample. Initially it is a matter of trial and error judging the thickness to give 10% scatter. Slightly hygroscopic salts can also be packed in this manner provided the sachet is packed and sealed in a dry box and the foil does not puncture. This also has the advantage that the background scatter from the container is almost zero.

For air sensitive and very hygroscopic substances samples are held in thin silica "cans". For the present experiments these were kindly prepared by the glass blowers at Durham. (Silica was used since normal glassware contains an appreciable amount of neutron absorbing elements, principally  $^{10}\text{B}$ ). These consist of two circular plates of 0.5mm thick silica separated by 0.3 to 0.5 mm. sealed around the edges, except for an entry tube which is attached. Powdered samples are rather laboriously tapped into the space and the can sealed with a ground glass stopper and picene wax; all operations being performed in a dry nitrogen atmosphere. Samples to be used in the 6H evacuated sample chamber require a special brass stopper with a pressure release screw (otherwise the cans burst under the vacuum).



Liquids must be held in silica cans of more solid design, otherwise volume changes on freezing can cause the cans to crack. Slightly thicker silica plates are used and dimpled at spots on the face so that the walls touch providing greater strength. A much smaller entry tube can be used, and then, after freezing down the liquid and evacuating the can on a vacuum line, this tube can be neatly melted and sealed off.

A few compounds which are gases at room temperature were studied as the solid in the present work. This required that the gases be liquified and sealed in strong silica containers. These operations are described later (Chapter 6).

A typical beryllium filter background spectrum for a silica can is shown in fig. ( 2.9 ) below a typical spectrum, both run on the same monitor count limit. As can be seen its effect on the spectrum is almost negligible and consequently all the beryllium filter spectra presented in the thesis have not been corrected. (Since the time-of-flight machines are used to calculate absolute scattering cross sections the blank spectrum must be subtracted.)

#### 2.4 Artificial Curve Resolution of beryllium filter spectra.

In interpreting the neutron spectra of these compounds considerable insight was gained with the use of a Du Pont 310 Curve Resolver, more often used on ESCA spectra. Lorentzian or Gaussian shaped functions similar to I.N.S. peaks are generated as a visual display which is superimposed on the spectrum to be analysed. Their size, width and position can be varied according to the controller and when

superimposed the functions add together to produce different shaped curves. Unless various conditions are imposed by the user many possible peak combinations could give the same shape of spectrum.

As has been seen, in the case of beryllium filter spectra the bandwidth for a single mode, full width at half maximum should usually be of the order of  $\sim 40 \text{ cm}^{-1}$ , so this condition was generally imposed on the generated functions. Rough criteria for expected peak intensities and numbers in each case also helped to reduce possibilities. It should be pointed out that in all the cases the general flat background level of the spectrum, where this could be seen, was taken as the base level for the curve resolver.

Quite clearly this method of approximate separations can be quite useful but the process is not infallible, and although in most cases quite close fits with sensible peak separations were obtained, results obtained by this method should be treated with some reservation .

References - Chapter 2.

1. D.A. Symon, Ph.D. Thesis, Durham (1972).
2. W. Marshall, S.W. Lovesey "Theory of Thermal Neutron Scattering"  
Clarendon, Oxford (1971).
3. P.A. Egelstaff, "Thermal Neutron Scattering", Academic Press,  
London and N.Y. (1965).
4. V.F. Turchin, "Slow Neutrons" Israel Program for Scientific  
Translations Jerusalem (1965).
5. P.A. Egelstaff, Proc. I.A.E.A. Symp. Vienna p.25 (1961).
6. C.G. Windsor, Chapter 1 of "Chemical Applications of Thermal  
Neutron Scattering" A.E.R.E. Harwell Series Edited by  
B.T.M. Willis, Oxford (1973).
7. J.W. White *ibid*, Chapter 3.
8. H. Boutin, S.Yip "Molecular Spectroscopy with Neutrons" M.I.T.  
Press (1968).
9. S.F. Trevino, Applied Spectroscopy 22, 659 (1968).
10. L.J. Bunce, D.H.C. Harris, G.C. Stirling, Harwell Report R6246  
H.M.S.O. (1970).
11. D.H.C. Harris, S.J. Cocking, P.A. Egelstaff, F.J. Webb Proc. Symp.  
I.A.E.A. Vienna p.107 (1963).
12. A.H. Baston "Collection and Processing of Data from Three Time of  
Flight Neutron Spectrometers" Harwell Report M2570  
H.M.S.O. (1972).
13. R.E. Ghosh, "Computer Programs for Analysis of Neutron Time of  
Flight Data" Unpublished Harwell Report (1971).

14. M.B.M. Harryman, J.B. Hayter, Unpublished Harwell Report (1972).
15. P.H. Gamlen, N.F. Hall, A.D. Taylor, Unpublished Harwell Report (1974).
16. E. Fermi, *Ricerca Scientifica* 1 13 (1936).
17. G. Allen, J.S. Higgins, *Rep. Prog. Phys.* 36, 1073 (1973).
18. G.F. Longster, J.W. White, *Molec. Phys.* 17, 1 (1969).



## CHAPTER 3

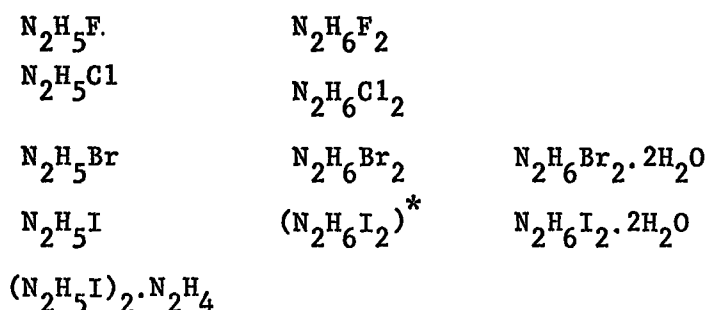
THE HYDRAZINIUM  $N_2H_6^{+2}$  SALTSIntroduction.

From the point of view of simplicity of interpretation of the torsional mode frequencies the hydrazinium dihalide salts  $N_2H_6^{+2} 2F^-$ ,  $2Cl^-$ ,  $2Br^-$  present an excellent case for study as mentioned in Chapter 1. Because of the symmetrical nature of the ion, which is isoelectronic with ethane, and of the external fields, observation of the two mode frequencies should permit direct calculation of both the internal and external barriers. Clearly the external barriers will give some information about the extent of the hydrogen-bonding in these systems.

X-ray and neutron diffraction structural data on  $N_2H_6SO_4$  (1), although indicating  $N_2H_6^{2+}$  ions, showed a degree of inequality in the two ends of the ion, with different H-bonding possibilities. This was therefore also studied to show the immediate effects of assymetry on the modes.

Section 1. Previous Studies.

A whole range of salts are formed between hydrazine and the halogeno acids. Milojević and Slivnik (2) give a summary and standard methods of preparation.



\* unstable ?

Opalovskii and Nazarov (3) studied the system  $\text{H}_2\text{O}/\text{N}_2\text{H}_6\text{F}_2/\text{HF}$  at  $0^\circ\text{C}$  and obtained three different species under different HF concentrations:

$\text{N}_2\text{H}_6\text{F}_2 \cdot \text{H}_2\text{O}$	0 - 5.42% HF
$\text{N}_2\text{H}_6\text{F}_2$	7.02 - 73.05%
$\text{N}_2\text{H}_6\text{F}_2 \cdot 2\text{HF}$	73.05 - 100%

The hydrated species showed additional I.R. bands due to water at 3460,  $1640\text{ cm}^{-1}$ , and the hydrofluorinated species bands at 1020,  $740\text{ cm}^{-1}$ .

### Spectra

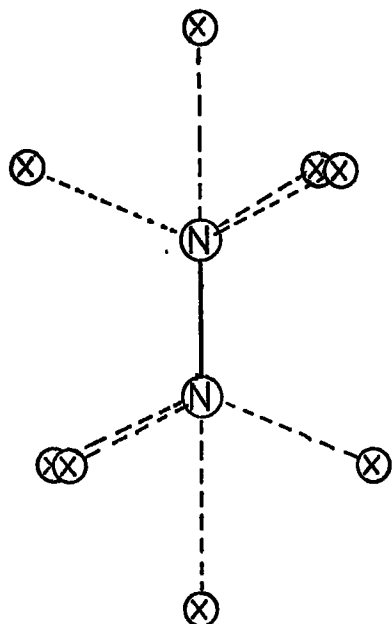
Edsall and coworkers (4,5) first studied the Raman spectra of  $\text{N}_2\text{H}_6\text{Cl}_2$  in solution and  $\text{N}_2\text{D}_6\text{Cl}_2$  in  $\text{D}_2\text{O}$  and made some assignments of fundamental modes. Further Raman studies on the solid chloride have been produced by Ananthakrishnan (6), and later by Couture and Mathieu (7) who made a number of assignments in terms of the crystal symmetry and attempted to calculate force constants for the lattice modes. This was followed by I.R. work by Snyder and Decius (8) who obtained spectra at liquid nitrogen temperatures of the fluoride as a thin film, and the chloride as nujol and perfluorokerosene mulls, over the range  $400\text{-}3500\text{ cm}^{-1}$ . This included work on the per deuterio salts. A broad band which they observed at  $455\text{ cm}^{-1}$  for the chloride at room temperature was assigned as the internal torsional mode. An I.R. study of the  $\text{SO}_4^{-2}$  salt (9) revealed a weak band at  $512\text{ cm}^{-1}$ , again assigned as a torsional mode.

Although most of the fundamentals have been assigned, some of these must be regarded with reservation especially in the high frequency region around the expected frequency of the N-H stretch where a very strong and broad absorption feature is seen with bands protruding through it. This feature which extends to well below the normal N-H stretching frequencies is characteristic of a strongly H-banded system (17 (p 85), 27).

A recent normal coordinate analysis of  $N_2H_4$ ,  $N_2H_5^+$ , and  $N_2H_6^{+2}$  (10) indicated from the potential energy distribution that there was practically no vibrational coupling of fundamental modes for  $N_2H_6^{+2}$ .

#### Structural Information.

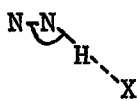
The crystal structures of  $N_2H_6F_2$  (11) and  $N_2H_6Cl_2$  (12) have been reported; the relevant data is summarised in table (4.1) below. An important feature with respect to the discussion later is that although they are not isostructural, the near environment of the  $N_2H_6^{+2}$  group is identical in both as indicated in figure (3.1).

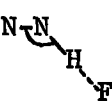


Assuming the hydrogens lie in the general direction of N----X a staggered configuration is implied, which would be expected as the most stable.

Table (3.1)

Structural Information

	$N_2H_6F_2$ (11)	$N_2H_6Cl_2$ (12)
Space	$D_{3d}^5 - R\bar{3}m$ (166)	$T_h^6 - Pa3$ (205)
Group	(hexagonal)	(cubic)
Z	3	4
Cell Parameters	$a_o = 4.43 \pm 0.01 \text{ \AA}$ $c_o = 14.37 \pm 0.02 \text{ \AA}$	$a_o = 7.87 \pm 0.01 \text{ \AA}$
N-N	$1.42 \pm 0.02 \text{ \AA}$	$1.42 \pm 0.04 \text{ \AA}$
N-H---X	$2.62 \pm 0.02 \text{ \AA}$	$3.10 \pm 0.02 \text{ \AA}$
N---X'	$2.78 \pm 0.02 \text{ \AA}$	$3.10 \pm 0.04 \text{ \AA}$
	$103^\circ$	$100 \pm 2^\circ$

The N---F' and  parameters were first reported as  $2.8 \text{ \AA}$  and  $110^\circ$  but Harker revised this in a private communication to Deeley and Richards (13). These two workers carried out N.M.R. studies of the fluoride and using second moments data calculated an N-H bond length of  $1.075 \text{ \AA}$ , however Ibers and Stevenson (14) later cast doubt on the validity of certain aspects of their calculations and recalculated the distance as  $1.05 \pm 0.03 \text{ \AA}$ . The main points to note from this structural data are

- a) The  $N_2H_6^{+2}$  ions and their immediate neighbourhood are  $D_{3d}$  symmetric.

b) The N-H---X distances are short indicating H-bonds.

N-H---F	2.62 $\overset{\circ}{\text{Å}}$	cf. (15) $\text{NH}_4\text{HF}_2$	2.76 $\overset{\circ}{\text{Å}}$
		$\text{NH}_4\text{F}$	2.68 $\overset{\circ}{\text{Å}}$
N-H---Cl	3.10 $\overset{\circ}{\text{Å}}$	cf. (16) $\text{NH}_4\text{Cl}$	3.26 $\overset{\circ}{\text{Å}}$ (NaCl type)
			3.35 $\overset{\circ}{\text{Å}}$ (CsCl type).

The structural study of  $\text{N}_2\text{H}_6\text{SO}_4$  was mentioned earlier (1) and relevant data is given below:

Space Group  $P2_12_12_1$        $Z = 4$

N-N = 1.426 $\overset{\circ}{\text{Å}}$  (neutron)

1.418 $\overset{\circ}{\text{Å}}$  (x-ray)

Table 3.2

Neutron Data	$\text{N}-\text{N}-\text{H}$	N-H $\overset{\circ}{\text{Å}}$
$\text{N}_1-\text{H}_1$	107.5 $^\circ$	1.036
$\text{N}_1-\text{H}_2$	107.8 $^\circ$	1.059
$\text{N}_1-\text{H}_3$	109.3 $^\circ$	1.039
$\text{N}_2-\text{H}_4$	110.0 $^\circ$	0.989
$\text{N}_2-\text{H}_5$	108.4 $^\circ$	0.989
$\text{N}_2-\text{H}_6$	109.5 $^\circ$	0.952

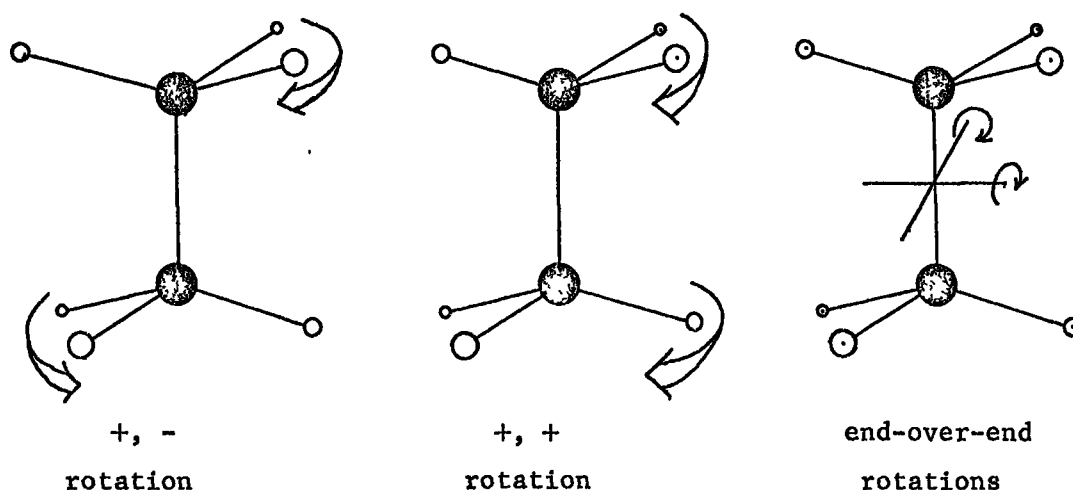
H---O contacts range between 2.627 - 1.646 $\overset{\circ}{\text{Å}}$ . Distances below  $\sim 2.4\overset{\circ}{\text{Å}}$  may be regarded as H-bonding according to the Hamilton-Ibers criterion (17). From the N-H bond lengths alone it is quite clear that one end is considerably different from the other. At the N(1)

end of the ion the H's are each associated with one O---H bond, whereas at the N(2) end one H associates with 3 O's and 2H's with 2O's each. The anisotropic thermal parameters for the hydrogens at each end are also very different. A large amplitude of vibration for the  $-N(2)H_3$  group around the N-N axis is indicated.

Marino and Oja (18) obtained nitrogen N.Q.R. data on the four salts with which we are concerned.  $N_2H_6F_2$  and  $N_2D_6Cl_2$  (they were unable to find any signal from  $N_2H_6Cl_2$ ) both gave field gradient asymmetry parameters  $\eta$  of zero as expected, the bromide gave  $\eta = 0.05585$  and the sulphate somewhat larger values. The main point of interest was that the sulphate gave two sets of signals again indicating nitrogens in two different environments.

N.M.R. spin lattice relaxation studies on the sulphate (19) indicated that reorientation of both  $-NH_3^+$  groups takes place with roughly similar correlation times, and an average activation energy of  $0.27 \text{ eV} \cong 2178 \text{ cm}^{-1}$ .

It would be useful to indicate visually here the four modes which are of most interest in the current work. Fig. (3.2).

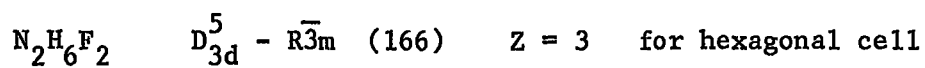


All become oscillations in the lattice.

Section 2. Factor Groups.

Snyder and Decius (8) carried out factor group analysis of the internal modes of the fluoride and chloride (a trivial matter for the fluoride) and Couture and Mathieu (7) also involved the lattice modes for the chloride.

Using the tables of Adams and Newton (20) the analysis for the lattice mode region is as follows:-



Primitive cell is rhombohedral  $Z = 1$

For  $D_{3d}$  point group the internal torsion is  $A_{1u}$  and the coaxial external rotation is  $A_{2g}$ , both I.R. and Raman inactive.

Assuming the centre of the N-N bond is an (a) site\*  
and the F's are on (c) sites\*

\* standard Wyckoff notation (21)

we have

$$T_o + T_A = A_{1g} + E_g + 2A_{2u} + 2E_u$$

$$T_A = A_{2u} + E_u$$

$$\therefore T_o = A_{1g} + E_g + A_{2u} + E_u$$

$$R = A_{2g} + E_g$$

where  $T_o =$  translational optic

$T_A =$  " acoustic

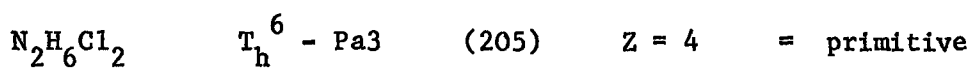
$R =$  rotor

I.R active modes are  $A_{2u}, E_u$

Raman active modes are  $A_{1g}, E_g$

for  $D_{3d}$

Hence we should see two I.R.  $T_o$  modes and two Raman  $T_o$  modes. Two of the whole body librations are degenerate and should be Raman active  $E_g$ . The  $C_3$  axis motions are both inactive but a combination band  $A_{1u} + A_{2g} \rightarrow A_{2u}$  would be I.R. active.



4 units per cell increases the number of possible modes from 12 (9 T's 3R's) to 48 (36 T's to 12R's) though some of these will be degenerate.

$$\begin{aligned} T_o + T_A &= A_g + E_g + 3F_g + 2A_u + 2E_u + 6F_u \\ T_A &= F_u \\ \therefore T_o &= A_g + E_g + 3F_g + 2A_u + 2E_u + 5F_u \\ R &= A_g + E_g + 3F_g \end{aligned}$$

I.R active mode is  $F_u$  for  $T_h$

Raman active modes  $A_g, E_g, F_g$

For comparison with the fluoride  $D_{3d}$

Rotations	$\frac{F}{A_{2g}}$	→	$\frac{Cl}{A_g + F_g}$
	$E_g$	→	$E_g + 2F_g$
Translations	$A_{1g}$	→	$A_g + F_g$
	$E_g$	→	$E_g + 2F_g$
	$2A_{2u}$	→	$2A_u + 2F_u$
	$2E_u$	→	$2E_u + 4F_u$

Also note that the torsion  $A_{1u}$  for  $D_{3d} \rightarrow A_u + F_u$  for  $T_h$ .



Hence five  $T_0$  modes may be seen in the I.R., five  $T_0$  in the Raman and the whole body librations may show three bands in the Raman. The interesting point is that the  $C_3$  external rotor mode should be Raman active and the torsion I.R. active.

Another point one should note is that for both fluoride and chloride no bands are both I.R. and Raman active.

### Section 3. Experimental.

The chloride and bromide were obtained commercially (B.D.H.Ltd) and purified by recrystallisation from dilute HCl, HBr respectively and dried on a vacuum line. The bromide crystallises as clear crystals of the dihydrate but vacuum drying, as shown by their spectra completely removes the water. A sample of the anhydrous product milled in air rapidly reverts to the hydrate as evidenced by the spectrum. The sulphate (a standard reagent) was also obtained commercially.

The fluoride was prepared by addition of hydrazine solution to HF solution in the correct molar ratios, and was recrystallised from water and vacuum dried. The I.R. spectrum was checked against that of Snyder and Decius (8) and the peaks observed in the

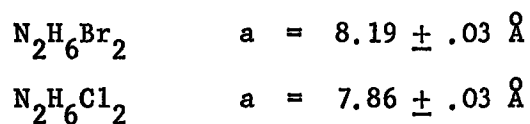
monohydrate and dihydrofluoridate (3) were not present. A discrepancy was noted in the literature over its air stability. The X-ray work (11) quotes air stable single crystals whereas two other references (8,13) say their fluoride was quite hygroscopic. The sample obtained did not appear to be so, and did not gain weight on exposure to the air. However the Raman spectrum showed two unexpected weak peaks at very low frequency one of which reduced in intensity after leaving the sample exposed to the air for several hours. I.R. and I.N.S. spectra of vacuum dried and air exposed samples showed no change. It was also noticed that the sample slightly etched glass containers, especially when open to the air, which might indicate presence of excess HF, or perhaps some dissociation. The I.R. spectra of  $N_2H_5F$  has been reported (22) so a search for traces of this in the spectrum of  $N_2H_6F_2$  was undertaken. However only one possibility was seen at  $970\text{ cm}^{-1}$ , a weak broad peak, which would correspond to the  $N_2H_5F$  N-N stretch at  $968\text{ cm}^{-1}$ , and the other strong peaks were absent.

An analysis for fluorine corrected for blank gave 48.8% (52.8% theoretical) uncorrected gave 52.4%, indicating there may be something slightly amiss. If some dissociation does occur and the HF is lost this would reduce the analysis (theoretical for  $N_2H_5F = 36.5\%$ ).

Section 4. X-ray powder data.

Observing a very close similarity of the spectra of the chloride and bromide it appeared likely that the two were isostructural. X-ray powder photographs of these salts were therefore obtained for comparison, together with those of the fluoride and hydrated bromide. A standard powder photograph camera was used with Cu radiation. The samples were finely powdered in a dry box and sealed in quartz capillary tubes. An additional sample of fluoride was loaded in air.

The pattern and intensities of lines observed on the photos of the anhydrous bromide and chloride were found to be almost identical, except that the bromide lines started at smaller angles, which would be consistent with a larger cell. Both photos were assigned on the basis of a cubic lattice with cell parameters:-



The  $1/d^2$  values for all the lines observed for the bromide are listed in table (3.3) together with several chloride values to show their identical nature. The chloride cell parameter compares very favourably with the single crystal value of  $a = 7.87 \pm 0.01 \text{ \AA}$  (12)

The hydrated bromide gives a completely different photo;  $1/d^2$  values are given in table (3.3). The picture is much more complicated and no simple analysis would fit. The two fluoride samples both showed a strong series of lines which readily analysed using the previous hexagonal parameters (11). However, the air

Table (3.3)

X-ray powder data: calculated  $1/d^2$  values ( $\text{\AA}^{-2}$ )

$(h^2+k^2+l^2)$	$1/d^2$		$(h^2+k^2+l^2)$	$1/d^2$	$1/d^2$
	$\text{N}_2\text{H}_6\text{Br}_2$	$\text{N}_2\text{H}_6\text{Cl}$			
3	0.0445	0.0483	53	0.7906	0.0275
4	0.0594	0.0640	54	0.8038	0.0473
5	0.0741	0.0809	56	0.8346	0.0652
6	0.0894	0.0971	57	0.8493	0.0778
8	0.1191	0.1299	59	0.8779	0.0871
9	0.1342	0.1452	61	0.9086	0.0993
11	0.1650	0.1784	62	0.9232	0.1096
12	0.1786	0.1943	65	0.9676	0.1290
13	0.1935	0.2106	66	0.9821	0.1465
14	0.2085	0.2274	69	1.0282	0.1654
16	0.2386	0.2594	70	1.0425	0.1702
17	0.2534	0.2755	73	1.0863	0.1853
20	0.2979	0.3241	74	1.1010	0.1960
21	0.3132	0.3405	77	1.1473	0.2010
22	0.3285	0.3572	81	1.2064	0.2075
24	0.3583	0.3893	86	1.2805	0.2229
25	0.3738		89	1.3247	0.2489
26	0.3876	0.4215	90	1.3399	0.2586
29	0.4329	0.4708	93	1.3845	0.2692
30	0.4478		94	1.3992	0.2823
32	0.4779		98	1.4574	0.2883
33	0.4919			1.4579	0.3788
36	0.5375		99	1.4723	0.3874
37	0.5519			1.4723	0.3995
38	0.5668		101	1.5014	0.4086
40	0.5971			1.5019	0.4315
41	0.6112		105	1.5611	0.4430
42	0.6254			1.5610	0.4770
44	0.6563		109	1.6206	0.4870
45	0.6710			1.6207	0.4943
46	0.6858		110	1.6349	0.5281
48	0.7147			1.6351	0.6095
49	0.7307				
50	0.7453				
52	0.7774				

exposed sample showed several other moderately strong but diffuse lines, which were also found as very faint traces on close examination of the dry sealed sample photo. This phenomenon may well have been due to etching of the quartz by HF aided by the presence of moisture, discussed earlier.

Returning to the data for the chloride and bromide a favourable comparison is obtained between the cell volumes of these and the ammonium salts in their CsCl type phases

$$\frac{N_2H_6Br_2}{N_2H_6Cl_2} = 1.13 \quad \frac{NH_4Br^*}{NH_4Cl^*} = 1.15 \quad \begin{array}{l} * \text{ data from} \\ \text{Wyckoff (16)} \end{array}$$

Further assuming for the moment that the two hydrazinium salts are isostructural and calculating the lengths of the unit cell diagonals along which the atoms lie (as shown for the chloride below) the following values are obtained:-

$$\begin{aligned} (Cl) &= 13.631 \text{ \AA} \\ (Br) &= 14.185 \text{ \AA} \\ \Delta(Br-Cl) &= 0.554 \text{ \AA} \end{aligned}$$

If the increased length is due entirely to the greater size of the bromides then the radius increase computes as  $0.554/4 = 0.139 \text{ \AA}$ . Comparison with ionic radii as given by Cotton and Wilkinson (23)

again shows a close correlation:-

	<u>Goldschmidt</u>	<u>Pauling</u>	<u>Radii</u>
$\text{Cl}^-$	1.81	1.81	in
$\text{Br}^-$	<u>1.96</u>	<u>1.95</u>	$\text{\AA}$
$\Delta$	<u>0.15</u>	<u>0.14</u>	

In view of all this evidence it would seem reasonable to assume that the bromide and chloride are isostructural. It would be useful to obtain further data in order to find the N-H---Br distance involved in the hydrogen bonds.

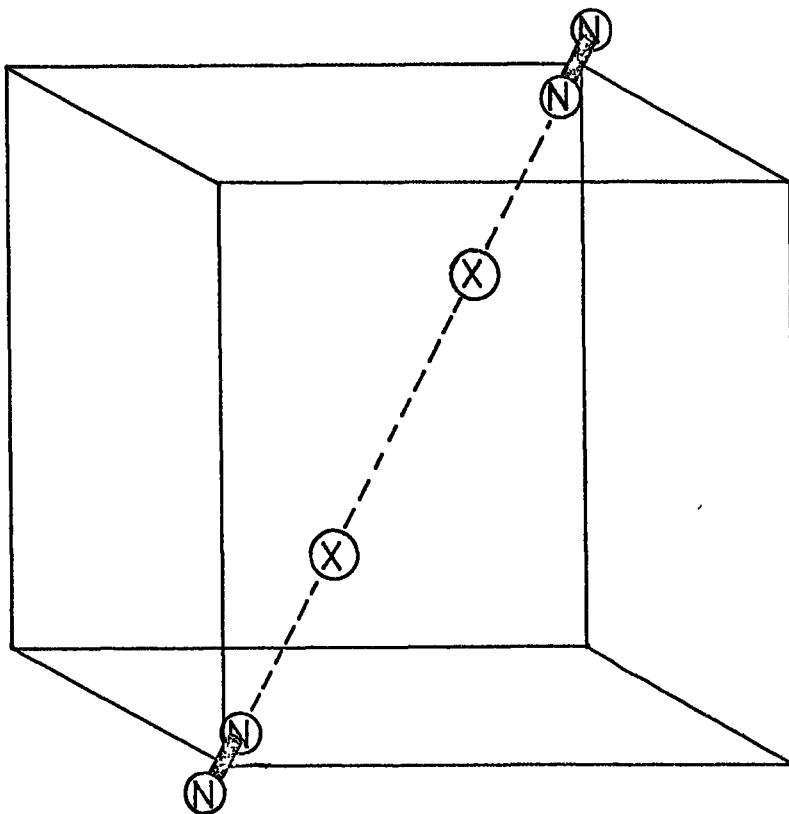


Fig. (3.3) Atoms lying along the diagonal of the cube unit cell of  $\text{N}_2\text{H}_6\text{Cl}_2$ .

(U.S. GOVERNMENT PRINTING OFFICE: 1960)

Section 5. Spectroscopic Data.

Near I.R. spectra of the halide salts as nujol and perfluorokerosene mulls were obtained at room temperature and nujol mulls were also run at liquid nitrogen temperatures, using CsI plates. Far I.R. spectra were obtained from nujol mulls at room and cold cell temperatures. A very thin disc of pure  $N_2H_6F_2$  was also run between  $600-200cm^{-1}$  as it was thought that the mulls were broadening the spectrum in this region. However the disc still produced a fairly broad band.

At first Raman spectra of the halides were kindly recorded by Drs Salthouse and Ware at Manchester, but later were repeated by ourselves on the samples used for the neutron work. I.N.S. spectra were obtained at liquid nitrogen temperatures on the beryllium filter spectrometer and at ambient temperatures on the 6H time-of-flight spectrometer.

The spectra of the sulphate are less complete as we were simply interested in finding the  $C_3$  torsion-libration modes.

Discussion of Spectra:

The  $F^-$ ,  $Cl^-$  frequencies did not differ significantly from the previous works (7,8) except for the Raman of the chloride which even at a spectral bandwidth of  $2cm^{-1}$  did not show the peak at  $223cm^{-1}$  reported by Couture and Mathieu (7), thus casting doubt on their low frequency assignments. Assignments of the new spectra were tentatively made by comparisons. At room temperature the band

observed in the chloride at  $455\text{cm}^{-1}$ , and assigned by Snyder and Decius (8), as the  $\nu_4$  torsion, was seen at  $407\text{ cm}^{-1}$  in the bromide. However the cold spectra show these at  $465$  and  $420\text{ cm}^{-1}$  respectively.

Tables (3.5-3.9) list the frequencies and as pointed out earlier (8) it is somewhat hazardous to place too much weight on some of the assignments. Table (3.4) gives the description of the fundamentals according to  $D_{3d}$  symmetry.

Table (3.4) Description of fundamentals in  $D_{3d}$  Symmetry.

Species	Designation		Description	
$A_{1g}$	$\nu_1$	NH	stretch	( $\nu$ )
	$\nu_2$	$\text{NH}_3$	deformation	( $\delta$ )
	$\nu_3$	$\text{NN}^3$	stretch	( $\nu$ )
$E_g$	$\nu_{10}$	NH	stretch	( $\nu$ )
	$\nu_{11}$	$\text{NH}_3$	deformation	( $\delta$ )
	$\nu_{12}$	$\text{NH}_3$	rock	( $\rho$ )
$A_{1u}$	$\nu_4$		internal torsion	
$A_{2u}$	$\nu_5$	NH	stretch	( $\nu$ )
	$\nu_6$	$\text{NH}_3$	deformation	( $\delta$ )
$E_u$	$\nu_7$	NH	stretch	( $\nu$ )
	$\nu_8$	$\text{NH}_3$	deformation	( $\delta$ )
	$\nu_9$	$\text{NH}_3$	rock	( $\rho$ )

An inspection of the beryllium filter neutron spectra immediately shows two very intense peaks at higher frequencies common to all four salts. These certainly do not appear in the I.R. or Raman of the fluoride, and since the factor group analysis shows us that only the



Table (3.5) I.R./Raman frequencies above  $700\text{ cm}^{-1}$  of solid  $\text{N}_2\text{H}_6\text{X}_2$  species (X = F, Cl, Br) ( $\text{cm}^{-1}$ )

$\text{N}_2\text{H}_6\text{F}_2$		I.R.*			RAMAN			
I.R.*	Raman	Assignment	$\text{N}_2\text{H}_6\text{Cl}_2$	$\text{N}_2\text{H}_6\text{Br}_2$	Assignment	$\text{N}_2\text{H}_6\text{Cl}_2$	$\text{N}_2\text{H}_6\text{Br}_2$	Assignment
2710 m	2896 v.s. 2771 s		(~3300) $\uparrow$ very broad band	(~3200) $\uparrow$ s.b ~2680 2610 s.b very broad band		3083 w 3048 w 2978s.sh	3052 w 3011 w 2955s.sh	
2426 m	2686 2556 m.b. } 2438	v <sub>5</sub> , v <sub>7</sub>	(~2100) $\downarrow$ 2110 v.w	(~2100) $\downarrow$ 2080 w		2948 s 2872v.s	2913 s 2839v.s	
2300 m	2234 s.b.		2065 m	2025 m		2809v.s	2749v.s,sh	
2190 m			1943 m	1897 m		2749v.s	2709v.s	v <sub>10</sub> ?
2060 m			1817 m	1778 m		2669m.sh	2632 m } 2587 m }	v <sub>1</sub> ?
1848 } 1805 } 1679 m	~2023 w.b		1610 w 1567 w	1520 w	v <sub>8</sub> ?	2552 s	2531 s	
1557 s	1660 m } 1617 m }	v <sub>8</sub> ? v <sub>2</sub> , v <sub>11</sub>	1535 w 1500 m	1095 s 1080 s	v <sub>6</sub>	~2000w.v.b	2020v.w 1982 w 1954 w	
1174 v.s 1094 w	1413 w	v <sub>12</sub> ? v <sub>9</sub>	1095 s 1080 s	1155 w 1080 s } 1070 s }	v <sub>9</sub>	1600 w.b 1524 m	1580 m 1503 m	v <sub>11</sub> v <sub>2</sub>
970 w	1041 v.s	v <sub>3</sub>	1005 w 877 w	1010 v.w 830 v.w		1255 w.b 1100 w.b	1125 w	v <sub>12</sub> ?
						1027 v.s	1014 v.s	v <sub>3</sub>

\* At liquid nitrogen temperatures.  
s = strong m = medium w = weak v = very sh = shoulder b = broad.

Table (3.6) Spectroscopic frequencies below 700 cm<sup>-1</sup>for N<sub>2</sub>H<sub>6</sub>F<sub>2</sub> (cm<sup>-1</sup>)

I.R.	RAMAN	I.N.S.		ASSIGNMENT
		6H	Be-filter	
{ ~ 548w. sh. ~ 273v.s brd	286v.s	270v.s	692 v.s.	} Torsion- libration $\nu_4, \nu_{Lib}$ Combination
			635 v.s.	
			329 m	} Translational $A_{2u}, E_u + E_g +$ libration
			268 v.s. (215v.v.w)	
159m.s 120m.s	135v.s	144s.sh 127s.	} $A_{1g} + E_g$ Translational Acoustic modes	
58.5m.w 15.5m.w	~ 85w.sh			} ?

Table (3.7) Spectroscopic frequencies below 700 cm<sup>-1</sup>for N<sub>2</sub>H<sub>6</sub>Cl<sub>2</sub> (cm<sup>-1</sup>)

I.R.	RAMAN	I.N.S.		ASSIGNMENT
		6H	Be-filter	
465(455)w. { 286 w. sh 266 m. 231 v.s 221 sh 161 m 125 v.w 84v.v.w	248v.s 232v.v.s	235v.s	494 v.s.	} Torsion- Libration $\nu_4, \nu_{Lib}$ Combination
			422 v.s.	
			w. broadening	} Degenerate Libration
			236 v.s. ↑	
			160 w 140w.sh	} Lattice Modes
			100 m	
			85 m	
			62 w	
85 m	85 m	72 m		

\* Liquid nitrogen temperatures except figure in brackets at room temperature.

Table (3.8) Spectroscopic Frequencies below 700  $\text{cm}^{-1}$   
for  $\text{N}_2\text{H}_6\text{Br}_2$  ( $\text{cm}^{-1}$ )

I.R.*	RAMAN	I.N.S.		Assignment
		6H	Be-filter	
420(407)w.		~ 400s. brd	462 v.s. 387 v.s.	} Torsion- Libration $\nu_4, \nu_{\text{Lib}}$ Combination
{ ~ 253 w. sh 242 s  208 v. s 201 sh 143 m	222m. s		w. broadening	
	209s	209v. s	209 v. s ↑	
	70s	138 m		} Lattice Modes
	53m	60 m		
		45 m		

\* Liquid nitrogen temperatures, except ( ) at room temperature.

Table (3.9) Frequencies  $\text{N}_2\text{H}_6\text{SO}_4$  ( $\text{cm}^{-1}$ )

I.R.	Be-filter	Assignment
~ 610 s		( $\nu_4 \text{SO}_4^{2-}$ )
	512 v. s. 426 v. s.	} Torsion- Libration
514 m brd		
468 w		Torsion? or Combination ( $\nu_2 \text{SO}_4^{2-}$ )
very brd. strong band into far I.R. ↓	~ 251 v. s. broad	Lattice Modes

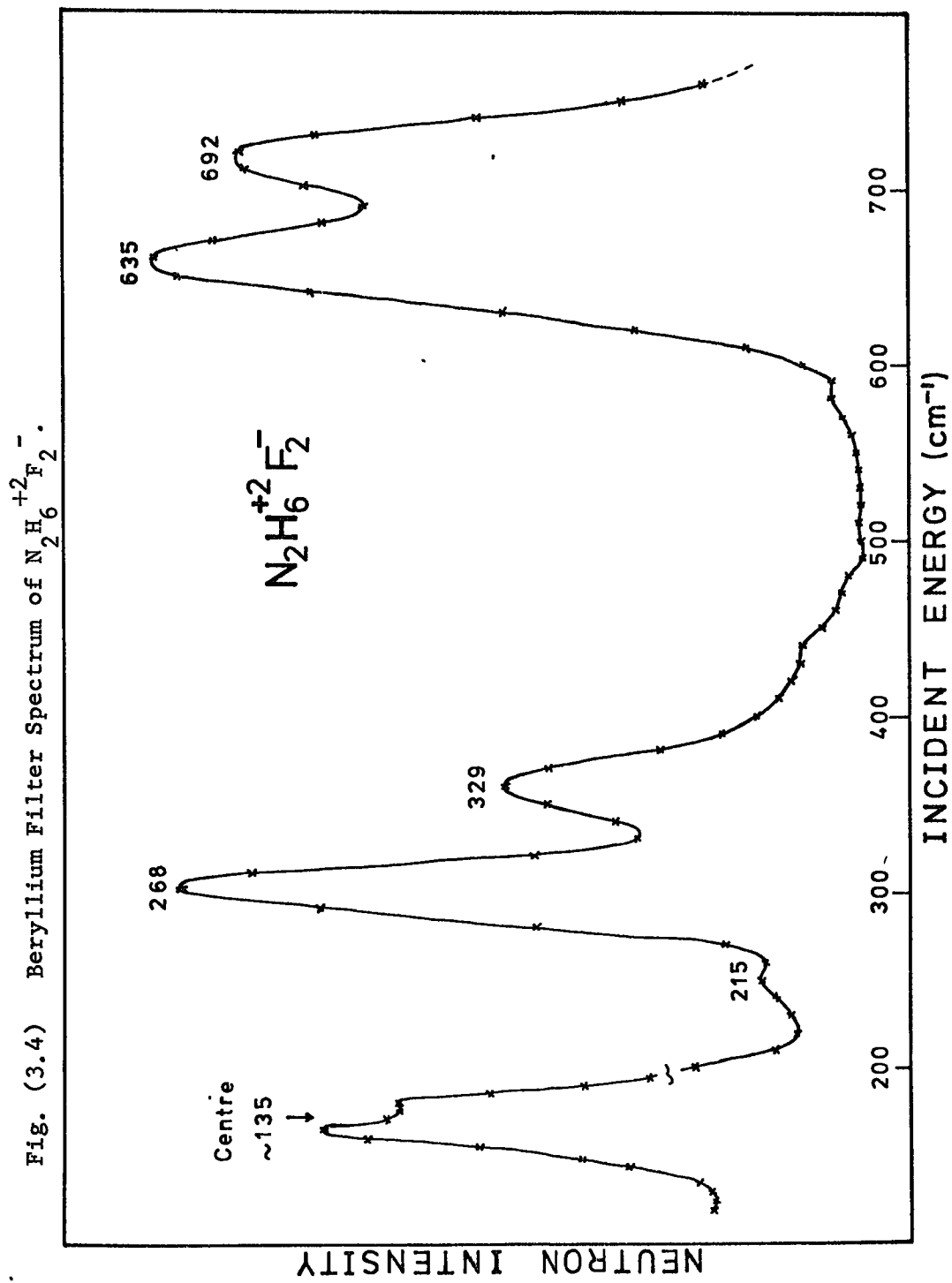
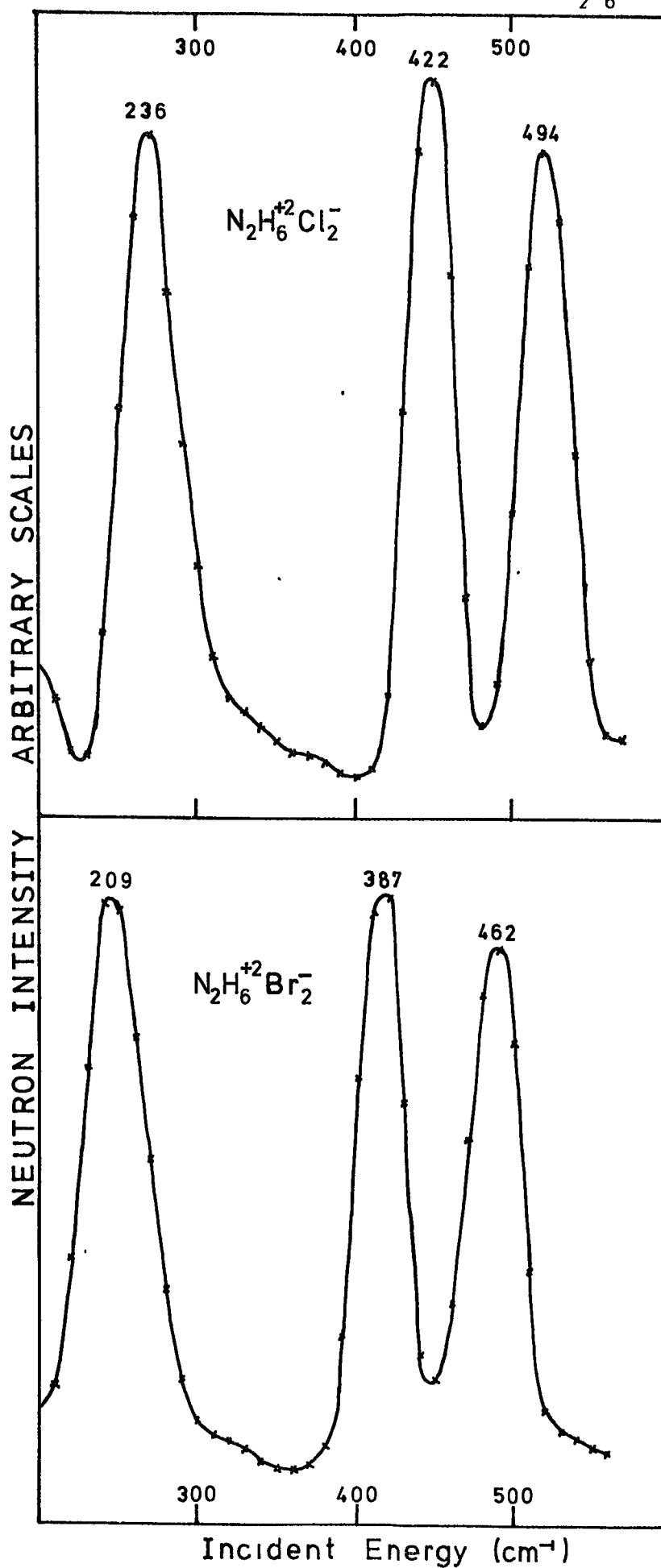


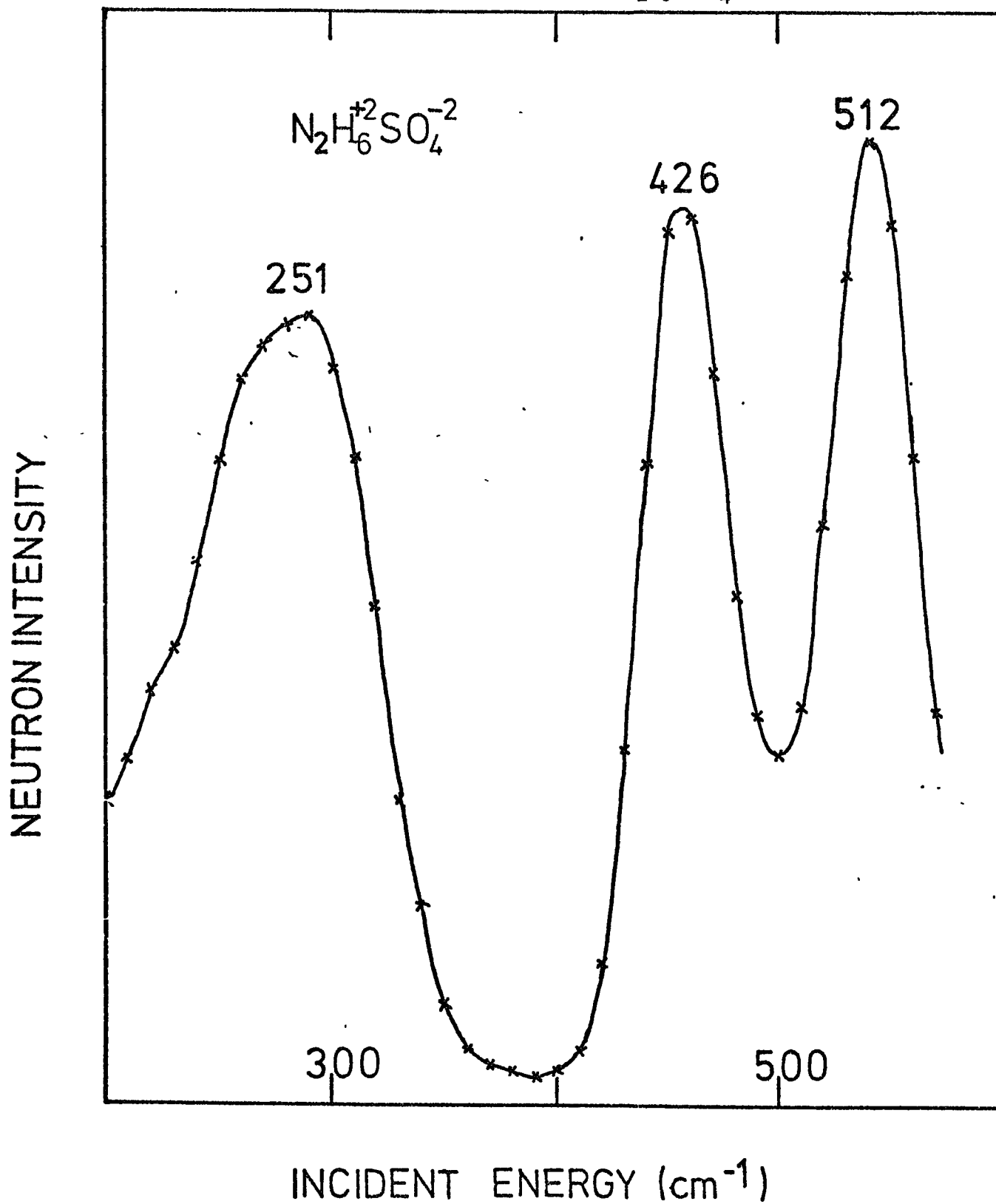
Fig. (3.5) Beryllium Filter Spectra of  $\text{N}_2\text{H}_6^{+2}\text{Cl}_2^-$  and  $\text{Br}_2^-$ .

$C_3$  axis torsion and libration are inactive one can immediately assign these. Combinations or overtones are ruled out as the parent peaks would be expected to be much stronger.

For the  $Cl^-$ ,  $Br^-$  cases there is one I.R. band which lies between the two neutron peaks. Either one is seeing a strong dispersion effect or the I.R. band was wrongly assigned by Snyder and Decius (8) and is not associated with the torsion at all. An overtone or combination band would seem highly plausible as an explanation; very strong I.R., Raman and neutron bands appear at about half the frequency, and on inspection the fluoride presents a similar situation:-

	<u>I.N.S.</u>	<u>I.R.</u>	<u>Raman</u>		<u>I.R.</u>	
Cl	236	231	232	} $\begin{array}{l} \text{Combination} \\ \text{(I.R. + Raman)} \\ \text{or} \\ \text{Overtone} \end{array}$	465	} $cm^{-1}$
Br	209	208	209		420	
F	269	273	286		548	

So it would seem that these neutron doublets are also I.R./Raman inactive. Even though the selection rules for the crystal permit such activity for the  $C_3$  torsion-libration, they do not guarantee their appearance. It would also be very unlikely that these neutron peaks could be translational modes as their frequencies would be unusually high, and they are higher than the remaining frequencies of the fluoride. Since the fluoride has the lightest anions and probably the strongest H-bonding its translational and whole-body-librational modes might be expected to be somewhat higher in frequency

Fig. (3.6) Beryllium Filter Spectrum of  $\text{N}_2\text{H}_6^{+2}\text{SO}_4^{-2}$ .

than the corresponding modes for the chloride and bromide. Hence the two higher frequency bands must again be assigned as the  $C_3$  axis torsion-libration.

It would seem reasonable to assign the similar bands of the sulphate by comparison. In this case the I.R. band at  $514\text{ cm}^{-1}$  may be the torsion, active due to assymetry (c.f. the  $\beta$ -methylammonium salts discussed later), although this is again in the region of twice the broad lattice mode centred around  $251\text{ cm}^{-1}$ .

Two other points of interest with respect to the I.N.S. spectrum of the sulphate are (1) the noticeable broadening of the torsional bands (a quantitative measurement of which is the full width at half maximum F.W.H.M.) and (2) the pattern of a slightly less intense higher frequency seen for the halides is reversed.

Table (3.10) Widths and relative intensities of the  $C_3$ -torsion-libration bands.

	F.W.H.M. ( $\text{cm}^{-1}$ )		Relative intensity $\nu_1:\nu_2$	
	$\nu_1^\dagger$	$\nu_2^*$	$\nu_1$	$\nu_2$
F	not sufficiently resolved		33	29
Cl	35	38	36	32
Br	35	40	29	26
SO <sub>4</sub>	48	49	31	34

$\dagger \nu_1$  = lower frequency \*  $\nu_2$  = higher frequency

These effects may again be due to the assymetry of the  $N_2H_6SO_4$  system.



Fig. (3.7) Time-of-Flight Data.

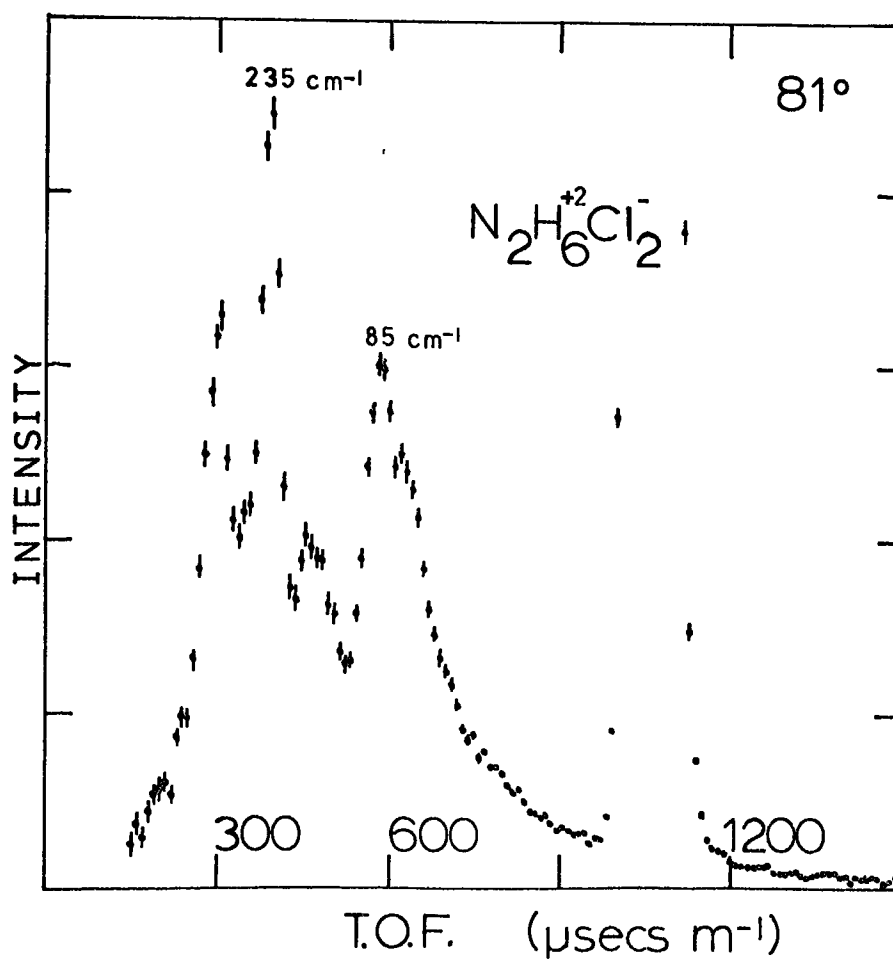
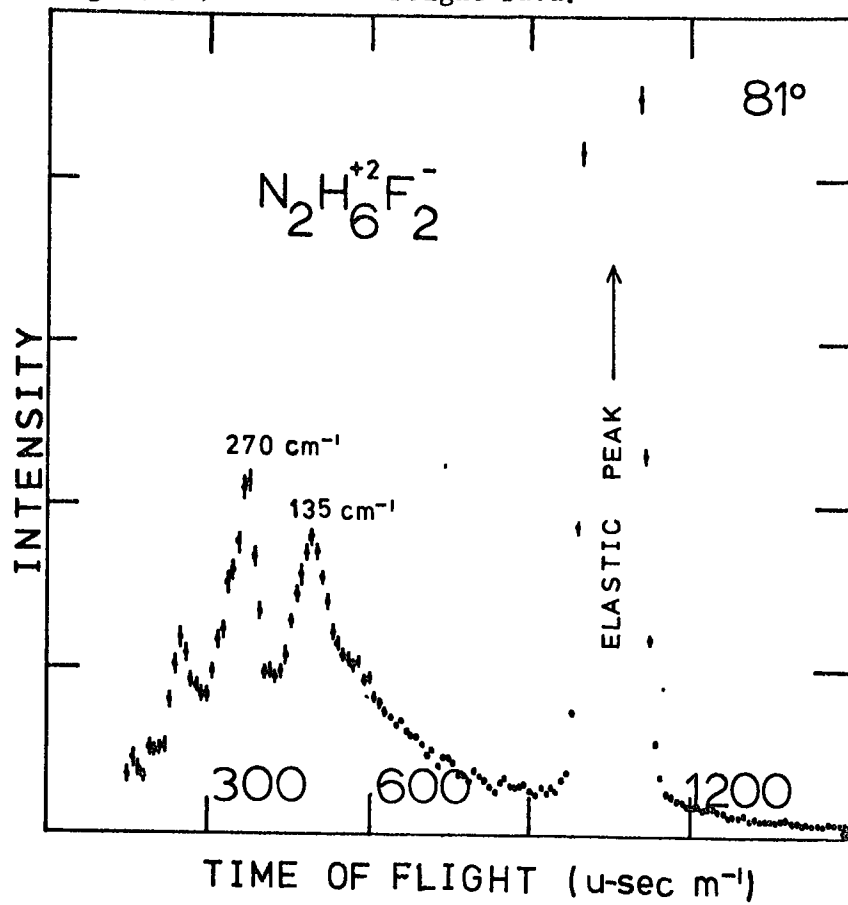
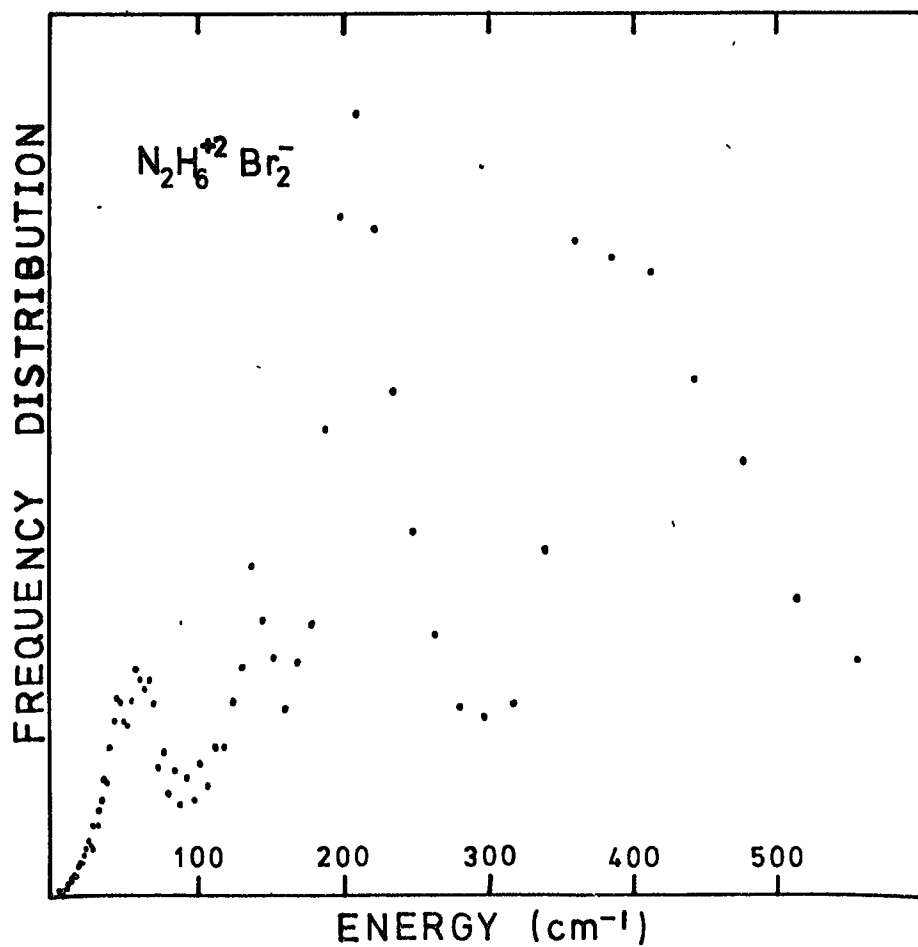
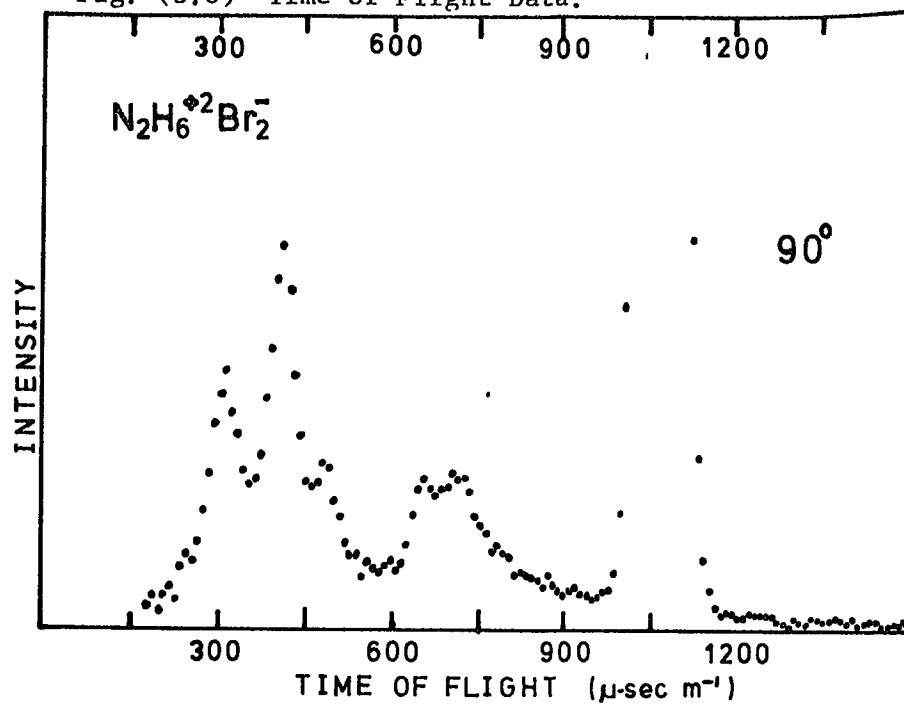


Fig. (3.8) Time-of-Flight Data.



It would be very useful now if the remaining whole body librational frequencies could be picked out from the lower frequency bands; a problem which has not been conclusively solved:-

The problem ought to be simplest for the fluoride since there are far fewer lattice modes, on account of there being only one unit in the primitive cell. Recalling the factor group analysis there should be 3 Raman bands ( $A_{1g} + 2E_g$ ) which includes the  $E_g$  libration, and 2 I.R. bands ( $A_{2u} + E_u$ ). I.N.S. spectra may also show the two remaining acoustic modes ( $A_{2u} + E_u$ ). In fact 3 Raman bands are seen at 286, 159 and  $120\text{cm}^{-1}$ , and the I.R. spectrum displays a very broad intense absorption centred at  $\sim 273\text{cm}^{-1}$ , the second I.R. band is probably masked beneath this. Looking at the I.N.S. spectrum the equivalents of all the frequencies above are seen, but an extra band appears at  $329\text{cm}^{-1}$ . At first it was thought that this might be an impurity, but re-running old and freshly recrystallised samples over the region showed no change whatsoever with respect to the stronger peak at  $268\text{cm}^{-1}$ . The possibility that it might be a hot band can be ruled out since its intensity does not appear to be any different for the time-of-flight room temperature spectrum. There do not appear to be any sensible candidates which might constitute an overtone or combination, so it must be concluded that the  $329\text{cm}^{-1}$  band is the equivalent of the missing I.R. band. The broad I.R. absorption is in fact much broader to higher frequencies and could amply cover the extra band.

The strongest I.N.S. band at  $268\text{cm}^{-1}$  must correlate with the  $273\text{cm}^{-1}$  (I.R.) and  $286\text{cm}^{-1}$  (Raman) bands though it is slightly odd that the Raman band is significantly higher, whereas in the

chloride and bromide the equivalent I.N.S. band coincides exactly with the I.R. and Raman bands, which in these cases are accidentally degenerate.

The remaining Raman bands at 120, 159  $\text{cm}^{-1}$  must correlate with the strong band at 135  $\text{cm}^{-1}$  in the 6H time-of-flight spectrum which appears to be resolved at 127, 144  $\text{cm}^{-1}$  in the beryllium filter spectrum. This area of the neutron spectrum might also contain the acoustic modes, and in fact a weak shoulder appears on the time-of-flight spectrum at  $\sim 85 \text{ cm}^{-1}$ . So now all the bands seem to have been located, but the problem remains as to which of the Raman frequencies is the librational mode. One would again expect this kind of motion to have a large proton amplitude and hence produce an intense peak, so on this argument the 268  $\text{cm}^{-1}$  I.N.S. peak would seem the most likely. However this also includes a contribution from the I.R. translational band at 273  $\text{cm}^{-1}$  so the separate intensity is not apparent, and the lower bands might then be as strong. However a comparison with the equivalent peaks in the I.N.S. of the chloride and bromide shows that their higher frequency peak is by far the most intense and their lower frequencies much less intense than a librational mode might be expected to give, especially so for the bromide. Here the intensity argument very much favours the higher frequency, so by comparison the fluoride would be expected to be even higher, which means that the 268  $\text{cm}^{-1}$  band must be chosen as the  $E_g$  libration.

Dealing now specifically with the chloride and bromide, their spectra are made more complex due to correlation splittings. The two strongest peaks in the I.N.S. spectra just mentioned, occur at

236  $\text{cm}^{-1}$  (chloride) and 209  $\text{cm}^{-1}$  (bromide), and both have accidentally degenerate I.R. and Raman bands at almost exactly the same frequencies. See tables (3.7, 3.8 ). The Raman bands do in fact show a splitting giving a slightly weaker peak to higher frequency and the I.R. spectra also have weaker bands to slightly higher frequency. These appear in the neutron spectra as a slight broadening on the strong peak.

The remaining I.R. and Raman lattice bands all appear to lower frequencies and none occur as intense peaks in the I.N.S. spectra, as can be seen in the figures.

Hence provisional assignments of the most likely degenerate librational frequencies can be made as:-

F	268	
Cl	236	$\text{cm}^{-1}$
Br	209	

A Raman polarisation study of a single crystal would prove extremely useful in narrowing down the possibilities for the libration. For the fluoride this should pick out which of the three bands is the  $A_{1g}$  mode, leaving only two  $E_g$  bands to choose between. It is worth noting that for  $D_{3d}$  symmetry no overtone of an  $E_g$ ,  $E_u$  or  $A_{2u}$  mode (the possible symmetries involved in the newly assigned band) would be I.R. active and hence the I.R. feature discussed earlier at about twice the frequency would have to be a combination ( $E_g + E_u$ ) or ( $E_g + A_{2u}$ ).

Section 6. Calculations.

a) Motions about the  $C_3$  axis.

From the theory given in chapter 1 (eq. 1.3.22,23) the simple equations relating frequencies to barriers for symmetrical  $N_2H_6^{+2}$  ions, in the S.H. approximation, are:-

$$\bar{\nu}_1^2 = \frac{9h \bar{V}_E}{8\pi^2 cI}, \quad (\bar{\nu}_2^2 - \bar{\nu}_1^2) = \frac{9h \bar{V}_I}{4\pi^2 cI}$$

where  $\bar{V}_E$ ,  $\bar{V}_I$  are external and internal barriers respectively,  $I$  is the moment of inertia of one  $-NH_3$  group. The frequencies of  $\bar{\nu}_1$ ,  $\bar{\nu}_2$  obtained from I.N.S. are summarised in the table (3.11) below together with  $\bar{\nu}_1^2$ ,  $(\bar{\nu}_2^2 - \bar{\nu}_1^2)$  and  $(\bar{\nu}_2^2 - \bar{\nu}_1^2)^{\frac{1}{2}}$  in  $cm^{-1}$  or  $(cm^{-1})^2$ .

Table (3.11) Summary of Frequencies in  $cm^{-1}$  for Torsion-Libration.

$N_2H_6^{+2}$	$\bar{\nu}_1$	$\bar{\nu}_2$	$\bar{\nu}_1^2$	$(\bar{\nu}_2^2 - \bar{\nu}_1^2)$	$(\bar{\nu}_2^2 - \bar{\nu}_1^2)^{\frac{1}{2}}$
$2F^-$	635	692	403225	75639	275
$2Cl^-$	422	494	178084	65952	257
$2Br^-$	387	462	149769	63675	252
$SO_4^{-2}$	426	512	181476	80668	284

The value of  $(\bar{\nu}_2^2 - \bar{\nu}_1^2)^{\frac{1}{2}}$ , at least for the symmetric cases, gives the effective "free ion" frequency.

Calculation of the moments of inertia presents a small problem in that there are no absolutely definite bond lengths and angles for N-H except for the sulphate. If one assumes that the hydrogens lie along the N-H---X<sup>-</sup> lines then one has an angle for the F, Cl cases (11,12).

However this assumption is rather dubious, since neutron diffraction has in many cases shown that the hydrogen bond need not be linear, larger deviations being seen for cases where  $X-H\cdots Y$  is  $> 2.7\text{\AA}$  i.e. weaker H-bonds. This is seen quite well in  $N_2H_6SO_4$  (1) (see earlier) which shows signs of bi and tri-furcated H-bonds; the  $N-N-H$  angles vary on either side of the tetrahedral angle, and the  $N-H\cdots O$  angles vary between  $109-167^\circ$ . Hence the fluoride which is strongly H-bonded with  $N\cdots F = 2.62\text{\AA}$  might well be more nearly linear than the chloride with  $N\cdots Cl = 3.10\text{\AA}$ . Hence in the calculations both  $N-N-X$  and the tetrahedral angles have been used as indicated.

As regards the N-H bond lengths no one seems to be agreed. The fluoride N.M.R. value of  $1.075\text{\AA}$  (13) was corrected to  $1.05\text{\AA}$  (14) but with large estimated errors. For the chloride and bromide no measurement has been attempted. Ibers and Stevenson (14) also corrected values for  $NH_4F \rightarrow 1.041\text{\AA}$  and  $NH_4Cl \rightarrow 1.032\text{\AA}$ . Neutron diffraction on  $NH_4Cl$  (24) has given  $N-H = 1.03\text{\AA}$  and in  $ND_4Br$  (25)  $N-D = 1.03$ , and according to Wyckoff (16) electron diffraction on  $NH_4Cl$  has yielded values of  $N-H = 1.03$  and  $0.98\text{\AA}$  respectively. Snyder and Decius (8) estimated the value for  $N_2H_6Cl_2$  as  $1.045\text{\AA}$  from a plot of the N-H bond lengths calculated by Ibers and Stevenson (14) vs. weight-averaged bond stretching frequency. Tsau and Gilson (26) also estimated  $N-H = 1.045\text{\AA}$  for use in their calculations on  $\beta$ -methylammonium chloride.

Clearly we might expect  $N_2H_6F_2$  to have a longer N-H distance than  $NH_4F$  since the H-bonding appears to be stronger;  $N\cdots F = 2.62$  and  $2.68\text{\AA}$  respectively, similarly for the chloride.

Consequently barriers have been calculated using the parameters indicated in the table of results below:-

Table (3.12) Simple Harmonic Barriers ( $\text{cm}^{-1}$ ) for  $\text{N}_2\text{H}_6\text{F}_2$ ,  $\text{Cl}_2$ ,  $\text{Br}_2$ .

	Bond Length (Å)	Crystal N-N...X			Tetrahedral N-N...H		
		I (a.m.u. Å <sup>2</sup> )	$\bar{V}_I$ (cm <sup>-1</sup> )	$\bar{V}_E$ (cm <sup>-1</sup> )	I (a.m.u. Å <sup>2</sup> )	$\bar{V}_I$ (cm <sup>-1</sup> )	$\bar{V}_E$ (cm <sup>-1</sup> )
F	1.06	3.225	804	8576	3.020	753	8030
	1.05	3.165	789	8415	2.963	739	7879
Cl	1.04	3.172	690	3724	2.907	632	3414
	1.03	3.111	676	3653	2.851	620	3348
Br	1.04				2.907	610	2871
	1.03				2.851	599	2816

Treating  $\text{N}_2\text{H}_6\text{SO}_4$  as asymmetric; if we assume that the internal barrier is not drastically affected and use values for  $\bar{V}_I$  of 680-620 $\text{cm}^{-1}$  (since the mode frequencies fall in the same range as the chloride and bromide, indicating a similar degree of H-bonding) we can now, using the more complex expressions, calculate approximately the barriers at each end. (Theory from Chapter 1, Section 3).

Moments of inertia were calculated from the neutron data given earlier:  $I_{N_1} = 2.9787$ ,  $I_{N_2} = 2.5676$  (a.m.u. Å<sup>2</sup>) where  $N_1$  is the end with strongest H-bonding.



$$\text{From the theory } \lambda_1 + \lambda_2 = d_A + d_B \quad (i)$$

$$\lambda_1 - \lambda_2 = \pm (d_A - d_B)^2 + d_I^2 \quad (ii)$$

$$\text{rearranging (ii) } d_A - d_B = (\lambda_1 - \lambda_2)^2 - d_I^2 \quad (iii)$$

$\lambda_1, \lambda_2$  relate directly to the frequencies (Eq. 1.3.12)

$d_I$  can be calculated assuming  $V_I$  (eq. 1.3.4).

$d_A, d_B$  can therefore be found by elimination from (i), (iii) and these then give the values of  $\bar{V}_{N_1}, \bar{V}_{N_2}$  respectively.

Table (3.13) Barriers in  $\text{cm}^{-1}$  and normal coordinates for  $\text{N}_2\text{H}_6\text{SO}_4$ .

$\bar{V}_I (\text{cm}^{-1})$ Assumed	$\bar{V}_{N_1} (\text{cm}^{-1})$	$\bar{V}_{N_2} (\text{cm}^{-1})$	Normal Coord vs. Symmetry Coord. Matrix
620	4163	2768	$\begin{matrix} \alpha_1 & \alpha_2 \\ a \begin{bmatrix} 1.513 & -0.770 \end{bmatrix} \\ b \begin{bmatrix} -0.830 & -1.405 \end{bmatrix} \end{matrix}$
680	3979	3815	$\begin{matrix} \alpha_1 & \alpha_2 \\ a \begin{bmatrix} 1.434 & -0.891 \end{bmatrix} \\ b \begin{bmatrix} -0.960 & -1.332 \end{bmatrix} \end{matrix}$

The "barrier" parameters in this case do not bear so much physical relationship to the true barrier as in the halide salts, since it really is an averaged value for the asymmetric potential.

b) The Lower Frequency Librations.

The kind of potential required for the end-over-end motion is not so clear as for the  $C_3$  axis motions, and since the movement would require much more space one might perhaps expect factors such as Van der Waals

or electrostatic repulsions from other  $N_2H_6^{+2}$  ions to enter into the barrier forces, as well as the hydrogen bending.

In the first approximation one would expect the molecule to be hindered by a two-fold barrier  $V_2$  caused by 6 hydrogen bonds, although other terms such as  $V_4$  may perhaps be an influence. A simple harmonic model can again be used for the two-fold case

$$\bar{\nu}^2 = \frac{h}{8\pi^2 c I} \cdot n^2 \bar{V}_2 \quad n = 2$$

The parameter  $(n^2 \bar{V})$  i.e.  $(4\bar{V}_2)$  in this case, can be regarded as a kind of force constant, and if it derives from 6 H-bonds it should be comparable with the value of  $2x(9\bar{V}_E)$  which can be obtained for the  $C_3$  axis motions. ( $\bar{V}_E$  was derived for one end of the molecule and so must be multiplied by two to account for 6 hydrogen bonds).

The moment of inertia for this heavier librational motion is not so much affected by small changes in geometry and using either the crystal geometry or Td angles gives a range of  $I \approx 20 \rightarrow 21$  a.m.u.  $\text{\AA}^2$ . So for the purposes of this crude calculation  $I = 20.5$  a.m.u.  $\text{\AA}^2$  has been used.

Initially values of  $2x(9\bar{V}_E)$  have been calculated from table (3.12), and then substituted as  $(4\bar{V}_2)$  in the two-fold equation. Predicted values of the libration frequency can then be calculated as follows:-

Table (3.14)

Calculated and observed libration frequencies ( $\text{cm}^{-1}$ )

	$2x(9\bar{V}_E)$	$(\bar{\nu}_{LIB})_{Calc.}$	$(\bar{\nu}_{LIB})_{Assigned}$
$F^-$	141822	341	268
$Cl^-$	61452	225	236
$Br^-$	51678	206	209

These results prove very interesting in that the chloride and bromide show quite a close correspondence with the assigned bands, but for the fluoride the calculated value is much closer to the band seen at  $329 \text{ cm}^{-1}$  in the I.N.S. This is somewhat worrying especially since some features of the Raman spectrum have already given rise to some discussion (i.e. the highest band not coinciding with the I.N.S. band), but the fact remains that the libration should be Raman active and the  $329 \text{ cm}^{-1}$  band certainly is not. This evidence emphasises that the assignment must be held with reserve until further investigations have been carried out.

If one retains the  $268 \text{ cm}^{-1}$  assignment for the fluoride its low frequency may perhaps be explained by its different structure. Quite possibly the structure may produce different steric repulsions which counteract the attractive H-bond forces. If one compares the value of  $(4\bar{V}_2)$  calculated from the assigned frequencies with that obtained from  $(18\bar{V}_E)$  for the 6 H-bonds, the difference should quantify the extra forces:-

Table (3.15) Additional forces.

	$(4\bar{V}_2)$	$(18\bar{V}_E)$	Difference	Origin
$\text{F}^-$	87382	141822	- 54440	Repulsive (Steric)
$\text{Cl}^-$	67761	61452	+ 6309	Attractive
$\text{Br}^-$	53143	51678	+ 1465	Attractive

The values for the chloride and bromide are hardly significant when errors and the crudity of the model are considered, though the repulsion term suggested for the fluoride is quite large.

### Section 7. Discussion.

The first point of interest is that the model for the  $C_3$  axis torsion-librational modes appears to work, and gives reasonably consistent values for the internal barrier. It is worth noting that the value increases as the external barrier increases which may be due to changing charge displacements in the different H-bonds.

The values obtained for the external barriers for the motions around the  $C_3$  axis show the expected pattern of decreasing H-bond strengths  $F^- \rightarrow Br^-$ . Fortunately the external frequency values can be compared with the librational frequencies obtained for the ammonium halides (28,29). Since the barrier is proportional to the frequency squared and the moments of inertia do not change substantially from one halide salt to the next, the ratio

$$\left[ \frac{\bar{\nu}_{N_2H_6}^{+2}}{\bar{\nu}_{NH_4}^{+}} \right]_{X^-}^2$$

should remain roughly the same for each pair of frequencies:

Table (3.16) Comparison of external modes.  $NH_4X/N_2H_6X_2$

$X^-$	$\bar{\nu}_{NH_4}^{+} (cm^{-1})$	$\bar{\nu}_{N_2H_6}^{+2} (cm^{-1})$	$(\bar{\nu}_{N_2H_6}^{+2} / \bar{\nu}_{NH_4}^{+})^2$
$F^-$	523 †	635	1.474
$Cl^-$	389 *	422	1.177
$Br^-$	335 *	387	<u>1.335</u>
$I^-$	293 *	x	Ave: 1.329

† Ref. (28)

\* Ref (29) I.N.S. frequency at 100°K.

The comparison is fairly consistent and if one takes the average ratio and uses this to calculate the frequency for  $N_2H_6I_2$ ,  $x = 338 \text{ cm}^{-1}$  which gives a 3-fold value for  $\bar{V}_E$  of  $2186 \text{ cm}^{-1}$ . (This estimated value may be of interest in later chapters).

The model also neatly shows that the barriers at each end of the  $N_2H_6^{+2}$  ion in the sulphate are substantially different. At the end which has three individual H-bonds the barrier indicated is slightly higher than for the chloride. (Out of interest; if the system had been assumed as symmetrical and using an average value of  $I_{NH_3}$  the barriers work out as  $\bar{V}_E = 3319 \text{ cm}^{-1}$   $\bar{V}_I = 738 \text{ cm}^{-1}$ . This higher value for  $\bar{V}_I$  would not fit into the pattern of increasing  $\bar{V}_I$  as  $\bar{V}_E$  increases discussed earlier.) Comparison with the N.M.R. activation energy (19) for  $-NH_3$  group rotation of  $2178 \text{ cm}^{-1}$  shows that this value is somewhat low. It should also be noted that this value does not separate internal and external effects.

Because of cross terms the sinusoidal potential functions cannot be separated, however the S.H. approximation separates the internal and external barriers very neatly, and in the symmetrical cases points to the "free" ion internal torsional frequency given by  $(\bar{v}_2^2 - \bar{v}_1^2)^{\frac{1}{2}}$  and the rigid librator frequency given by  $\bar{v}_1$ . Perhaps it is not too drastic to assume that these may be very nearly the pure separate mode frequencies of the system in a sinusoidal context, and that the barriers derived from Mathieu solutions using these frequencies might give a value nearer the physical reality. This has therefore been attempted using the values of  $I_{NH_3}$  indicated, the frequencies were given in table (3.11). The external barrier has to be calculated as for 6 H-bonds and using  $(2I_{NH_3})$  for the moment of inertia. The values

obtained are given in table (3.17) below:

Table (3.17) Cosine barriers ( $\text{cm}^{-1}$ )

	$I_{\text{NH}_3}$	S.H. $2x\bar{V}_E$	$\bar{V}_I$	Cosine $2\bar{V}_E$	$\bar{V}_I$
$\text{F}^-$	2.963	15758	739	16080	908
$\text{Cl}^-$	2.907	6828	632	7044	789
$\text{Br}^-$	2.907	5742	610	5940	764

Clearly the S.H. external barriers are in themselves quite good, but the internal barrier changes quite substantially as expected ( $\sim 24\%$  increase). If the external barriers ( $2\bar{V}_E$ ) are considered to be composed mainly of 6 H-bonds the following single N-H---X bond energies given in the conventional units are obtained:-

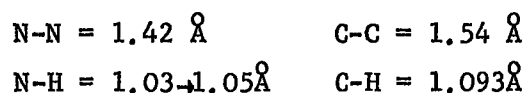
$\text{F}^-$	7.67	(k cal/mole)
$\text{Cl}^-$	3.36	
$\text{Br}^-$	2.83	

These values are in the usual range for asymmetrical H-bonds (17,27). Unfortunately there is no way of determining any steric repulsion contribution to the potential but since it may be opposite in sign to the H-bond potential any attempt to take account of it would increase the value determined for the H-bond energy.

The internal barrier is somewhat below that of the isoelectronic ethane (Chapter 1. Ref 40). For comparison:-

	S.H.	Cosine	
$(\text{N}_2\text{H}_6^{+2})\text{Cl}^-$	632	783	$\text{cm}^{-1}$
$\text{C}_2\text{H}_6$	860	1023	

Since all the bond lengths in  $\text{N}_2\text{H}_6^{+2}$  are shorter than in ethane:



one might have expected its internal hindrance to be greater. The most probable explanation is that the electronic charge distribution is somewhat different in  $\text{N}_2\text{H}_6^{+2}$  in order to accommodate the double positive charge, negative charge being pulled down onto the nitrogens i.e. the increased nuclear charge on the nitrogens spatially contracts the orbitals, thus reducing the Van der Waals repulsion energy. The increasing internal barriers observed for increasing H-bonding may then indicate that charge is being drawn back off the nitrogen towards the electronegative anion.

It would be very interesting to investigate an  $\text{N}_2\text{H}_6^{+2}$  salt which does not show any hydrogen bonding. The very much reduced external barriers (if any) would mean that a torsional band, due practically to the internal torsion alone, should appear, and if the ideas expressed above are correct the barrier calculated ought to be less than in the halide salts.

References - Chapter 3

1. P-G. Jönsson, W.C. Hamilton, *Acta. Cryst.* B26, 536 (1970).
2. M. Milojevic, J. Slivnik, *Therm. Anal., Proc. Int. Conf. 3rd*, (1971) 3, 19.
3. A.A. Opalovskii, A.S. Nazarov, *Izv. Sib. Otd. Akad. Nauk. SSSR, Ser. Khim. Nauk* 4, 3 (1968).
4. J.T. Edsall, *J. Chem. Phys.* 5, 225 (1937).
5. J.T. Edsall, H. Scheinberg, *ibid* 8, 520 (1940).
6. R. Ananthakrishnan, *Proc. Ind. Acad. Sci.* A5, 87 (1937).
7. L. Couture, J.P. Mathieu, *Ann. Phys., Paris* 9, 255 (1954).
8. R.G. Snyder, J.C. Decius, *Spectrochim Acta.* 13, 280 (1959).
9. A.V.R. Warriar, P.S. Narayanan, *Ind. J. Pure Appl. Phys.* 5(6), 216 (1967).
10. Z. Mielke, H. Ratajczak, *J. Mol. Struct.* 19, 751 (1973).
11. M.L. Kronberg, D. Harker, *J. Chem. Phys.* 10, 309 (1942).
12. J. Donohue, W.N. Lipscomb, *ibid* 15, 115 (1947).
13. C.M. Deeley, R.E. Richards, *Trans. Farad. Soc.* 50, 560 (1954).
14. J.A. Ibers, D.P. Stevenson, *J. Chem. Phys.* 28, 929 (1958).
15. L. Pauling, 'The Nature of the Chemical Bond' Cornell, Ithaca, N.Y. 1939.
16. Wyckoff, *Crystal Structures* 2nd Ed. 1, 88, 104.
17. W.C. Hamilton, J.A. Ibers 'Hydrogen Bonding in Solids: Methods of Molecular Structure Determination', N.Y. Benjamin (1968).
18. R.A. Marino, T. Oja, *J. Chem. Phys.* 56, 5453 (1972).
19. J.W. Harrell Jr., F.L. Harrell, *J. Mag. Res.* 8, 311 (1972).



20. D.M. Adams, D.C. Newton 'Tables for Factor Group and Point Group Analysis', Beckman.
21. International Tables for X-ray Crystallography 1.
22. P. Glavič, D. Hadži, Spectrochim. Acta. 28A, 1963 (1972).
23. F.A. Cotton, G. Wilkinson, 'Advanced Inorganic Chemistry', Interscience 2nd Edition p.45.
24. H.A. Levy, S.W. Peterson, Phys. Rev. 86, 766 (1952).
25. H.A. Levy, S.W. Peterson, J. Chem. Phys. 21, 366 (1953).
26. J. Tsau, D.F.R. Gilson, Can. J. Chem. 48, 717 (1970).
27. G.C. Pimentel, A.L. McClellan 'The Hydrogen Bond', Freeman, London (1959) Ch. 3.
28. R.C. Plumb, D.F. Hornig, J. Chem. Phys. 23, 947 (1955).
29. G. Venkataraman et al. J. Phys. Chem. Solids 27, 1103 (1966).

## CHAPTER 4

### MONOMETHYLAMMONIUM SALTS

#### Introduction.

The monomethylammonium,  $\text{CH}_3\text{NH}_3^+$ , salts present a more complicated system than the hydrazinium salts. In the first place the ion is no longer totally symmetric. Only the  $-\text{NH}_3^+$  group presents the possibility of strong H-bonding, and hence where this occurs one would expect a sizable external barrier to rotation for this group, provided the symmetry is correct to maximise the potential. A somewhat lower external barrier would be expected at the  $-\text{CH}_3$  group.

The halide salts studied in fact exist in a number of different phases, in some of which the barrier at the  $-\text{NH}_3^+$  group appears to be maximised (i.e. a  $\text{C}_3$  rotor in a 3-fold external field) and others where it is not (e.g. a  $\text{C}_3$  rotor in a 4-fold field, see Chapter 1 fig. (1.4)). The cases which do show a large external barrier provide a useful test of the full model developed in Chapter 1, section (3a). The  $\text{PF}_6^-$  salt was also studied as a special case where no H-bonding is expected, and overall external influences are likely to be small.

Considerable insight was also gained by studying the salts of the isotopic species  $\text{CD}_3\text{NH}_3^+$  and  $\text{CH}_3\text{ND}_3^+$ .

#### Section 1. Previous Studies.

##### a) Crystal Phase Changes

It has been found that the  $\text{CH}_3\text{NH}_3^+\text{X}^-$  salts ( $\text{X}^- = \text{halide}$ ) exist in several different, temperature dependent, crystalline phases, some of which correlate in properties from one halide to another.

The chloride was first studied thermodynamically by Aston and Ziemer (1) who found three phases;  $\alpha$  at room temperature  $\gamma$ ,  $\beta$  at cold temperatures. Bridgman (2) using temperatures up to 200°C and high pressures was able to find further phases.

Cabana and Sandorfy (3) observing temperature dependent changes in the I.R. spectra discovered 4 phases for the bromide;  $\alpha$  at elevated temperatures,  $\alpha'$  room temperature,  $\delta$ ,  $\beta$  at cold temperatures, where the  $\alpha$  and  $\beta$  spectra in all respects correlate with these phases of the chloride. The  $\gamma$ -Cl and  $\delta$ -Br do not however correlate. Two phases were found for the iodide  $\alpha'$ ,  $\delta$  correlating with the corresponding bromide phases. Also, spectra of the fluoride at room temperatures and -190°C were found to be different, indicating at least two phases. No further phases were found by Théorêt and Sandorfy (4) when they observed spectra down to 12°K.

Tsau and Gilson (5) using N.M.R. second moments data indicated that the bromide was in the process of a transition at 77°K, and set an upper limit for this of 250°K, however they do not indicate whether they were warming from the  $\delta$  or  $\beta$  phase. Very little change in the second moment occurred for the iodide between 77°-300°K, although I.R. data would indicate that the  $\delta \rightarrow \alpha'$  transition must occur within this range.

A higher  $\beta \rightarrow \gamma$  transition temperature for  $\text{CD}_3\text{NH}_3^+\text{Cl}^-$  than  $\text{CH}_3\text{NH}_3^+\text{Cl}^-$  and  $\text{CH}_3\text{ND}_3^+\text{Cl}^-$  was discovered by Albert and Ripmeester (6) again from N.M.R.

Table (4.1)

Summary of phases and temperature ranges where known  
for the methylammonium salts.

F (3)	2 distinct phases at 22°C, - 190°C
Cl <sup>-</sup> (1-4,6)	<p>Phase diagram for <math>\text{CD}_3\text{NH}_3\text{Cl}</math> showing transitions between phases <math>\alpha</math>, <math>\gamma</math>, and <math>\beta</math>. The diagram includes the following transitions and conditions:</p> <ul style="list-style-type: none"> <li>From <math>\alpha</math> to <math>\beta</math>: <math>264.5^\circ\text{K}</math> (Heat)</li> <li>From <math>\beta</math> to <math>\alpha</math>: <math>220.4^\circ\text{K}</math> (supercool)</li> <li>From <math>\beta</math> to <math>\gamma</math>: <math>245.5-248^\circ\text{K}</math></li> <li>From <math>\gamma</math> to <math>\alpha</math>: <math>(T^\circ?)</math></li> <li>From <math>\beta</math> to <math>\gamma</math>: <math>12^\circ\text{K}</math> (supercool)</li> <li>From <math>\alpha</math> to <math>\beta</math>: <math>12^\circ\text{K}</math> (supercool to <math>222^\circ\text{K}</math>)</li> <li>From <math>\alpha</math> to <math>\beta</math>: <math>12^\circ\text{K}</math> (+ pressure, room temp)</li> </ul>
Br <sup>-</sup> (3-5)	<p>Phase diagram for bromide salt showing transitions between phases <math>\alpha</math>, <math>\alpha'</math>, <math>\delta</math>, and <math>\beta</math>. The diagram includes the following transitions and conditions:</p> <ul style="list-style-type: none"> <li>From <math>\alpha</math> to <math>\alpha'</math>: <math>398^\circ\text{K}</math></li> <li>From <math>\alpha'</math> to <math>\delta</math>: rapid cooling (room temp.)</li> <li>From <math>\delta</math> to <math>\beta</math>: warm to <math>173^\circ\text{K}</math></li> <li>From <math>\delta</math> to <math>\beta</math>: <math>12^\circ\text{K}</math></li> <li>From <math>\beta</math> to <math>\delta</math>: <math>12^\circ\text{K}</math></li> </ul>
I <sup>-</sup> (3-5)	<p>Phase diagram for iodide salt showing transitions between phases <math>\alpha'</math> and <math>\delta</math>. The diagram includes the following transitions and conditions:</p> <ul style="list-style-type: none"> <li>From <math>\alpha'</math> to <math>\delta</math>: rapid cooling (room temp. <math>83^\circ\text{K}</math>)</li> <li>From <math>\delta</math> to <math>\alpha'</math>: no change</li> <li>From <math>\delta</math> to <math>\beta</math>: <math>12^\circ\text{K}</math></li> </ul>

#### b) X-ray Structural Information

Elucidation of the structures of the chloride, bromide and iodide salts at room temperature, already known to crystallise in the tetragonal system (7), was first attempted by Hendricks in 1928 (8) who obtained the following structural parameters:

Table (4.2)

$\text{CH}_3\text{NH}_3^+$	Molecules per unit cell (z)	a (Å)	c (Å)
$\text{Cl}^-$	1	4.28	5.13
$\text{Br}^-$	2	5.09	8.75
$\text{I}^-$	2	5.11	8.95

The bromide and iodide were found to be similar in form.

A redetermination of the chloride by Hughes and Lipscombe (9) showed Hendricks' result to be slightly incorrect. They found two molecules per unit cell ( $z = 2$ ),  $a = 6.04 \text{ \AA}$ ,  $c = 5.05 \text{ \AA}$  and space group  $D_{4h}^7 - P4/nmm$ . The relevant interatomic distances are summarised in fig. (4.1). The C-N bond coincides with the four-fold axis of the crystal, and hence the  $C_3$  distribution of H atoms on the C and N cannot conform to the space group unless they are freely rotating or orientationally disordered. The shortest N---Cl distance indicates some degree of H-bonding. As they point out, Hendricks had taken his unit cell base wrongly, as indicated by the small square instead of the large square in fig. (4.2):—

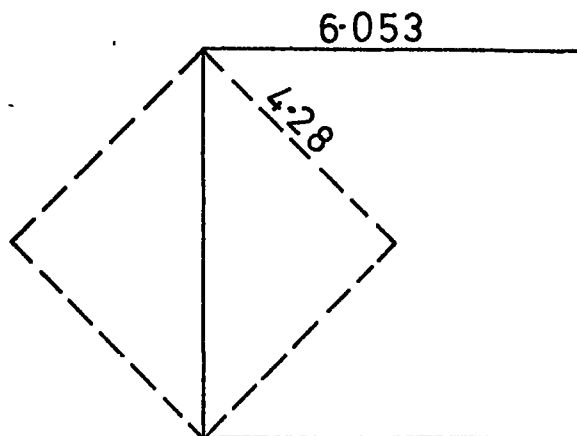


Fig. (4.1) Structure of  $\alpha\text{-CH}_3\text{NH}_3^+\text{Cl}^-$  (Distances in Å)

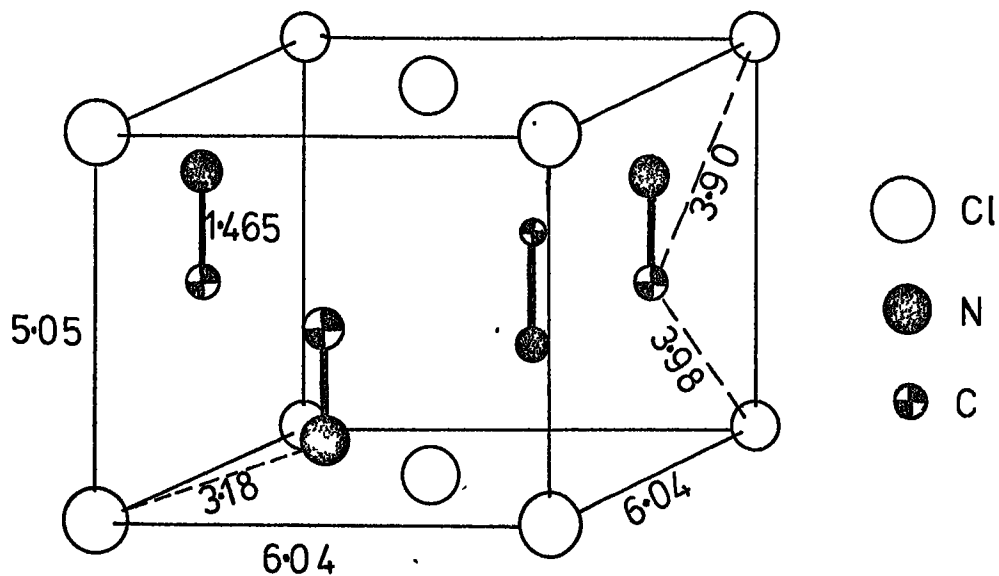
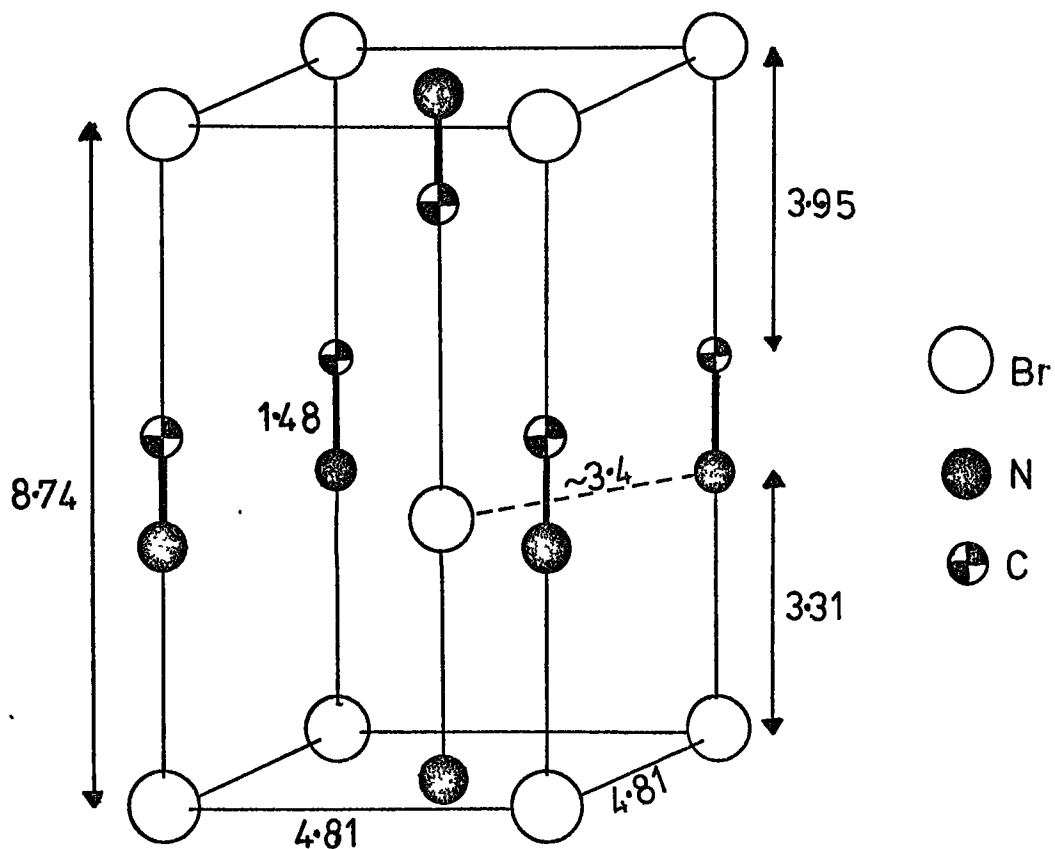


Fig. (4.3) Structure of  $\alpha'\text{-CH}_3\text{NH}_3^+\text{Br}^-$  (Distances in Å)



The bromide was also redetermined (Gabe (10)) and also found to be of space group  $P4/nmm$  with  $z = 2$ ,  $a = 4.81\text{\AA}$ ,  $c = 8.74\text{\AA}$  (c.f. Hendricks' values). This structure, of the  $\alpha'$ -phase, is slightly different from the chloride  $\alpha$ -phase, in that although the C-N bond is again sitting on a four-fold axis, there are also bromide ions on the same axis, see fig. (4.3). Considering Hendricks' and I.R. information it would seem plausible that the  $\alpha'$  iodide has a structure similar to this.

Powder photographs of the three phases of the chloride were obtained by Stammer (11) who found for the  $\alpha$ -phase  $z = 2$ ,  $a = 6.07\text{\AA}$ ,  $c = 5.07\text{\AA}$ , in good agreement with Hughes and Lipscombe. On going to the  $\gamma$ -phase the photographs became more complicated, even more so for the  $\beta$ -phase, and indexing was not possible, which indicates a lowering of symmetry.

#### c) Infra-red and Raman studies.

Early spectroscopic work was carried out by Edsall (12) who obtained Raman data for  $\text{CH}_3\text{NH}_3\text{Cl}$  in water and also for the N-deutero species in  $\text{D}_2\text{O}$ . Waldron (13) obtained I.R. spectra of the chloride and its N-deutero derivative in all three phases, and did single crystal, polarised I.R. work on the room temperature phase. Assuming  $C_{3v}$  symmetry he made assignments of the 18 internal modes and obtained reasonable agreement with a valence-field normal coordinate treatment and with the isotope product rule.

Table (4.3x) Description of modes under  $C_{3v}$  symmetry.

No	Symmetry	Description
$\nu_1$	$A_1$	Symmetric $NH_3^+$ stretch
$\nu_2$	$A_1$	Symmetric $CH_3$ stretch
$\nu_3$	$A_1$	Symmetric $NH_3^+$ bend
$\nu_4$	$A_1$	Symmetric $CH_3$ bend
$\nu_5$	$A_1$	C-N stretch
$\nu_6$	$A_2$	TORSION
$\nu_7$	E	Asymmetric $NH_3^+$ stretch
$\nu_8$	E	Asymmetric $CH_3$ stretch
$\nu_9$	E	Asymmetric $NH_3^+$ bend
$\nu_{10}$	E	Asymmetric $CH_3$ bend
$\nu_{11}$	E	Rocking
$\nu_{12}$	E	Rocking } mixed CH,NH character



Relevant facts to note from Waldron's work are as follows:

For  $C_{3v}$  symmetry there should be  $5A_1$ ,  $6E$  modes which are I.R.

allowed, and an  $A_2$  torsional mode which is forbidden. The normal mode descriptions and numbering are given in table (4.3x).

- 1) In the  $\alpha$ -phase no torsional mode is observed and the E bands, although broad, show no significant splitting, suggesting minimal field effects and no reduction of symmetry from  $C_{3v}$ .
- 2) In the  $\beta$  and  $\gamma$  phases a torsional band is observed, and the E bands split into 2 or more, with the effects most pronounced for the  $\beta$ -phase. This suggests a significant lowering of symmetry.
- 3) The N-H stretching frequencies in all phases were somewhat reduced from their non-interacting values, indicating the effect of H-bonding. See table (4.3).
- 4) The assigned  $\beta$ -phase torsional frequencies did not fit the product rule. Waldron realised this could be due to interaction of the internal and external rotations around the  $C_3$  axis, and tried a normal coordinate type treatment on these two modes. The secular determinant was solved to give two frequency roots in terms of three force constants, a procedure the same as the classical mechanical treatment in terms of barrier heights described in Chapter 1, section (3c). Had Waldron been able to obtain  $\bar{\nu}_6$  for  $CD_3NH_3^+Cl^-$  as well, he could have obtained values for all three of his force constants, but with only two pieces of information he could only make estimates.

Cabana and Sandorfy (3) studied the I.R. of the various phases of non-deuterated  $F^-$ ,  $Cl^-$ ,  $Br^-$  and  $I^-$  salts. This was the only study of the fluoride ever made; a torsional band was observed at both  $22^\circ C$  and  $-190^\circ C$  (see table (4.4)). Comparison of the N-H

stretching frequencies (Table (4.3)) with those for the  $\text{BF}_4^-$  and  $\text{BCl}_4^-$  (14) salts where little or no H-bonding occurs shows a down shift for all the halide salts indicating different degrees of H-bond interaction.

Table (4.3)

Reported N-H Stretching Frequencies for  $\text{CH}_3\text{NH}_3^+$  Salts.

N-H Stretch	$\text{F}^-$ (Room)	$\alpha\text{-Cl}^-$ (Room)	$\alpha'\text{-Br}^-$ (Room)	$\alpha'\text{-I}^-$ (Room)	CsCl soln 88°K	$\text{BF}_4^-$ (Room)	$\text{BCl}_4^-$ (Room)
Sym $\nu_1$	2740	2993	3035	3012	3045	3282	3214
Assym $\nu_7$	2573 2660	3080	3085	3098	3090	3223	3158
Ref.	3	3	3	3	20	14	14

Theoret and Sandorfy (4) then looked at the C-, N- and fully deuterated compounds and made some corrections to the assignments. Considering the  $\beta$ -phase torsional frequencies the shift for  $\text{CH}_3\text{ND}_3^+$  was seen to be much greater than for  $\text{CD}_3\text{NH}_3^+$  indicating a larger participation of the  $-\text{NH}_3^+$  end in this mode; they did not however make use of Waldron's model to calculate the three force constants. Far I.R. work on the fully protonated salts showed up rather broad lattice modes and also torsional bands for the  $\delta$ -Bromide and  $\delta$ -iodide. A summary of torsional frequencies in  $\text{cm}^{-1}$  is given in table (4.4).

Attention was drawn to a band which they assigned as the combination ( $\nu_6 + \nu_9$ ), torsion + asymmetric  $\text{NH}_3^+$  bend, which appeared in the  $\beta$  and  $\delta$  phases but not the  $\alpha$  and  $\alpha'$  phases. This is of some interest and is discussed later.

Table (4.4) Previously observed torsional bands ( $\text{cm}^{-1}$ )

	$\text{CH}_3\text{NH}_3^+$	$\text{CD}_3\text{NH}_3^+$	$\text{CH}_3\text{ND}_3^+$	$\text{CD}_3\text{ND}_3^+$
$\text{F}^-$	22°C 522 - 190°C 547			
$\gamma \text{Cl}^-$	473	458		
$\beta \text{Cl}^-$	487	475	373	347
$\beta \text{Br}^-$	449	437	357	338
$\delta \text{Br}^-$	312			
$\delta \text{I}^-$	281			

They also looked at the I.R. of isotopic solid solutions to determine the contributions of correlation and crystal field splittings in the cold phases. If a small amount of the deuterated species is mixed into the crystal of the non-deuterated species, so that statistically no two deuterated ions are next to each other, its spectra will still show crystal field effects but not correlation effects.  $\gamma$ ,  $\beta$  phases show both effects, whereas the  $\delta$  phases show strong correlation effects and the  $\delta$ -bromide shows a weak crystal field effect, but not the  $\delta$ -iodide.

The Raman spectra of the room temperature chloride as a powder (15) and the I.R. and Raman of a single crystal (16) have been obtained, though the low frequency assignments may be a little dubious.

Whalley (17) considered the effects that orientational disordering should have upon the spectra of the  $\alpha$ ,  $\alpha'$  phases and concluded that  $A_1$  bands should remain sharp, while E bands become

broadened, and points out that this is in fact observed. He quotes from the thermodynamic data (1) that the  $\gamma \rightarrow \alpha$  entropy change for the chloride is almost  $R \ln 4$  and that there is no drop of heat capacity that could be associated with the onset of free rotation.

However the  $R \ln 4$  fit may just be coincidental and clearly free rotation around the  $C_3$  axis would produce the same effect on the A and E modes.

Very recently Castellucci (20) obtained polarised I.R. and Raman spectra of  $\beta$ -,  $\gamma$ -  $\text{CH}_3\text{NH}_3^+\text{Cl}^-$  and also the I.R. of its solid solution in CsCl at room temperature and  $\sim 88^\circ\text{K}$ . He attempted to determine possible factor groups for the  $\beta$ ,  $\gamma$  phases using the observed splittings and obtained:

$\beta$ -phase	$D_{2h}$	orthorhombic	8 ions/primitive cell on sites with no symmetry
$\gamma$ -phase	$C_{2h}$	monoclinic	centrosymmetric

His polarised I.R. frequencies in  $\text{cm}^{-1}$  for the torsional mode are 486.4 ( $\beta$ ) and 467 ( $\gamma$ ) c.f. Sandorfy (3,4) 487 ( $\beta$ ), 473 ( $\gamma$ ).

However the Raman torsional frequency, obtained only for the  $\beta$ -phase, at a  $90^\circ$  scatter angle is considerably lower at  $471 \text{ cm}^{-1}$ . The solution (CsCl) at low temperature showed single, sharp bands. The torsional frequency was not seen, but estimated as  $517.5 \text{ cm}^{-1}$  from a band assigned as  $(\nu_6 + \nu_9)$ . At room temperature however all the bands were very weak and broad which Castellucci suggests indicates large amplitude motions over the rotation axes, whereas at  $88^\circ\text{K}$  the ion is strongly hindered. Considering the N-H stretching frequencies H-bonding is still important.

Normal coordinate calculations on the internal modes, but excluding the torsion have been done (18,19).

d) N.M.R. studies.

A number of papers on N.M.R. studies by line width, relaxation time and second moments have appeared in rapid succession (5, 21, 22, 23, 6) all on the chloride, except for a brief mention of the Bromide and Iodide by Tsau and Gilson (5). The most recent, very comprehensive study, including the C-, N- deuterio species, by Albert and Ripmeester (6) gives the present sum of knowledge. Static ( $T_1$ ) and rotating ( $T_{1p}$ ) frame spin-lattice relaxation times and second moments data were used. The relevant apparent facts are:-

$\beta$ -phase Both groups ( $\text{CH}_3$ ,  $\text{NH}_3^+$ ) undergo reorientations, but the  $\text{CH}_3$  is most mobile.

$\gamma$ -phase Again both groups reorientate, but the  $\text{CH}_3$  considerably more so and  $\text{NH}_3$  reorientation only gains importance as the temperature increases. Broadline spectra of  $\text{CH}_3\text{NH}_3^+\text{Cl}^-$  and  $\text{CH}_3\text{ND}_3^+\text{Cl}^-$  at 77°K show  $\text{CH}_3$  reorientating and  $\text{NH}_3^+$  rigid.

$\alpha$ -phase Both groups appear free to rotate and correlation times are short indicating the motion is fast. The measurements were insensitive to motions of the groups relative to each other. It is suggested that the observed spectrum is due to more or less whole ion rotation relative to the lattice.

Activation energy barriers have been calculated by several of the workers. In the case of  $\gamma$ ,  $\beta$  this was done for each end separately. Average values indicated in kcal/mole are given in table (4.5). Charge shift in the  $\beta$ -phase placing more + ve charge on the C has been suggested (3,6), as a possible explanation of why the  $\beta$  phase  $-\text{NH}_3$  barrier is lower than the  $\gamma$  whereas the  $\text{CH}_3$  barrier is moderately large.

Table (4.5)

N.M.R. Activation Energies, (kcal/mole)

	$\text{CH}_3^-$	$-\text{NH}_3^+$
$\alpha$	$\underbrace{\hspace{10em}}$ 1 For whole ion $\text{C}_3$ rotation in lattice	
$\gamma$	2	7.5
$\beta$	4.5	6

However from the consideration of the present work in which the two external and internal barriers are treated separately, it would seem that the two activation energies derived in these N.M.R. studies involve quite complicated contributions from the different motions of the whole system (i.e. the N.M.R. picture is of the overall effect observed at each end of the molecule).

c) N.Q.R.

A recent nitrogen N.Q.R. investigation (24) has indicated that the electronic charge occupations in the tetrahedral orbitals around the nitrogen are very nearly equal. The N-C bond has slightly less charge than the N-H's.

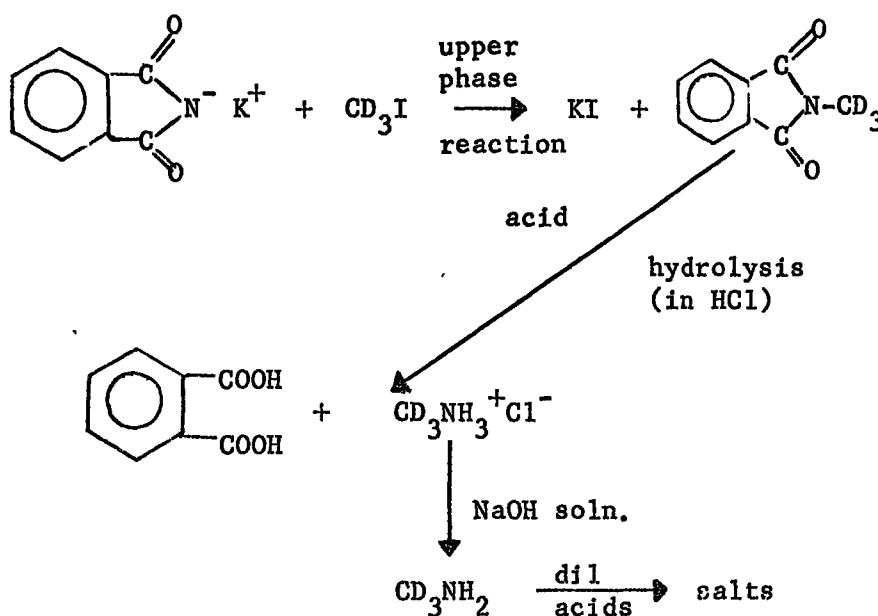
## Section 2. Experimental.

In all, twelve salts are discussed consisting of pairs of the following ions:

<u>Cations</u>	<u>Anions</u>
$\text{CH}_3\text{NH}_3^+$	$\text{Cl}^-$
$\text{CD}_3\text{NH}_3^+$	$\text{Br}^-$
$\text{CH}_3\text{ND}_3^+$	$\text{I}^-$
	$\text{PF}_6^-$

Nearly all the salts were kindly prepared by Dr C.J. Ludman and his assistants.

The  $\text{CH}_3\text{NH}_3^+$  and  $\text{CD}_3\text{NH}_3^+$  halide salts were prepared by passing  $\text{CH}_3\text{NH}_2$  or  $\text{CD}_3\text{NH}_2$  gas into dilute solutions of the appropriate acids, the amines being first produced by the action of caustic soda solution on a solution of their chloride salt. After neutralisation of all the dilute acid the salt solutions were evaporated to dryness. Salts prepared in this way were found to be quite pure spectroscopically.  $\text{CD}_3\text{NH}_3^+\text{Cl}^-$  was initially prepared by the method of Cox and Warne (28), the basic reactions of which are described very briefly in the scheme below:-



The  $\text{CH}_3\text{ND}_3^+$  salts were obtained from the corresponding  $\text{CH}_3\text{NH}_3^+$  salts by repeated dissolution in and evaporation from  $\text{D}_2\text{O}$ , until their spectra showed that the substitution was complete.

The  $\text{PF}_6^-$  salts were rather more difficult to prepare.  $\text{HPF}_6$  as a 60% solution was available but this contains an appreciable amount of HF impurity. The bifluoride salt which this would have produced would be rather difficult to remove and hence another method of preparation was used:- All operations were carried out on a vacuum line.  $\text{CH}_3\text{NH}_3^+\text{Cl}^-$  (or  $\text{CD}_3\text{NH}_3^+\text{Cl}^-$ ) was dissolved in liquid HCl at  $-95^\circ\text{C}$  (toluene slush bath) and then frozen to  $-196^\circ\text{C}$ . Excess  $\text{PF}_5$  was then frozen in. The reaction vessel was then warmed up again to  $-95^\circ\text{C}$ . The mixture reacted at some stage in the warming process to produce  $\text{PF}_6^-$  ions as follows:-



$\text{CH}_3\text{NH}_3^+\text{PF}_6^-$  is not soluble in HCl liquid and so this precipitated out leaving  $\text{PCl}_2\text{F}_3$  and excess  $\text{PF}_5$  in solution. The HCl and  $\text{PF}_5$  were pumped off at  $-95^\circ\text{C}$  and then the  $\text{PCl}_2\text{F}_3$  while warming up the vessel, leaving the desired product.

Once this salt has been prepared it can be handled without trouble in water and in fact the  $\text{CH}_3\text{ND}_3^+\text{PF}_6^-$  salt was prepared by repeatedly dissolving and evaporating the  $\text{CH}_3\text{NH}_3^+\text{PF}_6^-$  salt in  $\text{D}_2\text{O}$ .

All the salts are hygroscopic and hence were vacuum dried for several hours before use, and then were handled at all times in a dry box. Samples for the I.N.S. study were all sealed in thin silica cans.



Near and far I.R. spectra of nujol mulls and I.N.S. spectra of the powders were obtained for all the salts, although studies of the different phases were restricted somewhat by the conditions imposed by the various pieces of equipment available. Obtaining room and liquid nitrogen temperature I.R. spectra presented no problems, but attempts to produce phases at intermediate temperatures (e.g. the  $\gamma$ -phase chloride) by warming from liquid nitrogen temperatures and then recooling proved fruitless.

Beryllium filter I.N.S. spectra were obtained at temperatures approaching that of liquid nitrogen and hence gave the  $\beta$ -phase for the chlorides and  $\delta$ -phase for the iodides. The bromide proved rather difficult in that the  $\text{CH}_3\text{NH}_3^+\text{Br}^-$  salt first gave the spectrum of the  $\beta$ -phase but  $\text{CD}_3\text{NH}_3^+\text{Br}^-$  clearly gave a mixture of both  $\beta$  and  $\delta$  phases. When the spectrum of the  $\text{CH}_3\text{NH}_3^+\text{Br}^-$  salt was repeated at a later stage under identical conditions, it too produced a mixture of  $\delta$  and  $\beta$ . The possibility of a similar mixture in the case of the spectrum of  $\text{CH}_3\text{ND}_3^+\text{Br}^-$  is discussed later.

Time-of-flight spectra obtained using the 6H or 4H5 spectrometers at ambient temperatures had been obtained previously for the salts  $\text{CH}_3\text{NH}_3^+\text{Cl}^-$ ,  $\text{I}^-$  and  $\text{CH}_3\text{ND}_3^+\text{Br}^-$ ,  $\text{I}^-$  by Dr R.E. Ghosh, but had not been analysed. In the present work ambient temperature spectra for the remaining salts were obtained, and then using the variable cold temperature sample changer the I.N.S. spectra set out in Table 4.6 were also obtained on 6H.

The apparent phase as determined by a comparison with the beryllium filter data is also indicated. The higher of the two temperatures in the cases of the chlorides was an attempt to produce the  $\gamma$  phase; unfortunately there was no way of ascertaining the phase

Table (4.6)

Compound	Temperature °K	Resultant phase
$\text{CH}_3\text{NH}_3^+\text{Cl}^-$	219	$\gamma$
"	199	$\beta$
$\text{CD}_3\text{NH}_3^+\text{Cl}^-$	216	Supercool $\alpha$
"	255	$\beta$
$\text{CH}_3\text{ND}_3^+\text{Cl}^-$	200	Supercool $\alpha$
"	243	$\beta$
$\text{CH}_3\text{NH}_3^+\text{Br}^-$	207	$\beta$
$\text{CD}_3\text{NH}_3^+\text{Br}^-$	189	$\beta$
$\text{CH}_3\text{ND}_3^+\text{Br}$	189	$\beta$
$\text{CH}_3\text{NH}_3^+\text{I}^-$	199	$\delta$

at the time of the experiment and the final spectra proved to be of the supercooled  $\alpha$  phase for the  $\text{CD}_3\text{NH}_3^+$  and  $\text{CH}_3\text{ND}_3^+$  salts. The spectrum of the  $\text{CH}_3\text{NH}_3^+\text{Cl}^-$  salt at  $219^\circ\text{K}$  could not be assigned to either the  $\alpha$  or  $\beta$  phase, and hence must represent the  $\gamma$ -phase.

It would be interesting and useful to obtain Raman spectra of the cold phases when equipment becomes available. Only the room temperature  $\alpha$ -phase Raman spectrum of the  $\text{CH}_3\text{NH}_3^+\text{Br}^-$  salt was obtained after the recent acquisition of a spectrometer. Apart from this displaying a very good example of the broad E and sharp A bands discussed by Whalley (17) no further information relevant to the torsions was obtained to complement the I.R. and I.N.S. work.

### Section 3. Assignment of Spectra.

The optical spectra are not discussed in full here, their main purpose being to help as guides to the location of the torsional mode

frequencies in the I.N.S. spectra. Their salient features are described generally and any points of special interest are discussed.

a) Near I.R. Spectra:-

The near I.R. frequencies of the halides, including the cold phase torsional bands, are found to be in general agreement with Sandorfy's work (3,4) with the exception of the torsional mode of  $\beta$ - $\text{CH}_3\text{ND}_3\text{Br}$  which is observed lower at  $\sim 340 \text{ cm}^{-1}$  (v.w). Spectra of the  $\delta$ -bromides were not obtained, but the torsional bands of the  $\delta$   $\text{CH}_3\text{NH}_3^+\text{I}^-$  and  $\text{CD}_3\text{NH}_3^+\text{I}^-$  salts are observed at 279 and  $263 \text{ cm}^{-1}$  respectively, and are quite broad compared to the torsional bands seen for the  $\beta$ -chlorides and bromides. The equivalent band in the  $\delta$   $\text{CH}_3\text{ND}_3^+\text{I}^-$  salt would be expected below the range of the P.E. 457 and, none of the weak  $\delta$ -phase torsions are seen in the F.S.720 spectra.

The spectra of the  $\text{PF}_6^-$  salts do not show any drastic changes in appearance, which might indicate no phase changes on cooling to liquid nitrogen temperatures, although the bands sharpen up a little and some very slight frequency increases are observed. As expected, the  $\nu_1$  and  $\nu_7$  N-H stretching bands are above  $3000 \text{ cm}^{-1}$  in the  $\text{PF}_6^-$  salts and are quite sharp indicating the absence of H-bonds. Four frequencies appear in this region for the  $\text{CH}_3\text{NH}_3^+\text{PF}_6^-$  salt:-

{	3315	m. broad
{	3269	m. sharp shoulder
{	3212	w.
{	3190	w.

Exactly which pair corresponds to  $\nu_1$  and  $\nu_7$  would require further investigation, but the point is emphasised that the system is not H-bonded, by a favourable comparison with the frequencies of  $\text{BF}_4^-$  and  $\text{BCl}_4^-$  salts given in table (4.3). No torsional bands are in evidence in the  $\text{PF}_6^-$  salts spectra. The frequencies of the interesting ( $\nu_6 + \nu_9$ ) I.R. band as observed in the present work for the cold phases, and the values of  $\nu_9$  and  $\nu_6$  where these have been sorted out, are given in table (4.7) below:-

Table (4.7) The ( $\nu_6 + \nu_9$ ) torsion and asymmetric  $\text{NH}_3$  bend combination band. (I.R. data)

Salt	( $\nu_6 + \nu_9$ ) $\text{cm}^{-1}$	$\nu_9$ $\text{cm}^{-1}$	Predicted $\nu_6$ $\text{cm}^{-1}$	Observed $\nu_6$ $\text{cm}^{-1}$
$\beta\text{CH}_3\text{NH}_3^+\text{Cl}^-$	2070	1610	460	487
$\beta\text{CD}_3\text{NH}_3^+\text{Cl}^-$	2069	1612	457	475
$\beta\text{CH}_3\text{ND}_3^+\text{Cl}^-$	1510 ?	1170 ?	340	373
$\beta\text{CH}_3\text{NH}_3^+\text{Br}^-$	2020	1600	420	449
$\delta\text{CH}_3\text{NH}_3^+\text{I}^-$	1820	1560	260	279
$\delta\text{CD}_3\text{NH}_3^+\text{I}^-$	$\sim 1840$ ?	1560	280 ?	263

As can be seen the predicted frequency is in the right area and in the cases of the  $\beta$ -phases falls consistently below the observed frequency. In the room temperature phases several of the authors (3,4,13) have observed weak bands in the region of  $1800\text{-}1900\text{cm}^{-1}$  for the  $\text{CH}_3\text{NH}_3^+$  and  $\text{CD}_3\text{NH}_3^+$  salts which they have variously assigned as combinations and

overtones, but never suggested the possibility that it might be  $(\nu_6 + \nu_9)$ . These bands are seen in the present spectra and are rather broad and not very strong. They appear strongest in the chlorides and bromides and only very weakly in the iodide. The possibility that these may in fact be the  $(\nu_6 + \nu_9)$  band is discussed later but their approximate band centre frequencies, and  $\nu_9$  are listed and subtracted below.

Table (4.8) Frequencies of  $\nu_9$  and a possible  $(\nu_6 + \nu_9)$  combination in  $\text{cm}^{-1}$  for the room temperature halides. (I.R.)

Salt	Combination	$\nu_9$	Difference
$\alpha\text{CH}_3\text{NH}_3^+\text{Cl}^-$	~ 1890 w	~ 1570	320
$\alpha\text{CD}_3\text{NH}_3^+\text{Cl}^-$	~ 1885 m.w	~ 1570	315
$\alpha'\text{CH}_3\text{NH}_3^+\text{Br}^-$	~ 1850 w	1568	282
$\alpha'\text{CD}_3\text{NH}_3^+\text{Br}^-$	~ 1840 m.w	1568	272
$\alpha'\text{CD}_3\text{NH}_3^+\text{I}^-$	~ 1800 v.w	1550	250

b) Far I.R. Spectra.

All the far I.R. spectra show broad strong absorptions between  $250 \rightarrow 80\text{cm}^{-1}$ .

Factor group analyses for the lattice modes of the  $\alpha$ -chloride and  $\alpha'$ -bromide using the X-ray data predict in both cases 3 I.R. bands and 5 Raman:

$\alpha$   $\text{CH}_3\text{NH}_3^+\text{Cl}^-$  has C, N on Wyckoff sites (c) and Cl on sites (a) or (b)

$$T_{\text{ACOUSTIC}} = A_{2u} + E_u$$

$$T_{\text{OPTIC}} = \frac{A_{1g} + B_{1g} + 2Eg}{\text{Raman}} + \frac{A_{2u} + E_u}{\text{I.R.}}$$

$$\text{ROTATIONAL} = A_{2g} + \frac{Eg}{\text{Raman}} + A_{1u} + \frac{E_u}{\text{I.R.}}$$

The rotation coaxial with the torsion consists of  $A_{2g} + A_{1u}$  (inactive), leaving  $Eg + E_u$  for the end-over-end librations.

$\alpha'$   $\text{CH}_3\text{NH}_3^+\text{Br}^-$  has C, N and Br on Wyckoff sites (c)

$$T_{\text{ACOUSTIC}} = A_{2u} + E_u$$

$$T_{\text{OPTIC}} = \frac{2A_{1g} + 2Eg}{\text{Raman}} + \frac{A_{2u} + E_u}{\text{I.R.}}$$

$$\text{ROTATIONAL} = A_{2g} + \frac{Eg}{\text{Raman}} + A_{1u} + \frac{E_u}{\text{I.R.}}$$

The  $\alpha'$  iodides very clearly show three I.R. bands, whereas the bromide and chloride show only two with certainty, although the third may be masked. In general the halide spectra present a strong absorption centre on the higher frequency side of the whole broad region, with the other weaker centres at lower frequency. On cooling to liquid nitrogen temperatures the only prominent change in the halide spectra is that the higher frequency absorption increases in intensity relative to the

others (It has been assumed that like the cold spectra obtained on the P.E.457 the phases obtained for the chlorides and bromides in the far I.R. spectra are probably the  $\beta$ -phases). The  $\text{PF}_6^-$  salts present only one very strong and broad band centred  $\sim 130\text{cm}^{-1}$ .

In all cases very little if any down shift in frequency can be seen on deuteration, and indeed no drastic shift would be expected for translational lattice modes and the degenerate end-over-end librations of the whole ion. Frequencies are included in tables (4.9 - 4.13).

c) The Raman Spectrum of  $\alpha'$ - $\text{CH}_3\text{NH}_3^+\text{Br}^-$ .

At the low frequency end of this spectrum the 5 predicted bands do appear, although one is only hinted as a shoulder on the strongest peak. None of the bands are very strong:-

133	sh }	m.w	
130	}		
108	broad v.w		$\text{cm}^{-1}$
69	broad v.w		
33	w		

This one spectrum is very useful in that since the end-over-end librations are predicted as active in both I.R. and Raman, the higher frequency I.R. band at  $\sim 170\text{cm}^{-1}$  for this compound is therefore not likely to be a librational band unless the modes are strongly split. Furthermore the I.R. bands go no further down than  $100\text{cm}^{-1}$  and the Raman no higher than  $133\text{cm}^{-1}$  and so the librations probably lie in the  $100\text{-}130\text{cm}^{-1}$  region.

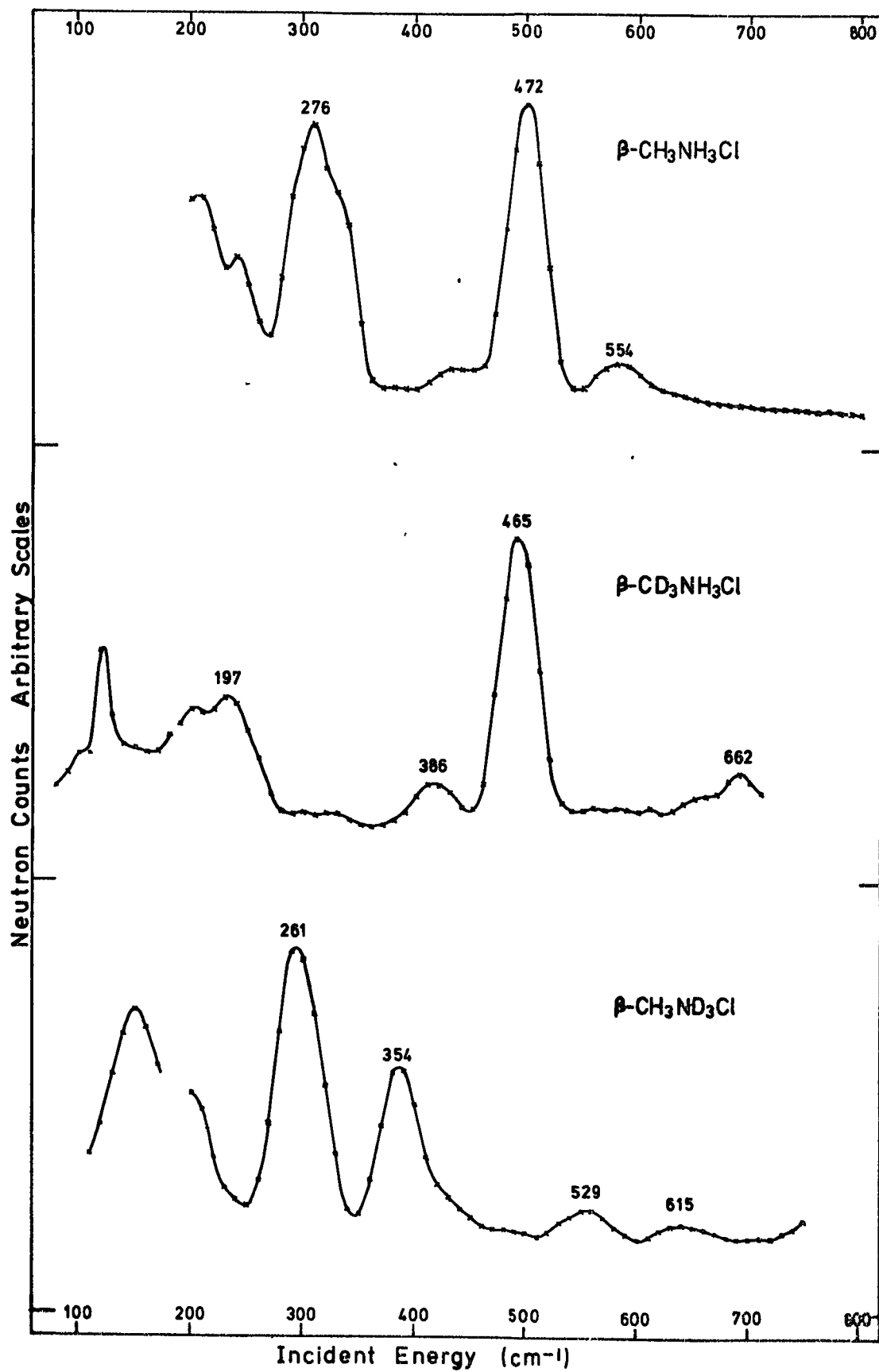
d) I.N.S. Spectra

The assignment of the cold phase spectra is clearer than for the room temperature phases and hence is dealt with first. For cases where the external barriers are quite high one might expect to see two peaks as was the case with the hydraziniums, with frequencies dependent on the three barrier heights and the moments of inertia of the tops (Chapter 1, Section 3).

(i) Beryllium filter spectra of the chlorides and bromides:

Considering first the spectra of the chloride salts: As seen from the I.R. studies one of the torsion-libration bands is active and the manner of the shifts on deuteration have indicated that the mode involves mainly  $-\text{NH}_3^+$  motion. The beryllium filter spectra shown in fig. (4.4) confirm this assignment. Although the frequencies of these strong bands are somewhat below the I.R. values it is interesting that the one known Raman frequency (20) is in agreement. The  $\text{CH}_3\text{NH}_3^+$  and  $\text{CH}_3\text{ND}_3^+$  cases also clearly show another intense beryllium filter band which is still well clear of the far I.R. bands, and can only reasonably be assigned as the remaining torsion-libration. The location of this band for the  $\text{CD}_3\text{NH}_3^+$  case is not immediately apparent, as no very intense band appears to lower frequency. Two very relevant points about the effects of deuteration should be made here:- (a) with respect to the higher frequency peak N-deuteration produces a much greater shift than C-deuteration, and Sandorfy (4) suggested that if the lower frequency could be observed this pattern would probably be reversed. It is easily seen that the lower  $\text{CH}_3\text{ND}_3^+$  peak is not much shifted below that of  $\text{CH}_3\text{NH}_3^+$  and that a larger shift for  $\text{CD}_3\text{NH}_3^+$  could well place it



Fig. (4.4) Beryllium filter spectra of the  $\beta$ -chlorides.

below  $200\text{ cm}^{-1}$  overlapping with the I.R. frequencies. (b) If the higher frequency is mainly an  $-\text{NH}_3^+$  motion then N-deuteration should reduce its intensity relative to the lower peak, which is in fact observed. Likewise the lower frequency being largely a  $-\text{CH}_3$  motion should reduce in intensity relative to the higher peak upon C-deuteration, which would explain why this band does not stand out for  $\text{CD}_3\text{NH}_3^+\text{Cl}^-$ .

The  $\text{CD}_3\text{NH}_3^+\text{Cl}^-$  spectrum also shows a weak feature at  $386\text{ cm}^{-1}$  which has no optical counterpart and is most probably the overtone of the lower torsion-libration. Half this value would place the main peak at  $193\text{ cm}^{-1}$  and the beryllium filter spectrum rises to a point at  $\sim 197\text{ cm}^{-1}$  on the high frequency edge of the broad band. This would fit quite well with the shift and intensity arguments, and is therefore assigned as the lower torsion-libration.

At the lower frequency end of the  $\text{CH}_3\text{NH}_3^+\text{Cl}^-$  spectrum the intensity increases to a peak at  $170\text{ cm}^{-1}$ . The equivalent of the strongest far I.R. band at  $215\text{ cm}^{-1}$  is only weakly in evidence. The I.N.S. spectrum of  $\text{CH}_3\text{ND}_3^+\text{Cl}^-$  does not even show the equivalent I.R. band at  $\sim 190\text{ cm}^{-1}$ . Hence if the strong I.R. band at  $\sim 190\text{ cm}^{-1}$  for  $\text{CD}_3\text{NH}_3^+\text{Cl}^-$  does not show up strongly in the I.N.S. then the  $197\text{ cm}^{-1}$  I.N.S. band has no optical counterpart; further evidence for its assignment as the lower torsion-libration frequency.

Having shown that the higher band is associated mainly with  $-\text{NH}_3^+$  motion and the lower one mainly  $\text{CH}_3$  motion, it can be qualitatively said at this stage that the barrier at the  $-\text{NH}_3^+$  end is larger than at the  $-\text{CH}_3$  end.

Since the two modes which would have been a pure torsion  $\nu_6$  and a pure libration ( $R_z$ ) are obviously intermixed, the following labelling

Table (4.9)

Frequencies of the  $\beta$ -phase methylammonium chlorides ( $\text{cm}^{-1}$ )

	I.R.	I.N.S.		Assignment
		T. of F.	Be-filter	
$\text{CH}_3\text{NH}_3^+\text{Cl}^-$	<u>487</u> v.w  215 v.s  ~ 140 m ~ 125 m	~ <u>460</u> v.s  ~ <u>275</u> v.s  ~ 170 s  <u>115</u> v.s ~ 75 m.sh	554 w <u>472</u> v.s ~ 406 v.w { ~ 300 w.sh <u>276</u> v.s  { ~ 203 w.sh 170 m.s	2x $\nu_{\text{ctor}}$ $\nu_{\text{ntor}}$  $\nu_{\text{ctor}}$  } Lattice Modes  $\nu_{\text{elib}}$ Lattice Mode
$\text{CD}_3\text{NH}_3^+\text{Cl}^-$	<u>475</u> v.w  190 v.s  ~ 140 v.w	{ ~ <u>470</u> v.s ~ 350 w.sh ~ <u>195</u> m.s  ~ 150 m.sh  <u>105</u> m.s ~ 75 m.sh	662 w <u>465</u> v.s 386 m.w <u>197</u> m.s  ~ 169 m  (~ 95 m?)	$\nu_{\text{ntor}} + \nu_{\text{ctor}}$ $\nu_{\text{ntor}}$ 2x $\nu_{\text{ctor}}$ $\nu_{\text{ctor}}$  } Lattice Modes  $\nu_{\text{elib}}$ Lattice Mode
$\text{CH}_3\text{ND}_3^+\text{Cl}^-$	<u>373</u> v.w  190 v.s  140 w	~ <u>340</u> m ~ <u>260</u> s  ~ 165 m ~ 135 m <u>106</u> v.s ~ 70 v.w.sh	615 v.w.brd ~ 528 w.brd <u>354</u> s <u>261</u> v.s  (~ <u>110</u> m.s?)	$\nu_{\text{ntor}} + \nu_{\text{ctor}}$ 2x $\nu_{\text{ctor}}$ $\nu_{\text{ntor}}$ $\nu_{\text{ctor}}$  } Lattice Modes  $\nu_{\text{elib}}$ Lattice Mode

scheme has been adopted for the halide salts:-

$$\begin{aligned} \nu_{\text{NTOR}} &= \text{higher frequency torsion-libration} \\ \nu_{\text{CTOR}} &= \text{lower frequency} \quad " \quad " \end{aligned}$$

(and the end-over-end librations in all cases will be labelled  $\nu_{\text{ELIB}}$ ).

The assigned frequencies for the  $\beta$ -chlorides appear in table (4.9).

All the spectra show weaker bands at frequencies higher than the torsion-libration bands which could correspond with combinations of these modes or overtones. (The total percentage scatter, which can be obtained from the time of flight data indicates that double scattering should not be a significant factor). It could be mentioned in passing that in an earlier survey scan on  $\beta\text{-CD}_3\text{NH}_3^+\text{Cl}^-$  the spectrum was obtained up to about  $850 \text{ cm}^{-1}$ . No intense bands were observed until a medium one at  $787 \text{ cm}^{-1}$  which corresponds well with the I.R. bands of the  $\nu_{12}$   $\text{CD}_3$  rocking mode. The fact that this is moderately strong must mean that some mixing with other modes has occurred, bringing in proton motions.

A finer detail of the torsion-libration bands of considerable interest is their bandwidth (F.W.H.M.) - see table (4.14). In fact the lower band  $\nu_{\text{CTOR}}$  of  $\beta\text{-CH}_3\text{NH}_3^+\text{Cl}^-$  shows a definite shoulder on its higher frequency side at  $\sim 295 \text{ cm}^{-1}$ . The same band in  $\text{CH}_3\text{ND}_3^+\text{Cl}^-$  shows a significant broadening with the weight to higher frequency. All three salts have a bandwidth for the higher frequency  $\nu_{\text{NTOR}}$  which is only slightly greater than for the values seen in the hydrazinium chloride, c.f. table (3.10).

Table (4.14) F.W.H.M. in  $\text{cm}^{-1}$  for the torsion-libration bands of the  $\beta$ -chlorides.

Cation	$\nu_{\text{CTOR}}$ Lower Frequency Band	$\nu_{\text{NTOR}}$ Higher Frequency Band
$\text{CH}_3\text{NH}_3^+$	62	41
$\text{CD}_3\text{NH}_3^+$	unresolved	42
$\text{CH}_3\text{ND}_3^+$	49	44

Unfortunately the  $\nu_{\text{CTOR}}$  band in  $\text{CD}_3\text{NH}_3^+\text{Cl}^-$  overlaps on its lower frequency side with other bands, but the higher frequency side shows a considerable broadening (see fig. (4. 4 )). This effect, probably due to asymmetry, is discussed later.

Considering now the  $\beta$ -bromide beryllium filter spectra the same patterns are repeated at slightly lower frequencies except that as mentioned earlier complications arise due to the co-existence of the  $\delta$ -phase. Spectra are shown in figs.(4,5,6 ), frequencies in table (4.10). The first run on  $\text{CH}_3\text{NH}_3^+\text{Br}^-$  showed pure  $\beta$  and is almost an exact copy of the chloride spectrum. The shoulder on the lower band is perhaps a little clearer. (The second run shows the strong  $\delta$  phase torsion-libration( $\nu_{\text{NTOR}}$ ) band overlapping this region, peaking at  $305 \text{ cm}^{-1}$  in good agreement with the I.R. value of  $312 \text{ cm}^{-1}$ ).

$\text{CD}_3\text{NH}_3^+\text{Br}^-$  shows the strong  $\beta$ -phase higher frequency  $\nu_{\text{NTOR}}$  at  $427 \text{ cm}^{-1}$  and a strong broad band centred  $\sim 156 \text{ cm}^{-1}$ . The weak band assumed to be the overtone of the lower torsion-libration mode ( $2x \nu_{\text{CTOR}}$ ) again

Fig. (4.5) Beryllium filter spectra of the cold bromides.

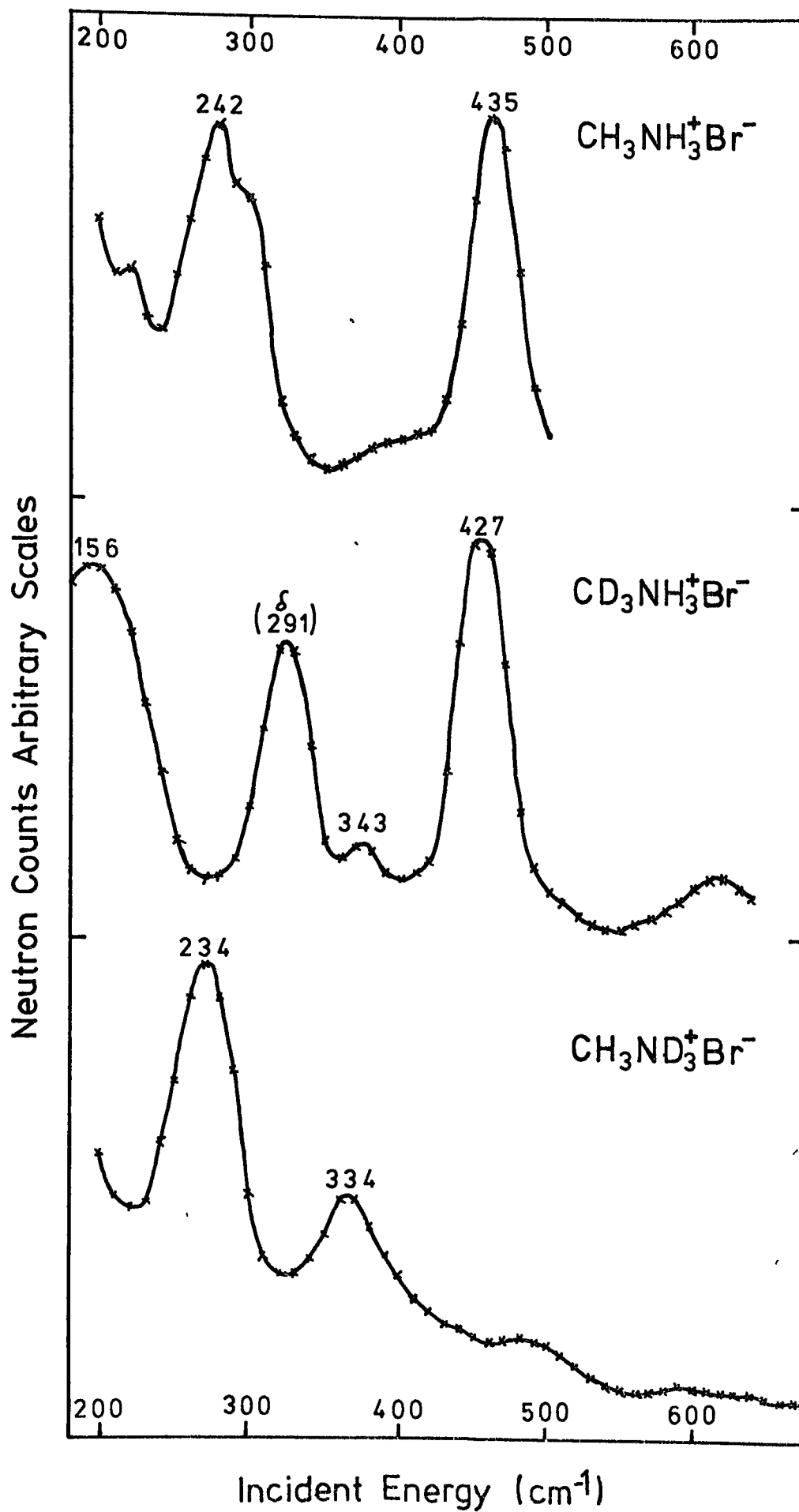


Fig. (4.6) Beryllium filter spectrum of  $\beta\text{-CH}_3\text{NH}_3^+\text{Br}^-$  complicated by the  $\delta$ -phase.  
 $\beta + \delta - \text{CH}_3\text{NH}_3\text{Br}$

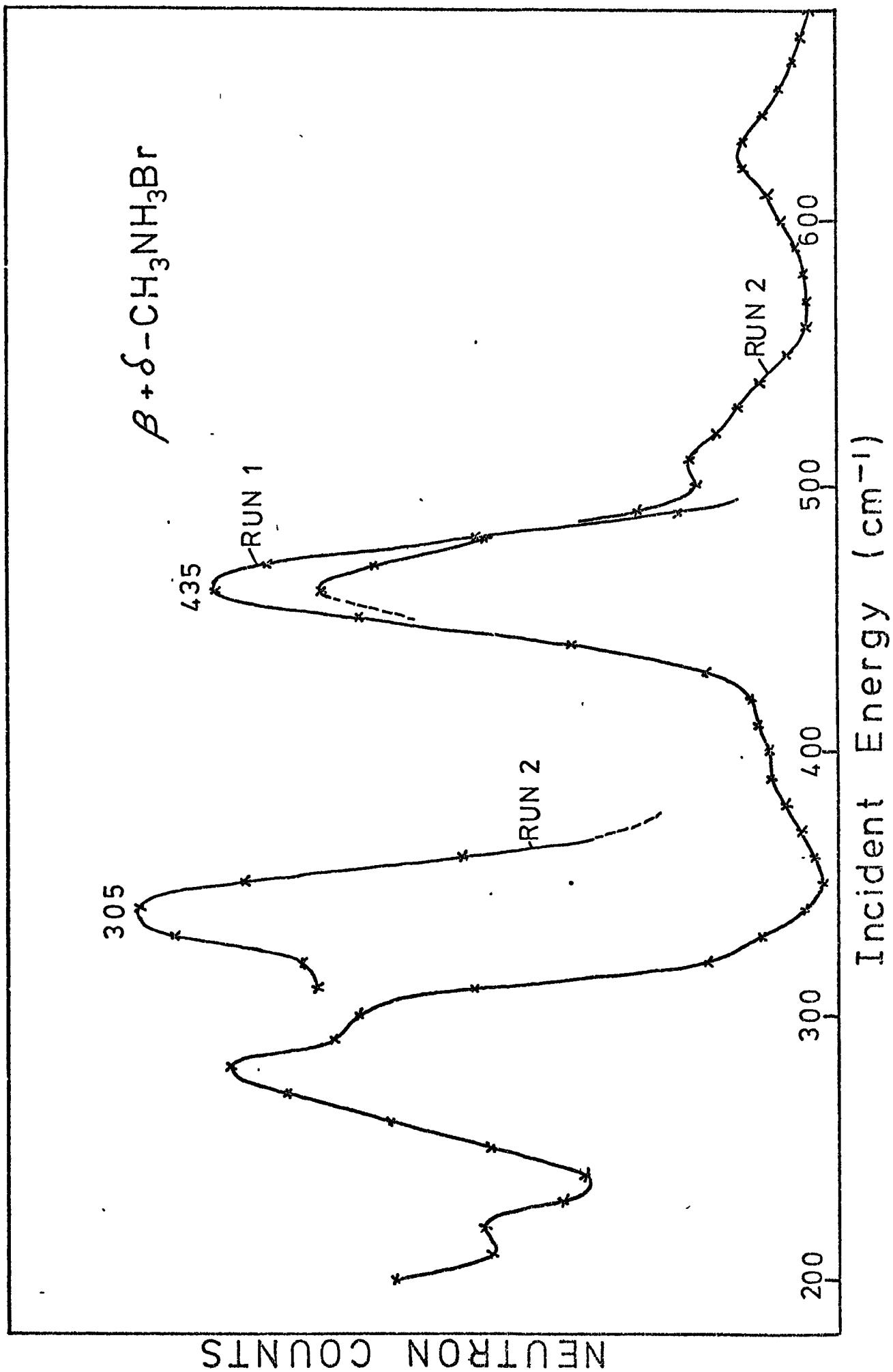


Table (4.10)

Frequencies of the  $\beta$ -phase\* methylammonium bromides ( $\text{cm}^{-1}$ )

	I.R.	I.N.S.		Assignment
		T. of F.	Be-filter	
$\text{CH}_3\text{NH}_3^+\text{Br}^-$	<u>449</u> v.w (312) 177 v.s 125 w	$\sim$ <u>440</u> m, brd  $\sim$ <u>245</u> v.s  $\sim$ 140 m.s  <u>113</u> s 50 m.w	(600 w) 480 w, sh <u>435</u> v.s 361 w (305 v.s) 270 w, sh 242 v.s	(2x $\delta$ - $\nu_{\text{ntor}}$ ) 2x $\nu_{\text{ctor}}$ $\nu_{\text{ntor}}$ ( $\delta$ - $\nu_{\text{ntor}}$ ) $\nu_{\text{ctor}}$ Lattice Modes $\nu_{\text{elib}}$ Lattice Mode
$\text{CD}_3\text{NH}_3^+\text{Br}^-$	<u>437</u> v.w 176 v.s 120 m.w	$\sim$ <u>420</u> s $\sim$ 320 w  $\sim$ <u>170</u> v.s  $\sim$ 140 sh  <u>106</u> m 48 m.w	590 w <u>427</u> v.s 343 w (291 m.s)  (156 v.s, brd)	$\nu_{\text{ntor}} + \nu_{\text{ctor}}$ $\nu_{\text{ntor}}$ 2x $\nu_{\text{ctor}}$ ( $\delta$ - $\nu_{\text{ntor}}$ ) Lattice Mode $\nu_{\text{ctor}}$ ( $\delta$ -interference) Lattice Modes $\nu_{\text{elib}}$ Lattice Mode
$\text{CH}_3\text{ND}_3^+\text{Br}^-$	$\sim$ <u>340</u> v.v.w 167 v.s 120 m	$\sim$ <u>340</u> m $\sim$ <u>235</u> s  $\sim$ 150 w } sh $\sim$ 130 m }  <u>107</u> v.s $\sim$ 45 w	459 w, brd <u>334</u> m, brd <u>234</u> v.s, brd	2x $\nu_{\text{ctor}}$ $\nu_{\text{ntor}}$ $\nu_{\text{ctor}} + (\delta$ - $\nu_{\text{ntor}}?)$ Lattice Modes $\nu_{\text{elib}}$ Lattice Mode

\* Torsion-libration bands of the  $\delta$ -phase are included in brackets where they occurred in the I.N.S. spectra.



appears at  $343 \text{ cm}^{-1}$ ; half of which is  $171 \text{ cm}^{-1}$ , covered by the broad band. There then remains another relatively strong sharp band at  $291 \text{ cm}^{-1}$  which can only be assigned to the  $\delta$ -phase  $\nu_{\text{NTOR}}$  mode. It is of relevance that the band at low frequency in the  $\beta\text{-CH}_3\text{NH}_3^+\text{Br}^-$  spectrum increases remarkably in intensity when the  $\delta$ -phase is present (see spectra) relative to the other peaks. The lower torsion-libration of the  $\delta$ -phase ( $\nu_{\text{CTOR}}$ ) may well be located in this band. This could explain the increased intensity at the low frequency of  $156 \text{ cm}^{-1}$  seen in the  $\text{CD}_3\text{NH}_3^+\text{Br}^-$  spectrum.

The spectrum of  $\text{CH}_3\text{ND}_3^+\text{Br}^-$  might at first sight seem to indicate pure  $\beta$ -phase, however a comparison with the equivalent chloride casts some doubt on this. The lower frequency has increased markedly in intensity relative to the higher, and now shows a greater broadening to lower frequency. Having seen the interference from the  $\delta$ -phase in the other salts the possibility cannot be excluded that perhaps one is seeing its  $\nu_{\text{NTOR}}$  mode at  $\sim 208 \text{ cm}^{-1}$  beneath the lower frequency side of the  $\beta$ -phase peak. Since this would be the higher of two modes the fact that it has shifted more than for  $\delta\text{-CD}_3\text{NH}_3^+\text{Br}^-$  again fits the pattern. Another odd feature of this spectrum is the shape of the higher frequency peak and its considerable broadening, which may perhaps be due to underlying combination bands of the  $\delta$ -phase.

(ii) Time-of-flight spectra of the  $\beta$ -chlorides and  $\beta$ -bromides.

The main purpose of obtaining cold temperature time-of-flight spectra (figs. 4.7 - 4.8) was to look for the remaining, possibly degenerate end-over-end type libration ( $\nu_{\text{ELIB}}$ ) since resolution of frequencies above  $\sim 200 \text{ cm}^{-1}$  is very poor. However the torsion-libration bands found in the beryllium filter spectra are found to show up quite strongly in the appropriate frequency regions and it can be ascertained

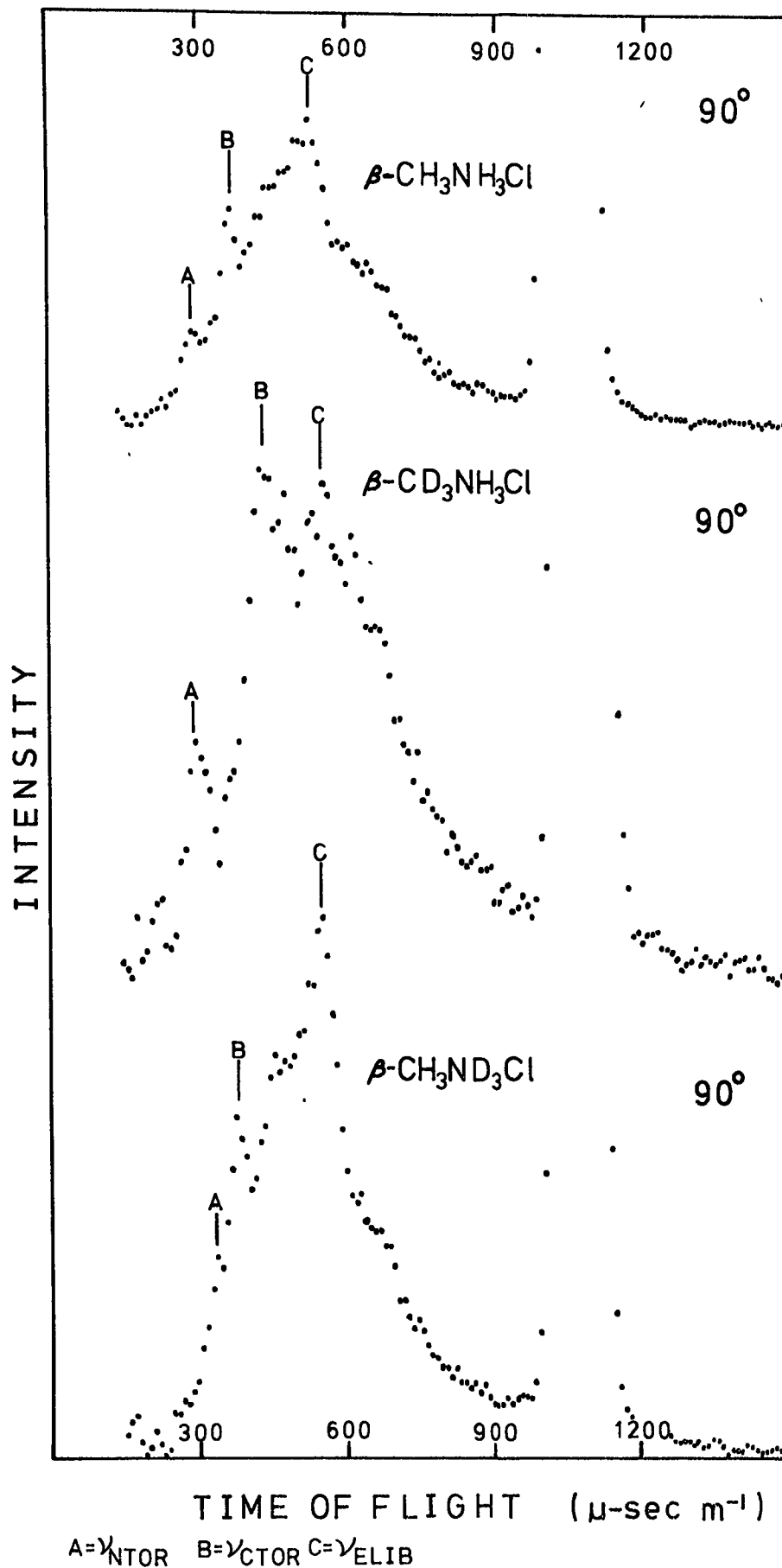
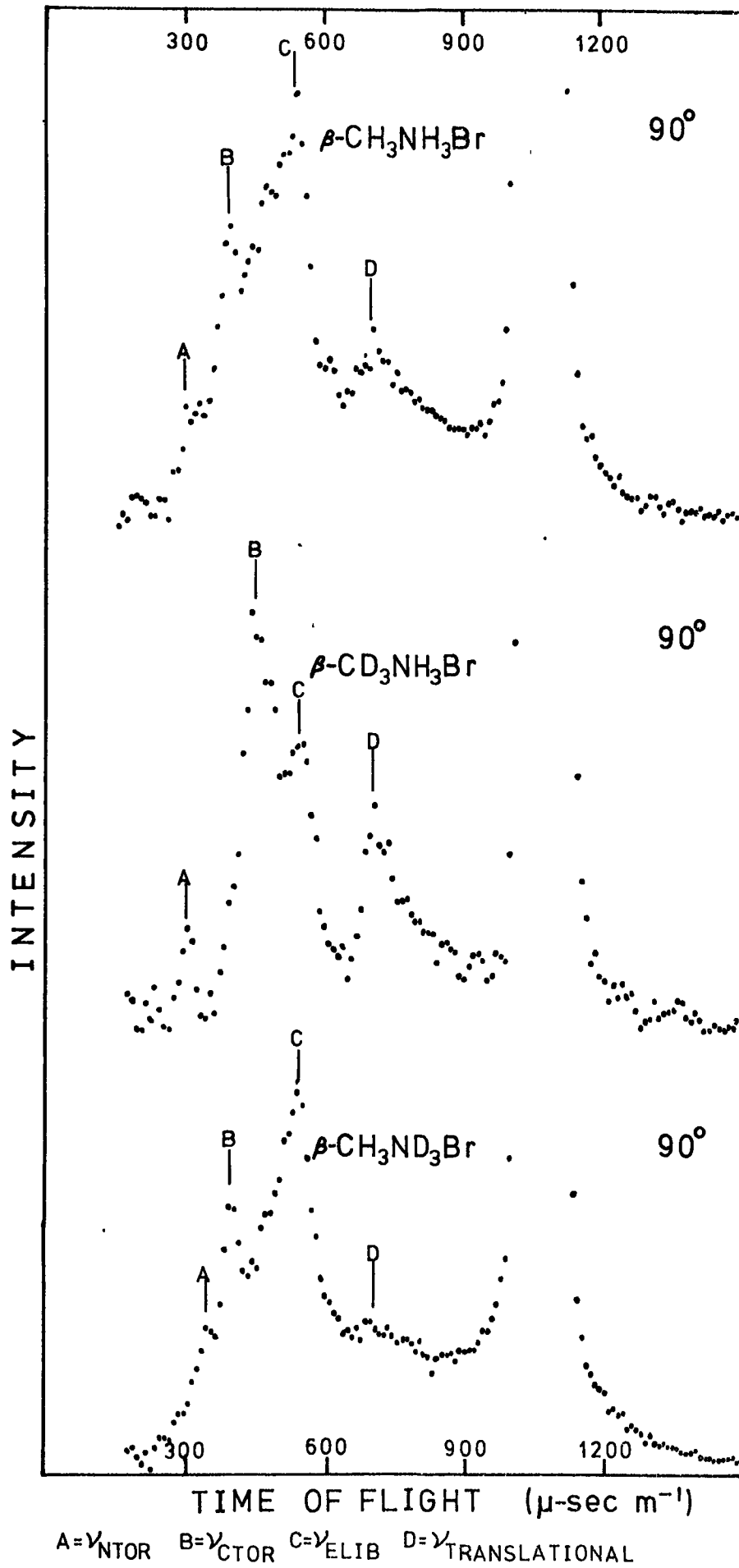
Fig. (4.7) Time-of-flight spectra of the  $\beta$ -chlorides.

Fig. (4.8) Time-of-flight spectra of the  $\beta$ -bromides.

from these, at least for  $\text{CH}_3\text{NH}_3^+$  and  $\text{CD}_3\text{NH}_3^+\text{Br}^-$ , that the  $\delta$ -phases are not seen to any appreciable amount in the spectra. In the case of  $\text{CH}_3\text{ND}_3^+\text{Br}^-$  where the  $\delta$ -phase peak may be hidden under the lower  $\beta$ -phase torsion-libration ( $\nu_{\text{CTOR}}$ ) peak the situation cannot be assessed properly, although the broadening of the  $\delta$ -phase  $\nu_{\text{CTOR}}$  band is still apparent. For the purpose of assignment it was assumed that the spectrum was principally of the  $\beta$ -phase.

A comparison of the three spectra for each halide in the 150-200  $\text{cm}^{-1}$  region shows a strong feature unique to the  $\text{CD}_3\text{NH}_3^+$  salts at  $\sim 195 \text{ cm}^{-1}$ , (chloride) and  $\sim 170 \text{ cm}^{-1}$  (bromide). This confirms the assignment of the lower torsion-libration band ( $\nu_{\text{CTOR}}$ ) of  $\text{CD}_3\text{NH}_3^+\text{Cl}^-$  and the band also shows the broadening to higher frequency. The near absence of the  $\delta$  phase in  $\text{CD}_3\text{NH}_3^+\text{Br}^-$  clearly shows that the  $\beta$ -phase  $\nu_{\text{CTOR}}$  band is at  $\sim 170 \text{ cm}^{-1}$ . This confirms that the broad band centred in the beryllium filter spectrum at  $\sim 156 \text{ cm}^{-1}$  probably involves the lower  $\delta$ -phase band, but that half the overtone band at  $343 \text{ cm}^{-1}$  is in fact a good indicator for the  $\beta$ -phase frequency.

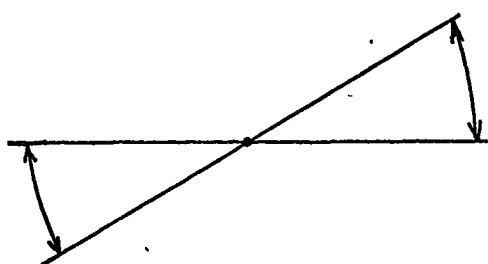
Considering now the modes to lower frequency one would expect a rather complex spectrum containing all the lattice modes and the remaining end-over-end librations. In fact all the spectra show a broad quite intense band between about 60 and 180  $\text{cm}^{-1}$ , which is least intense in the case of the  $\text{CD}_3\text{NH}_3^+$  salts. This band does in most cases show at least two peaks resolved on top of the general shape; some show a third band or a shoulder. The frequencies are listed in tables (4.9,4.10) and the comparison with the I.R. spectra shows that the strongest I.R. peak at the high frequency end does not show strongly in the I.N.S. spectrum. In fact there is very little

correspondence throughout between the two sets of frequencies, which probably means that all the I.R. frequencies show only weak I.N.S. bands.

The strongest band would once again seem the most likely candidate for the end-over-end librations ( $\nu_{\text{ELIB}}$ ). This occurs at  $\sim 115 \text{ cm}^{-1}$  for  $\text{CH}_3\text{NH}_3^+\text{Cl}^-$ , and about  $106 \text{ cm}^{-1}$  for the two deuterio species, similar values are observed for the bromide. The most interesting feature of these peaks however is their intensity relative to the rest of the spectrum. In the  $\text{CH}_3\text{NH}_3^+$  cases the relative intensity of this band is quite strong, in the  $\text{CH}_3\text{ND}_3^+$  cases it is even stronger, but in the  $\text{CD}_3\text{NH}_3^+$  cases it is much less intense. This in itself would tend to confirm the assignment on the basis of the following argument:-

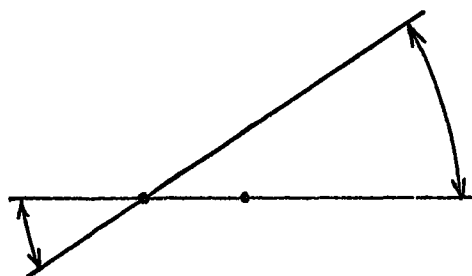
Since the fields at each end of the ion are different the centre of motion will not be at the centre of mass. The nitrogen end being tied down more will tend to move less than the carbon end, and hence the amplitude of proton motion at each end will be different. This is illustrated simply in fig.(4.9).

Symmetrical case  
(Hydrazinium salts)



Identical amplitudes

Asymmetrical case  
(Methylammonium Halides)



Non-identical amplitudes

In the I.N.S. spectrum the  $\text{CH}_3\text{ND}_3^+$  should only show the large amplitude  $-\text{CH}_3$  motion, whereas  $\text{CD}_3\text{NH}_3^+$  should only show the lower amplitude  $-\text{NH}_3^+$  motion. Relative to the peaks from translational modes in the vicinity, which should not show such effects (both scattering from 3 protons), the intensity of the librational band in the  $\text{CH}_3\text{ND}_3^+$  spectrum would be expected to be somewhat greater than in the  $\text{CD}_3\text{NH}_3^+$  spectrum. A similar comparison of this band with translational bands in the  $\text{CH}_3\text{NH}_3^+$  case should give a relative intensity which is the average of the intensities of the two deuterated species, since the comparison is of the cumulative scattering from the  $-\text{NH}_3^+$  and  $-\text{CH}_3$  motion against the translational motion of six protons.

A little below the librational band in the spectra of the bromides a weaker band appears (at  $\sim 50 \text{ cm}^{-1}$  in  $\text{CH}_3\text{NH}_3^+\text{Br}^-$ ), the equivalent band appearing as a shoulder in the chloride spectra (at  $\sim 75 \text{ cm}^{-1}$  in  $\text{CH}_3\text{NH}_3^+\text{Cl}^-$ ). This band is most likely to be a translational mode, the shift of  $\sim 25 \text{ cm}^{-1}$  being due to the change in the anion mass  $\text{Cl} \rightarrow \text{Br}$  more than anything else, and hence provides a good comparison point for the librational bands. Giving this band an intensity of unity in each case the following rough intensity ratios for the librational bands are observed:-

Table (4.15) Relative intensities of lower librational modes.

	$\text{Cl}^-$		$\text{Br}^-$	
	Trans.	Lib.	Trans.	Lib.
$\text{CH}_3\text{NH}_3^+$	1	: 1.6	1	: 2.9
$\text{CD}_3\text{NH}_3^+$	1	: 1.1	1	: 1.9
$\text{CH}_3\text{ND}_3^+$	1	: 2.1	1	: 3.7

In both cases the values follow  $\text{CD}_3\text{NH}_3^+ < \text{CH}_3\text{NH}_3^+ < \text{CH}_3\text{ND}_3^+$  as expected, with the approximate ratio 2:3:4, and the  $\text{CH}_3\text{NH}_3^+$  values are roughly the average of those for the deuterio species.

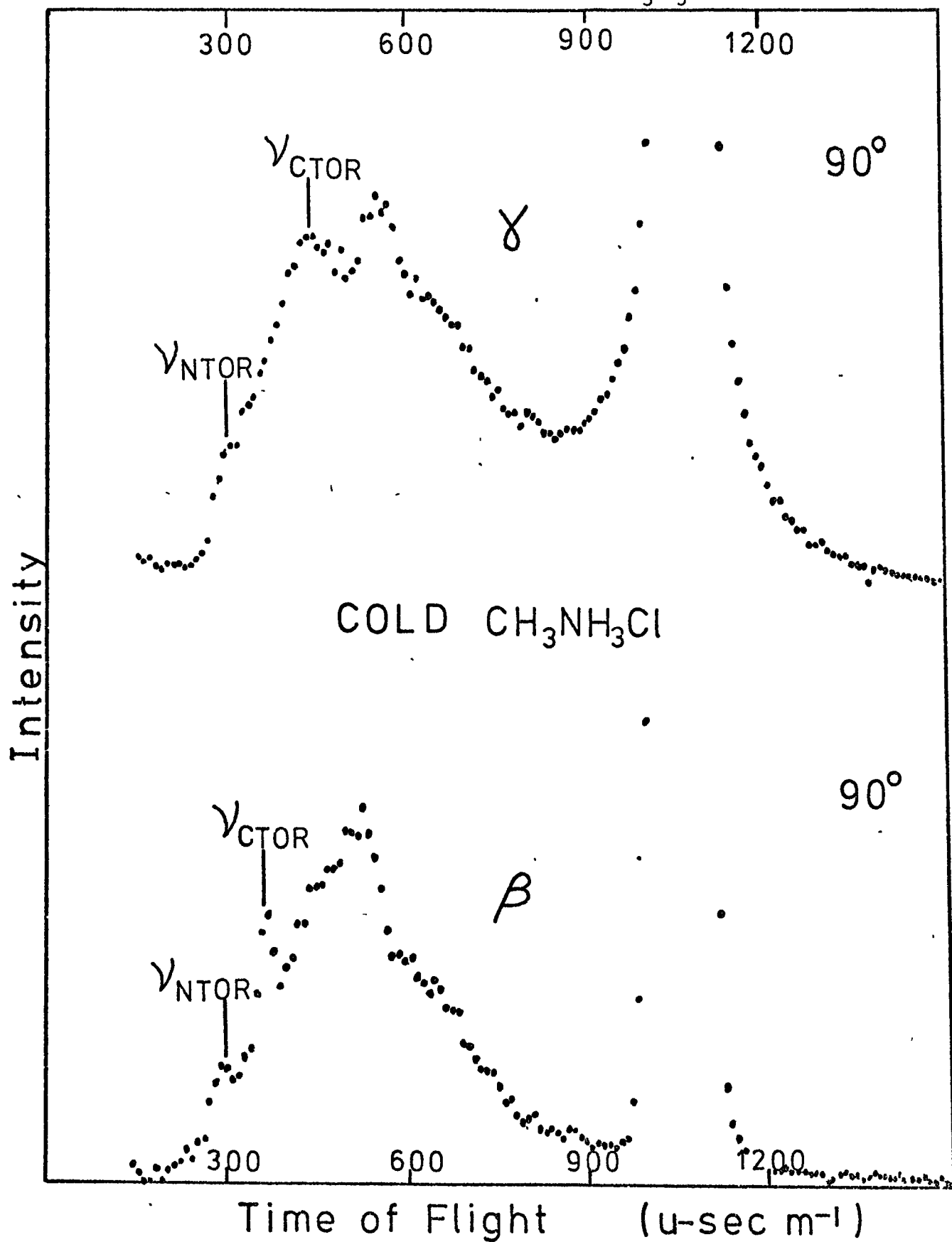
The remaining features in the I.N.S. spectra must then be translational modes or perhaps  $2 \rightarrow 0$  transitions from the overtone levels of the end-over-end ( $\nu_{\text{ELIB}}$ ) libration. (The potential for the  $\nu_{\text{ELIB}}$  mode is much more likely to deviate from simple harmonic for levels above the ground state than the torsion-libration modes).

(iii) The  $\gamma$ -phase of  $\text{CH}_3\text{NH}_3^+\text{Cl}^-$ .

As mentioned earlier it seems likely that the attempt to attain the  $\gamma$ -phase of this salt succeeded, in that the spectrum is not the same as that of the  $\beta$  phase already discussed or the  $\alpha$ -phase discussed later.

The time-of-flight spectrum (at 219<sup>o</sup>K) shows a vague band between 400-500  $\text{cm}^{-1}$  which would correspond with the band seen in the I.R. at 473  $\text{cm}^{-1}$  by Sandorfy(4) and at 467  $\text{cm}^{-1}$  by Castellucci (20). This can only be assigned as  $\nu_{\text{NTOR}}$ . The spectrum then shows no other feature until it rises to an intense broad feature about 60  $\text{cm}^{-1}$  wide centred at  $\sim 190 \text{ cm}^{-1}$ . A slightly stronger but sharper peak occurs at 100  $\text{cm}^{-1}$  with a moderate shoulder at  $\sim 70 \text{ cm}^{-1}$ . Time-of-flight spectra of this and the  $\beta$ -phase are shown in fig. (4.10) for comparison and the obvious conclusion to draw is that the lower torsion-libration band ( $\nu_{\text{CTOR}}$ ) has moved down in the  $\gamma$ -phase into the band at 190  $\text{cm}^{-1}$ .

The overtone of this would be at  $\sim 380 \text{ cm}^{-1}$  which may be helping to blanket the upper torsion-libration mode, somewhat reducing its apparent intensity.

Fig. (4.10) Time-of-flight spectra of  $\gamma$  and  $\beta$   $\text{CH}_3\text{NH}_3^+\text{Cl}^-$ .



The band at  $100\text{ cm}^{-1}$  must again be assigned as the end-over-end libration ( $\nu_{\text{ELIB}}$ ).

It would be very interesting to obtain the beryllium filter spectra of the supercooled  $\gamma$ -phase. Although the lower band is at lower frequencies considerable insight might be gained from its overtone as in the case of  $\beta\text{-CD}_3\text{NH}_3^+\text{Cl}^-$ . However this experiment must await a more sophisticated variable temperature cryostat.

(iv) The  $\text{PF}_6^-$  salts.

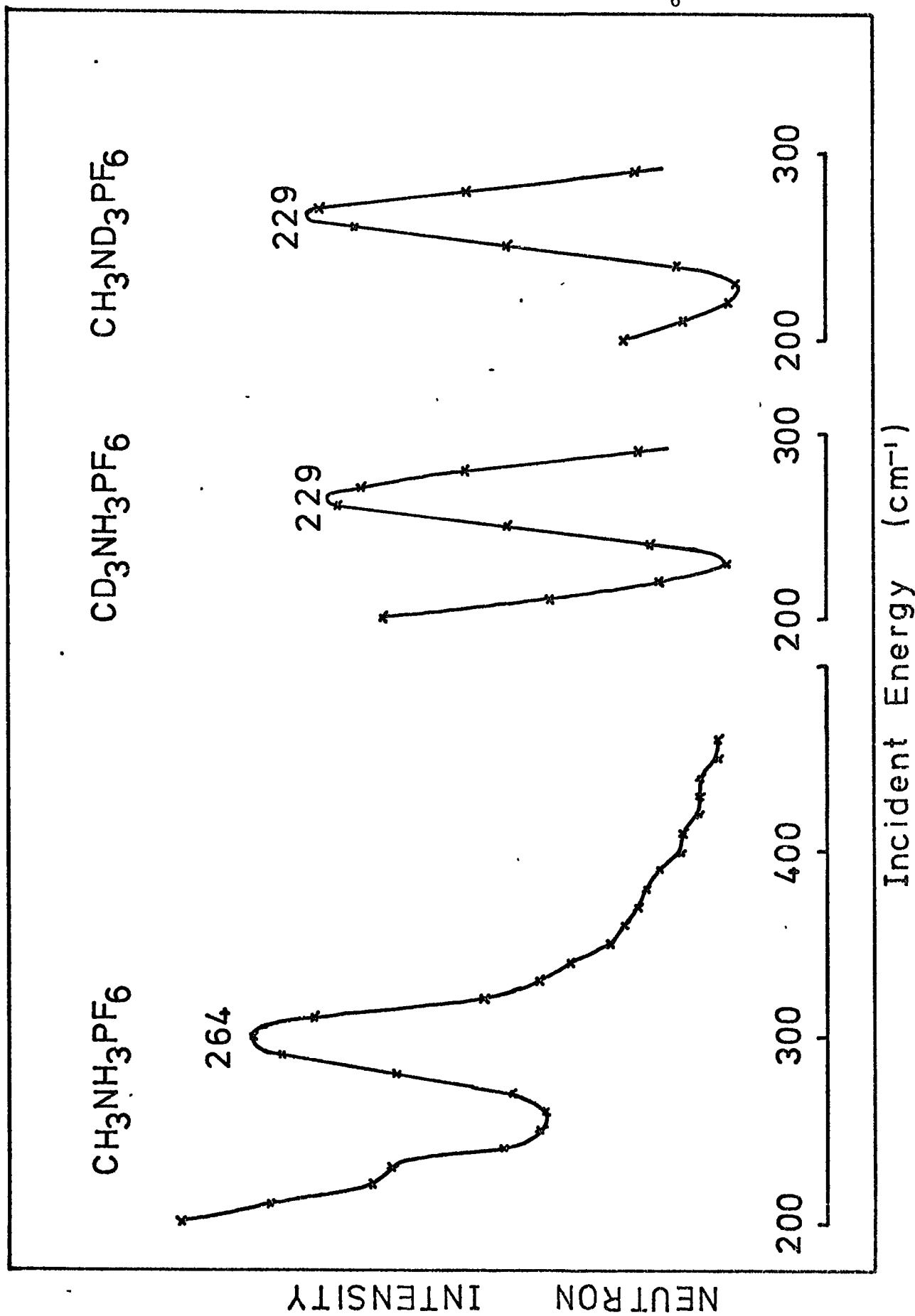
Table (4.11) Frequencies of the methylammonium  $\text{PF}_6^-$  salts ( $\text{cm}^{-1}$ )

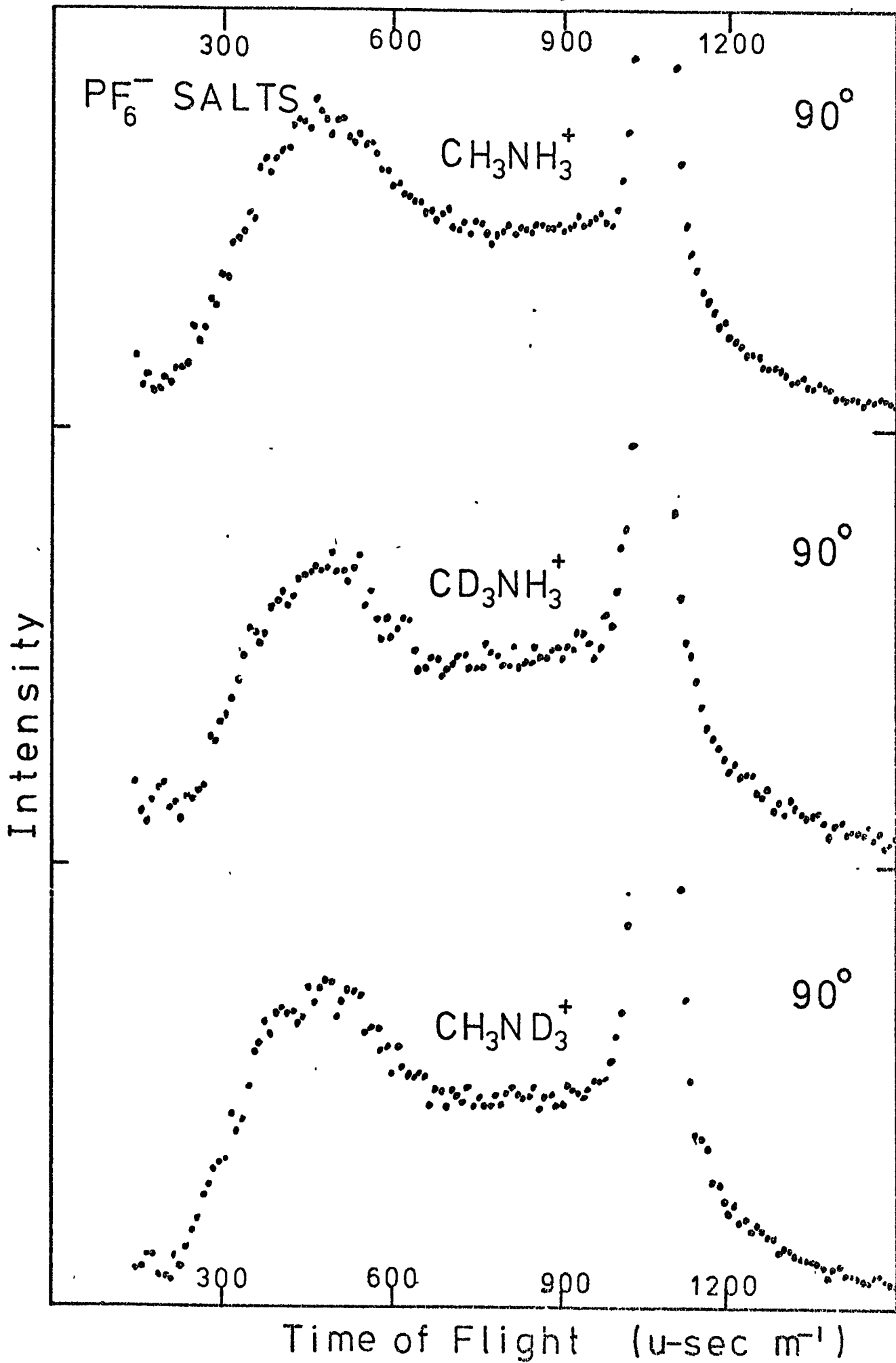
	I.R. (Room or Cold)	I.N.S.		Assignment
		T. of F. (Room)	Be-filter (Cold)	
$\text{CH}_3\text{NH}_3^+\text{PF}_6^-$	Strong broad band, centre $\sim 135$	$\sim 265\text{ m}$ Strong broad band max $\sim 130$	$264\text{ s}$ Rising at 172	$\nu_{\text{NTOR}}$ LATTICE MODES + POSSIBLY $\nu_{\text{CTOR}}$ $\nu_{\text{ELIB}}$
$\text{CD}_3\text{NH}_3^+\text{PF}_6^-$	Strong broad band, centre $\sim 130$	$\sim 225\text{ m}$ Strong broad band max $\sim 120$	$229\text{ s}$ Rising at 172	$\nu_{\text{NTOR}}$ LATTICE MODES + POSSIBLY $\nu_{\text{CTOR}}$ $\nu_{\text{ELIB}}$
$\text{CH}_3\text{ND}_3^+\text{PF}_6^-$	Strong broad band, centre $\sim 130$	$\sim 225\text{ m}$ Strong broad band max $\sim 120$	$229\text{ s}$ Rising at 172	$\nu_{\text{NTOR}}$ LATTICE MODES + POSSIBLY $\nu_{\text{CTOR}}$ $\nu_{\text{ELIB}}$

Before considering the rest of the spectra it is very useful to look at the spectra of the  $\text{PF}_6^-$  salts. It has already been observed from the I.R. spectra that this salt is not H-bonded, and consequently the external forces at each end are much more likely to be equal than in the halide salts. Deuteration of either end of the ion should therefore produce very similar shifts of the torsional frequencies.

The beryllium filter spectra of these salts fig. (4. 11 ) show an isolated strong sharp peak at  $264 \text{ cm}^{-1}$  for  $\text{CH}_3\text{NH}_3^+\text{PF}_6^-$  and at  $229 \text{ cm}^{-1}$  for both of the deuterio salts. These are not I.R. active, and can only be assigned as the torsional bands ( $\nu_{\text{NTOR}}$ ). They clearly display the identical nature of external effects discussed above. What is even more interesting is that the frequency for  $\text{CH}_3\text{NH}_3^+$  of  $264 \text{ cm}^{-1}$  is between that of the torsion of  $\text{CH}_3\text{CH}_3$  at  $289 \text{ cm}^{-1}$  and the "free ion" torsions for the  $^+\text{NH}_3\text{NH}_3^+$  systems at  $252 \text{ cm}^{-1}$  (bromide) and  $257 \text{ cm}^{-1}$  (chloride) derived in Chapter 3. It would not seem too unreasonable to have expected the "free ion" torsional frequency of  $\text{CH}_3\text{NH}_3^+$  to fit this pattern, and the observed frequency therefore indicates that the external barriers are very low, if not zero. (The external symmetry is probably not 3-fold and so any forces involved add up destructively). The theory of chapter 1 section (3b) shows that as the external barriers tend to zero the modes are best described as a whole ion free rotation and an internal torsion.

Another point which emphasises that the band is a torsional mode is that the observed deuteration shift corresponds with those calculated on the basis of the change of reduced moments of inertia:

Fig. (4.11) Beryllium filter, torsional peaks of the  $\text{PF}_6^-$  salts.



$$\frac{I_{\text{CH}_3\text{ND}_3^+}}{I_{\text{CH}_3\text{NH}_3^+}} = 0.7354 \quad \sqrt{x} \times 264 \rightarrow 226 \text{ cm}^{-1}$$

$$\frac{I_{\text{CD}_3\text{NH}_3^+}}{I_{\text{CH}_3\text{NH}_3^+}} = 0.7646 \quad \sqrt{x} \times 264 \rightarrow 231 \text{ cm}^{-1}$$

These are in very good agreement with the observed bands at  $229 \text{ cm}^{-1}$ . It is difficult to show in brief, but it should be pointed out that this relationship should hold for the free ion case, and also for cases with equal external barriers, so that this observation in itself does not indicate whether the barriers have reduced to zero.

As mentioned earlier there does not appear to be any phase change between room and cold temperatures for this salt, and hence the time-of-flight I.N.S. spectra taken at room temperature should be comparable with the beryllium filter spectra. Their immediate interest is that they do not show the pattern of drastic intensity change associated with the librational modes which was seen in the  $\beta$ -phase chlorides and bromides, a point which again favours the parity of external effects at each end of the ion. All three I.N.S. spectra show a very broad band rising fairly rapidly from 0 to a maximum between  $\sim 100\text{-}140 \text{ cm}^{-1}$  and then falling away more slowly to higher frequency. The very strong broad I.R. band lies neatly below the centre of this I.N.S. band but does not extend as far to higher frequency. Using this information the frequencies of the torsional bands must lie in the higher wing of the I.N.S. spectrum which the I.R. spectrum does not cover. The approximate values obtained agree reasonably with the beryllium-filter data.

The main I.N.S. band must contain all the lattice modes, the two end-over-end librations and possibly the  $C_3$  axis rotation. One might still expect the end-over-end librations to be quite strongly hindered due to steric repulsions by the large  $PF_6^-$  ion, and these may give rise to the rather sharp maximum of the band.

To add some speculation about the overall external motion about the  $C_3$  axis; if the external barriers are not quite zero the energy levels of what would have been a pure rotor will be raised and in the time-of-flight spectra both the deuterio salts show a moderately strong broad shoulder at  $\sim 40-55 \text{ cm}^{-1}$ . The  $CH_3NH_3^+$  salt only shows a slight broadening in this region and so the equivalent band is probably slightly higher in frequency and well under the wing of the main I.N.S. peak. The  $C_3$  axis external rotation may possibly be associated with this band, indicating some slight external interaction. On the other hand the effect which a free rotation about one axis should produce on the neutron spectrum would be a general broad contribution to the intensity of the spectrum below  $\sim 100 \text{ cm}^{-1}$  due to a Boltzmann distribution among numerous levels all of which would have slightly different scattering amplitudes, and no sharp peak would appear. The choice between these two possibilities can only be left open.

(v) I.N.S. spectra of the  $\delta$ -iodides.

In the preliminary stages of the investigation, as was done with  $\beta$ - $CD_3NH_3Cl$ , a beryllium filter scan of  $\delta$ - $CH_3NH_3I$  was taken up to  $\sim 1000 \text{ cm}^{-1}$ , on fairly low neutron counts. The torsional band already seen in the

I.R. showed quite strongly at  $\sim 276 \text{ cm}^{-1}$  and no other intense peaks were noted from there up to the region of  $\sim 900 \text{ cm}^{-1}$  plus. In this higher region a moderately strong structured band was observed which would correspond with the  $\nu_{12} \text{ CH}_3$  rocking mode and other internal modes to higher frequency.

Table (4.12)

Frequencies of the  $\delta$ -phase methylammonium Iodides ( $\text{cm}^{-1}$ )

$\text{CH}_3\text{NH}_3^+\text{I}^-$			$\text{CD}_3\text{NH}_3^+\text{I}^-$		$\text{CH}_3\text{ND}_3^+\text{I}^-$		Assignment
I.R.	I.N.S.		I.R.	I.N.S. Be-F	I.R.	I.N.S. Be-F	
	T. of F.	Be-F					
<u>279</u> w	$\sim 265\text{m.s}$	$\sim 380\text{w, brd}$ <u>276</u> v.s	<u>263</u> m	$\sim 510\text{w}$ 417w <u>259</u> v.s		$\sim 410\text{w, sh}$ $\sim 308\text{m, brd}$ <u>219</u> v.s $\sim 179\text{w, sh}$	$2 \times \nu_{\text{NTOR}}$ $\nu_{\text{NTOR}}$
166 v.s	broad $\sim 160\text{m}$ band	$\updownarrow$	165v.s		165v.s		LATTICE MODES REGION POSSIBLY INCLUDES $\nu_{\text{CTOR}}?$
<u>112</u> m	<u>110</u> v.s $\sim 45\text{w}$		<u>146</u> s, sh <u>107</u> m	$\sim 147\text{m.s}$	<u>143</u> s, sh <u>109</u> m		$\nu_{\text{ELIB}}$ LATTICE MODE OR $\nu_{\text{CTOR}}?$

The beryllium filter spectra of all three  $\delta$ -iodides (with much better statistics) are presented in fig. (4.13) and all show one intense band assigned as the torsional mode ( $\nu_{\text{NTOR}}$ ) with much weaker bands to higher frequency which may be overtones and combinations. The frequencies of the  $\nu_{\text{NTOR}}$  bands again follow the shift pattern seen in the  $\beta$ -chlorides and bromides:

$\delta\text{-CH}_3\text{NH}_3\text{I}$	276	
$\delta\text{-CD}_3\text{NH}_3\text{I}$	259	$\text{cm}^{-1}$
$\delta\text{-CH}_3\text{ND}_3\text{I}$	219	

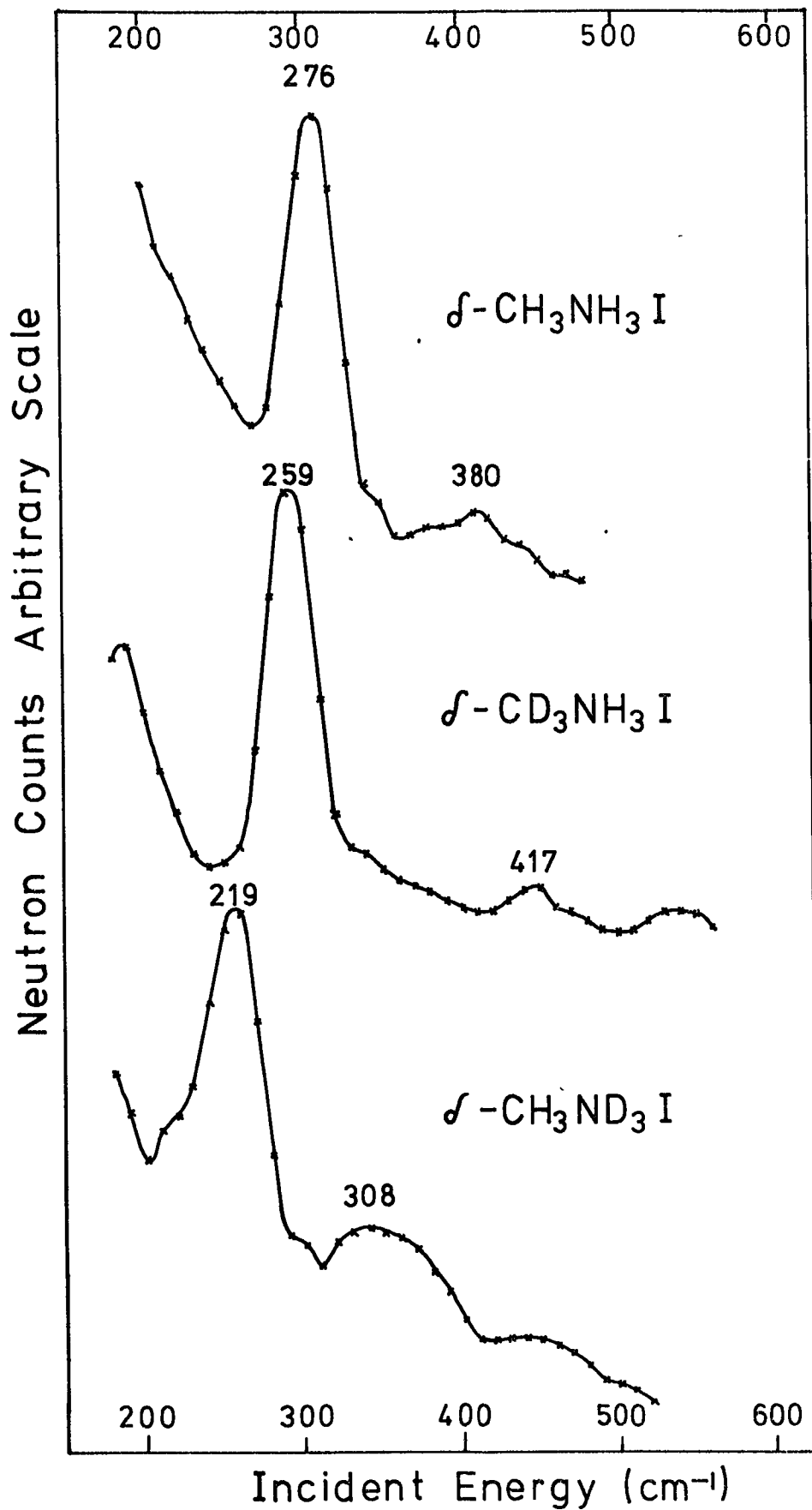
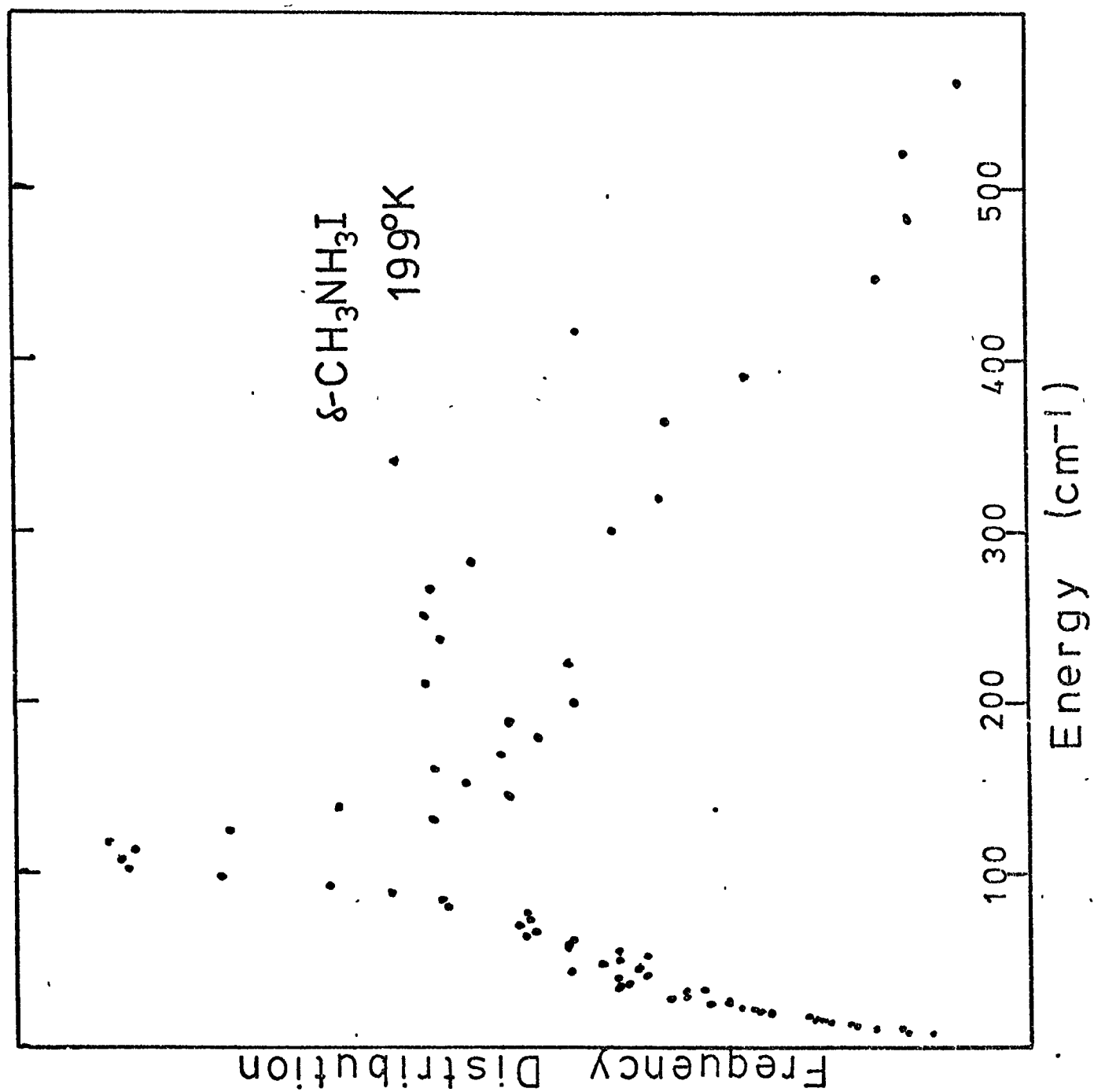
Fig. (4.13) Beryllium filter spectra of the  $\delta$ -iodides.



Fig. (4.14) Time-of-flight spectrum of  $\delta\text{-CH}_3\text{NH}_3^+\text{I}^-$ .

and this implies again an asymmetry of the fields at each end of the molecule. Bands would also be expected at lower frequency showing the reverse pattern of shifts, but these are not in evidence in the lower parts of the beryllium filter spectra. However the frequency of the band observed in  $\delta\text{-CH}_3\text{NH}_3^+\text{I}^-$  is only  $12\text{ cm}^{-1}$  higher than for the  $\text{PF}_6^-$  salt which would indicate that the external barriers are still very small. Consequently the other torsion-libration band ( $\nu_{\text{CTOR}}$ ) might be expected to be quite low (i.e. the model is approaching that of separate internal torsion and external rotation).

Unfortunately only the  $\text{CH}_3\text{NH}_3^+\text{I}^-$  salt has been studied by the time-of-flight instrument at cold temperatures. The spectrum was obtained at  $199^\circ\text{K}$  and appears sufficiently different from the room temperature spectrum to enable it to be labelled as  $\delta$ -phase. The torsional band appears rather broader than in the beryllium-filter spectrum (though this is probably an effect of poorer resolution). The general features are very similar to those of the  $\text{PF}_6^-$  spectrum; a very broad moderately strong and rounded band appears, ranging from  $0 \rightarrow 200\text{ cm}^{-1}$  plus, centred at about  $100\text{ cm}^{-1}$ . However this time it is much more obvious that another band is superimposed on this giving an intense peak centred at  $\sim 110\text{ cm}^{-1}$ , which is most probably the end-over-end librational mode. This band is now clearly present in the far I.R. spectrum.

The strongest far I.R. band of  $\delta\text{-CH}_3\text{NH}_3^+\text{I}^-$  at  $166\text{ cm}^{-1}$  does not appear to contribute much to the I.N.S. spectrum, and the equivalent I.R. bands of the deuterio species are not in evidence at all in the beryllium filter spectra, however the  $\text{CD}_3\text{NH}_3^+\text{I}^-$  salt does show a moderate

I.N.S. band at  $\sim 147 \text{ cm}^{-1}$  corresponding to the next strongest I.R. band at  $146 \text{ cm}^{-1}$ . The same band in the  $\text{CH}_3\text{NH}_3^+\text{I}^-$  I.N.S. spectrum is covered by the main band. These may all reasonably be assigned to lattice modes since they do not show appreciable shifts on deuteration.

(vi) The time-of-flight spectra of the  $\alpha$  and  $\alpha'$  phases.

The  $\alpha'$  phases of the bromide and iodide show very similar I.N.S. time-of-flight spectra, but the  $\alpha$ -chloride although similar in general respects does show a slight variation. Spectra are shown in figs (4.15-4.19).

All the compounds produce a very broad intense band with complex features, which rises from  $0 \text{ cm}^{-1}$  and extends as far as  $350 \text{ cm}^{-1}$  in the case of  $\text{CH}_3\text{NH}_3^+\text{Cl}^-$ . The most striking feature is that a band which appears in the region of  $\sim 100\text{-}110 \text{ cm}^{-1}$  for the bromides and iodides and  $\sim 70\text{-}100 \text{ cm}^{-1}$  for the chlorides again shows the same drastic intensity variations as was seen for the  $\beta$ -phases, and consequently this band is assigned to the end-over-end librations ( $\nu_{\text{ELIB}}$ ). This band also shows the main difference between the  $\alpha$  and  $\alpha'$  phases in that the frequencies seen for the chlorides are about  $20 \text{ cm}^{-1}$  lower than the bromides and iodides. It is interesting to note that the observation made earlier with respect to the Raman spectrum of  $\alpha'\text{-CH}_3\text{NH}_3^+\text{Br}^-$  that the libration probably lay within the region  $100\text{-}130 \text{ cm}^{-1}$  is in fact true and that the I.N.S. band is at  $108 \text{ cm}^{-1}$ , exactly the same as one Raman band.

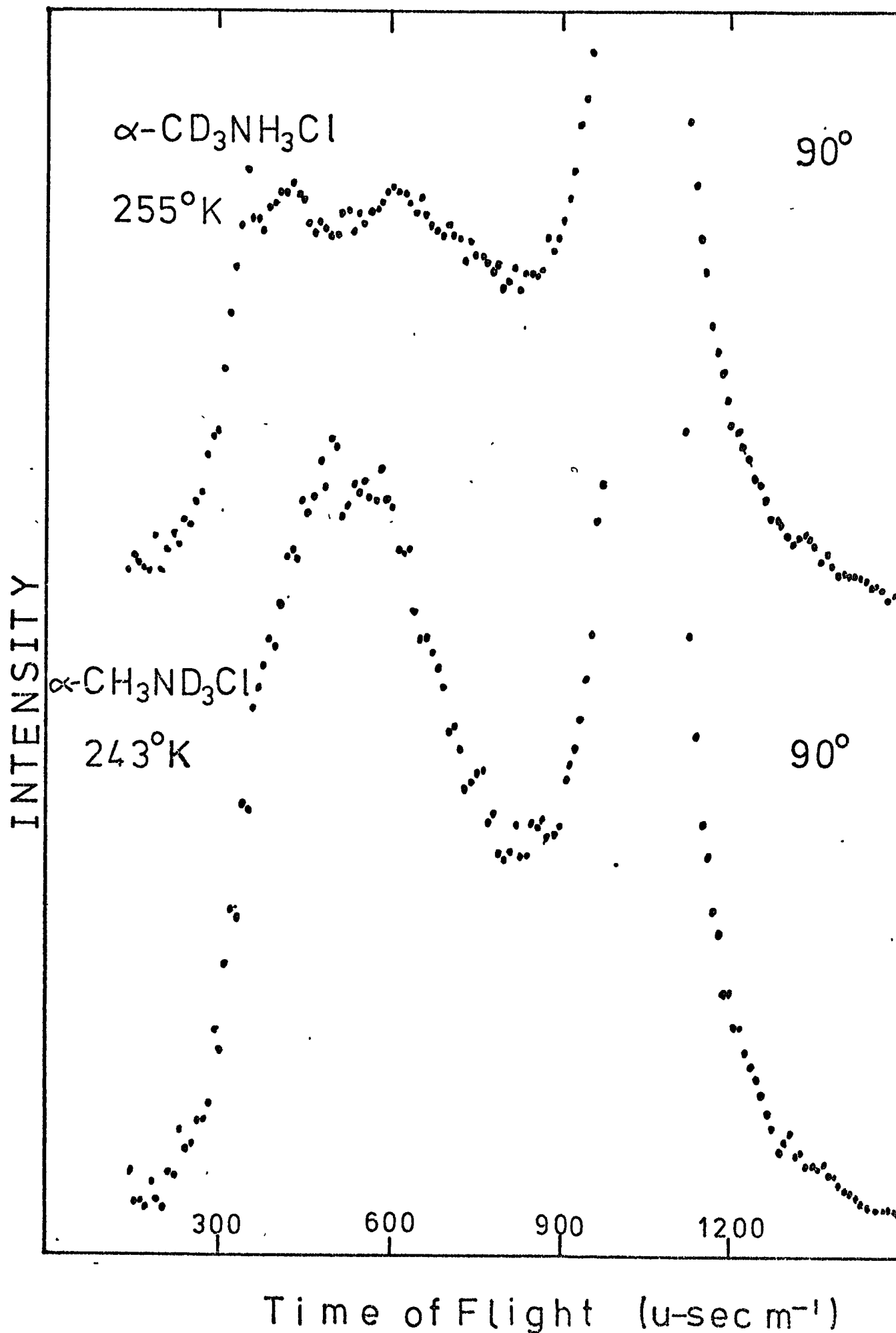


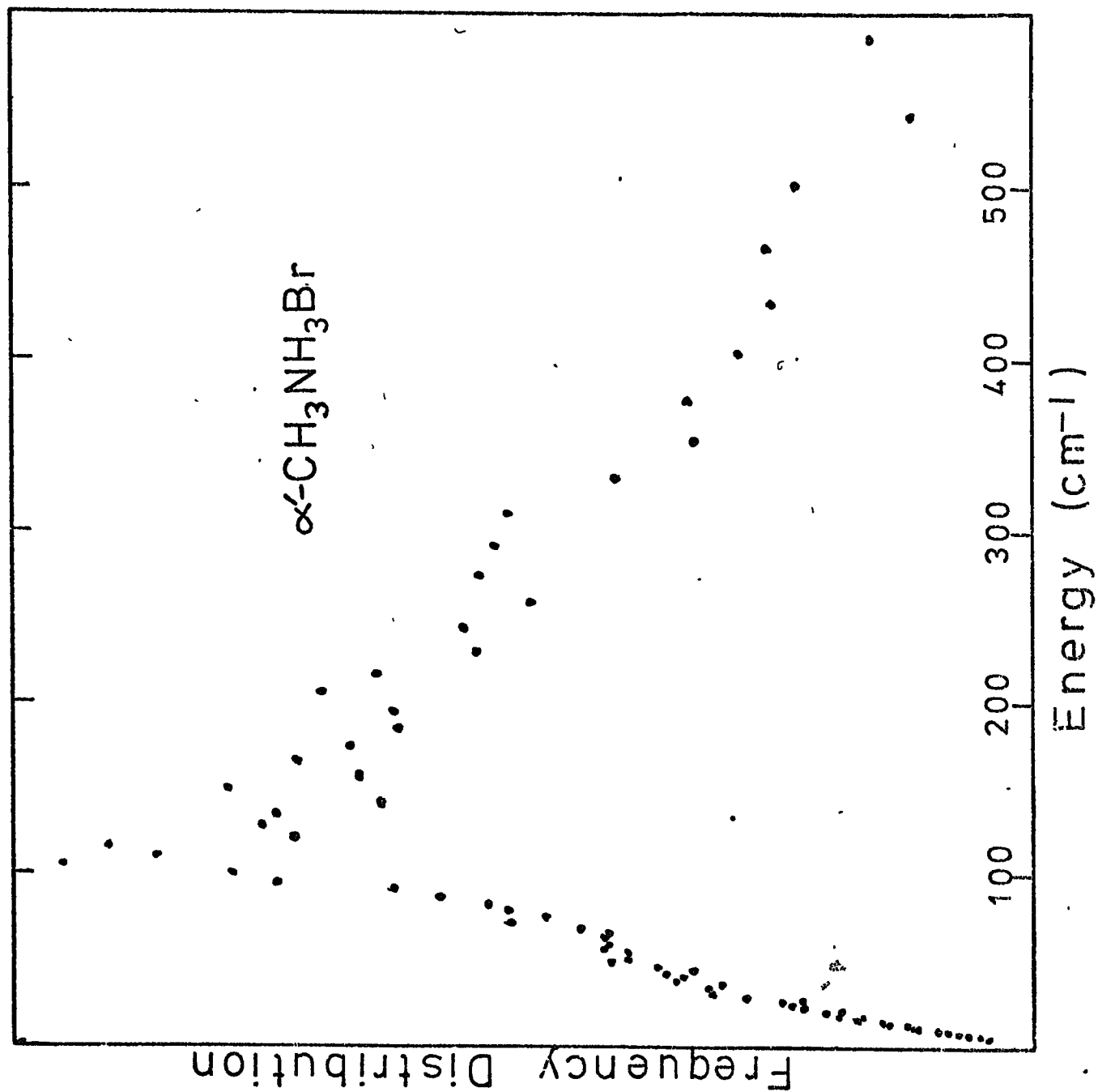
Fig. (4.16) Time-of-flight spectrum of  $\alpha\text{-CH}_3\text{NH}_3^+\text{Br}^-$ .

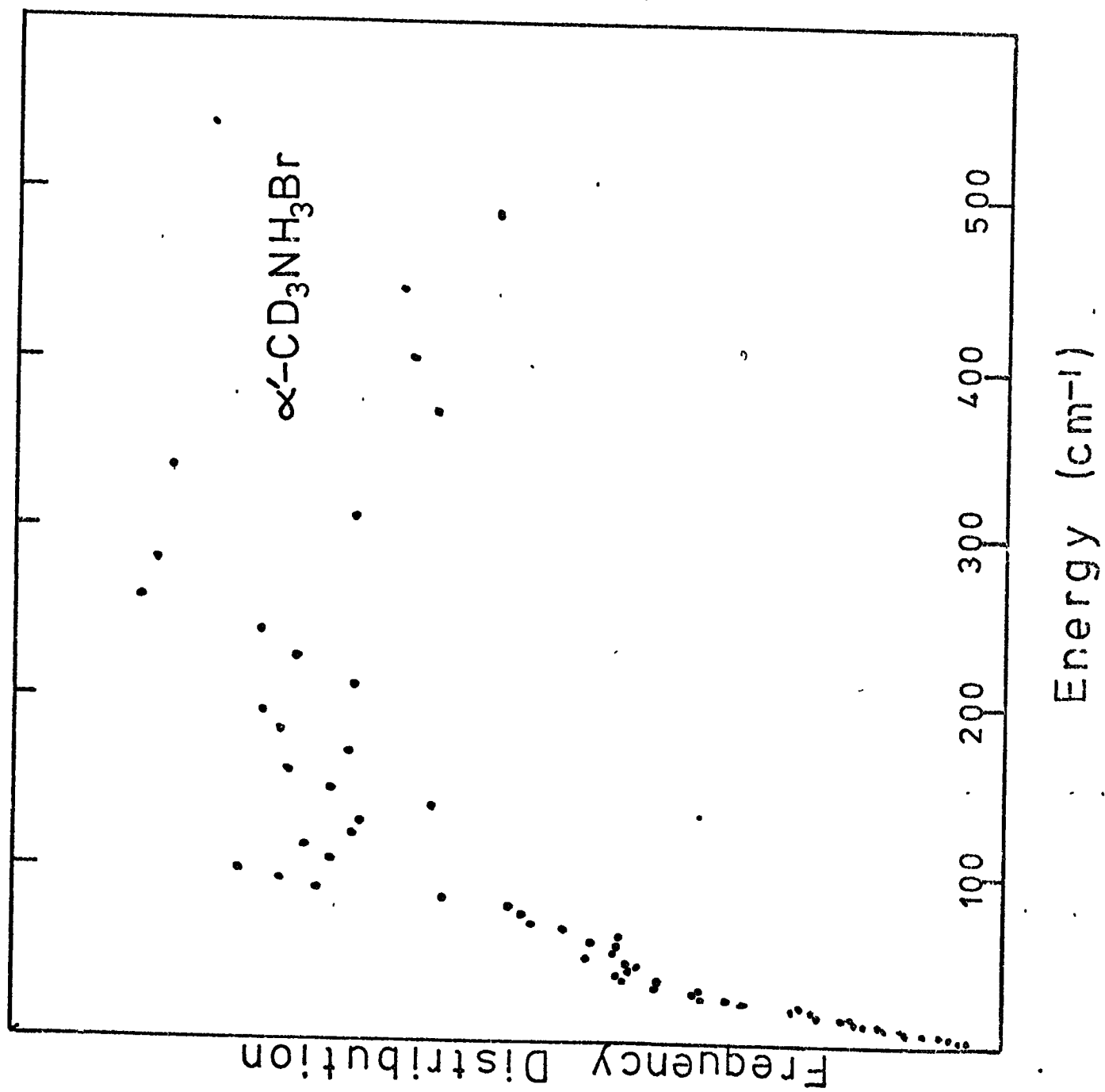
Fig. (4.17) Time-of-flight spectrum of  $\alpha'$ -CD<sub>3</sub>NH<sub>3</sub><sup>+</sup>Br<sup>-</sup>.

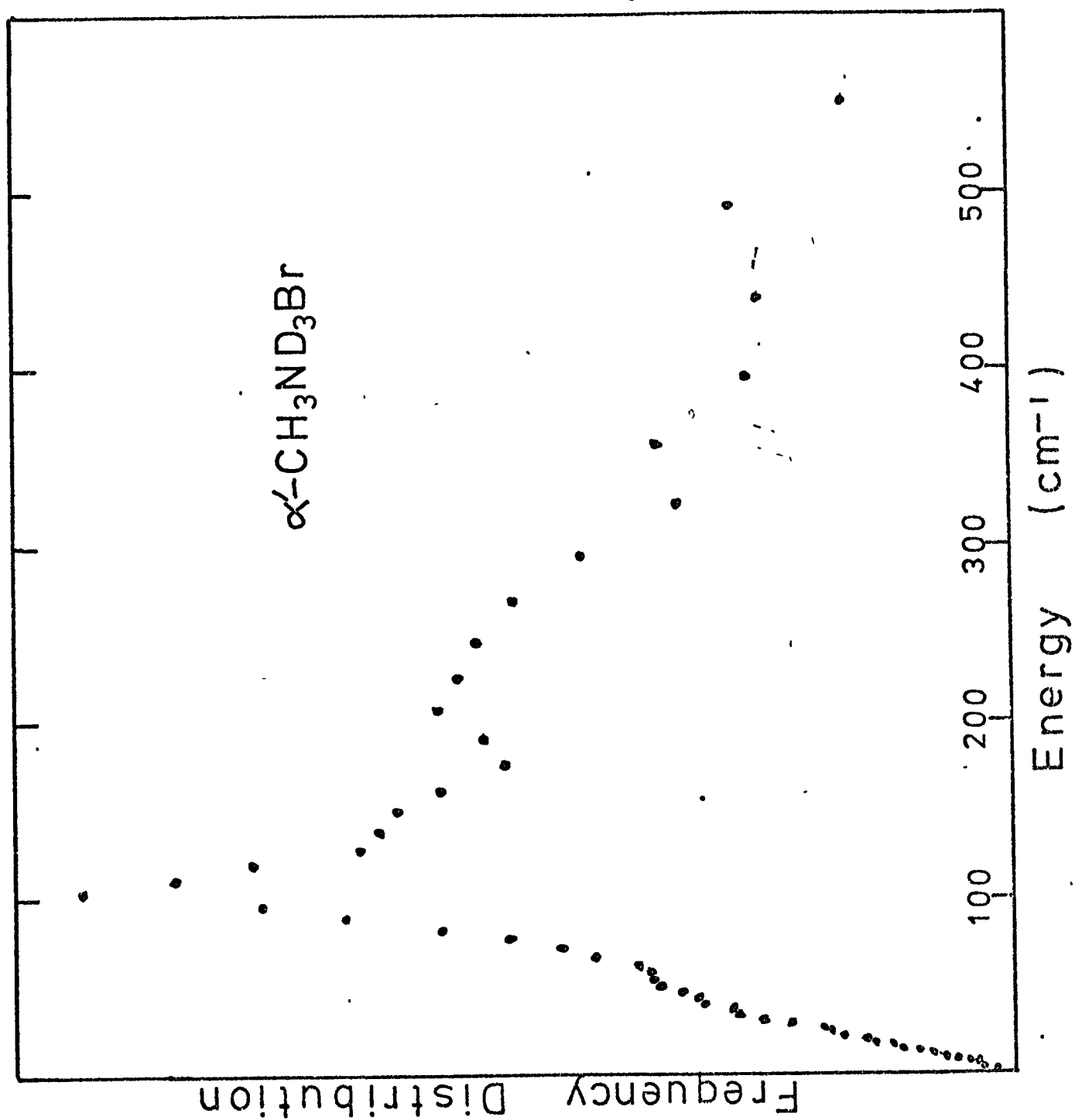
Fig. (4.18) Time-of-flight spectrum of  $\alpha'$ -CH<sub>3</sub>ND<sub>3</sub><sup>+</sup>Br<sup>-</sup>.

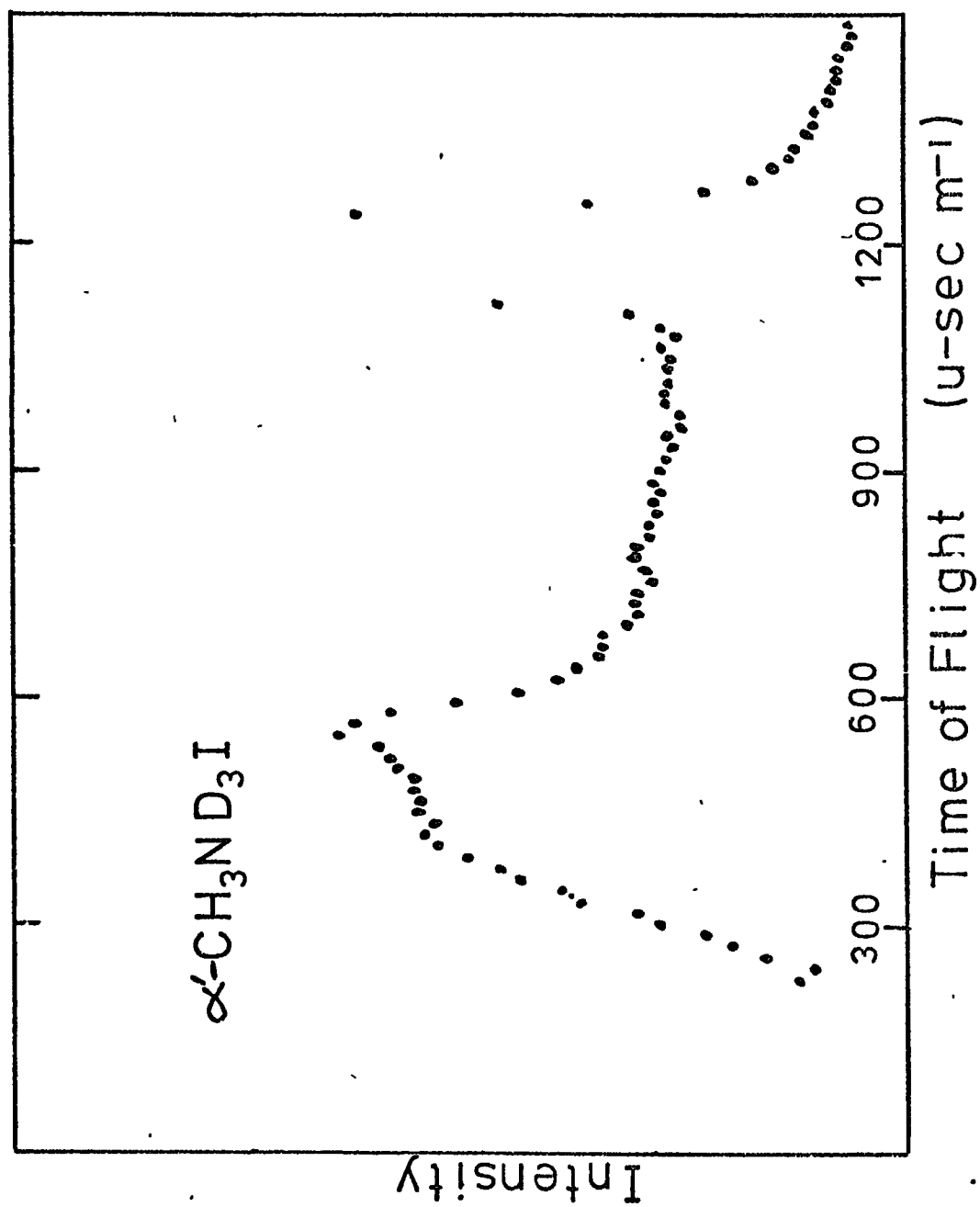
Fig. (4.19) Time-of-flight spectrum of  $\alpha'$ -CH<sub>3</sub>ND<sub>3</sub><sup>+</sup>I<sup>-</sup>.



Table (4.13)

Frequencies of the room temperature phases of the  
methylammonium halides ( $\text{cm}^{-1}$ )

	$\text{CH}_3\text{NH}_3^+$		$\text{CD}_3\text{NH}_3^+$		$\text{CH}_3\text{ND}_3^+$		Assignment
	I.R.	I.N.S. T. of F.	I.R.	I.N.S. T. of F.	I.R.	I.N.S. T. of F.	
$\alpha$ -CHLORIDES	215vs ~ 140m ~ 125m	~ 310m.s ~ 205s 140s  ~ 95s	~ 190v.s ~ 140w	~ 300v.s ~ 185v.s  ~ 110m.sh ~ 75s ~ 50sh	~ 190v.s ~ 140  ~ 110m	~ 250m ~ 190m.s 145m ~ 125v.s  ~ 80v.s ~ 50w.sh	$\nu_{\text{NTOR}}$ LATTICE MODES AND POSSIBLY $\nu_{\text{CTOR}}$ $\nu_{\text{ELIB}}$
$\alpha'$ -BROMIDES	169s 145s  125m	~ 290m ~ 185s broad ~ 130sh  108v.s ~ 60m.sh	163s 143m.sh  120m	~ 265v.s ~ 170s broad region  ~ 100m.w ~ 50m.sh	162s 142m.sh  120m	~ 210m ~ 175m broad ~ 140m  107v.s ~ 55w.sh	$\nu_{\text{NTOR}}$ LATTICE MODES + POSSIBLY $\nu_{\text{CTOR}}$ $\nu_{\text{ELIB}}$
$\alpha'$ -IODIDES	164m 145m  112m	~ 260s ~ 170s broad ~ 130s  110v.s ~ 60m.sh	160s 146s  107m	~ 250 broad region centred ~ 160s  ~ 98s ~ 50m.sh	163w 143s  109m.s	~ 210w broad region ~ 155m  105v.s ~ 50m.sh	$\nu_{\text{NTOR}}$ LATTICE MODES + POSSIBLY $\nu_{\text{CTOR}}$ $\nu_{\text{ELIB}}$

A comparison with the I.R. data shows that the rest of the broad I.N.S. band extends considerably further than the I.R. band. The centre of this additional band can only be estimated roughly, see table (4.13) but this still enables one to see that the old pattern of N-deuteration causing a greater shift than C-deuteration is present. Consequently this band is assigned as the higher torsion-libration  $\nu_{\text{NTOR}}$ . The estimated frequencies for iodide show a similarity to the  $\delta$ -phase values, but for the bromide the values are less than for the  $\delta$ -phase, and the chloride values are a little higher than for the bromide. It is fairly obvious from this that H-bonding is still affecting the mode, albeit weakly. This is discussed with reference to the crystal structures later. The whereabouts of the lower torsion-libration mode  $\nu_{\text{CTOR}}$  can again only be surmised as lying somewhere in the lower envelope of the broad band; the bromides and iodides do in fact show a moderate shoulder at  $\sim 50 \text{ cm}^{-1}$  or less.

The remaining intensity in the middle of the I.N.S. band does show some rough correspondence with the I.R. translational bands, though it may also include overtones of the end-over-end libration.

Frequencies are listed in table (4.13) and if one compares the values of the  $\nu_{\text{NTOR}}$  bands with the values given in table (4.8) which were derived from the difference between  $\nu_9$  and a combination band, (I.R. data), the correspondence is quite reasonable. This is in favour of labelling the combination band as  $(\nu_6 + \nu_9)$ , where  $\nu_6 \equiv \nu_{\text{NTOR}}$ .

Section 4. Barrier calculations and related discussion.

(a) On the data obtained for the  $\beta$ -phase Chloride and Bromide Torsion-Libration modes.

The  $\beta$ -phases of the chloride and bromide provide a suitable case for application of the model described in Chapter 1 Section 3.

Unfortunately their structures are not known, although Castelluci (20) suggested a  $D_{2h}$  factor group for the chloride. However  $C_2H_5NH_3^+Cl^-$ ,  $Br^-$  and  $I^-$  show structures (25) which display the  $-NH_3^+$  group with anions in an arrangement around it similar to that seen in  $N_2H_6F_2$ ,  $Cl_2$ .

Also their I.R. spectra are directly analogous to the  $\beta$ -phases of  $CH_3NH_3^+Cl^-$ ,  $Br^-$ ; in that a high frequency torsional band appears around  $500-400\text{ cm}^{-1}$  and also the characteristic  $\beta$ -phase ( $\nu_6 + \nu_9$ ) band appears (26). Sandorfy (26,27) points out that several alkyl- and aryl-ammonium halides, whose structures are known to have a three-fold anion arrangement around the  $-NH_3^+$  rotor at distances which imply H-bonding, also display the  $\beta$ - type of spectrum. However, it should be noted that in these structures the N---Cl distances are not all equivalent nor are the C-N \begin{array}{l} \diagdown \\ \text{Cl} \end{array} angles, which would be a cause for the crystal field splittings observed in the  $\beta$ - type spectra.

It should be noted that the higher torsional frequencies in  $\beta$   $CH_3NH_3^+Cl^-$ ,  $Br^-$  are in the same region as those for the  $N_2H_6^{+2}$  salts, which might indicate that this is largely associated with  $-NH_3^+$  motion, and more importantly a high frequency means a deep well indicating strong interactions for all three hydrogens at the equilibrium position.

Hence all the evidence points in favour of the  $\beta$ -phases having a 3-fold H-bonded system around the nitrogen but with some slight

distortion from true  $C_3$  symmetry. With respect to the  $-CH_3$  group we can only assume that a near  $C_3$  environment prevails for this also. This latter assumption does not affect the overall calculation since it is the force constant ( $n^2V$ ) parameter which is important and  $\bar{V}_3$  is only obtained from this by dividing it by 9.

Problems again arise in deciding bond lengths and angles, so Td angles have been used with 1.04 or 1.03 Å bond lengths for N-H (as for the  $N_2H_6^{+2}$  salts) and a 1.0945 Å bond length for C-H. The latter value is a compromise between 1.093 and 1.096 Å which seem to appear with equal frequency in the literature, and using Td angles gives the value  $I_{CH_3} = 3.220 \text{ a.m.u. \AA}^2$ .

Table (4.16) A Summary of the torsion-libration frequencies.

		$CH_3NH_3^+$	$CD_3NH_3^+$	$CH_3ND_3^+$	$CD_3ND_3^+$	$\frac{1}{\sqrt{2}} \times CH_3NH_3^+$
$Cl^-$	I.R. (4)	487	475	373	347	344.4
	Raman (20)	471				
		472	465	354		
	I.N.S.	276 + sh.	197	261		
$Br^-$	I.R. (4)	449	437	357	338	317.5
		435	427	334		
	I.N.S.	242 + sh	172	234		

Attention should be drawn to the calculated  $1/\sqrt{2}$  change in frequency on full deuteration, which should occur for a perfect S.H. system.

A comparison with the observed values shows that there may be a good fit to the S.H. model for the  $Cl^-$  case, but some departure occurs for the  $Br^-$

case. Another point of interest is the apparent large difference in frequencies obtained between I.R. and Raman/I.N.S. methods. One can only speculate on the cause of this because the I.R. technique is only a surface probe, surface charge effects may affect the frequency particularly for finely divided samples, whereas Raman and I.N.S. probe right into the crystal, and hence see the bulk frequency. (30)

As mentioned earlier a knowledge of the higher torsional frequency  $\bar{\nu}_{\text{NTOR}}$  for three isotopic species should alone enable the calculation of the three barriers. Recalling the theory of Chapter 1 section 3a the expressions for the torsion-libration frequencies can now be written as:

$$2\pi^2 c^2 \bar{\nu}_{\text{NTOR}}^2 = \lambda_{\text{N}} = \frac{1}{2} [d_{\text{N}} + d_{\text{c}} + \{(d_{\text{N}} - d_{\text{c}})^2 + d_{\text{I}}^2\}^{\frac{1}{2}}] \quad (4.1)$$

$$2\pi^2 c^2 \bar{\nu}_{\text{CTOR}}^2 = \lambda_{\text{c}} = \frac{1}{2} [d_{\text{N}} + d_{\text{c}} - \{(d_{\text{N}} - d_{\text{c}})^2 + d_{\text{I}}^2\}^{\frac{1}{2}}] \quad (4.2)$$

$$\text{and} \quad \lambda_{\text{N}} + \lambda_{\text{c}} = d_{\text{N}} + d_{\text{c}} \quad (4.3)$$

$$\lambda_{\text{N}} - \lambda_{\text{c}} = \pm \{(d_{\text{N}} - d_{\text{c}})^2 + d_{\text{I}}^2\}^{\frac{1}{2}} \quad (4.4)$$

where

$$d_{\text{N}} = \frac{9}{4} \left[ \frac{\bar{\nu}_{\text{N}} + \bar{\nu}_{\text{I}}}{I_{\text{N}}} \right], \quad d_{\text{c}} = \frac{9}{4} \left[ \frac{\bar{\nu}_{\text{c}} + \bar{\nu}_{\text{I}}}{I_{\text{c}}} \right], \quad d_{\text{I}} = -\frac{9}{2} \frac{\bar{\nu}_{\text{I}}}{(I_{\text{N}} I_{\text{c}})^{\frac{1}{2}}}$$

and

$\bar{\nu}_{\text{N}}$	nitrogen end	}	external barriers
$\bar{\nu}_{\text{c}}$	carbon end		
$\bar{\nu}_{\text{I}}$	internal barrier		
$I_{\text{N}}$	- NH <sub>3</sub> group	}	moments of inertia
$I_{\text{c}}$	- CH <sub>3</sub> group		

Three equations can then be written from the higher frequency expression (in  $\lambda_N$ ) for the three isotopic species, making the necessary divisions by 2 to account for the mass changes on deuteration. These values of  $\lambda$  will be labelled as:-

$$\begin{array}{lll} \lambda_{N1} & \text{for } \text{CH}_3\text{NH}_3^+ & \text{involving terms in } d_N, d_c, d_I \\ \lambda_{N2} & \text{for } \text{CD}_3\text{NH}_3^+ & \text{" " } d_N, d_c/2, d_I/2 \\ \lambda_{N3} & \text{for } \text{CH}_3\text{ND}_3^+ & \text{" " } d_{N/2}, d_c, d_I/2 \end{array}$$

Complicated manipulation of these three expressions then yields the three following equations in  $d_N$  and  $d_c$

$$(d_N + d_c) = \frac{\lambda_{N1} - 2 \left[ \frac{\lambda_{N2} \lambda_{N3}}{\lambda_{N1}} \right]}{1 - 3 \left[ \frac{\lambda_{N2} \lambda_{N3}}{\lambda_{N1}} \right] \left[ \frac{1}{\lambda_{N2} + \lambda_{N3}} \right]} \quad (4.5)$$

$$(d_N + \frac{d_c}{2}) = \lambda_{N2} + \frac{1}{2} \left[ \frac{\lambda_{N1}}{\lambda_{N2}} \right] \left[ (d_N + d_c) - \lambda_{N1} \right] \quad (4.6)$$

$$\left( \frac{d_N}{2} + d_c \right) = \lambda_{N3} + \frac{1}{2} \left[ \frac{\lambda_{N1}}{\lambda_{N3}} \right] \left[ (d_N + d_c) - \lambda_{N1} \right] \quad (4.7)$$

Since  $\lambda_N = 2\pi^2 c^2 v_{\text{NTOR}}^{-2}$  use of the three  $\bar{v}_{\text{NTOR}}$  frequencies from the isotopic species in (4.5)-(4.7) enables the derivation of the  $(d_N + d_c)$  parameters on their left hand side. Then from equation (4.3):

$$\begin{array}{lll} (d_N + d_c) & = \lambda_{N1} + \lambda_{c1} & \text{for } \text{CH}_3\text{NH}_3^+ \\ (d_N + \frac{d_c}{2}) & = \lambda_{N2} + \lambda_{c2} & \text{" } \text{CD}_3\text{NH}_3^+ \\ \left( \frac{d_N}{2} + d_c \right) & = \lambda_{N3} + \lambda_{c3} & \text{" } \text{CH}_3\text{ND}_3^+ \end{array}$$

Consequently the  $\lambda_c$  and hence  $\bar{\nu}_{\text{CTOR}}$  values can be calculated for the three isotopic species. If the system is truly S.H. these values should compare favourably with the observed  $\bar{\nu}_{\text{CTOR}}$  values. An important point to note is that this calculation does not involve any moment of inertia values and hence any errors are entirely due to the  $\bar{\nu}_{\text{NTOR}}$  values. Table (4.17) shows the results of this calculation using the I.R. and then I.N.S. values, and contrasts them with the observed lower frequency I.N.S. values.

Table (4.17) Calculated and observed values of the lower torsion-libration frequency  $\bar{\nu}_{\text{CTOR}}$  of  $\beta$ -monomethylammonium chloride and bromide ( $\text{cm}^{-1}$ ).

Compound		Calculated $\bar{\nu}_{\text{CTOR}}$		Observed $\bar{\nu}_{\text{CTOR}}$ (I.N.S)
		From I.R. $\bar{\nu}_{\text{NTOR}}$	From I.N.S. $\bar{\nu}_{\text{NTOR}}$	
Cl <sup>-</sup>	CH <sub>3</sub> NH <sub>3</sub> <sup>+</sup>	272	277	276
	CD <sub>3</sub> NH <sub>3</sub> <sup>+</sup>	197	199	197
	CH <sub>3</sub> ND <sub>3</sub> <sup>+</sup>	251	261	261
Br <sup>-</sup>	CH <sub>3</sub> NH <sub>3</sub> <sup>+</sup>	297	275	242
	CD <sub>3</sub> NH <sub>3</sub> <sup>+</sup>	216	198	172
	CH <sub>3</sub> ND <sub>3</sub> <sup>+</sup>	264	253	234

This clearly shows that the behaviour of the chloride is very nearly S.H., whereas the bromide shows some breakdown of the model. It is also evident that the I.R. frequencies used do not fit as well as the I.N.S. values.

From the derived ( $d_N + d_C$ ) values of equations (4.5)-(4.7) simple elimination yields the values of  $d_N$  and  $d_C$ , from which ( $\bar{V}_N + \bar{V}_I$ ) and ( $\bar{V}_C + \bar{V}_I$ ) can be obtained by introducing the moments of inertia. The value of  $d_I$  (which yields  $\bar{V}_I$ ) can be derived from the expression:-

$$d_I^2 = 4[\lambda_{NI}^2 - \lambda_{NI}(d_N + d_C) + d_N d_C] \quad (4.8)$$

(This can be obtained by manipulation of the basic equations).

Consequently all three barriers can be calculated.

Since the chloride shows S.H. behaviour its barriers can be calculated directly from the ( $d_N + d_C$ ) values of equations (4.5)-(4.7) and  $d_I$  of equation (4.8). The results are as follows:-

Table (4.18) Calculated barrier parameters (S.H.) for  $\beta$ -monomethylammonium chloride.

N-H ( $\text{\AA}$ )	$\bar{V}_I$	$\bar{V}_N$	$\bar{V}_C$	
1.04	771	3293	1088	cm <sup>-1</sup>
1.03	763	3222	1096	

The  $\bar{V}_N$  barrier compares very favourably with the hydrazinium value of 3414 cm<sup>-1</sup> (N-H = 1.04  $\text{\AA}$ ), and also as might be expected the internal barrier lies between the S.H. barriers for  $N_2H_6^{+2}Cl_2$  and  $C_2H_6$  of 632 cm<sup>-1</sup> and 860 cm<sup>-1</sup> respectively. What is also of considerable interest is the fact that the  $\bar{V}_C$  barrier is by no means small.

The slightly decreased value of the  $\bar{V}_N$  barrier may well be caused by a slight distortion from  $C_3$  symmetry around the  $-NH_3^+$  group, which as mentioned earlier is a feature of other salts with  $\beta$ - type spectra.

Recalling the theory (Chapter 1 section 3) once again it will be remembered that the rotor coordinates  $\alpha_C$  and  $\alpha_N$  are related to the



normal coordinates a and b by the expressions

$$\begin{aligned} a &= I_N^{\frac{1}{2}} \cos \theta \alpha_N + I_C^{\frac{1}{2}} \sin \theta \alpha_C \\ b &= I_N^{\frac{1}{2}} \sin \theta \alpha_N - I_C^{\frac{1}{2}} \cos \theta \alpha_C \end{aligned} \quad (4.9)$$

and that  $\theta$  is found from the relation  $\tan 2\theta = \frac{d_I}{d_N - d_C}$

Hence it is relatively easy to calculate the transformation matrix between the normal and symmetry coordinates for each species.

For N-H = 1.04 Å this gives:-

	$\text{CH}_3\text{NH}_3^+\text{Cl}^-$	$\text{CD}_3\text{NH}_3^+\text{Cl}^-$	$\text{CH}_3\text{ND}_3^+\text{Cl}^-$
	$\alpha_N$	$\alpha_C$	
a	$\begin{bmatrix} 1.64 & -0.49 \\ -0.46 & -1.73 \end{bmatrix}$	$\begin{bmatrix} 1.68 & -0.39 \\ -0.26 & -2.51 \end{bmatrix}$	$\begin{bmatrix} 1.96 & -1.04 \\ -1.40 & -1.46 \end{bmatrix}$
b			

where a and b are associated with the high and low frequencies respectively. These are in fact the equivalents of the  $L^{-1}$  matrices of a normal coordinate analysis.

It is apparent from these matrices that both normal modes involve motion of both the  $-\text{NH}_3^+$  and  $-\text{CH}_3$  groups, the lower frequency mode having both groups rotating in the same sense and the higher frequency mode has the groups contra-rotating. For the  $\text{CH}_3\text{NH}_3^+$  and  $\text{CD}_3\text{NH}_3^+$  cases the higher frequency is mainly  $-\text{NH}_3^+$  motion and the lower frequency mainly  $-\text{CH}_3$  motion whereas for  $\text{CH}_3\text{ND}_3^+$  both frequencies show a more nearly equal participation of the two rotor motions, especially so for the lower frequency mode. Consequently it would be expected that the higher frequency I.N.S. peak for  $\beta$   $\text{CD}_3\text{NH}_3^+\text{Cl}^-$  should be much more intense than the lower frequency, whereas for  $\beta$   $\text{CH}_3\text{ND}_3^+\text{Cl}^-$  although

the lower frequency peak should now be the most intense the higher frequency peak should not be very much weaker. This is exactly what is shown by the beryllium filter spectra; although the peak at  $197 \text{ cm}^{-1}$  for  $\text{CD}_3\text{NH}_3^+\text{Cl}^-$  may have a weak underlying translational mode, even if this fact is ignored the peak is less than half the intensity of the higher frequency, whereas for  $\text{CH}_3\text{ND}_3^+\text{Cl}^-$  the relative intensities are about 13:8 for the  $261 \text{ cm}^{-1}$  and  $354 \text{ cm}^{-1}$  peaks.

This can be taken one step further. The I.N.S. intensity is in part proportional to the squared amplitude of the motions of the scattering atoms of the mode concerned. Cyvin (29) has given methods of obtaining amplitudes. For a particular quantum level  $n$  of a normal mode the mean square amplitude is given by

$$\langle Q_n^2 \rangle = \frac{h}{4\pi^2 c \omega} \left( n + \frac{1}{2} \right) \quad (4.10)$$

( $Q$ , from the normal coordinate treatment is usually mass weighted  $Q = m^{\frac{1}{2}} x$ . Where  $x$  is a pure displacement coordinate; and  $\omega$  is the mode frequency).

The amplitude of motions in other types of coordinates can then be derived if the relevant conversion matrix is known.

Using matrix notation  $S = LQ$

where  $S$  = symmetry coordinate matrix  
 $Q$  = normal coordinate matrix  
 $L$  = conversion matrix

or  $Q = L^{-1}S$  where  $L^{-1}$  is the conversion matrix derived a little earlier.

The amplitude matrix of the symmetry coordinates is then given by

$$\langle SS' \rangle = L \langle Q Q' \rangle L'$$

Hence in the present case  $S = LQ$  is given by

$$\begin{bmatrix} \alpha_N \\ \alpha_c \end{bmatrix} = \begin{bmatrix} \frac{\cos \theta}{\sqrt{I_N}} & \frac{\sin \theta}{\sqrt{I_N}} \\ -\frac{\sin \theta}{\sqrt{I_c}} & -\frac{\cos \theta}{\sqrt{I_c}} \end{bmatrix} \begin{bmatrix} a \\ b \end{bmatrix}$$

and  $\langle SS' \rangle = L \langle QQ' \rangle L'$  is

$$\begin{bmatrix} \langle \alpha_N^2 \rangle & \langle \alpha_N \alpha_c \rangle \\ \langle \alpha_N \alpha_c \rangle & \langle \alpha_c^2 \rangle \end{bmatrix} = \begin{bmatrix} \frac{\langle a^2 \rangle \cos^2 \theta + \langle b^2 \rangle \sin^2 \theta}{I_N} & \frac{(\langle a^2 \rangle - \langle b^2 \rangle) \sin \theta \cos \theta}{(I_N I_c)^{\frac{1}{2}}} \\ \frac{(\langle a^2 \rangle - \langle b^2 \rangle) \sin \theta \cos \theta}{(I_N I_c)^{\frac{1}{2}}} & \frac{\langle a^2 \rangle \sin^2 \theta + \langle b^2 \rangle \cos^2 \theta}{I_c} \end{bmatrix}$$

(Cross terms  $ab \rightarrow 0$  by the definition of normal coordinates)

If one now substitutes for

$$\langle a^2 \rangle = \frac{h}{8\pi^2 c \bar{\nu}_{NTOR}} \quad \text{and} \quad \langle b^2 \rangle = \frac{h}{8\pi^2 c \bar{\nu}_{CTOR}}$$

and for all the other parameters, the numerical values of the mean square symmetry coordinate amplitudes can be calculated. Hence

for the  $\beta$ -phase chloride:-

	$\text{CH}_3\text{NH}_3^+$	$\text{CD}_3\text{NH}_3^+$	$\text{CH}_3\text{ND}_3^+$
$\langle \alpha_N^2 \rangle$	0.0129	0.0128	0.0092
$\langle \alpha_c^2 \rangle$	0.0184	0.0131	0.0183
$\langle \alpha_N \alpha_c \rangle$	0.0022	0.0017	0.0019

Since  $\alpha_N$  and  $\alpha_c$  are described in radians the following angular displacements can be calculated.

Table (4.19) Group angular displacement amplitudes for the  $\beta$ -chlorides.

	$\text{CH}_3\text{NH}_3^+$	$\text{CD}_3\text{NH}_3^+$	$\text{CH}_3\text{ND}_3^+$
$\langle \alpha_N^2 \rangle^{\frac{1}{2}}$	$6.5^\circ$	$6.5^\circ$	$5.5^\circ$
$\langle \alpha_c^2 \rangle^{\frac{1}{2}}$	$7.8^\circ$	$6.6^\circ$	$7.8^\circ$

Just to see what this means in terms of a distance displacement on the circle of rotation; for  $\text{CH}_3\text{NH}_3^+$

$$\langle \alpha_N^2 \rangle^{\frac{1}{2}} = 0.1114 \text{ \AA} \quad \text{and} \quad \langle \alpha_c^2 \rangle^{\frac{1}{2}} = 0.1399 \text{ \AA}$$

This quite clearly shows that the  $-\text{NH}_3^+$  group is tied down to smaller oscillations than the  $-\text{CH}_3$  group as would be expected from the size of the external barriers. It is also quite interesting to note that the amplitude of  $-\text{NH}_3^+$  motion is the same in both  $\text{CH}_3\text{NH}_3^+$  and  $\text{CD}_3\text{NH}_3^+$ ; similarly for the  $-\text{CH}_3$  motion in  $\text{CH}_3\text{NH}_3^+$  and  $\text{CH}_3\text{ND}_3^+$ . The cross terms  $\langle \alpha_N \alpha_c \rangle$  are also seen to be somewhat smaller in comparison.

From expressions (4.9):

$$\begin{aligned} a^2 &= I_N \cos^2 \theta \alpha_N^2 + I_c \sin^2 \theta \alpha_c^2 + 2(I_N I_c)^{\frac{1}{2}} \sin \theta \cos \theta \alpha_N \alpha_c \\ b^2 &= I_N \sin^2 \theta \alpha_N^2 + I_c \cos^2 \theta \alpha_c^2 + 2(I_N I_c)^{\frac{1}{2}} \sin \theta \cos \theta \alpha_N \alpha_c \end{aligned}$$

Hence the ratios of the contributions of the amplitudes  $\langle \alpha_N^2 \rangle$  and  $\langle \alpha_c^2 \rangle$  to the normal mode amplitudes are given by

$$\frac{\cos^2 \theta}{\sin^2 \theta} \quad \text{for } \alpha_N^2, \quad \frac{\sin^2 \theta}{\cos^2 \theta} \quad \text{for } \alpha_c^2.$$

This suggests that for  $\text{CH}_3\text{ND}_3^+$  the amplitude contributions to the I.N.S. intensity from the  $\text{CH}_3$  group are

$$\nu_{\text{CTOR}} : \nu_{\text{NTOR}} \quad 1.95 : 1$$

and for  $\text{CD}_3\text{NH}_3^+$  from the  $\text{NH}_3^+$  group,  $\nu_{\text{CTOR}} : \nu_{\text{NTOR}} \quad 1:41$ .

The latter ratio looks to be very wide of the observed intensity ratios but it must be remembered that several other factors are involved in the double differential scattering cross scattering equation.

Returning now to the data for the  $\beta$ -bromide, it was seen that the predicted and observed lower frequencies were considerably different. This indicates some departure from S.H. behaviour and means that the  $d_{\text{N}}$ ,  $d_{\text{C}}$  and  $d_{\text{I}}$  values derived solely from the higher frequencies may be considerably in error. Since a model has not been developed for a case such as this a "close" solution within the framework of the S.H. treatment has been sought using all the six observed I.N.S. frequencies, by first ascertaining the range of possible values for  $\bar{V}_{\text{N}}$ ,  $\bar{V}_{\text{C}}$  and  $\bar{V}_{\text{I}}$  and then making sensible restrictions on the  $\bar{V}_{\text{I}}$  parameter:-

The calculations are not drastically affected by the different moments of inertia for N-H = 1.04 or 1.03 Å, and so 1.03 Å has specifically been used. Recalling equations (4.3) and (4.4)

$$\lambda_{\text{N}} + \lambda_{\text{C}} = d_{\text{N}} + d_{\text{C}} \quad (4.3)$$

$$\lambda_{\text{N}} - \lambda_{\text{C}} = \pm \{(d_{\text{N}} - d_{\text{C}})^2 + d_{\text{I}}^2\}^{\frac{1}{2}} \quad (4.4)$$

(4.4) can be rearranged to give

$$d_N - d_C = \pm \{(\lambda_N - \lambda_C)^2 - d_I^2\}^{\frac{1}{2}} \quad (4.12)$$

where

$$\lambda_N = 2\pi^2 c^2 \bar{\nu}_{NTOR}^{-2} \quad \lambda_C = 2\pi^2 c^2 \bar{\nu}_{CTOR}^{-2}$$

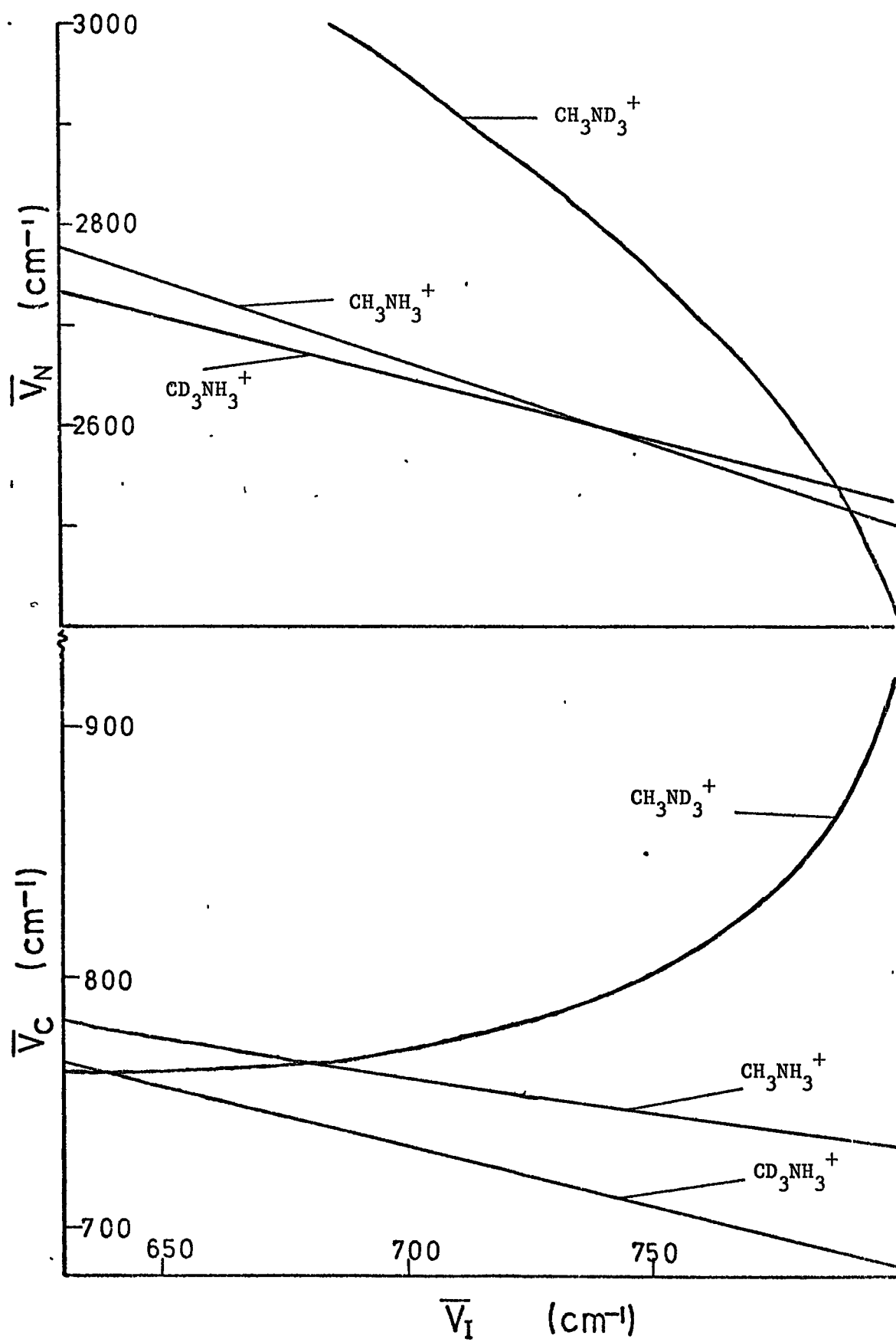
Values of  $d_I$  can be calculated for a series of  $\bar{\nu}_I$  values, then substituting for  $\lambda_N$ ,  $\lambda_C$  and  $d_I$  in (4.3) and (4.12) and eliminating between the two,  $d_N$  and  $d_C$  can be found and consequently  $\bar{\nu}_N$  and  $\bar{\nu}_C$ . By plotting the change of  $\bar{\nu}_N$  and  $\bar{\nu}_C$  vs.  $\bar{\nu}_I$  for each of the three isotopic species their points of intersection can be found. Fig. (4.20) shows this graphically, and whereas for the chloride all the plots would intersect at the same values, for the bromide the intersections are all separate:-

Table (4.20) Points of intersection of bromide parameters ( $\text{cm}^{-1}$ )

	$\bar{\nu}_I$ vs. $\bar{\nu}_N$	$\bar{\nu}_I$ vs. $\bar{\nu}_C$
$\left. \begin{array}{l} \text{CH}_3\text{NH}_3^+ \\ \text{CD}_3\text{NH}_3^+ \end{array} \right\}$	740      2601	437      887
$\left. \begin{array}{l} \text{CH}_3\text{NH}_3^+ \\ \text{CH}_3\text{ND}_3^+ \end{array} \right\}$	791      2515	682      766
$\left. \begin{array}{l} \text{CD}_3\text{NH}_3^+ \\ \text{CH}_3\text{ND}_3^+ \end{array} \right\}$	788      2540	641      762

What is immediately clear is that the agreement in the  $\bar{\nu}_I$  vs.  $\bar{\nu}_N$  case is much closer than for the  $\bar{\nu}_I$  vs.  $\bar{\nu}_C$  case. The indicated

Fig. (4.20)



magnitude of  $\bar{V}_N$  is a little less than the barrier of  $2816 \text{ cm}^{-1}$  seen in  $\text{N}_2\text{H}_6^{+2}\text{Br}_2^-$ , but a reduction in  $\bar{V}_N$  was also seen for the chloride.

Considering the values of  $\bar{V}_I$ , it would not be unreasonable to expect that this should have a value similar to that obtained for the chloride ( $\text{N-H} = 1.03 \text{ \AA}$  gave this as  $763 \text{ cm}^{-1}$ ). It was seen in the chapter on the hydrazinium salts that the internal barrier of  $\text{N}_2\text{H}_6^{+2}$  decreased by  $\sim 20 \text{ cm}^{-1}$  on going from the chloride to the bromide, and so the expected range for the internal barrier in  $\text{CH}_3\text{NH}_3^+\text{Br}^-$  would be  $\sim 740\text{-}750 \text{ cm}^{-1}$ . It will also be seen shortly that the S.H. barrier to internal rotation in  $\text{CH}_3\text{NH}_3^+\text{PF}_6^-$  where external influences are minimal is  $\sim 700 \text{ cm}^{-1}$  and so the barrier for the bromide would certainly not be expected below this value.

The graphs also show that the  $\bar{V}_N$  plots begin to diverge below  $\bar{V}_I \sim 790 \text{ cm}^{-1}$  and that the  $\bar{V}_C$  have converged to very similar values by  $\bar{V}_I \sim 680 \text{ cm}^{-1}$ . One would expect the best fit to lie somewhere between these values. (The best fit at a particular value of  $\bar{V}_I$  being given by the average values of  $\bar{V}_N$  and  $\bar{V}_C$  at that value). Having suggested that the optimum reasonable value of  $\bar{V}_I$  should be  $\sim 740\text{-}750 \text{ cm}^{-1}$  averaged values of  $\bar{V}_N$  and  $\bar{V}_C$  at  $\bar{V}_I = 740$  and  $750 \text{ cm}^{-1}$  have been calculated. The two sets of parameters have then been resubstituted in the basic equations to give the frequencies. These are given in table (4.21) with the deviations from the observed frequencies in brackets.

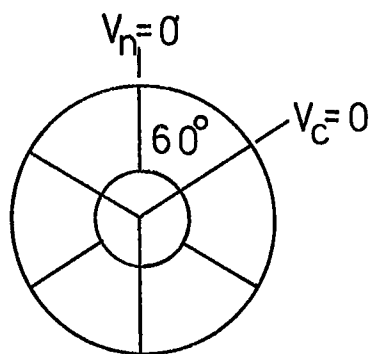
The interesting feature of these 'close fits' is that  $\bar{V}_I \approx \bar{V}_C$  and a barrier of  $750 \text{ cm}^{-1}$  is in the region where the S.H. approximation is beginning to get much poorer.



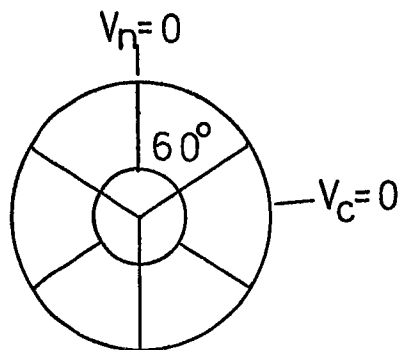
Table (4. 21) Calculated frequency fits (All values in  $\text{cm}^{-1}$ )

Parameter Set		$\bar{\nu}_{\text{NTOR}}$	$\bar{\nu}_{\text{CTOR}}$
$\bar{\nu}_{\text{I}} = 740$	$\text{CH}_3\text{NH}_3^+$	439 (+ 4)	243 (+ 1)
$\bar{\nu}_{\text{N}} = 2667 \text{ ave.}$	$\text{CD}_3\text{NH}_3^+$	431 (+ 4)	175 (+ 3)
$\bar{\nu}_{\text{c}} = 751 \text{ ave.}$	$\text{CH}_3\text{ND}_3^+$	329 (- 5)	229 (- 5)
$\bar{\nu}_{\text{I}} = 750$	$\text{CH}_3\text{NH}_3^+$	438 (+ 3)	243 (+ 1)
$\bar{\nu}_{\text{N}} = 2643 \text{ ave.}$	$\text{CD}_3\text{NH}_3^+$	430 (+ 3)	175 (+ 3)
$\bar{\nu}_{\text{c}} = 752 \text{ ave.}$	$\text{CH}_3\text{ND}_3^+$	330 (- 4)	228 (- 6)

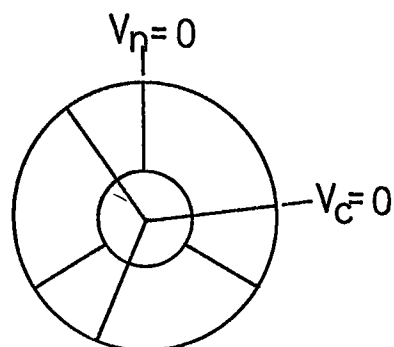
Another possible factor which may interfere should now be considered: The whole model so far discussed has assumed that in the crystals the external fields are so arranged so that the equilibrium position of the  $\text{CH}_3\text{NH}_3^+$  ion is simultaneously at the individual minima of all three potentials, which would require that the external potentials are staggered at  $60^\circ$  to each other. What happens if these potentials are not at  $60^\circ$  on account of the crystal structure? If the field at the nitrogen end is regarded as strong enough to maintain the minimum external potential for that end of the ion, i.e. regard it for the moment as fixed, then the  $\text{CH}_3$  group will position itself at the minimum of the total potential it experiences which may be at the minimum of the internal potential or at the minimum of its external potential or neither. This is expressed diagrammatically in fig. (4.21).



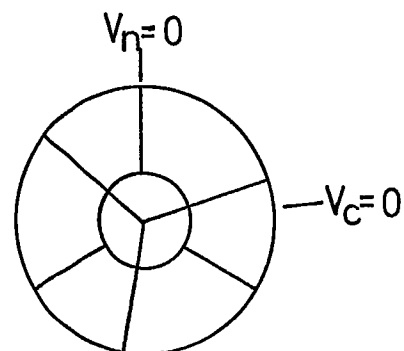
$V_N, V_c, V_I$  all at  
minima.



$V_c$  not at minimum



$V_I$  not at minimum.



$V_c, V_I$  not at minima.

The question then arises as to what effect this would have on the energy levels of the system. Since unless either one of  $\bar{V}_I$  or  $\bar{V}_c$  was much larger than the other, there would not be a specific centre about which to perform S.H. motion. The potential would probably be a very complicated function possibly with double minimum wells, and consequently give rise to a more complicated pattern of energy levels.

This may be an explanation of the shoulder which appears on the  $\nu_{\text{CTOR}}$  peaks of both  $\beta\text{-CH}_3\text{NH}_3^+\text{Cl}^-$  and  $\text{Br}^-$  and the broadening of the  $\nu_{\text{CTOR}}$  peak of  $\beta\text{-CH}_3\text{ND}_3^+\text{Cl}^-$ , where a splitting of the levels has probably occurred. (Attempts to take account of a different angle between the external fields in a S.H. model have not proved too successful and clearly a more detailed treatment would be needed.)

The only other possible cause for the shoulder which immediately springs to mind is that the rotor groups are substantially distorted from  $C_3$  symmetry by the external fields causing the internal potential to

distort considerably, again producing energy level splittings.

The magnitude of the external  $\bar{V}_c$  barriers in these  $\beta$ -phases also requires some comment. One would initially expect that this should be caused by steric effects building up constructively to give moderately deep wells just as for the individual N-H---X bonding. It has however also been reported (see Chapter 7 for references) that methyl groups can hydrogen bond to some extent with such ions as  $\text{Cl}^-$  and  $\text{Br}^-$ , and this may also contribute to the barrier (although it should be mentioned that previous cases have usually suggested that only one proton of the  $\text{CH}_3$  group participates).

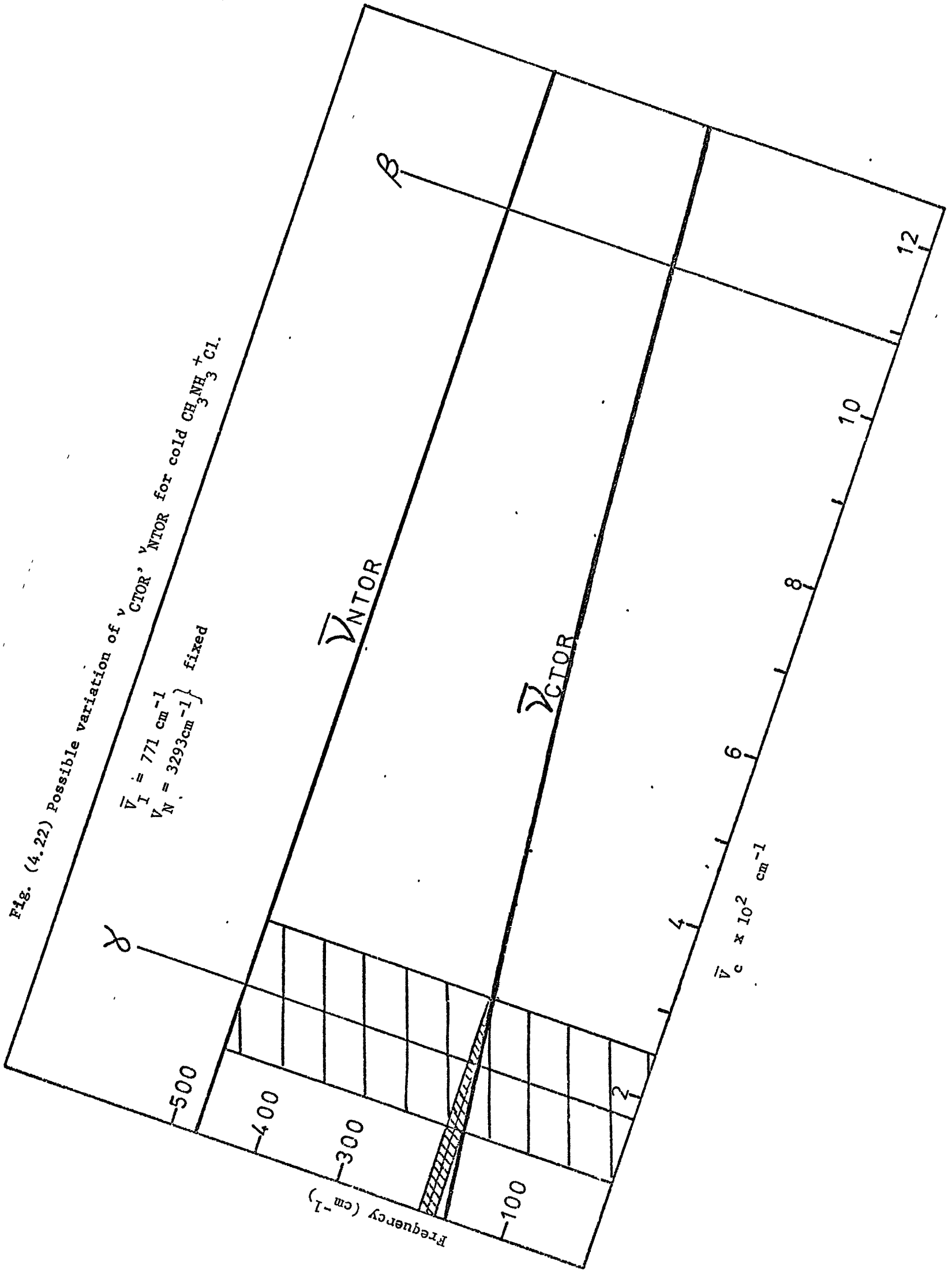
b) A consideration of the  $\gamma$ -phase of the chloride.

Using the information obtained in the time-of-flight spectrum of  $\gamma\text{-CH}_3\text{NH}_3^+\text{Cl}^-$  where  $\bar{\nu}_{\text{CTOR}}$  was observed to have moved to much lower frequency, probably to  $\sim 190 \text{ cm}^{-1}$ , some conjecture can be made regarding the external barriers in this phase.

The frequency of  $\bar{\nu}_{\text{NTOR}}$  which is slightly below that of the  $\beta$ -phase clearly indicates that the  $-\text{NH}_3^+$  group still partakes in 3 H-bonds, with an environment not too dissimilar to that of the  $\beta$ -phase. Having found the internal barrier, and the external barrier at the nitrogen end for the  $\beta$ -phase these can be used to calculate  $\bar{\nu}_{\text{NTOR}}$  and  $\bar{\nu}_{\text{CTOR}}$  as the external barrier at the carbon end  $\bar{V}_c$  is changed. The result is shown graphically in fig. (4.22) and clearly indicates for frequencies of  $\bar{\nu}_{\text{CTOR}}$  between  $190 \pm 10 \text{ cm}^{-1}$  the external barrier to rotation of  $-\text{CH}_3$  is of the order of  $175 \pm 75 \text{ cm}^{-1}$ , and even falls to zero for  $\bar{\nu}_{\text{CTOR}} \sim 170 \text{ cm}^{-1}$ . At the same time it is seen that  $\bar{\nu}_{\text{NTOR}}$  is only slightly reduced. This would agree with the N.M.R. data (6) which also shows a much reduced activation energy for the  $-\text{CH}_3$  group reorientation in the  $\gamma$  phase.

Fig. (4.22) Possible variation of  $\nu_{CTOR}$ ,  $\nu_{NTOR}$  for cold  $CH_3NH_3Cl$ .

$\bar{\nu}_I = 771 \text{ cm}^{-1}$   
 $\bar{\nu}_N = 3293 \text{ cm}^{-1}$  } fixed



c) The internal barrier of the 'free' ion.

It has been seen that the  $\text{PF}_6^-$  salts do not show any of the effects of hydrogen bonding and that the external barriers are most probably very small if not zero. Consequently this salt provides an indicator of the 'free ion' internal torsion. Using the torsional frequency of  $264 \text{ cm}^{-1}$  for  $\text{CH}_3\text{NH}_3^+\text{PF}_6^-$  the S.H. and sinusoidal  $\bar{V}_3$  barriers calculate as follows:-

$$\text{S.H. } \bar{V}_3 \quad \underline{695 \text{ cm}^{-1}} \qquad \text{Mathieu } \bar{V}_3 \quad \underline{857 \text{ cm}^{-1}}$$

Using the value of  $229 \text{ cm}^{-1}$  for the internal torsional frequency of the deuterated salts yields the following barriers:-

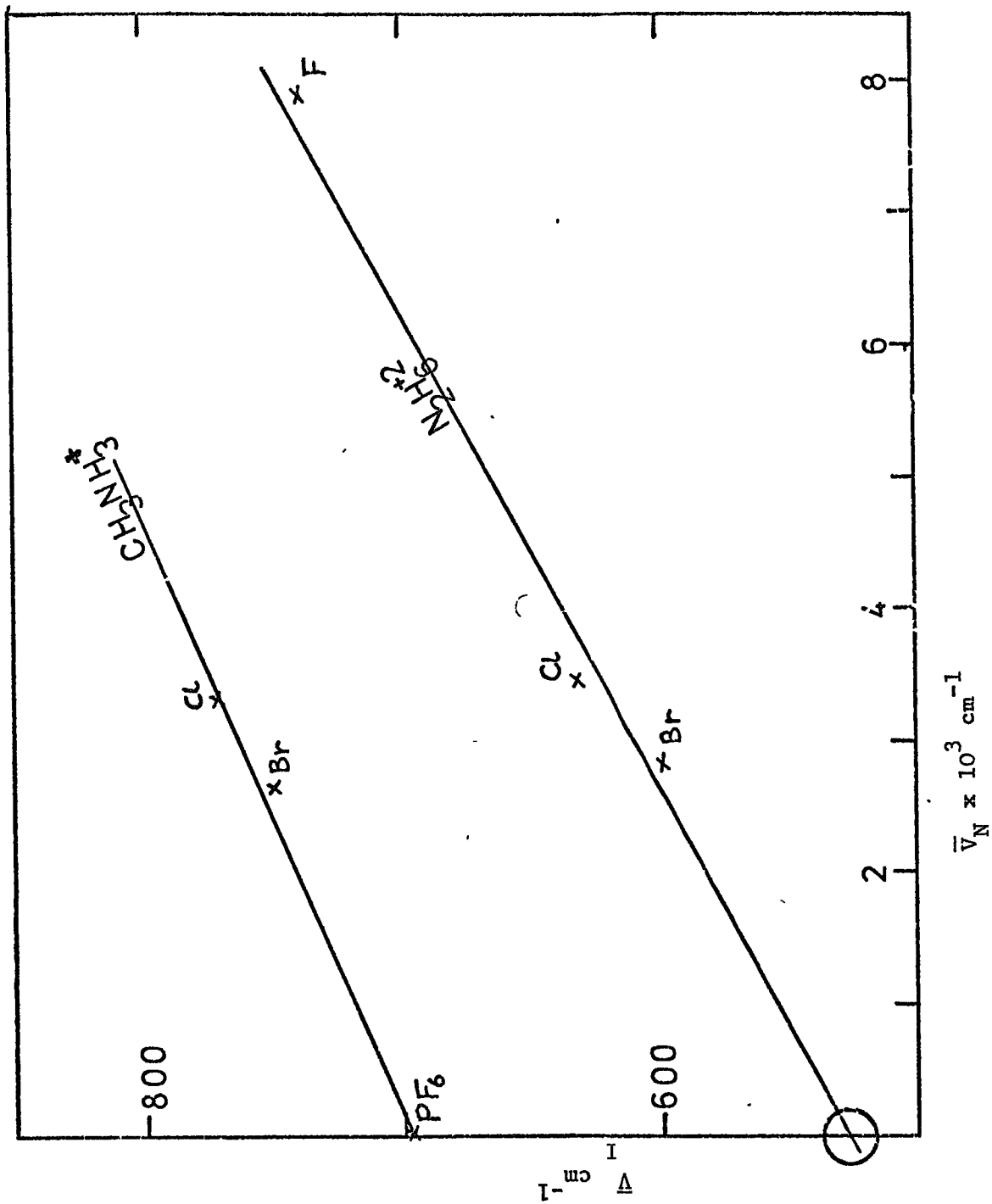
	<u>S.H.</u>	<u>Mathieu</u>
$\text{CD}_3\text{NH}_3^+$	$683 \text{ cm}^{-1}$	$825 \text{ cm}^{-1}$
$\text{CH}_3\text{ND}_3^+$	$712 \text{ cm}^{-1}$	$847 \text{ cm}^{-1}$

Consequently the average S.H. barrier is  $697 \text{ cm}^{-1}$ . These calculations in fact give maximum figures since any external barriers would mean that the observed torsional frequencies would be larger than the 'free ion' frequencies.

The interesting point about this is that it is still significantly lower than for the  $\beta\text{-CH}_3\text{NH}_3^+\text{Cl}^-$  case. This may help to confirm the idea of charge migration due to hydrogen bonding increasing the internal barrier, as suggested for the hydrazinium salts. It also suggests that the 'free ion' barrier for  $\text{N}_2\text{H}_6^{2+}$  may be considerably lower than the area of  $635 \text{ cm}^{-1}$  observed in its chloride salt.

A plot of  $\bar{V}_I$  vs.  $\bar{V}_N$  for the  $\text{CH}_3\text{NH}_3^+$  and  $\text{N}_2\text{H}_6^{2+}$  salts is shown in fig. (4.23) and if, as these suggest, the relationship is linear

Fig. (4.23) Variation of internal barrier with external H-bonding potential



the projected free ion non-H-bonded frequency for  $N_2H_6^{+2}$  is of the order of  $\sim 525 \text{ cm}^{-1}$ .

d) The  $\delta$  and  $\alpha'$  phases of the bromide and iodide and the  $\alpha$  phase chloride.

It became clear in making the assignments that the observed  $\bar{\nu}_{\text{NTOR}}$  bands of the  $\delta$ ,  $\alpha'$  and  $\alpha$  phases all have considerably lower frequencies than the  $\beta$ -phases. This would indicate that the external barriers have been much reduced and are probably too low for the three barrier S.H. model to hold rigorously. However they still show the frequency shift pattern on deuteration associated with a larger external barrier at the nitrogen end, which would also indicate that a "free ion" model would not hold.

However a number of qualitative points can be made from order of magnitude calculations and a consideration of what would happen to the three barrier S.H. model as the external barriers tend to zero. Fig. (4.24) shows graphically the variation of the torsion-libration frequencies ( $\bar{\nu}_{\text{NTOR}}$  and  $\bar{\nu}_{\text{CTOR}}$ ) for values of  $\bar{V}_N$  (the nitrogen end external barrier) from 0-1000  $\text{cm}^{-1}$ , when  $\bar{V}_I = 700 \text{ cm}^{-1}$  (probably the minimum internal barrier for H-bonded systems) and  $\bar{V}_c = 0$ . This shows that both frequencies decrease as  $\bar{V}_N$  decreases and that below  $\bar{V}_N \sim 200 \text{ cm}^{-1}$   $\bar{\nu}_{\text{CTOR}}$  falls rapidly to zero. Further calculations show that if  $\bar{V}_I$  were to increase by  $50 \text{ cm}^{-1}$  both frequencies would also increase but only slightly. If  $\bar{V}_c$  were to increase to say  $200 \text{ cm}^{-1}$  again both frequencies increase but  $\bar{\nu}_{\text{CTOR}}$  would increase much more than  $\bar{\nu}_{\text{NTOR}}$ . Fig.(4.25).

What is of immediate interest is that  $\bar{\nu}_{\text{CTOR}}$  is by no means zero for values of  $\bar{V}_N$  about  $300 \text{ cm}^{-1}$ ; the predicted frequencies are higher

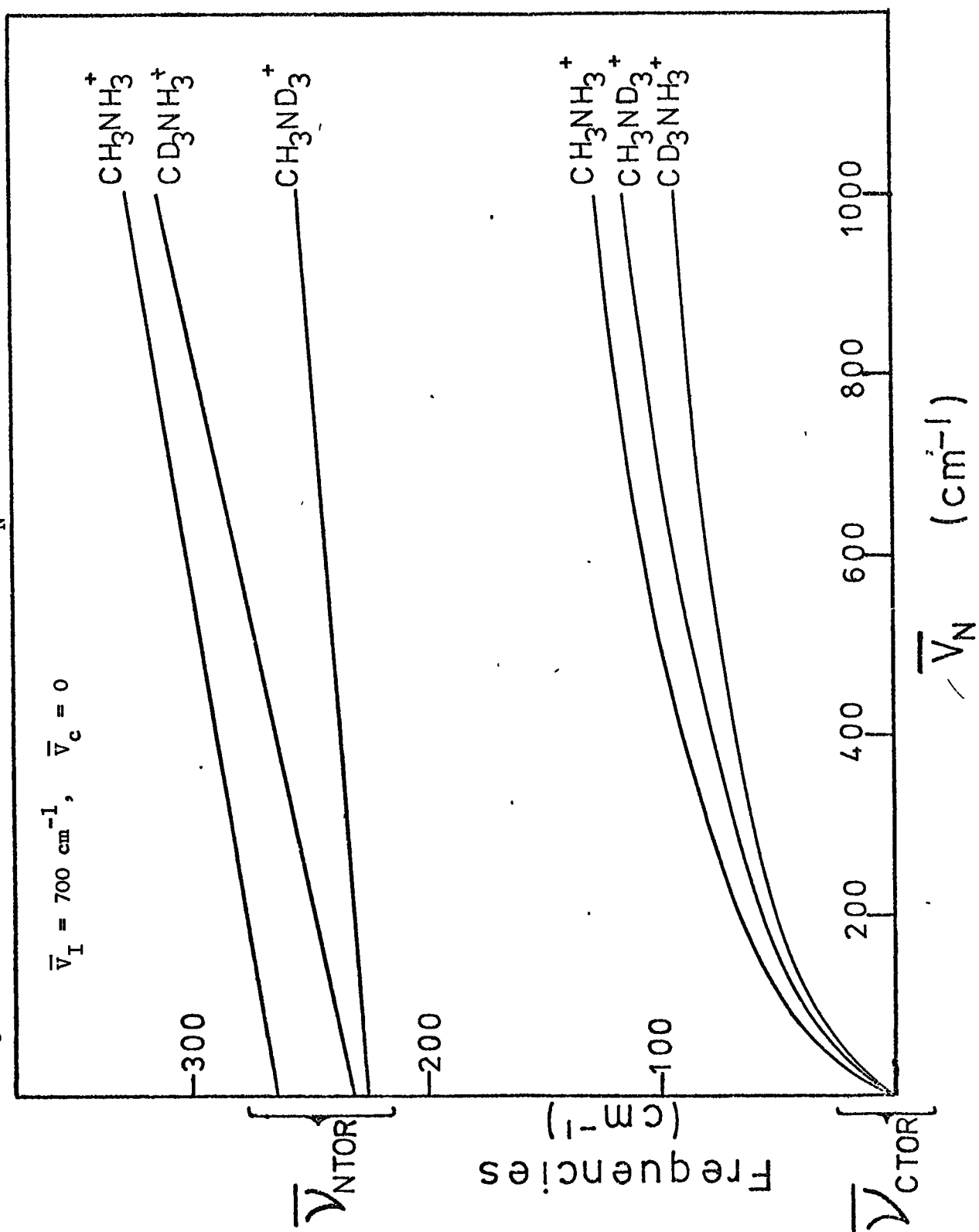
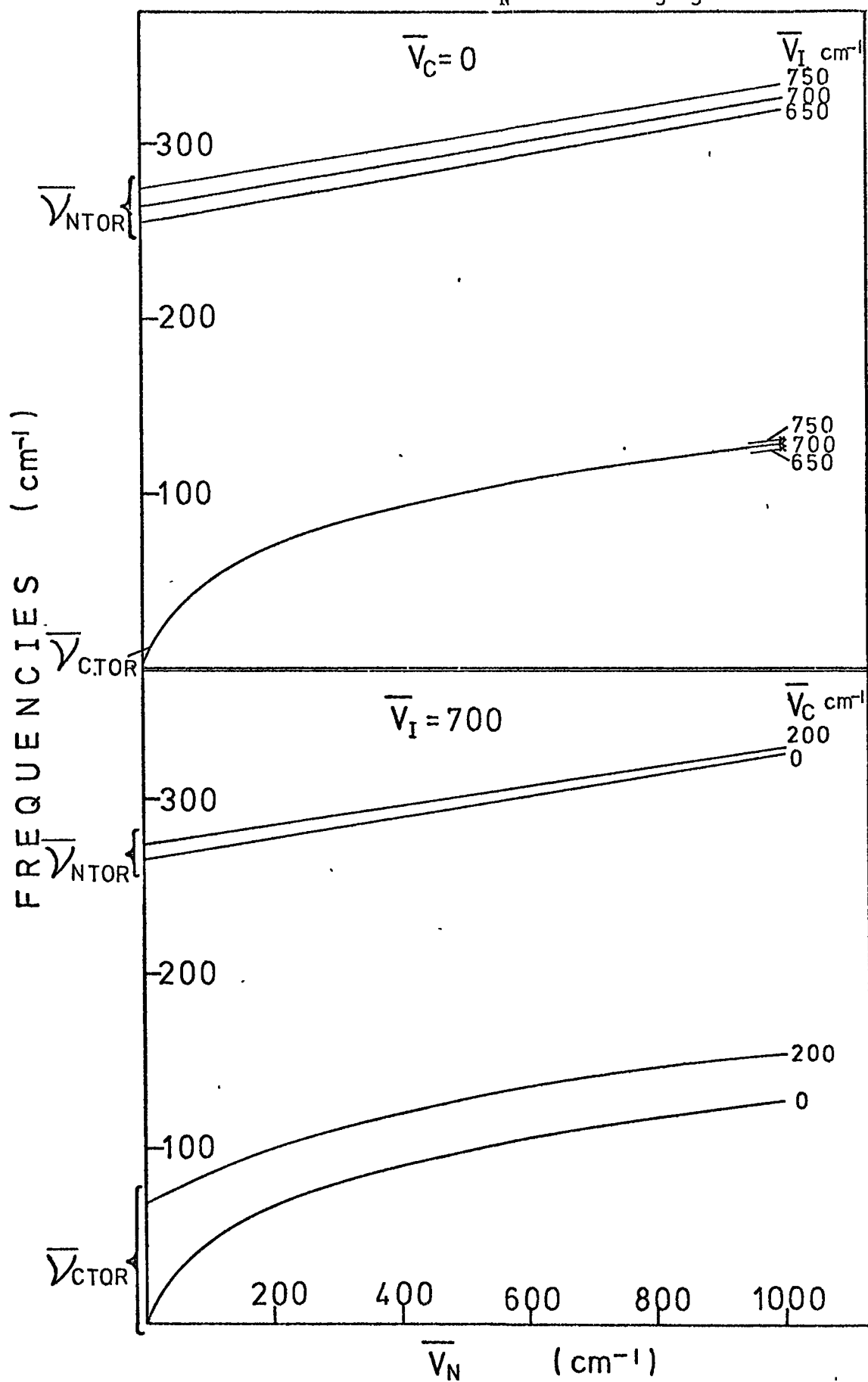
Fig. (4.24) Variation of frequencies as  $\bar{\nu}_N \rightarrow 0$ .



Fig. (4.25) Variation of  $\nu_{\text{NTOR}}$ ,  $\nu_{\text{CTOR}}$  under different conditions, as  $\bar{\nu}_{\text{N}} \rightarrow 0$  (for  $\text{CH}_3\text{NH}_3^+$  only).



than  $60 \text{ cm}^{-1}$ . (Although it should be remembered that the S.H. model does not work very well for such low barriers, it may still provide an indicator). Consequently  $\bar{\nu}_{\text{CTOR}}$  may well lie within the broad strong bands which appear in the I.N.S. time-of-flight spectra.

Since only the  $\bar{\nu}_{\text{NTOR}}$  band could be assigned for the  $\delta$ ,  $\alpha'$  and  $\alpha$  phases the effects of changing  $\bar{V}_N$  are of primary interest. The highest frequency observed for these phases was  $310 \text{ cm}^{-1}$  and since the graph (fig. 4.24) shows frequencies up to  $325 \text{ cm}^{-1}$  these should all be covered by the plots. The behaviour on deuteration is interesting. As was seen for the  $\beta$ -phases the calculated  $\bar{\nu}_{\text{NTOR}}$  for  $\text{CD}_3\text{NH}_3^+$  lies close to that of  $\text{CH}_3\text{NH}_3^+$  for higher external barriers, and that for  $\text{CH}_3\text{ND}_3^+$  lies much lower; then as the barrier reduces the  $\bar{\nu}_{\text{NTOR}}$  frequency of  $\text{CD}_3\text{NH}_3^+$  moves lower, away from the value for  $\text{CH}_3\text{NH}_3^+$  whereas  $\text{CH}_3\text{ND}_3^+$  gets closer. At  $\bar{V}_N = 0$  the calculated values for both deuterated species are very similar, as was in fact seen for the  $\text{PF}_6^-$  salts. All the available frequencies for the  $\delta$ ,  $\alpha'$  and  $\alpha$  phases indicate that the difference between the frequencies of  $\text{CH}_3\text{NH}_3^+$  and  $\text{CD}_3\text{NH}_3^+$  is less than that between  $\text{CD}_3\text{NH}_3^+$  and  $\text{CH}_3\text{ND}_3^+$ . On the graph this situation occurs above  $\bar{V}_N \sim 400 \text{ cm}^{-1}$ , although to be realistic, since the model is breaking down all one can say is that the situation implies that  $V_N$  is still somewhat greater than zero.

Considering the  $\delta$  phase of the bromide, it has already been found that 3 N-H---Br bonds produce a barrier of  $\sim 2800 \text{ cm}^{-1}$ . If only 2 or 1 H-bonds can form, the expected barriers (neglecting any effects from the free N-H bonds) would be  $\sim 1870 \text{ cm}^{-1}$  and  $\sim 933 \text{ cm}^{-1}$  respectively.

(Again one should really multiply by 9 here to express the figures in terms of  $(n^2\bar{V})$ , the force constant, rather than a three-fold barrier). A  $\bar{V}_N$  barrier of  $1870 \text{ cm}^{-1}$  would give much too high a frequency for  $\bar{\nu}_{\text{NTOR}}$ , whereas  $\bar{V}_N = 933 \text{ cm}^{-1}$  (from the graph) gives a  $\bar{\nu}_{\text{NTOR}}$  of  $\sim 320 \text{ cm}^{-1}$  compared with  $305 \text{ cm}^{-1}$  observed for  $\delta \text{ CH}_3\text{NH}_3^+\text{Br}^-$ . This would perhaps indicate that for the  $\delta$ -phase bromide at best only one H-bond is formed. This would mean that the  $-\text{NH}_3^+$  group would become slightly asymmetric and may produce a crystal field splitting of the group modes. Sandorfy (4) reported slight splittings for the  $\delta$ -bromide but saw only correlation effects for the  $\delta$ -iodide. However the effect in the iodide may be very weak; its torsional frequency of  $276 \text{ cm}^{-1}$  is only  $12 \text{ cm}^{-1}$  greater than the 'free ion' frequency indicating a very low external barrier.

The  $\alpha$  and  $\alpha'$  phases present a different problem in that it is known from their crystal structures that the external field is 4-fold. The frequencies observed for these phases clearly indicate something of a barrier at the nitrogen end and the only way this could be accounted for is in a twelve fold barrier. Considering  $\alpha \text{ CH}_3\text{NH}_3^+\text{Cl}^-$  the  $\bar{\nu}_{\text{NTOR}}$  band appears at  $\sim 310 \text{ cm}^{-1}$ . On the graph (fig. 4.24) this corresponds to a force constant of  $\sim (9 \times 750) = (n^2\bar{V}_N)$ . For  $n = 12$  the twelve-fold barrier  $(\bar{V}_N)_{12}$  calculated from this would be  $\sim 47 \text{ cm}^{-1}$ . This is certainly not sufficient to localise the rotor to one position, and so the idea of orientational disordering must be replaced by rotation above the barriers. The same must hold for the  $\alpha'$  phases of the bromide and iodide since their  $\bar{\nu}_{\text{NTOR}}$  frequencies are even lower. The  $\alpha'$  to  $\delta$  phase transition in these two salts may be a distortion from 4-fold symmetry which moves one N-H into the field of a halide ion and the other two N-H's further away.

e) A consideration of the reported fluoride data (3).

It may be worthwhile speculating about the number of hydrogen bonds present in the  $\text{CH}_3\text{NH}_3^+\text{F}^-$  salt. Sandorfy (3) observed a torsional band at  $547\text{ cm}^{-1}$  at cold temperatures for this salt. This is somewhat below the frequency of the external mode in  $\text{N}_2\text{H}_6^{+2}\text{F}_2^-$  at  $635\text{ cm}^{-1}$ . Again by trying external barrier values equivalent to  $1/3$  or  $2/3$  of the barrier in  $\text{N}_2\text{H}_6^{+2}\text{F}_2^-$  and assuming that the internal barrier will be higher than for the chloride, say  $\sim 800\text{ cm}^{-1}$  torsional frequencies can be calculated and compared with the observed frequency.

For 2H-bonds:-

$$\bar{V}_N = 5252\text{ cm}^{-1}$$

$$\bar{V}_I = 800$$

$$\bar{V}_c = 0$$

$$\bar{v}_{\text{NTOR}} = 562\text{ cm}^{-1}$$

$$(\bar{v}_{\text{CTOR}} = 179\text{ cm}^{-1})$$

or if  $\bar{V}_c = 1000\text{ cm}^{-1}$

$$\bar{v}_{\text{NTOR}} = 563\text{ cm}^{-1}$$

$$(\bar{v}_{\text{CTOR}} = 279\text{ cm}^{-1})$$

For 1 H-bond:

$$\bar{V}_N = 2626\text{ cm}^{-1}$$

$$\bar{V}_I = 800$$

$$\bar{V}_c = 0$$

$$\bar{v}_{\text{NTOR}} = 431\text{ cm}^{-1}$$

$$(\bar{v}_{\text{CTOR}} = 165\text{ cm}^{-1})$$

or if

$$\bar{V}_c = 1000\text{ cm}^{-1}$$

$$\bar{v}_{\text{NTOR}} = 436\text{ cm}^{-1}$$

$$(\bar{v}_{\text{CTOR}} = 265\text{ cm}^{-1})$$

It can be seen that for  $\bar{V}_c = 0$  or  $1000\text{ cm}^{-1}$  the values of  $\bar{v}_{\text{NTOR}}$  is not much affected, and that the observed torsional frequency at  $547\text{ cm}^{-1}$

would best fit a situation involving only two H-bonds.

This would seem rather odd in view of the fact that in  $N_2H_6^{+2}F_2^-$  (see Chapter 3) and  $NH_4^+F^-$  (31) the structures indicate that all possible N-H---F bonds are formed.

In  $CH_3NH_3^+F^-$  the H-bonding should be still much stronger than in the other  $CH_3NH_3^+$  halide salts and one would rather have expected to see 3 N-H---F bonds involved, especially since the  $\beta$ -chloride and bromide show that this situation is possible for even weaker H-bonds, so perhaps the assignment is wrong.

f) The end-over-end modes.

A plausible argument to explain the changing intensity of these librational bands was given earlier. It would unfortunately be rather a difficult if not impossible task to attempt to calculate barriers for this kind of motion, since some way of determining the centre of motion must be found before the moments of inertia can be calculated. This is rather an important parameter and does change quite markedly as the centre of motion moves along the C-N axis:- e.g. for  $CH_3NH_3^+$  the motion around the centre of mass, at 0.691 Å from the nitrogen along the C-N axis, gives  $I = 21.12 \text{ a.m.u. \AA}^2$ . Shifting the centre of rotation to 0.295 Å from the nitrogen (a shift of only  $\sim 0.4 \text{ \AA}$ ) increases  $I$  to 26.13 a.m.u.  $\text{\AA}^2$ . The two different selective deuterations also causes the centre of motion to shift slightly, increasing the complexity of the problem. Consequently one would not feel justified in using the present data on more than a qualitative basis. The reason why the end-over-end libration frequency in the  $\alpha$ ,  $\alpha'$  phases is as high as the  $\beta$ -phases even though the N-H's are apparently not fixed in

localised H-bonds may be sought in the model described in fig. (1.4) of Chapter 1. It was shown that for a 3-fold rotor in a 4-fold environment the potential around the  $C_3$  axis was flat but the interactions are still present and the potential is raised, consequently motions around the other two axes will still pull on the (H-bonding) potential at the nitrogen end.

References - Chapter 4

1. J.G. Aston, C.W. Ziemer, J.A.C.S. 68, 1405 (1946).
2. P. Bridgman, Proc. Am. Acad. Arts Sci. 72, 227 (1938);  
ibid 76, 71 (1948).
3. A. Cabana, C. Sandorfy, Spectrochim. Acta. 18, 843 (1962).
4. A. Theoret, C. Sandorfy, Spectrochim. Acta 23A, 519 (1967).
5. J. Tsau, D.F.R. Gilson, Can. J. Chem. 48, 717 (1970).
6. S. Albert, J. Ripmeester, J. Chem. Phys. 58, 541 (1973).
7. P. Groth, Chemische Krystallographie, 1, 168 (1906).
8. S.B. Hendricks, Z. Kristallog. 67, 106 (1928).
9. E.W. Hughes, W.N. Lipscombe, J.A.C.S. 68, 1970 (1946).
10. E.J. Gabe, Acta. Cryst. 14, 1296 (1961).
11. M. Stammer, J. Inorg. Nucl. Chem. 29, 2203 (1967).
12. J.T. Edsall and J.T. Edsall, H. Scheinberg, J. Chem. Phys. 4,  
1 (1936); ibid 8, 520 (1940).
13. R.D. Waldron, J. Chem. Phys. 21, 734 (1953).
14. W. Kynaston, B.E. Larcombe, H.S. Turner, J.C.S. 1772 (1960).
15. P. Schmidt, P.S. Narayanan, J. Indian Inst. Sci. 52, 28 (1970).
16. N. Lenain, J.P. Mathieu, H. Poulet, Compt. Rendu. Acad. Sci.  
Ser. B 270, 753 (1970).
17. E. Whalley, J. Chem. Phys. 51, 4040 (1969).
18. A. Nakamura, T. Takenishi, M. Tsuboi, Symp. Molecular Structure  
and Spectroscopy, Tokyo (1962).
19. G. Borch, U. Anthoni, P.H. Nielsen, Acta Chem. Scand. 25, 784 (1971).

20. E. Castellucci, J. Mol. Struct. 23, 449 (1974).
21. J. Tegenfeldt, L. Odberg, J. Phys. Chem. Solids, 33, 215 (1972).
22. J. Tegenfeldt, T. Kedwsim, C. Saterkvist, Acta. Chem. Scand. 26, 3524 (1972).
23. E.R. Andrew, P.C. Canepa, J. Magn. Resonance, 7, 429 (1972).
24. D.T. Edmonds, M.J. Hunt, A.L. Mackay, J. Magn. Resonance, 9, 66 (1973).
25. F. Jellinek, Acta. Cryst. 11, 626 (1958).
26. P. Chevalier, C. Sandorfy, Symp. Molecular Structure and Spectroscopy Tokyo (1962).
27. A. Cabana, C. Sandorfy, Can. J. Chem. 40, 622 (1962).
28. J.D. Cox, R.D. Warne, J.C.S., 1896 (1951).
29. S.J. Cyvin, "Molecular Vibrations and Mean Square Amplitudes" Elsevier, Amsterdam 1968.
30. R. Ruppin, R. Englman, Rep. Prog. Phys. 33, 149 (1970).
31. R.C. Plumb, D.F. Hornig, J. Chem. Phys. 23, 947 (1955).



CHAPTER 5ANILINE HYDROCHLORIDE AND HYDROBROMIDEIntroduction

Work on the internal rotation of such molecules as toluene and its analogues has indicated that the potential barrier is extremely low. A microwave study on toluene itself (1) gave  $V_6 = 13.94 \pm 0.1$  cal/mole and recent work by Dempster, Powell and Sheppard (2) on the fine structure observed in the perpendicular stretching modes of the  $-\text{CH}_3$  group has shown that this is consistent with almost free rotation. On the basis of the discussion in the theory (Chapter 1) this is hardly surprising; the individual contributions of the three parts of the rotor against a 2-fold hindrance sum up to zero for the first term  $V_3$  of the expanded potential function and the  $V_6$  term produces a 6-fold ripple. Only when there are ortho substituents does the barrier increase significantly (3).

It might therefore be expected that a very similar situation should occur in the anilinium ion  $\text{C}_6\text{H}_5\text{NH}_3^+$ . This presents the attractive possibility of observing the separate  $-\text{NH}_3^+$  group motion hindered almost solely by an external crystal field, and similarly the separate externally hindered ring motion. A study of the halide salts should give a reasonable check of the external barriers obtained for  $-\text{NH}_3^+$  groups in the hydrazinium and methylammonium salts, provided that the symmetry of the external field is 3-fold and the internal barrier negligible in comparison.

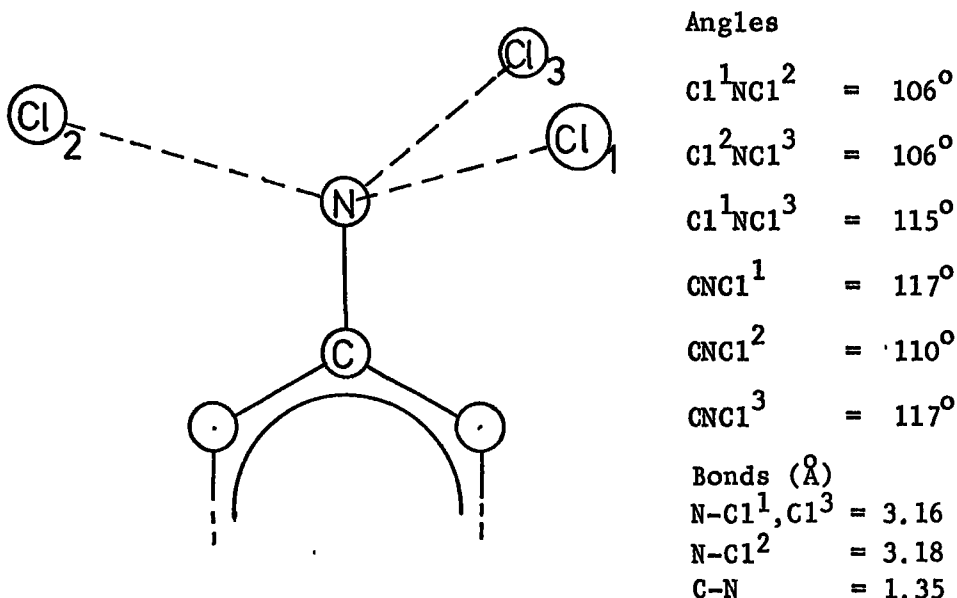
Structural studies of the chloride and bromide salts have been done (see below) and so these compounds were chosen for spectral work.

### Section 1. Previous Studies.

Brown (4) determined the room temperature X-ray crystal structure of the chloride, and no phase changes on cooling have been reported:-

Space group  $C_c$   $z = 4$  Monoclinic  $\beta = 101^\circ \pm 30'$   
 $a = 15.84 \pm 0.03$ ,  $b = 5.33 \pm 0.03$ ,  $c = 8.58 \pm 0.03 \text{ \AA}$

The most important feature is the fact that 3  $\text{Cl}^-$  ions sit around the  $-\text{NH}_3^+$  group as shown in fig. (5.1).



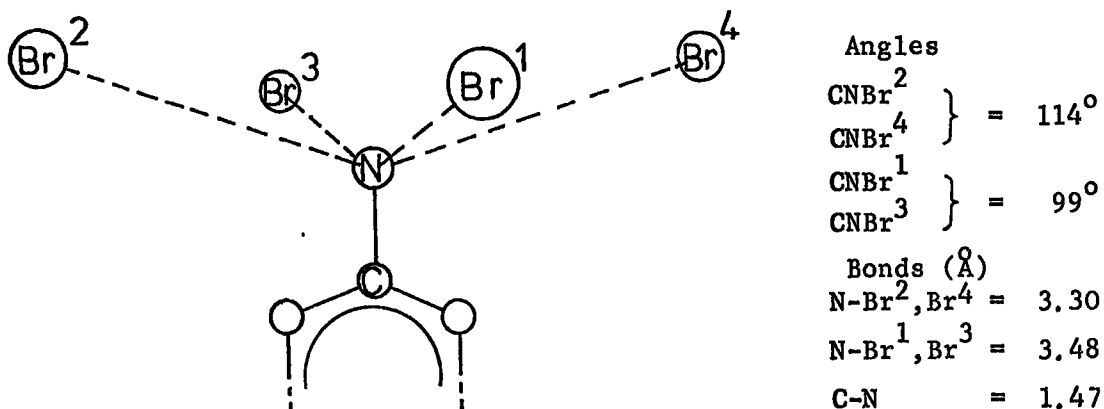
None of these angles are far removed from the  $T_d$  angle but there is some asymmetry.

The planes of neighbouring rings make an angle of  $64^\circ$  with each other and have nearest C---C approaches of  $3.85 \text{ \AA}$ .

The bromide was studied by Taguchi et al (5) who discovered two phases. The higher temperature orthorhombic structure has been reported in full (5) but that of the cold monoclinic phase was not published, although Taguchi (6) described the phase change and gave the space group, from which the essential features can be surmised:-

Temperature	70°	-110°
Space Group	$D_{2h}^{10} - P_{naa}$	$C_{2h}^5 - P2_1/a$
a	$16.77 \pm 0.06 \text{ \AA}$	$16.725 \pm 0.06 \text{ \AA}$
b	$6.05 \pm 0.03$	$5.95 \pm 0.03$
c	$6.86 \pm 0.03$	$6.81 \pm 0.03$
$\beta$	90°	91° 22'
	z = 4	z = 4

The environment of the  $-\text{NH}_3^+$  group in the orthorhombic phase is indicated in fig. (5.2):—

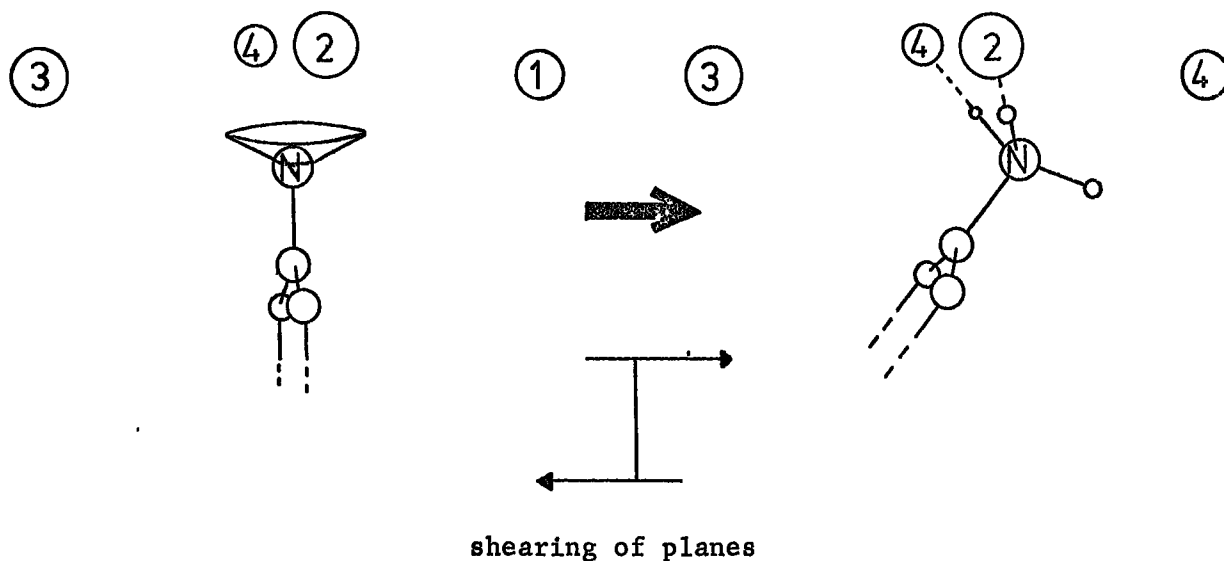


The planes of neighbouring rings make an angle of 45° to each other.

This time there are 4  $\text{Br}^-$  ions around the  $-\text{NH}_3^+$  but it should be noted that two are nearer than the other two and the C-N-Br angles of these pairs are also different. On cooling below  $27.5^\circ\text{C}$  the substance undergoes a  $\lambda$  type phase transition where the axial angle  $\beta$  slowly increases from  $90^\circ$ , the transition being completed by about  $-70^\circ\text{C}$ . Tuguchi (6) described the process as a kind of shearing. He also pointed out that the  $-\text{NH}_3^+$  group can take up a fixed position in the low temperature form whereas the crystal symmetry of the orthorhombic form requires free rotation or disordering, and that the transition might be merely order-disorder. This was confirmed by Suga (7) who performed a calorimetric study of the salt and observed a typical order-disorder process with a critical temperature of  $22^\circ\text{C}$ . A calculation assuming a transition between the ordered state and one disordered over two positions gave an entropy change of 1.06 e.u. compared with 1.10 e.u. observed, although it should be pointed out that other effects had to be accounted for in this calculation. Hence it was pointed out that disordering over two positions for the room temperature phase is only a possibility.

Effectively the picture which one envisages is that the cell is sheared a little so that two of the hydrogens approach two bromide ions close enough to become fixed in H-bonds, the third moving further away from a third bromine, fig. (5.3). The results of the present investigation would tend to favour this picture.

Fig. (5.3) Probable mechanism of phase transition.



Some comment should also be made on the reported C-N lengths for these two salts, of 1.35 Å (chloride) and 1.47 Å (bromide). The change in the chloride is somewhat drastic compared with values seen for example in  $\text{CH}_3\text{NH}_3^+$  of 1.465 Å (chloride) and 1.48 Å (bromide) (Refs 9, 10 Chapter 4). The change of bond length from  $\text{CH}_3\text{-CH}_3$  to  $\text{CH}_3\text{-C}_6\text{H}_5$  is also small; 1.543  $\rightarrow$  1.52 respectively (13) and consequently one would tend to place more faith in the value of 1.47 Å as the C-N length in the anilinium ion.

Sandorfy et al (8-10) obtained I.R. spectra of the aniline hydrohalides between 4000-1500 $\text{cm}^{-1}$  and later Sandorfy and Cabana (11) extended this to 600  $\text{cm}^{-1}$  and cold temperatures. This effectively confirmed that the chloride had no phase change on cooling as far as  $-190^\circ$  and that the bromide did not show any more phases down to this temperature. As might be expected from the crystal structures the spectra of the two phases of the bromide were quite different from each other and also from the chloride. The spectrum of the chloride was related to the  $\beta$ -phase spectra of the methylammonium salts with a combination band reminiscent of ( $\nu_6 + \nu_9$ ), a characteristic of these

phases appearing at  $\sim 2040 \text{ cm}^{-1}$ . The room temperature bromide gave a spectrum with broad features on some bands reminiscent of the  $\alpha$  phase methylammonium salts where the external symmetry is fourfold. On going to the cold phase, which Sandorfy suggested might be similar to the  $\delta$ -phases of the methylammonium salts, the broad features sharpened up and a combination band appeared at  $\sim 1850 \text{ cm}^{-1}$ , this time not very strong. Sandorfy was unwilling to compare this band with the  $(\nu_6 + \nu_9)$   $\beta$ -methylammonium band which he thought should be higher, and suggested it was a combination of  $\nu_9$  + a lattice vibration at about  $300 \text{ cm}^{-1}$ .

Because of the complexity of the spectra due to the ring not all bands were assigned. (However for convenience the  $-\text{NH}_3^+$  rotor motion or torsion will be referred to as  $\nu_6$  and the asymmetric  $-\text{NH}_3^+$  bend as  $\nu_9$  so that the interesting combination may be referred to again as  $(\nu_6 + \nu_9)$  ).

## Section 2. Experimental.

Samples of the two salts were readily available and purified by recrystallisation from ethanol. Their room temperature I.R. spectra were identical to those reported earlier (8-11).

A 6H time-of-flight neutron spectrum of a sample of the chloride had been obtained previously but not analysed by a former colleague Dr M. Jinks who kindly passed this on. This showed a very intense peak  $\sim 438 \text{ cm}^{-1}$  which is at the poor resolution region of the 6H machine. Both salts were therefore run on the Be-filter

machine at liquid nitrogen temperatures. I.R. spectra were obtained at room and liquid nitrogen temperatures down to  $250\text{ cm}^{-1}$  on the P.E. 457 and at room temperature for the chloride and cold for the bromide on the F.S. 720, in the far I.R.

Raman spectra of the low frequencies were obtained using the red laser since the green laser caused decomposition, and even in red light the bromide showed fluorescence and gave a poor spectrum.

The neutron spectra are shown in figs. (5.4 - 5.5 )

Frequencies are given in tables (5.1, 5.2). The bands with shoulders seen in the neutron spectra were analysed with the curve resolver using peak functions with a full width at half maximum of  $40\text{ cm}^{-1}$ . The resolved bands are indicated in the tables by the prefix R.

### Section 3. Assignment of torsional bands.

Looking for the strongest peaks in the beryllium filter spectra immediately suggests that the bands at  $442\text{ cm}^{-1}$  for the chloride and  $294\text{ cm}^{-1}$  for the bromide are torsional frequencies. For the chloride comparison with the I.R. spectrum also shows a total absence of this band whereas the other bands are all present. (The room and cold temperature I.R.s are also confirmed as identical apart from some slight intensity changes). The cold bromide I.R. spectrum however does show an intense sharp band at  $298\text{ cm}^{-1}$  corresponding with the neutron band, but it should be noted that this is not present for the room temperature phase, whereas all the other bands are common to both phases. It will also be noticed that the remaining spectral

Fig. (5.4) Time-of-flight spectrum of the chloride.

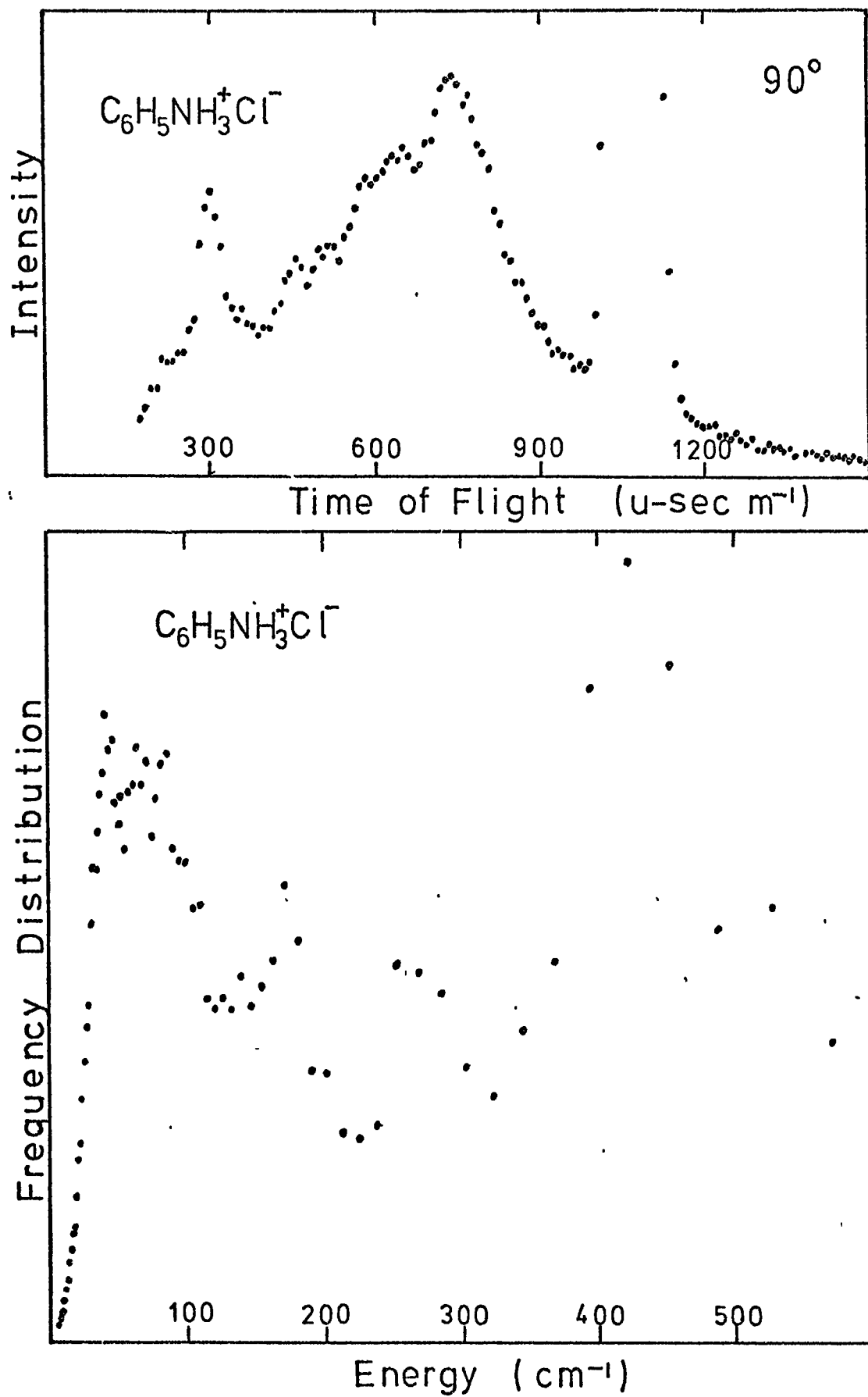




Fig. (5.5) Beryllium filter spectra.

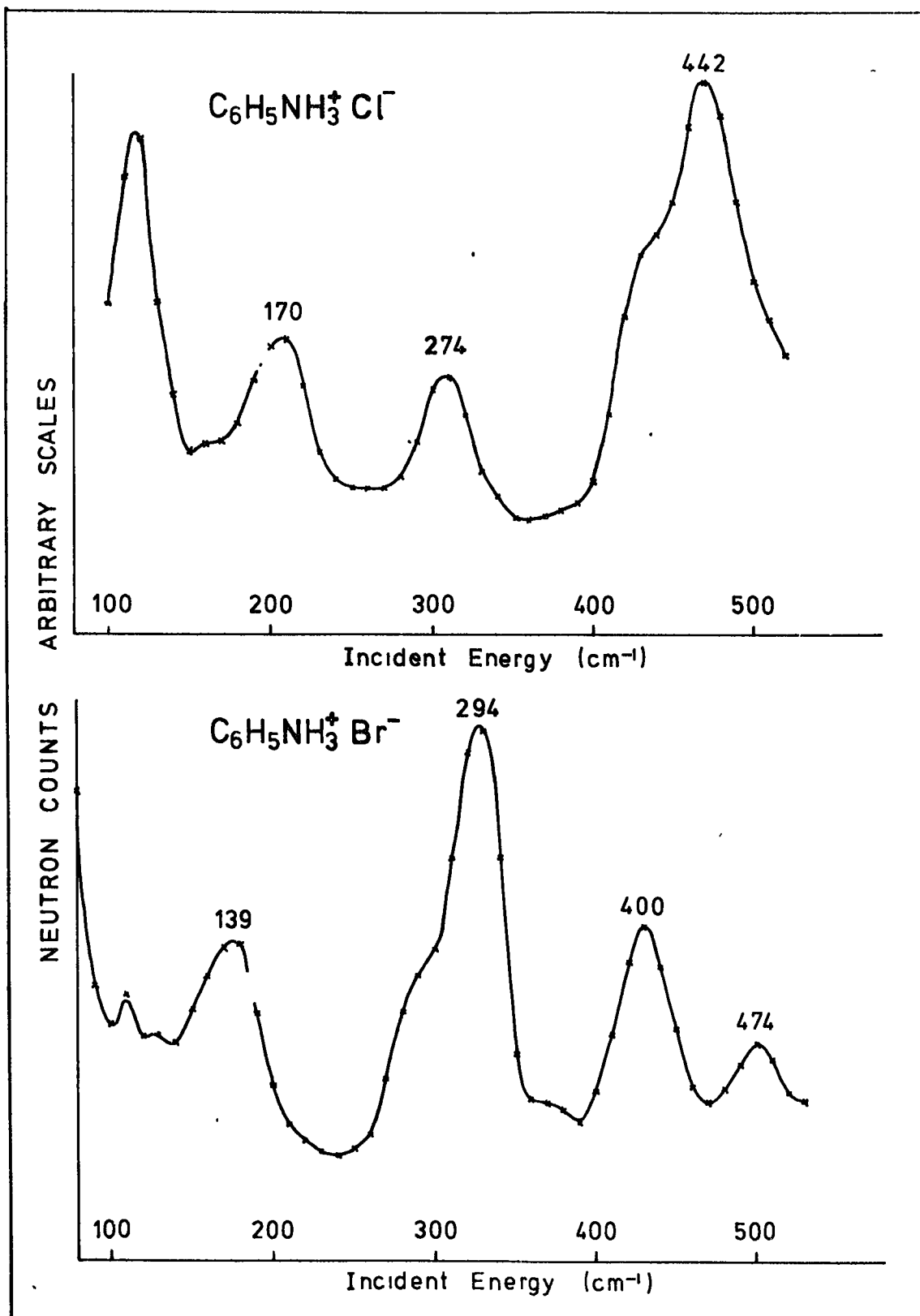


Table (5.1)

Spectroscopic frequencies of  $C_6H_5NH_3^+Cl^-$  ( $cm^{-1}$ )

I. R. *	Raman ‡	I. N. S		Assignment
		6H‡	Be-filter *	
621 w	~ 615 v.w			} Ring Modes
	~ 579 v.w			
527 w	~ 524 v.w		R 478 m	} $-NH_3^+$ Torsion( $\nu_6$ )
479 s		~ 438 v.s	442 v.s.	
406 v.s			R 404 m.s.	} Ring Modes
281 } v.s				
272 }		~ 275m. brd	274 m	} Ring Mode or Translation?
171 brd v.s	172 w	171 m	170 m	
141 m.s		~ 140 v.w?		} Translational Modes
	~ 120 v.w			
	{ 94 m.s	~ 96 m.sh		} $C_6H_5^-$ , and
	{ 89sh.	~ 86 s		
	64 v.w	~ 68 s		} $2 \times C_6H_5NH_3$
	{ 54 sh.w			
	{ 47 v.s	43 v.s		} Librations + Underlying Translations

\* At liquid nitrogen temperatures

‡ At room temperature

R = frequency obtained using curve resolver.

Table (5.2)

Spectroscopic frequencies of  $C_6H_5NH_3^+Br^-$  ( $cm^{-1}$ )

I.R.		I.N.S.	Assignment
Room Phase	Cold Phase	Be-filter (Cold Phase)	
616 v.w	~ 619 v.w		} Ring Modes
	565 v.w. brd		
528 w	526 w		
{ 478 m.s	{ 481 v.s	474 w	
{ 470 m	{ 470 m.s		
393 m	396 v.s	400 m.s	
	<u>298 v.s</u>	<u>294 v.s</u>	-NH <sub>3</sub> <sup>+</sup> Torsion ( $\nu_6$ )
Broad band { centred at ~ 255	259 brd v.s	R 252 m	Ring Mode
	{ 157 sh		} Ring Mode or Translation
	{ 145 } v.s	139 m.s	
	125 m		} Translations
	91 m		

bands of the bromide are similar to those of the chloride, but slightly shifted to lower frequencies.

Considering now Sandorfy's assignment of  $(\nu_6 + \nu_9)$  for the chloride and using the frequencies obtained in the present experiment  $(\nu_6 + \nu_9) - \nu_9 = 2020 - 1578 \rightarrow 442 \text{ cm}^{-1}$  for the  $-\text{NH}_3^+$  torsional frequency. Further assuming the combination band observed in the cold bromide is also  $(\nu_6 + \nu_9)$  the same arithmetic gives  $1850 - 1560 = 290 \text{ cm}^{-1}$  for the  $-\text{NH}_3^+$  torsion. Both figures correspond quite well with the suspected bands. It would therefore seem very reasonable to assign the strongest I.N.S. peaks as torsional frequencies.

Although the main object of this brief study has now been achieved, a short discussion of the rest of the spectral frequencies is in order. Without a much more detailed study, description of the peaks below  $300 \text{ cm}^{-1}$  can only be very broad. The I.N.S. and I.R. peaks which occur in both salts at  $\sim 400$  and  $\sim 475 \text{ cm}^{-1}$  can reasonably be assigned as ring bending modes. The I.N.S. peaks at  $274 \text{ cm}^{-1}$  (chloride) and  $252 \text{ cm}^{-1}$  (bromide) with I.R. counterparts may also fall into this category, and also the ones at  $170 \text{ cm}^{-1}$  (chloride) and  $139 \text{ cm}^{-1}$  (bromide) which have both I.R. and Raman counterparts. The fact that these 'internal' modes shift from chloride to bromide may be because they also involve some motion of the  $-\text{NH}_3$  side group which is affected by hydrogen bonding to different extents. (A more intense study of aniline itself (12) has shown that a number of the ring bending modes are sensitive to the  $-\text{NH}_2$  side group). The lower band could also possibly be explained as a

translational mode, though the shift is rather large, chloride to bromide.

The spectrum should also contain the three remaining librational modes i.e. the libration of the  $C_6H_5$  unit about the C-N axis, and the two end over end type librations. Unfortunately only the time-of-flight I.N.S. spectra of the chloride is available. On past record the librations would be expected to show up fairly strongly and indeed in the strong broad band below  $\sim 100\text{ cm}^{-1}$  three peaks are evident; a very strong sharp band at  $43\text{ cm}^{-1}$ , with two less clear but still strong at  $\sim 68$  and  $\sim 86\text{ cm}^{-1}$ . The barriers to the end-over-end rotations would on the grounds of steric hindrance alone be expected to be higher, but on top of this they also include the hydrogen bonding at the  $-NH_3$  end, with which the  $C_6H_5$ -unit rotation about the C-N axis is not involved. On these grounds one might expect that the band at  $43\text{ cm}^{-1}$  is the  $C_6H_5$ -motion. However it should also be pointed out that the moment of inertia of this mode ( $\sim 89\text{ a.m.u. \AA}^2$ ) is likely to be somewhat less than for the end-over-end motions, and so on these grounds its frequency relative to the two others ought to be pushed up. Hence the assignments of these three peaks are difficult to decide, but a  $C_6D_5-NH_3$  study ought to resolve the problem since in the I.N.S. spectrum the  $C_6D_5$ -libration should be inactive.

#### Section 4. Discussion and Calculation of Barriers.

The immediate point of interest is that the frequency of the  $-NH_3^+$  group motion for the chloride  $442\text{ cm}^{-1}$  is in the proximity of the external frequency of  $N_2H_6Cl_2$  at  $422\text{ cm}^{-1}$  as would be expected if the barrier is totally external but the band in the bromide at  $294\text{ cm}^{-1}$

is nowhere near the value of  $387 \text{ cm}^{-1}$  for  $\text{N}_2\text{H}_6\text{Br}_2$ . This would not seem unreasonable in view of the different structures.

Considering the chloride, the torsional frequency being  $20 \text{ cm}^{-1}$  higher than in  $\text{N}_2\text{H}_6\text{Cl}_2$  requires some comment. In  $\text{N}_2\text{H}_6\text{Cl}_2$  the N--Cl distances are  $3.10 \text{ \AA}$  and hence shorter than those in  $\text{C}_6\text{H}_5\text{NH}_3^+\text{Cl}^-$ , which would indicate slightly stronger H-bonding in the former case and suggests on this basis alone that the magnitudes of the frequencies ought to be the other way round. Also if the  $-\text{NH}_3^+$  rotor is rigidly  $\text{C}_3$  the slight distortion from true  $\text{C}_3$  external symmetry in  $\text{C}_6\text{H}_5\text{NH}_3^+\text{Cl}^-$  would be expected to result in a reduction in the barrier, since the contributions from each proton would be slightly out of phase and hence not add up to the maximum barrier value. This again should produce a lower frequency. However, it is quite possible, if the rotor is able to distort, that at the equilibrium configuration of the torsional oscillation each proton is at a position of maximum H-bond interaction.

This change of rotor geometry would also affect the moment of inertia, to which the frequencies are quite sensitive. In fact if the protons lie on the N---Cl lines the moment of inertia of  $-\text{NH}_3^+$  for  $\text{C}_6\text{H}_5\text{NH}_3^+\text{Cl}^-$  would be smaller than for  $\text{N}_2\text{H}_6\text{Cl}_2$ . Then since  $\bar{\nu}^2 \propto \bar{V}_3 / I_{\text{NH}_3}$  if these two compounds had the same barrier ( $\bar{V}_3$ ) then  $\text{N}_2\text{H}_6\text{Cl}_2$  would have the lower frequency. However in the absence of a knowledge of the proton positions this can only be speculation.

Aside from the discussion above, the most plausible reason for the slightly higher frequency is that it is due to a small coupling with the ring via the  $V_6$  barrier which is not strictly zero. However the model used for the  $\text{CH}_3\text{NH}_3^+$  salts has not been developed

for such small perturbations and hence the present situation must be approximated to a pure external barrier to  $-\text{NH}_3$  rotation.

Barrier values have been calculated using the simple expression

$$\bar{V}_E = \frac{8\pi^2 c I_{\text{NH}_3}}{9h} \bar{\nu}^2$$

with moments of inertia calculated for Td C-N-H angles and for the C-N--Cl angles of the structure. The S.H. results for  $\text{N}_2\text{H}_6\text{Cl}_2$  are presented alongside for comparison.

Table (5.3) Barrier to  $-\text{NH}_3^+$  group motion in  $\text{C}_6\text{H}_5\text{NH}_3^+\text{Cl}^-$ .

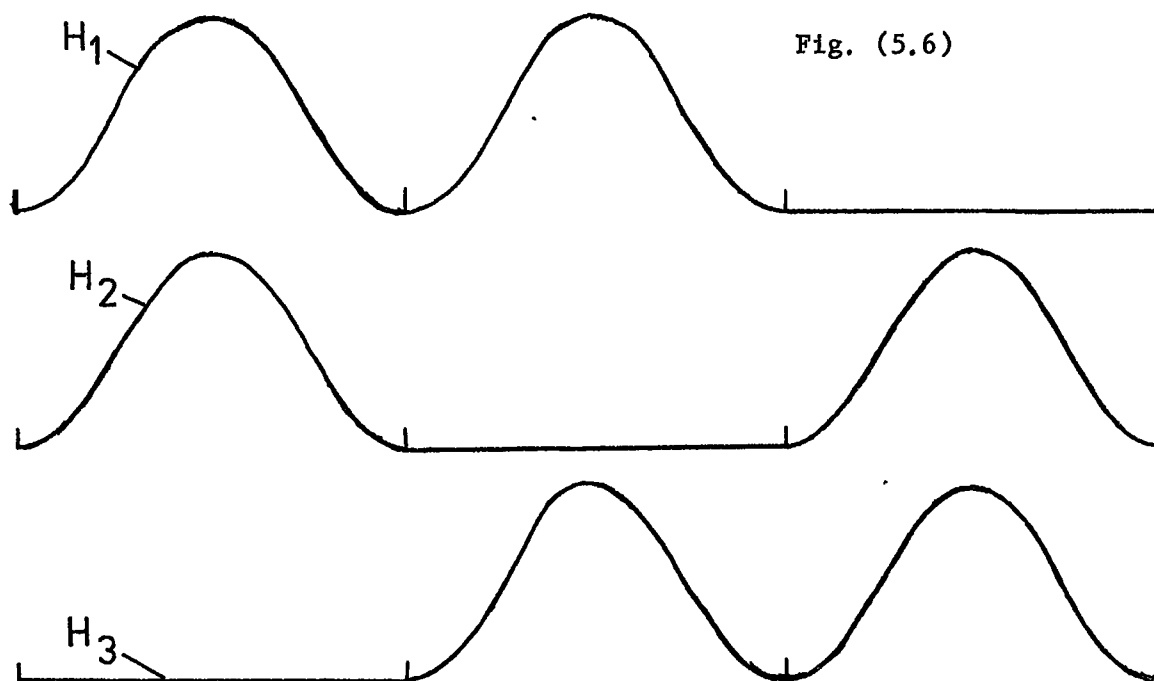
	N-H $\text{\AA}$	$\text{C}_6\text{H}_5\text{NH}_3\text{Cl}$		$\text{N}_2\text{H}_6\text{Cl}_2$	
		$I_{\text{NH}_3}$ a.m.u. $\text{\AA}^2$	$\bar{V}_E$ $\text{cm}^{-1}$	$I_{\text{NH}_3}$ a.m.u. $\text{\AA}^2$	$\bar{V}_E$ $\text{cm}^{-1}$
Td	1.04	2.907	3745	2.907	3414
Angles	1.03	2.851	3673	2.851	3348
Crystal	1.04	2.693	3470	3.172	3724
Geometry	1.03	2.642	3403	3.111	3653

It is interesting to note that using the geometry of the crystals the barrier calculated for  $\text{N}_2\text{H}_6\text{Cl}_2$  is in fact the higher, but what is most relevant is the fact that values for the barriers are of the same order.

The bromide frequency  $294 \text{ cm}^{-1}$  emphasises the fact that the external symmetry does not maximise the barrier, so strictly speaking the usual direct calculation should not be attempted. However, a crude approximation permits an estimate using the S.H. model:

Consider the monoclinic phase arrangement described earlier (fig. (5.3))

where there are probably only 2 strong H-bond interactions. The sum of the interactions of the 3 protons turned through  $2\pi$  still crudely produces a 3-fold potential as indicated in fig. (5.6) but the barrier height is only  $2/3$  that for 3 H-bonds. The biggest approximations here are assuming (a) the potential away



from the two bromides is zero, and (b) the phase relationship is  $2\pi/3$ .

If as is suggested, the two H-bonds are strong enough to localise the rotor protons to oscillations in the potential well, then the S.H. model can again be used.

The results of this calculation using Td configuration of  $-\text{NH}_3^+$  are shown below together with the equivalent  $\text{N}_2\text{H}_6\text{Br}_2$  data.



Table (5.4)

Barrier to  $-\text{NH}_3^+$  group motion in the cold phase of  
 $\text{C}_6\text{H}_5\text{NH}_3^+\text{Br}^-$ .

$\frac{\text{N-H}}{\text{Å}}$	$I_{\text{NH}_3}$ a.m.u. Å <sup>2</sup>	$\text{C}_6\text{H}_5\text{NH}_3\text{Br}$ $\bar{\nu}_E$ (cm <sup>-1</sup> )	$\text{N}_2\text{H}_6\text{Br}_2$ $\bar{\nu}_E$ (cm <sup>-1</sup> )
1.04	2.907	1657	$2871 \times 2/3 = 1914$
1.03	2.851	1625	$2816 \times 2/3 = 1877$

Clearly the correspondence is not nearly so good but the results are again in the same area, so perhaps the crude picture of the situation is not too far from the truth. The situation also contrasts with that in the  $\delta$ -phases of the  $\text{CH}_3\text{NH}_3^+\text{Br}^-$ ,  $\text{I}^-$  salts where it has been shown that probably only one H-bond is present.

A point should be made about the I.R. activities of the two compounds. The  $(\nu_6 + \nu_9)$  combination band seems to be characteristic of species with localised  $-\text{NH}_3^+$  group protons and hence this appears in both chloride and cold bromide.

The appearance or non-appearance of the  $(\nu_6 + \nu_9)$  type band is discussed in a wider context in Chapter 8. The chloride rather interestingly does not show the torsional band and so compares with the symmetrical hydrazinium salts, whereas the cold bromide shows this up very strongly (more so than in the  $\beta$ -methylammonium salts) which may be indicative of much greater assymetry. This again would fit the idea of only two strong H-bond interactions.

Clearly there is a great deal of room for further work on these salts. Selectively deuterated  $C_6D_5NH_3^+$  salts should help to sort out the lower frequency librations as well as the ring bending modes. This would also help to verify the decoupling (due to zero internal barrier) of the  $-NH_3^+$  and  $C_6H_5^-$  motions, depending on whether the  $-NH_3^+$  torsional band shifts or not. Selective N-deuteration should show a  $\sqrt{2}$  frequency shift for the  $-ND_3^+$  torsional mode of cold  $C_6H_5ND_3^+Br^-$  in its I.R. spectrum, and this band should not appear in the I.N.S. spectrum of either  $C_6H_5ND_3^+Cl^-$  or  $Br^-$ . Both these predictions depend on the total decoupling of the  $-ND_3^+$  and  $C_6H_5^-$  motions.

It would again be very useful and interesting to investigate say the  $PF_6^-$  salt, where the  $-NH_3^+$  motion may very well be nearly free, and the fundamental frequency very low.

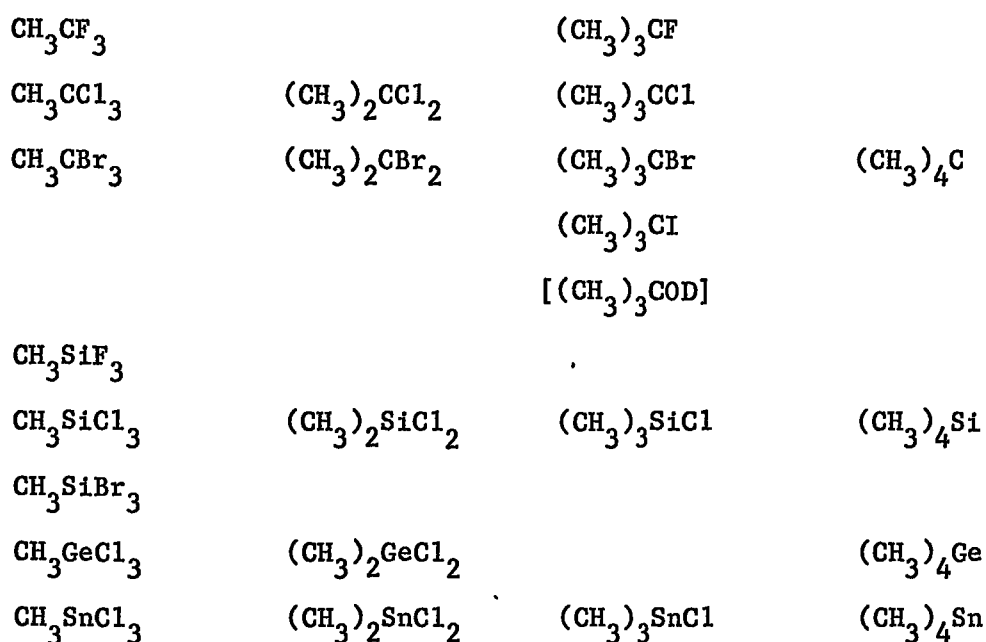
References - Chapter 5

1. H.D. Rudolph, H. Dreizler, A. Jaeschke, P. Wendline,  
Z. Naturforsch 22A, 940 (1967).
2. A.B. Dempster, D.B. Powell, N. Sheppard, Spectrochim. Acta  
31A, 245 (1975).
3. K.M. Jinks, T.C. Waddington, unpublished results.
4. C.J. Brown, Acta. Cryst. 2, 228 (1949).
5. I. Nitta, T. Watanabe, I. Taguchi, Bull. Chem. Soc. Jap. 34,  
1405 (1961).
6. I. Taguchi, *ibid* 34, 392 (1961).
7. H. Suga, *ibid* 34, 426 (1961).
8. B. Chenon, C. Sandorfy, Can. J. Chem. 36, 1181 (1958).
9. C. Brisette, C. Sandorfy, *ibid* 38, 34 (1960).
10. P. Chevalier, C. Sandorfy, *ibid* 38, 2524 (1960).
11. A. Cabana, C. Sandorfy, *ibid* 40, 622 (1962).
12. J.C. Evans, Spectrochim Acta 16, 428 (1960).
13. J.D. Roberts, M.C. Caserio 'Basic Principles of Organic Chemistry',  
Benjamin, N.Y. (1965) Pg.248.

CHAPTER 6METHYL HALOGENO COMPOUNDS OF GROUP IV ELEMENTSIntroduction

In order to observe the effects of multiple rotor internal interactions without too much interference from external effects, it was thought that it would be useful to study series of compounds such as  $(\text{CH}_3)_n\text{MX}_{(4-n)}$  where M is C, Si, Ge, Sn and X = F, Cl, Br, I ( $n = 1 \rightarrow 4$ ). A large amount of work has recently been done on many of these compounds using I.R., taking advantage of the breakdown of selection rules in the solid phase, and Raman studies of overtones in the gas phase. Since these methods often make assignments of extremely weak features, in areas which for some cases are complicated by other modes, we thought it would be useful to obtain neutron spectra both as an independent check and for comparison purposes. Earlier workers in the neutron field have looked at a few of these compounds using time-of-flight techniques, but were unable to attain anything like the resolution of the beryllium filter machine in the region of the torsional peaks.

A list of the compounds whose neutron spectra were obtained is given below. Completion of the various series was very dependent on availability of compounds, many of which were purchased and some prepared independently, but some gaps remain, leaving possible work for a future date.

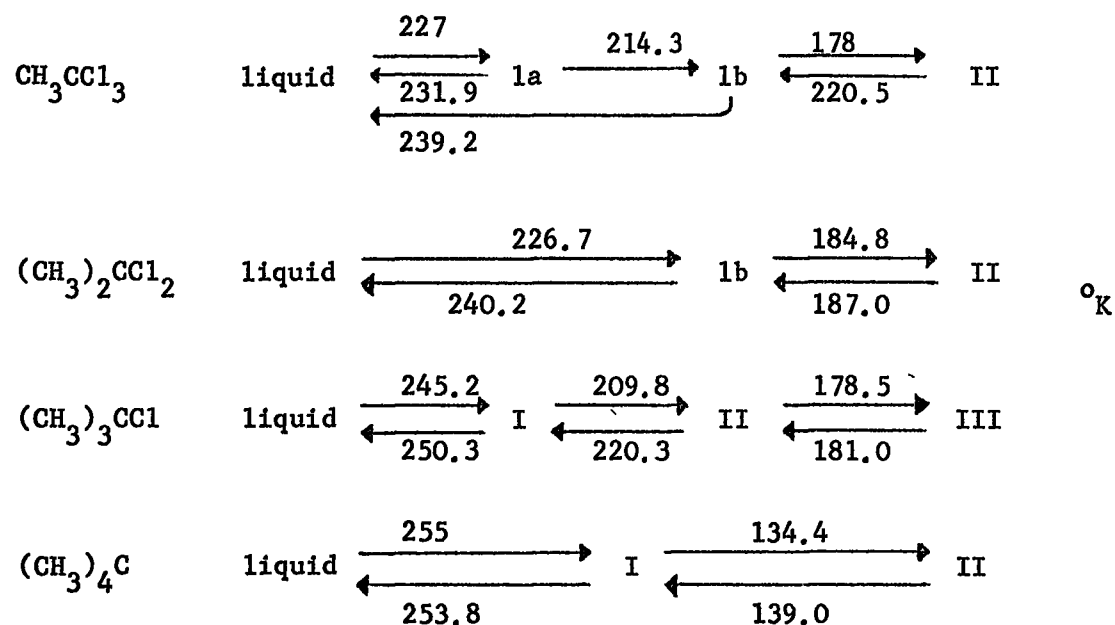


Methyl chloroform  $\text{CH}_3\text{CCl}_3$  and neopentane  $(\text{CH}_3)_4\text{C}$  alone have been the topics of a vast amount of research and many of the other compounds also appear in a number of papers. It would therefore be rather tedious to review each paper individually, so only a brief resumé of information will be presented here with numerous references. Relevant detailed data will be discussed along with the results of the present work for correlation and comparison. Compounds of the different group IV elements will be treated initially under separate sections, with cross-correlations at the end of the Chapter.

PART A : THE CARBON SERIESSection A1. Previous Work.

Many of these compounds have an almost spherical external nature, especially neopentane, and have thus been called "globular". They tend to form plastic crystals in their higher temperature phases in which the molecules still have a relatively large amount of rotational and translational freedom.

A differential scanning calorimetric study (1) has shown that compounds of the chlorine series have a number of phases.



So clearly any work done at liquid Nitrogen temperatures would involve their lowest phase. Other thermodynamics studies (2-5) have been done to obtain barriers but these are not all in agreement with determinations by other techniques, see table (6.23).

Only a few compounds have been studied by X-rays (6-10) at low temperature, from which some useful structural information for

calculating moments of inertia is available. The structure of  $\text{CH}_3\text{CCl}_3$  (9) clearly shows some distortion of the  $-\text{CCl}_3$  group which would account for breakdown of I.R. selection rules.

Microwave studies have principally been of the simpler  $\text{CH}_3\text{CX}_3$  types (11-15), although  $(\text{CH}_3)_3\text{CF}$  and  $(\text{CH}_3)_3\text{CH}$  have been studied (16) as well as  $(\text{CH}_3)_2\text{CHCl}$  (18) and  $(\text{CH}_3)_2\text{CH}_2$  (17). These again provide useful structural information (although strictly for the gas phase), and barrier parameters in some cases, which are given later.

I.R. and Raman spectra of most of the carbon series in one phase or another have been obtained and assigned (19-43). Durig and coworkers have made quite a large contribution in the low frequency area, in particular obtaining I.R. active torsional frequencies from the solids (23,24,37,42) and in a number of cases attempting to verify the assignment by isotopic substitution (i.e. seeing whether the peak shifts by an amount predicted by a simple calculation). Durig has also used the Raman technique to observe transitions of the torsion in the gas phase, for the transitions  $2 \leftarrow 0$ ,  $3 \leftarrow 1$  and sometimes  $4 \leftarrow 2$ ,  $5 \leftarrow 3$  (27). However the two compounds  $(\text{CH}_3)_2\text{CX}_2$ ,  $\text{X} = \text{Cl}, \text{Br}$  have not been investigated in the solid phase for torsional modes. An important feature of many of the spectra is that some of the fundamentals are of quite low frequency and hence complicate the assignment of torsions, especially so for the latter two compounds.

Normal coordinate treatments have appeared for  $\text{CH}_3\text{CX}_3$ ,  $\text{X} = \text{F}, \text{Cl}, \text{Br}$  (44, 21),  $(\text{CH}_3)_2\text{CCl}_2$  (30,31) and for neopentane (45,46), which can be usefully correlated with the intensity of I.N.S. peaks.

If a particular normal mode has a significant amount of H motion then it should appear in the I.N.S. spectrum with an intensity proportional to the proton amplitude.

I.N.S. spectra at various stages of development of the technique have appeared for  $\text{CH}_3\text{CF}_3$  gas,  $\text{CH}_3\text{CCl}_3$  liquid and solid, and neopentane liquid and solid (47-51).

N.M.R. investigations of  $(\text{CH}_3)_n\text{CCl}_{4-n}$  ( $n = 1 \rightarrow 4$ ) have again been undertaken at various stages of development of the technique (52-57) and also Chlorine N.Q.R. relaxation studies (58-61). Activation energies have been obtained from both line-width and  $T_1$  experiments. Since these were observed over a range of temperatures several of the crystal phases were involved; the motions causing the effects were shown to be essentially  $-\text{CH}_3$  group tunnelling for the coldest phase with molecular reorientation increasing in importance as the temperature was raised. In the case of  $\text{CH}_3\text{CCl}_3$  some effects may be due to  $-\text{CCl}_3$  reorientation.

#### Section A2. Experimental.

All the compounds of the carbon set except  $\text{CH}_3\text{CBr}_3$  were obtained from commercial sources:-

$\text{CH}_3\text{CF}_3$ ,  $(\text{CH}_3)_3\text{CF}$  from P.C.R. Inc. Gainesville, Florida;  
 $\text{CH}_3\text{CCl}_3$ ,  $(\text{CH}_3)_3\text{CX}$  ( $X = \text{Cl}, \text{Br}, \text{I}$ ) from B.D.H. Laboratories;  
 $(\text{CH}_3)_2\text{CCl}_2$  from I.C.N. Pharmaceuticals Inc., Plainview, N.Y.;  
 $(\text{CH}_3)_2\text{CBr}_2$  from C.P.L. Inc., College Point, N.Y.;  $(\text{CH}_3)_3\text{COD}$   
 from Merck, Sharp and Dohme, Montreal, Canada.

Samples were redistilled, and checked for impurities spectroscopically by comparing with literature values.



$\text{CH}_3\text{CBr}_3$  was kindly prepared by Dr C.J. Ludman and his assistants by the method of Stengle and Taylor (21), using the reaction of  $\text{CH}_3\text{CCl}_3$  with  $\text{AlBr}_3$  in dry  $\text{CS}_2$  in the presence of  $\text{HBr}$  at  $0^\circ\text{C}$ . The product thus formed was found to have some remnant C-Cl, probably  $\text{CH}_3\text{CBr}_2\text{Cl}$ , shown by I.R. mass spectrograph and V.P.C. The final sample of pure  $\text{CH}_3\text{CBr}_3$  was obtained using a gas chromatogram at  $125^\circ\text{C}$ , and this gave an I.R. spectrum identical to that reported by Durig (24).

Most of these compounds are liquids and as such were sealed into the silica liquid cans described earlier in Chapter 2 for the neutron work. This was generally performed using a vacuum-line, the liquid first being degassed by successive freezing and melting under reduced pressure and then distilled, where possible, under vacuum into the silica can held at liquid nitrogen temperature. The fluorine compounds and neopentane are gases under normal conditions and so required special handling. Neopentane could fortunately be held as a liquid under slight pressure in a dimpled silica can, but the fluorine samples could only be contained as liquids in stronger small bore sealed tubes. (This operation was kindly performed by Dr C.J. Ludman). Several of these were then fixed onto an aluminium sheet. This gave samples a little thicker than desirable for neutron experiments, although data collection was much faster.

The compounds  $\text{CH}_3\text{CI}_3$ ,  $(\text{CH}_3)_2\text{CI}_2$  and  $(\text{CH}_3)_3\text{CI}$  are photosensitive and hence difficult to handle, however  $(\text{CH}_3)_3\text{CI}$  was obtained. It was also found to decompose in the presence of air, and so was purified by vacuum distillation, the process being repeated several

times until a clear liquid resulted. This was sealed in a can and immediately wrapped in Al-foil. (The sample stored in this manner did not appear to have decomposed over the course of a year).

$\text{CH}_3\text{CBr}_3$  can be liquified by warming in the hand (m.p.  $\sim 30^\circ\text{C}$ ) and as such was run into an ordinary solids can and allowed to solidify.

Nearly all the compounds reduced to about  $3/4$  to  $2/3$  the volume of the liquid when frozen, a fact which had to be remembered when positioning the sample in the cryostat in the neutron beam.

Since the torsional frequencies of interest were expected to lie in the regions above  $\sim 200 \text{ cm}^{-1}$  all spectra were run only on the beryllium filter spectrometer at liquid nitrogen temperatures. Running at this temperature also had the advantage of reducing the complexity of the spectra since most of the transitions observed would be from a highly populated ground level e.g.  $0 \rightarrow 1$  or  $0 \rightarrow 2$ . A blank spectrum of silica tubes used for the fluoro compounds showed that these produced a background scatter of  $\sim 1/10$  of the base level of the samples, and hence it can be safely said that these should have no observable effect. I.R. spectra of the solids were only obtained where necessary for clarification.

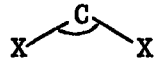
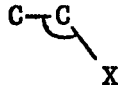
I.N.S. spectra are presented in figs (6.1 - 6.6 ) and the tables (6.2 - 6.15 ) also include equivalent I.R. and Raman data. It was found useful and necessary to use the curve resolver on a number of the I.N.S. peaks; some of the fits are shown superimposed on the spectra.

Section A3. Assignment and Discussion of Spectra.

(a) CH<sub>3</sub>CX<sub>3</sub> types.

The symmetry modes of these compounds are usually labelled as in the table below and the frequencies in previous studies have generally been labelled the same number with the same description, however the normal coördinate treatments clearly show that certain mode descriptions change from one compound to another.

Table (6.1)

Symmetry	Label *	Description †	
A <sub>1</sub>	S <sub>1</sub>	ν C-H	* S <sub>x</sub> = symmetry mode † ν = stretching mode δ = bending within the group i.e.  ρ = bending outside the group i.e.  sometimes called deformation.
	S <sub>2</sub>	δ CH <sub>3</sub>	
	S <sub>3</sub>	ν C-C	
	S <sub>4</sub>	ν C-X	
	S <sub>5</sub>	δ CX <sub>3</sub>	
A <sub>2</sub>	S <sub>6</sub>	torsion	
E	S <sub>7</sub>	ν C-H	
	S <sub>8</sub>	δ CH <sub>3</sub>	
	S <sub>9</sub>	ρ CH <sub>3</sub>	
	S <sub>10</sub>	ν C-X	
	S <sub>11</sub>	δ CX <sub>3</sub>	
	S <sub>12</sub>	ρ CX <sub>3</sub>	

The beryllium filter spectrum of CH<sub>3</sub>CF<sub>3</sub> fig. (6.1) clearly shows a very sharp intense band at 208 cm<sup>-1</sup>. Since the lowest of the other fundamentals is above 300 cm<sup>-1</sup> this can only be assigned as the torsion ν<sub>6</sub>, and compares with the I.R. value of 220 cm<sup>-1</sup> for the solid (23) and 220 ± 15 cm<sup>-1</sup> from the I.N.S. of the gas (50).

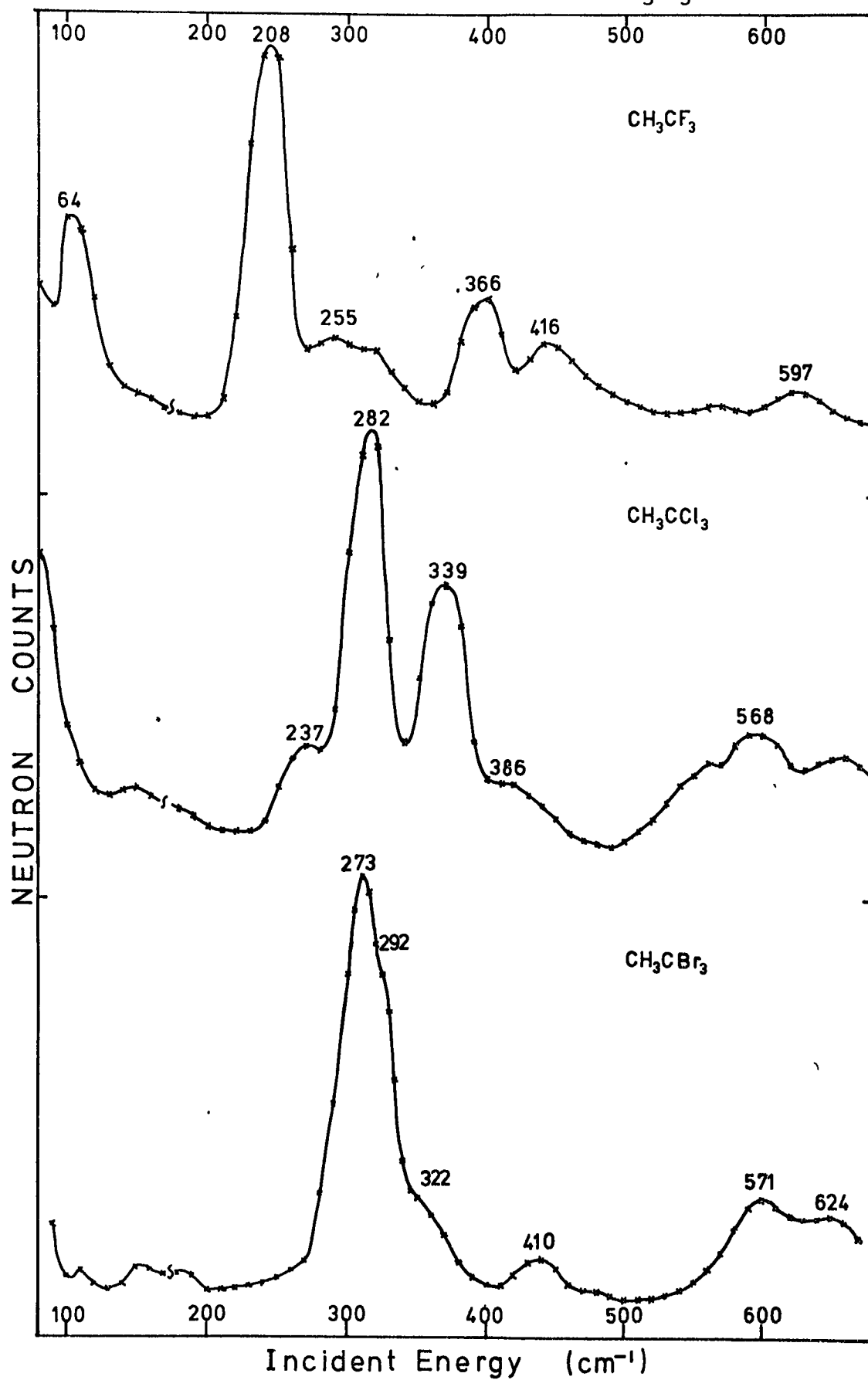
Fig. (6.1) Beryllium filter spectra of the  $\text{CH}_3\text{CX}_3$  types.

Table (6.2) Spectroscopic Frequencies  $\text{CH}_3\text{CF}_3$  ( $\text{cm}^{-1}$ )

I.R. (23)	Raman (21) Liquid 0°C	I.N.S. Solid	Assignment
377 (liq)	600	597 w	$\nu_5 \delta \text{CF}_3$
	538	(~ 540 vvw)	$\nu_{11} \delta \text{CF}_3$
	366	416 w	Double Scatter
		366 mw	$\nu_{12} \rho \text{CF}_3$
		~ 281 w	Double Scatter
<u>220</u> (solid)		~ 255 w	" "
		<u>208</u> v.s	$\nu_6$ Torsion
		~ 64 s	E Libration

The peak at  $366 \text{ cm}^{-1}$  identifies as  $\nu_{12}$  ( $\rho \text{CF}_3$ ), and shows an appreciable amount of H motion; this will be discussed shortly in the light of the normal coordinate analysis.  $\nu_5$  ( $\delta \text{CF}_3$ ) appears at  $597 \text{ cm}^{-1}$  and a faint trace of  $\nu_{11}$  ( $\delta \text{CF}_3$ ) at  $540 \text{ cm}^{-1}$ . This leaves a band at  $416 \text{ cm}^{-1}$  which at first sight might be assigned as the  $2 \leftarrow 0$  torsion, but some worry as to whether this might be double scattering on account of the greater thickness of the sample casts doubt on this. If this was the case, considering the peak at  $208 \text{ cm}^{-1}$  as the elastic centre the double scattered peak should appear at  $416 \text{ cm}^{-1}$ , and the equivalent of the  $366 \text{ cm}^{-1}$  peak should appear at  $\sim 582 \text{ cm}^{-1}$  with  $1/3$  the intensity of the  $416 \text{ cm}^{-1}$  peak. This does not appear, although it could be hidden under the wing of the  $597 \text{ cm}^{-1}$  band. A strong point in favour of double scattering

in this case is the result that a Mathieu type solution using  $208 \text{ cm}^{-1}$  as  $1 \leftarrow 0$  predicts  $2 \leftarrow 0$  at  $404 \text{ cm}^{-1}$ ,  $12 \text{ cm}^{-1}$  lower than the peak observed. Thus although this may be present beneath the  $416 \text{ cm}^{-1}$  peak, which appears slightly broadened, the main peak probably is due to double scattering. The remaining broad bands at about  $255, 281 \text{ cm}^{-1}$  could then be either combinations (less likely) or double scatter of the bands at  $\sim 64 \text{ cm}^{-1}$  (111 plane) and lower. The strong sharp feature in the Al 111 plane spectrum at  $\sim 64 \text{ cm}^{-1}$  is most probably the degenerate (E) whole body libration. A crude calculation of moments of inertia for this and the whole body principal axis rotation (A) gives  $I_E \sim 96 \text{ a.m.u. \AA}^2$ ,  $I_A \sim 92 \text{ a.m.u. \AA}^2$  i.e. roughly the same, but since the E mode needs more room to perform the motion it is likely to be more hindered and hence give the higher frequency.

Table (6.3) Spectroscopic Frequencies  $\text{CH}_3\text{CCl}_3$  ( $\text{cm}^{-1}$ )

I.R. Solid	Raman (21) Liquid	I.N.S. Solid	Assignment
563 w		568 mw	$2\nu_6$ Torsion $2 \leftarrow 0$
524 m	523	$\sim 525$ mw (386 w)	$\nu_4$ $\nu$ C1-C1 ? combination
346 m	343	339s	$\left\{ \begin{array}{l} \nu_5 \delta \text{ CCl}_3 \\ \nu_{11\rho} \text{ CCl}_3 \end{array} \right.$
<u>290</u> v.vw		<u>282</u> v.s	$\nu_6$ Torsion
<u>290</u> vw *			
249 m *	238	237 m.w	$\nu_{12} \delta \text{ CCl}_3$

\* = ref (23)

The neutron spectrum of  $\text{CH}_3\text{CCl}_3$  fig. (6.1) shows the much greater resolution of the beryllium filter instrument over that used earlier by Rush (47), who was only able to observe an unresolved band at  $\sim 300 \text{ cm}^{-1}$ . The strongest band at  $282 \text{ cm}^{-1}$  would agree with Durig's assignment of the torsion at  $290 \text{ cm}^{-1}$  in the I.R. (23). The I.R. of the solid was checked and apart from an almost invisible peak at 290, a weak band was also observed at  $563 \text{ cm}^{-1}$  which would fit the observed  $2 \leftarrow 0$  transition assigned by Durig (27) at  $564 \text{ cm}^{-1}$  in the gas phase Raman spectrum.

The peaks at 237, 339 can be correlated unambiguously with corresponding I.R. and Raman peaks, but the most striking feature of the spectrum is the high intensity of the  $339 \text{ cm}^{-1}$  band, which has been assigned to the two modes  $\nu_5$  ( $\delta \text{ CCl}_3$ ), and  $\nu_{11}$  ( $\rho \text{ CCl}_3$ ). Although chlorine has an incoherent cross section of 3.5 barns this small contribution to the scattering cannot explain the intensity; a large amount of hydrogen motion must therefore be involved.

An interesting feature of the neutron torsional bands for both compounds discussed so far is their full width at half maximum (F.W.H.M.) which is between  $36\text{-}40 \text{ cm}^{-1}$ , which is the minimum width allowed by the resolution response function for the machine.

Looking now at the  $\text{CH}_3\text{CBr}_3$  neutron spectrum fig. (6.1) the picture is more confused. The strongest band is centered at  $278 \text{ cm}^{-1}$  but shows a definite broadening and a shoulder to higher frequency (F.W.H.M. =  $46 \text{ cm}^{-1}$ ), and a weaker shoulder even higher. The problem now presented is that a strong band appears in the I.R. and Raman at  $\sim 278 \text{ cm}^{-1}$  assigned as  $\nu_{11}$  ( $\rho \text{ CBr}_3$ ) and Durig has

Table (6.4) Spectroscopic Frequencies  $\text{CH}_3\text{CBr}_3$  ( $\text{cm}^{-1}$ )

I.R. $\sim 290^\circ\text{K}$	I.R. (liq. $\text{N}_2$ )	I.R. Solid (24)	Raman (21) Liquid	I.N.S. * Solid	Assignment
625 vs	{ 621 vs 609 sh		628	624 mw	$\nu_{10}$ $\nu$ C-Br
564 vw	565 vvw			571 mw	$2\nu_6$
414 w	417 w		408	410 w	$\nu_4$ $\delta$ $\text{CBr}_3$
		(310)		R 322 w	( $\nu_6$ + Lib.)?
	297 vw	<u>304</u> vw		R <u>292</u> s	$\nu_6$ Torsion
278 w	278 w	277		R 273 vs	$\nu_{11}$ $\rho$ $\text{CBr}_3$
216		220	211	-	$\nu_5$ $\nu$ C-Br
152		154		143 vw	$\nu_{12}$ $\delta$ $\text{CBr}_3$
		146		115 vw	
				68 vw	

\* R = Frequency obtained using curve resolver.

assigned the torsion  $\nu_6$  as a weak I.R. band in the solid at  $304 \text{ cm}^{-1}$  (24), however no deuterated compound was studied to confirm this.

When curve resolution was attempted, in no way could a fit be obtained using a stronger peak on the higher frequency side, within the constraints of the usual bandwidth. Using two main peaks the best fit frequencies with their relative intensities in brackets were: 273 (10), 292 (7) and the weak shoulder at  $332 (2) \text{ cm}^{-1}$ , although this was by no means perfect. Considering the shifts in frequency seen for the fluoride and chloride between I.R. and I.N.S.,  $292 \text{ cm}^{-1}$  would agree reasonably with Durig's  $304 \text{ cm}^{-1}$ , whereas  $273 \text{ cm}^{-1}$  would be outrageous. If the higher frequency is the torsion the usual rule that this is the most intense band would appear to have broken down. The only other possible explanation is that the lower frequency conceals more than one band.



Fortunately further evidence regarding the torsion can be extracted from the rest of the neutron spectrum. Weak bands equivalent to  $\nu_4$  ( $\delta$   $\text{CBr}_3$ ) and  $\nu_{10}$  ( $\nu\text{C-Br}$ ) can be seen but also an extra stronger one at  $571 \text{ cm}^{-1}$ . Since this sample was packed in a thin solids can double scatter should not present a significant problem. Even if it did the band at  $278 \text{ cm}^{-1}$  would be the equivalent of the elastic peak and the main double scatter peak should then appear at  $2 \times 278 = 556 \text{ cm}^{-1}$ , which is somewhat below the one observed. Hence the most probable explanation of the peak at  $571 \text{ cm}^{-1}$  is that it is the torsional  $2 \leftarrow 0$  transition. The I.R. of the cold solid also gave a weak band at  $\sim 565 \text{ cm}^{-1}$ , although this has previously been assigned as  $2\nu_{11}$  ( $\rho$   $\text{CBr}_3$ ) (24), and Durig (27) has assigned  $2 \leftarrow 0$  and  $3 \leftarrow 1$  overtones in the gas phase Raman at  $583$  and  $553 \text{ cm}^{-1}$ . When  $292 \text{ cm}^{-1}$  is used as the  $1 \leftarrow 0$  frequency in a Mathieu type solution, the equivalent  $2 \leftarrow 0$  transition calculates at  $572 \text{ cm}^{-1}$ , which is coincident with the observed band. If  $278 \text{ cm}^{-1}$  is used as  $1 \leftarrow 0$ ,  $2 \leftarrow 0$  would come at  $\sim 546 \text{ cm}^{-1}$  and there is no evidence of a band here in the neutron spectrum. Hence the assignment would seem fairly reasonable.

The only band now requiring explanation is the weak one at  $\sim 332 \text{ cm}^{-1}$  which does not seem to have any counterpart in the I.R. or Raman. Unless it is some impurity the most probable origin is a combination of  $\nu_6$  (torsion) and the principal axis external libration which is expected to be at very low frequency. Subtraction would place this at  $\sim 40 \text{ cm}^{-1}$  and the spectrum on the (111) plane data shows the neutron intensity rising sharply in this region. A cold

run on the 6H machine would clarify the picture.

The remaining point of immediate interest with respect to band intensities is that the band at  $143 \text{ cm}^{-1}$  ( $\nu_{12} \delta \text{ CBr}_3$ ) is very weak and that  $\nu_5$  ( $\nu\text{C-Br}$ ) expected at  $\sim 210 \rightarrow 220 \text{ cm}^{-1}$  does not show at all, indicating little or no proton motions in these modes.

### Band Intensities.

Remembering from Chapter 2 that the intensity of an I.N.S. peak is proportional to the mean square amplitude of vibration of the scattering atoms, the intensity spectrum of a compound could in theory be calculated with a knowledge of these parameters, but this is a rather long and complicated process and has not been attempted in the present study (for a recent example see ref. (62)). However a much simpler qualitative approach can be made: Since the amplitude of a normal mode is given by the mean square of the coordinate any assessment of the make up of the mode should be very instructive. A consideration of the symmetry coordinates which are involved in a normal mode or the distribution of the potential energy of the normal mode among the symmetry species, indicates whether or not hydrogen motions are involved, and whether to a greater or lesser extent.

Most normal coordinate treatments present matrices relating the normal and symmetry coordinates

$$Q = L^{-1}S$$

Q = normal coordinate matrix  
S = symmetry coordinate "

or  $S = LQ$                        $L^{-1} = \text{conversion}$                       "

or the potential energy distribution matrix (P.E.D.) the elements of which are given by

$$(\text{p.e.d.})_{ij} = \frac{l_{ij}^2 f_{ij}}{w_j}$$

where  $i = i^{\text{th}}$  symmetry mode     $j = j^{\text{th}}$  normal mode

$w =$  mode frequency     $f =$  element of potential energy.

The I.N.S. intensity is proportional to the mean square of the absolute displacements of the atoms, but the coordinates used in most normal coordinate treatments are mass weighted. This will be one source of error in this rather crude qualitative approach.

However applying these ideas to the present subject of study Stengle and Taylor (21) give P.E.D. values for all three compounds just discussed whereas Lafon and Nielsen (44) give  $L^{-1}$  for  $\text{CH}_3\text{CF}_3$ . There are some slight differences between the two but the main features are the same. The relevant P.E.D. values taken for convenience from Stengle and Taylor's tables are given in table (6.5). The symmetry coordinates marked H contain proton motions. What is immediately apparent is that the main symmetry contributions to  $\nu_{11}$ ,  $\nu_{12}$  ( $\delta, \rho \text{ CX}_3$ ) reverse on going from the fluoride to the chloride and bromide, as they also do in  $\nu_4$ ,  $\nu_5$  ( $\nu\text{C-X}$ ,  $\delta \text{ CX}_3$ ) for the bromide.

The total % P.E.D. contribution from hydrogen active symmetry modes to a given frequency can be taken from table (6.5). From this one then ought to be able to predict the degree of I.N.S.

Table (6.5) P.E.D. expressed as a %, for the low frequency modes,  
from ref (21).

	CH <sub>3</sub> CF <sub>3</sub>		CH <sub>3</sub> CCl <sub>3</sub>		CH <sub>3</sub> CBr <sub>3</sub>			
		$\nu_5$ 600cm <sup>-1</sup>	$\nu_4$ 525cm <sup>-1</sup>	$\nu_5$ 343cm <sup>-1</sup>		$\nu_4$ 408cm <sup>-1</sup>	$\nu_5$ 211cm <sup>-1</sup>	
A <sub>1</sub>								
HS <sub>1</sub>		0	0	0		0	0	
HS <sub>2</sub>		2	-1	0		-3	1	
S <sub>3</sub>		27	40	4		35	0	
S <sub>4</sub>		16	54	22		31	58	
S <sub>5</sub>		55	6	74		36	41	
		$\nu_{11}$ 538cm <sup>-1</sup>	$\nu_{12}$ 366cm <sup>-1</sup>	$\nu_{11}$ 343cm <sup>-1</sup>	$\nu_{12}$ 238cm <sup>-1</sup>	$\nu_{10}$ 628cm <sup>-1</sup>	$\nu_{11}$ 275cm <sup>-1</sup>	$\nu_{12}$ 145cm <sup>-1</sup>
E								
HS <sub>7</sub>	0	0	0	0	0	0	0	
HS <sub>8</sub>	1	1	1	0	0	1	0	
HS <sub>9</sub>	8	12	4	1	6	9	0	
S <sub>10</sub>	16	0	0	14	92	-15	20	
S <sub>11</sub>	51	25	19	63	19	5	74	
S <sub>12</sub>	24	63	76	0	17	100	5	

S = symmetry coordinate, see table (6.1)

Table (6.6) Predicted and observed I.N.S. activities of the  
CH<sub>3</sub>CX<sub>3</sub> (X = F, Cl, Br) compounds.

Compound	Mode Frequency (cm <sup>-1</sup> )	% P.E.D. total proton active symmetry modes	Prediction *	Observed * I.N.S.
CH <sub>3</sub> CF <sub>3</sub>	A <sub>1</sub> 600	2	✓ w	✓ w
	E {538 366}	9 13	✓ m ✓ s	? v.v.w. ✓ m
CH <sub>3</sub> CCl <sub>3</sub>	A <sub>1</sub> 525	-1	✓ w	✓ w
	E {343 238}	5 1	✓ m ✓ w	✓ s ✓ w
CH <sub>3</sub> CBr <sub>3</sub>	A <sub>1</sub> {408 211}	-3 1	✓ w ✓ v.w	✓ w X
	E {628 275 145}	6 10 0	✓ m ✓ s X	✓ m ✓ v.s. ✓ v.w.

\* ✓ = neutron active    X = inactive  
w = weak    s = strong    m = moderate    v = very

activity which might be expected to be seen for the mode; see Table (6.6) which includes the mode frequencies of interest.

It is clear from this that the predicted contributions are not too accurate; however it is interesting to note that the band with most intensity predicted is in fact the strongest observed band in each spectrum. This mode in each case is also best described as the deformation  $\rho$   $CX_3$  (see table (6.5)), so the effect of inertia on the massive  $CX_3$  group may be causing a wagging of the  $-CH_3$  group, giving rise to a large proton amplitude for the mode. In fact the P.E.D. table indicates that the  $\rho$   $CH_3$  symmetry coordinate contributes most of the proton motion in the mode. This inertia effect may well also account for the increasing I.N.S. intensity of the mode as the weight of the group  $CX_3$  increases,  $F \rightarrow Br$ .

(b)  $(CH_3)_2CCl_2$  and  $(CH_3)_2CBr_2$ .

The increased number of atoms in these compounds leading to 27 normal internal modes, none of which are symmetrically degenerate, means that the spectrum becomes much more complicated. The lower symmetry also gives the possibility of greater mixing of modes. The numbering and nominal description of the frequencies were given in an early work by Tobin (64), see table (6.7).

The two recently reported spectra do not agree on all points of assignment. Green and Harrison (30) seem to think that Klaboe's (29) sample of  $(CH_3)_2CCl_2$  was impure, which would be rather unfortunate in that Cyvin et al (31) used his frequencies in their force field and amplitude calculations. Cyvin gives the amplitude

Table (6.7)

	A <sub>1</sub>	A <sub>2</sub>	B <sub>1</sub>	B <sub>2</sub>
v C-H assym.	v <sub>1</sub>	v <sub>10</sub>	v <sub>15</sub>	v <sub>22</sub>
v C-H sym.	v <sub>2</sub>		v <sub>16</sub>	
δ CH <sub>3</sub> assym.	v <sub>3</sub>	v <sub>11</sub>	v <sub>17</sub>	v <sub>23</sub>
δ CH <sub>3</sub> sym.	v <sub>4</sub>		v <sub>18</sub>	
ρ CH <sub>3</sub>	v <sub>5</sub>	v <sub>12</sub>	v <sub>19</sub>	v <sub>24</sub>
v C-C	v <sub>6</sub>		v <sub>20</sub>	
v C-X	v <sub>7</sub>			v <sub>25</sub>
δ C-C-C	v <sub>8</sub>			
δ CX <sub>3</sub>	v <sub>9</sub>			
Skeletal twist		v <sub>13</sub>		
ρ Skeletal			v <sub>21</sub>	v <sub>26</sub>
CH <sub>3</sub> torsions		v <sub>14</sub>		v <sub>27</sub>
Optical Activity :-	Raman (P) I.R.	Raman	Raman I.R.	Raman I.R.

in terms of inter-atom displacements, unfortunately with no indication of their contribution to each normal mode, although it does show quite large movements between protons on different methyls. He also puts down 6 modes in B<sub>1</sub> and 7 in B<sub>2</sub> whereas all other authors have used 7, 6 respectively. A number of authors seem to have done the same thing in connection with the spectra of (CH<sub>3</sub>)<sub>2</sub>GeCl<sub>2</sub> and (CH<sub>3</sub>)<sub>2</sub>SnCl<sub>2</sub>. However this ambiguity could arise if during the molecular point group analysis the x and y axes were interchanged. In the present work the axes have been taken as in fig (6.7) and this gives the torsions as A<sub>2</sub> and B<sub>2</sub> symmetry. Exchanging the x and y axial labels gives the torsions as A<sub>2</sub> and B<sub>1</sub> and effectively all the B<sub>1</sub> and B<sub>2</sub> modes also interchange labels.

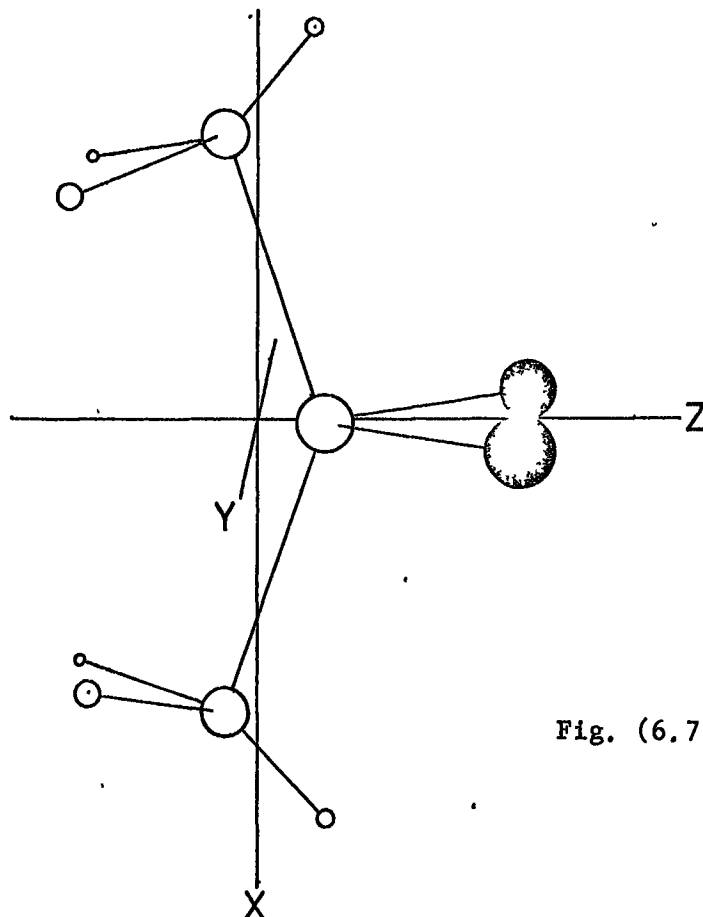


Fig. (6.7)

The P.E.D. calculated by Green and Harrison unfortunately only includes contributions of over 5%, so that all the lower frequencies appear to be composed of skeletal and C-X motions. The neutron spectrum again clearly shows considerable proton motions in some of these modes.

The neutron spectrum of the chloride (fig. 6.2) displays a moderately strong band at  $\sim 358 \text{ cm}^{-1}$  with a weak shoulder at higher frequency. This would correspond well with the solid I.R. bands at  $360 (\nu_{26}, \nu_8)$  and  $388 \text{ cm}^{-1} (\nu_{21})$ . The very strong neutron band centred at  $279 \text{ cm}^{-1}$  with a maximum at  $286 \text{ cm}^{-1}$  has quite obviously some underlying peaks; its F.W.H.M.  $\approx 70 \text{ cm}^{-1}$ . There is little doubt that this band contains the two torsional modes since their frequencies would not be expected to shift drastically from the value for  $\text{CH}_3\text{CCl}_3$ . The two torsions may be expected to have roughly equal intensities in the neutron spectrum, so assuming for the moment that these make up the band a curve analysis using only

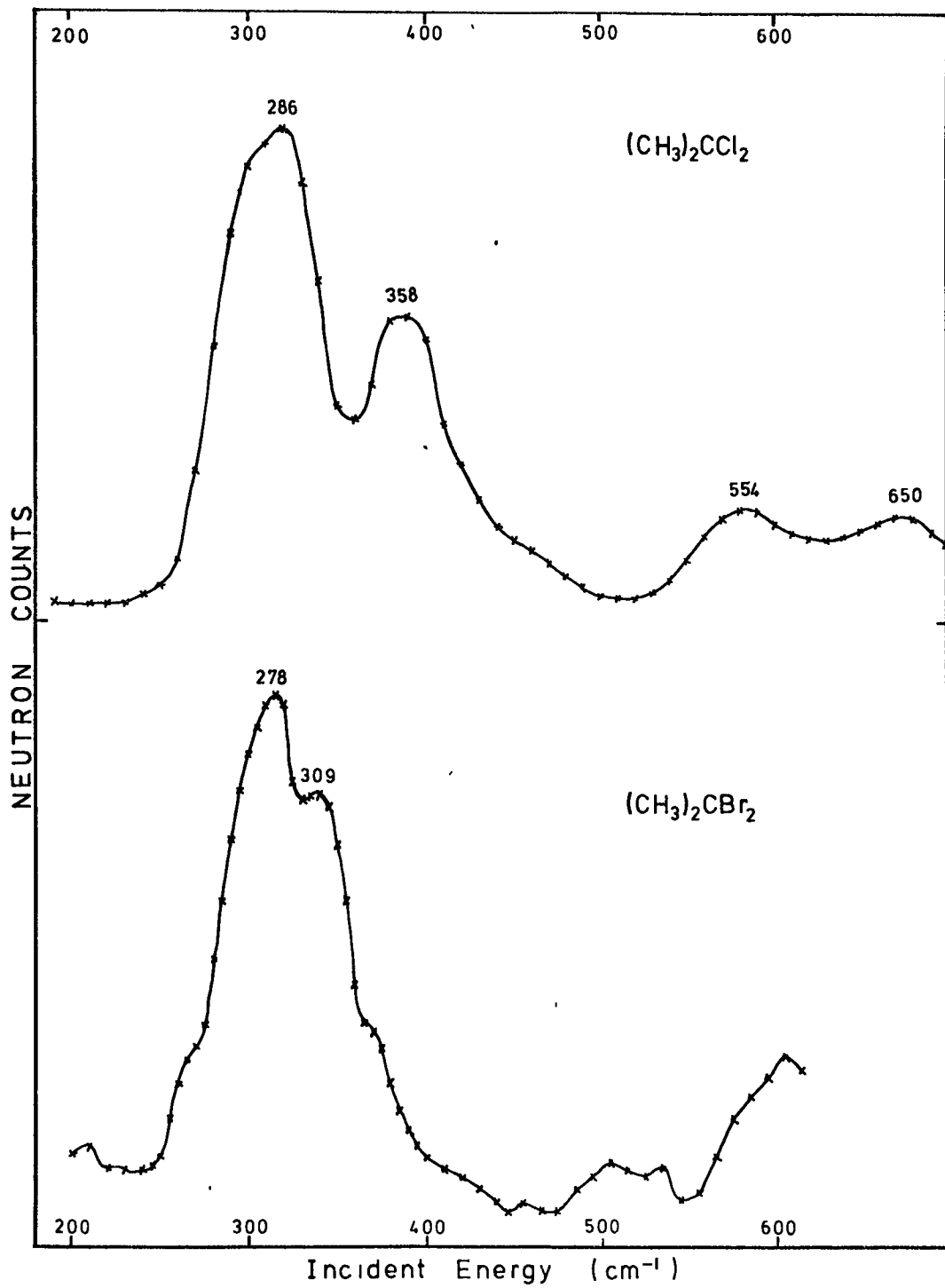
Fig. (6.2) Beryllium filter spectra of the  $(\text{CH}_3)_2\text{CX}_2$  types.



Table (6.8) Spectroscopic frequencies of  $(\text{CH}_3)_2\text{CCl}_2$  ( $\text{cm}^{-1}$ )

I.R. Liquid	I.R. Solid	Raman Liquid (29)	I.N.S.	Assignment (Tentative)
560 s		565 v.s P	650 w 554 w.brd	$\nu_7 \nu_{\text{C-Cl}}$ + overtones
		511 w		$\nu_{13}$ ( ) ?
388 m	388 s	388 w D	390 w.sh 358 m	$\nu_{21}$ $\rho$ Skeletal
360 s	360 s	367 vs P		$\nu_8$ $\delta$ C-C-C
	{ 319 vw 302 w			?
		<u>287 m D</u>	<u>R 290 s</u>	$\nu_{27}$ Torsion + ?
257 m	{ 259 253sh m 246sh		<u>R 257 s</u>	$\nu_{14}$ Torsion
250 sh		252 s		$\nu_9$ ? $\delta$ $\text{CCl}_2$
		192 m D		? (Not $\nu_{27}$ )

P = polarised    D = depolarised    R = resolved by curve analyser

two peaks places these at 290 (18) and 257 (16)  $\text{cm}^{-1}$  (relative intensities in parenthesis). Unfortunately no confirmation of this can be obtained from overtones. For the 2 top case the first overtone should appear as 3 bands (65). In this case these would be expected in the region of  $\sim 550 \text{ cm}^{-1}$ , but there are other modes in this area to complicate matters. Only a weak unresolved broad band centred at  $\sim 554 \text{ cm}^{-1}$  appears. However as will be seen later, the separation of the two peaks due to 2 top interaction is in general agreement with the 3-top interaction splitting for the t-butyl compound where the two modes are resolved.

On the other hand Klaboe (29) assigned two frequencies as the torsions for both the chloride and bromide seen in the

Cl	Br	
287	252	cm <sup>-1</sup>
192	187	

Raman of the liquid, whereas in (30) 287 cm<sup>-1</sup> is assigned as  $\nu_{13}$  (A<sub>2</sub> skeletal twist) and the band at 192 cm<sup>-1</sup> was not observed. Such a large separation would in any case mean rather an unreasonable interaction term, so although the higher frequencies may seem credible on the basis that they are in the region of the values for the CH<sub>3</sub>CX<sub>3</sub> types the lower ones are highly suspect. In fact the I.N.S. spectra of both compounds are completely flat at these frequencies.

Some consideration of contributions to the I.N.S. band by modes other than the torsions should now be made. A band appears at ~257 cm<sup>-1</sup> in both I.R. and Raman spectra which has been assigned as  $\nu_9$  (A<sub>1</sub>  $\delta$  CCl<sub>2</sub>) and as suggested above the Raman band at 287 cm<sup>-1</sup> may be  $\nu_{13}$  (A<sub>2</sub> skeletal twist) and not a torsion. The optically active band at 257 cm<sup>-1</sup> coincides with the neutron band again, which at first suggests it might be wrongly assigned. However the present investigation of the I.R. of the liquid and solid showed the presence of two bands at 257 and 250 cm<sup>-1</sup> in the liquid and a further split in the solid, so there may just be some accidental near-degeneracy. At this point some insight may be gained by comparison with equivalent bands in the bromide.

Table (6.9) Spectroscopic frequencies of  $(\text{CH}_3)_2\text{CBr}_2$  ( $\text{cm}^{-1}$ )

I.R. Liquid	I.R. Solid	Raman Liquid (29)	I.N.S.	Assignments (Tentative)
483 s	484 s	484 s P	$\sim 579$	? Torsion Overtones
		401 s	$\sim 477$ w brd	$\nu_7$ $\nu$ C-Br
337 w	333 w	342 w D	$\sim 338$ v.w.sh	$\nu_{13}$ Skeletal twist
304 m	306 m	312vs P	<u>R 309 s</u>	? $\nu_{27}$ Torsion
299 sh	300 sh	299vw D		
288 sh	278 m	288 vw	<u>R 278 s</u>	? $\nu_{14}$ Torsion
278 sh	273 sh			
264v.wsh	260v.wsh	252 m D	R 260 m	? $\nu_8$ $\delta$ C-C-C
			R 234 vw	?
		187 vw		? (not $\nu_{27}$ )
		167 vs P		$\nu_9$ $\delta$ CBr <sub>2</sub>

R = resolved by curve analyser

The I.N.S. spectrum of the bromide (fig. 6. 2 ) shows that all the strong bands have again coalesced as was the case with  $\text{CH}_3\text{CBr}_3$ . A very strong broad band with F.W.H.M.  $\sim 75 \text{ cm}^{-1}$  is centred about  $283 \text{ cm}^{-1}$ . A maximum is observed at  $281 \text{ cm}^{-1}$  broadening to lower frequency with a strong shoulder about  $306 \text{ cm}^{-1}$ . Much weaker shoulders appear on the low and high frequency fringes.

$\nu_9$  ( $A_1 \delta$  CBr<sub>2</sub>) has been assigned at  $167 \text{ cm}^{-1}$  in the Raman spectrum (29). The neutron spectrum shows a very weak feature at  $\sim 170 \text{ cm}^{-1}$  which is really insignificant taking into account statistical errors, so it seems likely that  $\nu_9$  in the chloride in the region of  $257 \text{ cm}^{-1}$  should not contribute significantly to the

neutron intensity. As mentioned earlier Klaboe (29) assigned the higher torsional band as  $252 \text{ cm}^{-1}$  for the bromide ( $\equiv 287 \text{ cm}^{-1}$  chloride), but this corresponds with a point on the low frequency side of the neutron band, leaving no room for another torsional band of about the same intensity to lower frequency so it would seem that this is not the higher torsion. Unfortunately its actual contribution to the I.N.S. band cannot immediately be seen. This now also suggests that the optically active band at  $287 \text{ cm}^{-1}$  in the chloride spectrum may have some non-torsional contribution, which might account for the slight disparity in the intensities of its two neutron peaks:- 257 (16), 290 (18), relative intensity in brackets.

An accurate peak resolution of the bromide I.N.S. is virtually impossible since it contains; (a) the two torsional bands (b) the equivalent of the  $358 \text{ cm}^{-1}$  ( $\nu_8$ ) chloride band which is quite strong (c) contributions from the  $252 \text{ cm}^{-1}$  band and the equivalent of  $\nu_{21}$  ( $B_1$  skeletal deformation) at  $388 \text{ cm}^{-1}$  in the chloride, only weakly in evidence in the neutron spectrum. Klaboe assigned  $\nu_8$  ( $A_1$  skeletal bend) as  $290 \text{ cm}^{-1}$  and  $\nu_{21}$  as  $306 \text{ cm}^{-1}$  although several other bands occur in this area. A repeat of the I.R. spectrum on the liquid and solid showed that the band is quite complex, although some of the bands are resolved in the solid. The strongest I.R. band appeared at 306 with shoulders at 300, 278, 273 and  $260 \text{ cm}^{-1}$ . A weak band at  $\sim 342 \text{ cm}^{-1}$  may well correspond with the weaker higher frequency I.N.S. shoulder at  $338 \text{ cm}^{-1}$ .

On the whole one gains the impression that the assignments

should be held with some reserve, especially as a number have already proved wrong. An isotopic substitution study should really be made to clear up the problem.

In an attempt to gain something from the neutron band a curve analysis was undertaken using just three strong peaks as for the chloride with two of equal intensity. Two possible fits were obtained:

(1)	(2)
265 (12) $\nu_{14}$	259 (9)
283 (10)	278 (12) $\nu_{14}$
308 (12) $\nu_{27}$	309 (12) $\nu_{27}$

Fit (2) constrains the equal intensity peaks to a separation about the same as for the chloride torsions. (As will be discussed and demonstrated later this is not unreasonable). Both fits give the higher frequency torsion at  $\sim 308 \text{ cm}^{-1}$  which is a larger shift from the value in  $\text{CH}_3\text{CBr}_3$  than in the equivalent chlorides (although it should be remembered that Durig (24) assigned  $304 \text{ cm}^{-1}$  as the  $\text{CH}_3\text{CBr}_3$  torsion). Fit (1) gives a rather drastic separation of the two torsions if they are constrained to equal intensities, so fit (2) is probably the better.

Whether or not one wishes to rely on the curve analysis, if it is assumed that the torsions do make the largest contributions to the intensity the higher frequency can be given an upper limit of  $\sim 308 \text{ cm}^{-1}$  and the lower frequency a lower limit of  $\sim 265 \text{ cm}^{-1}$  without too much argument. Then assuming a splitting of about  $32 \text{ cm}^{-1}$  (c.f. the chloride) two sets of possible maximum and minimum

frequencies are obtained:-

	<u>minimum</u>	<u>maximum</u>	
A <sub>2</sub> v <sub>14</sub>	265	276	cm <sup>-1</sup>
B <sub>2</sub> v <sub>27</sub>	297	308	

The maximum set does in fact correspond closely with fit (2), but both sets have been used in the barrier calculations, which are given along with the 3 and 4 top cases later.

(c) (CH<sub>3</sub>)<sub>3</sub>CX compounds.

The spectra of these compounds should be less complex than the previous set since the higher symmetry of the species means that a number of modes are doubly degenerate. The usual classification after Tobin (64) is as follows:

Table (6.10)

	A <sub>1</sub>	A <sub>2</sub>	E
v C-H assym.	v <sub>1</sub>	v <sub>9</sub>	v <sub>13</sub> , v <sub>14</sub>
v C-H sym.	v <sub>2</sub>		v <sub>15</sub>
δ C-H assym.	v <sub>3</sub>	v <sub>10</sub>	v <sub>16</sub> , v <sub>17</sub>
δ C-H sym.	v <sub>4</sub>		v <sub>18</sub>
ρ CH <sub>3</sub>	v <sub>5</sub>	v <sub>11</sub>	v <sub>19</sub> , v <sub>20</sub>
v C-C	v <sub>6</sub>		v <sub>21</sub>
v C-X	v <sub>7</sub>		
δ CC <sub>3</sub>	v <sub>8</sub>		v <sub>22</sub>
ρ Skeletal C-C-X			v <sub>23</sub>
CH <sub>3</sub> Torsion		v <sub>12</sub>	v <sub>24</sub>
Optical Activity:-	Raman (P) I.R.	Inactive	Raman I.R.

It should be noted that the description for certain frequencies changes from one compound to another, in particular v<sub>7</sub> and v<sub>8</sub> become

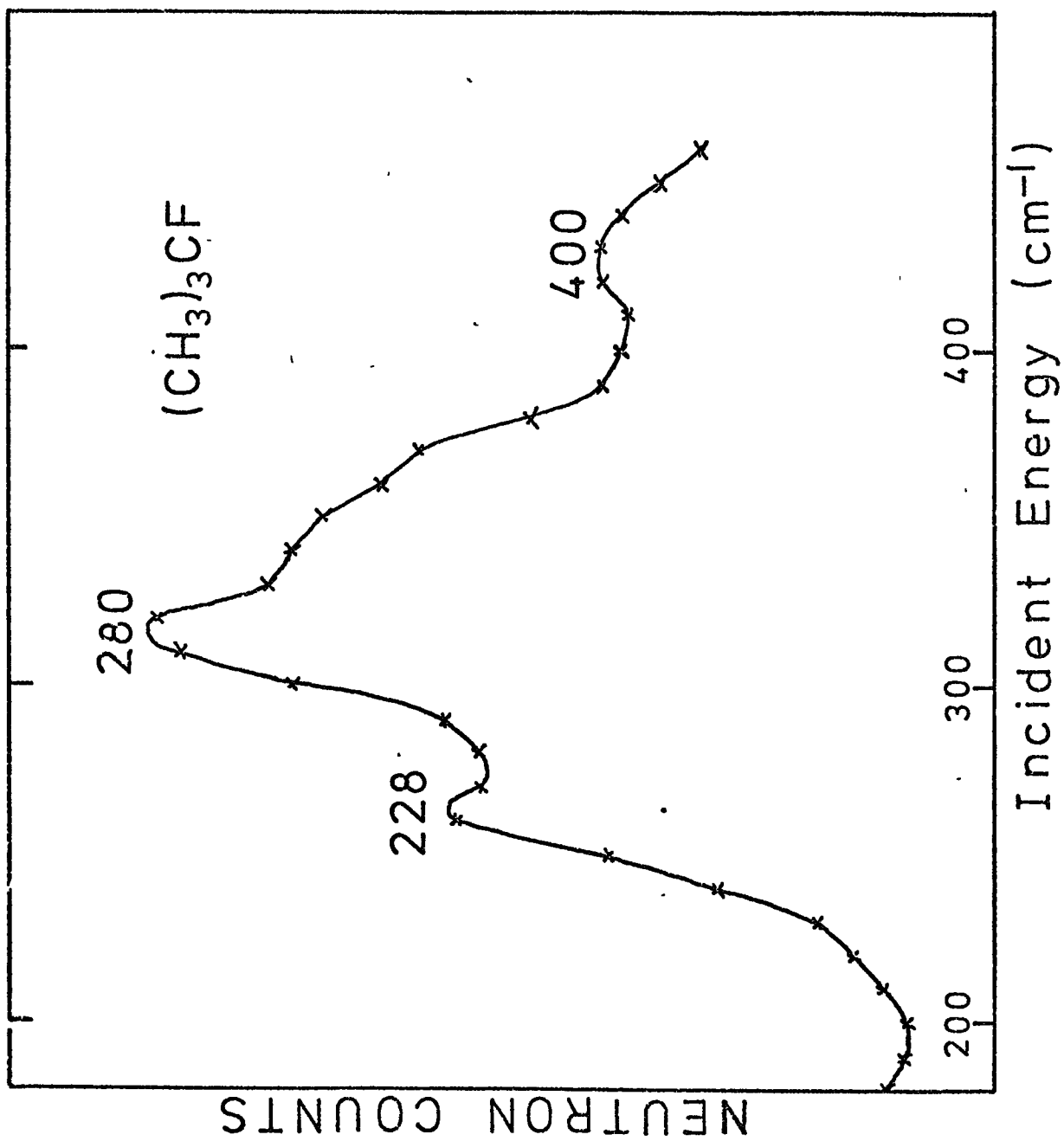
more intermixed  $F \rightarrow I$ . All the bands are I.R./Raman active except for the four  $A_2$  modes which include the  $\nu_{12}$  torsion. Beryllium filter I.N.S. spectra of the compounds studied are shown in figs. (6.3 - 6.6).

Table (6.11) Spectroscopic frequencies of  $(CH_3)_3CF$  ( $cm^{-1}$ )

I.R. (67)	Raman Liquid	I.N.S. Solid	Assignment
751	750 v.s		$\nu_7$ $\nu$ C-F $A_1$
460	464 m 417 m sh	~ 400 m	$\nu_{22}$ $\delta$ $CC_3$ E
409			$\nu_8$ $\delta$ $CC_3$ $A_1$
335	345 m	{ broad shoulder 280 v.s 228 m.s	$\nu_{23}$ $\rho$ skeletal + double scatter?
			$\nu_{24}$ E } Torsion
			$\nu_{12}$ $A_2$ }

No one appears to have reported any observation of the torsional modes in  $(CH_3)_3CF$  and the lowest remaining fundamental  $\nu_{23}$  occurs at  $\sim 340$   $cm^{-1}$ . This facilitates the assignment of the torsional modes in the I.N.S. spectrum which shows the strongest peak at 280  $cm^{-1}$  and one at 228  $cm^{-1}$  which is about half as intense. These can only be assigned as the E and  $A_2$  torsions ( $\nu_{24}, \nu_{12}$ ) respectively.

The optically active band,  $\nu_8$  skeletal bending mode ( $A_1$ ) appears at  $\sim 400$   $cm^{-1}$  and the lowest remaining fundamental  $\nu_{23}$  skeletal deformation (E) constitutes the higher frequency part of the broad shoulder. This leaves some remnant intensity between the torsional peak and  $\nu_{23}$  to be explained. The most likely

Fig. (6.3) Beryllium filter spectrum of  $(\text{CH}_3)_3\text{CF}$ .



explanation is that it is due to double scattering, since the sample had to be contained in Si tubes and was consequently quite thick. (It probably arises from a very low lying librational mode, double scattering neutrons which have already been scattered by the torsional mode at  $280 \text{ cm}^{-1}$ )

Table (6.12) Spectroscopic frequencies of  $(\text{CH}_3)_3\text{CCl}$  ( $\text{cm}^{-1}$ )

I.R. Liquid	I.R. Solid (37)	Raman Liquid	I.N.S. * Solid	Assignment
571 vs		569		$\nu_7 \nu \text{ C-Cl } A_1$
			554 w	? Torsion overtones
408 w		404	R 401 (9)	$\nu_{22} \text{ CC}_3 \text{ def. E}$
372 s		369	R 354 (10)	$\nu_8 \text{ CC}_3 \text{ def. } A_1$
301 m	301 m	302	R 301 (4)	$\nu_{23} \text{ C-C-Cl def. E}$
	<u>290</u> vw		R <u>292</u> (23)	$\nu_{24} \text{ E}$
	<u>246</u> v.v.w		R <u>244</u> (11)	$\nu_{12} A_2$ } Torsion

\* R = resolved by curve analyser

Durig (37) has assigned both torsional bands in the solid chloride at  $290 \text{ cm}^{-1}$  (E) and  $246 \text{ cm}^{-1}$  ( $A_2$ ) with a confirmation using  $(\text{CD}_3)_3\text{CCl}$  giving bands at  $217 \text{ cm}^{-1}$  (E) and  $176 \text{ cm}^{-1}$  ( $A_2$ ) (shift factors of 1.33 and 1.40; very close to  $\sqrt{2}$ ). Other modes in the region of interest as given by Evans and Lo (34) are

E	C-C-Cl def.	302	
$A_1$	C-C <sub>3</sub> def.	369	
E	C-C <sub>3</sub> def.	404	$\text{cm}^{-1}$
$A_1$	C-Cl stretch	570	

NEUTRON COUNTS

100 200 300 400 500 600

Incident Energy (cm<sup>-1</sup>)

(CH<sub>3</sub>)<sub>3</sub>CCl

COMBINED

SEPARATE

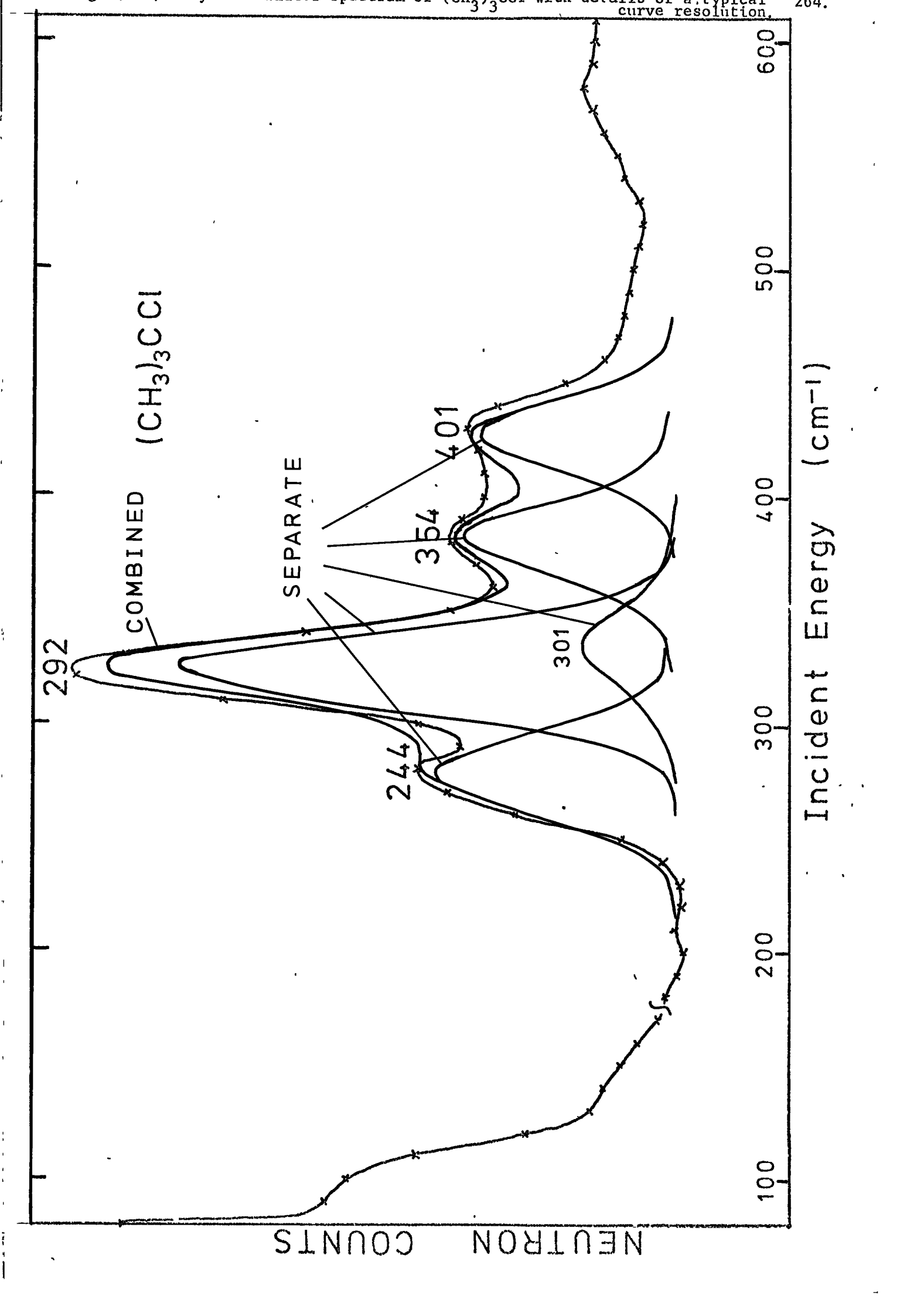
292

244

354

401

301



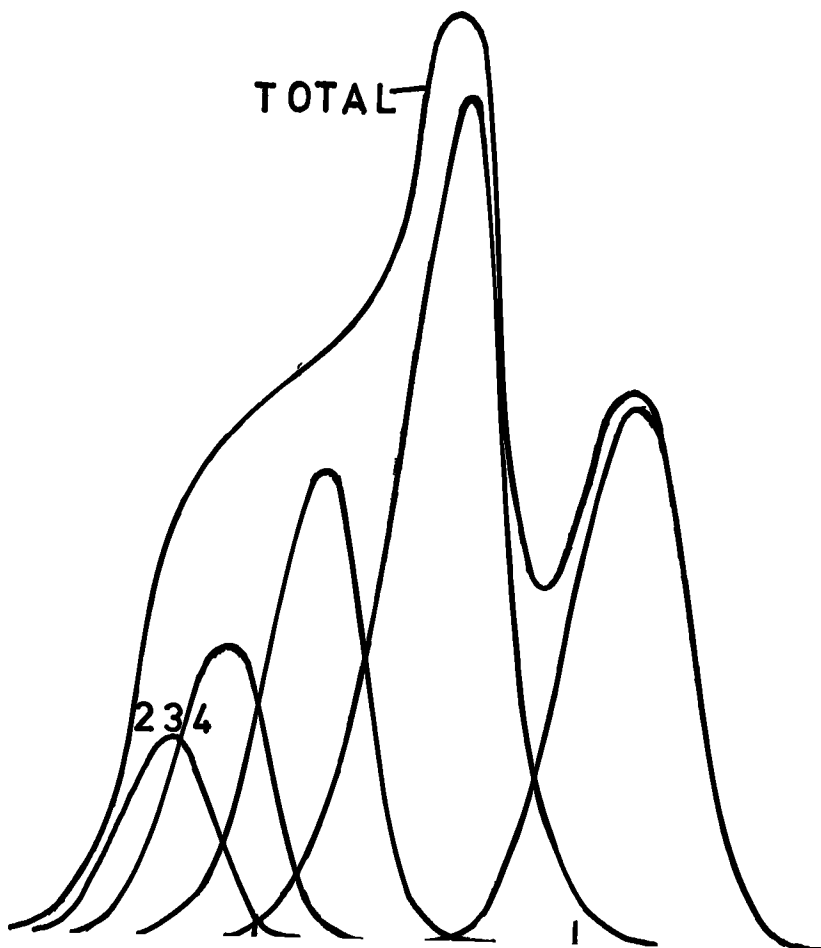
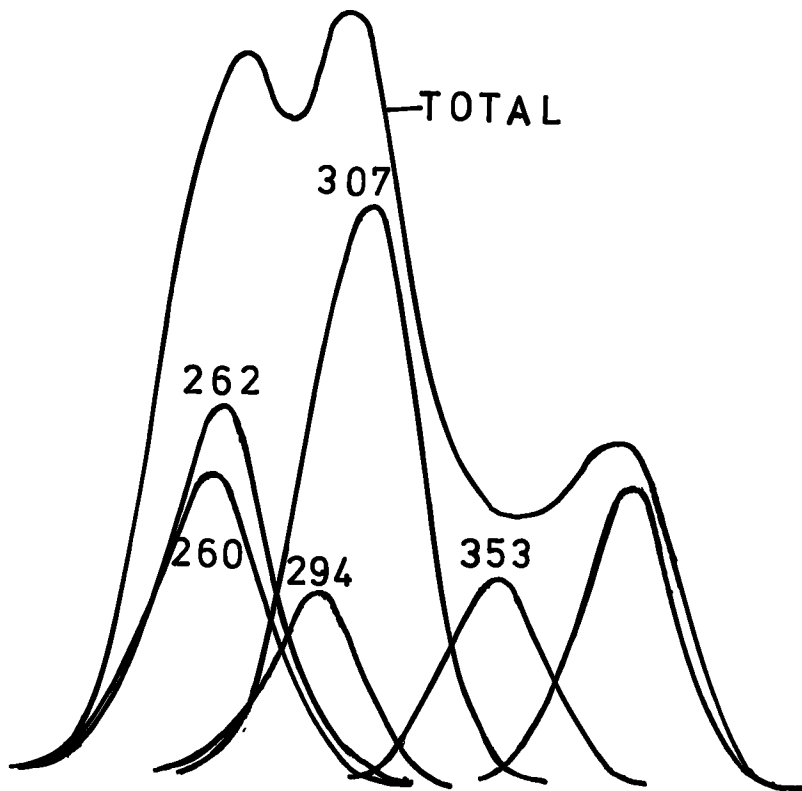
This all correlates very well with the neutron spectrum shown in fig. (6.4). The torsional bands appear at  $\sim 244 \text{ cm}^{-1}$  and  $\sim 290 \text{ cm}^{-1}$  again with a roughly 1:2 intensity ratio due to their  $A_2$ , E natures. Bands appear at  $353 \text{ cm}^{-1}$  and  $401 \text{ cm}^{-1}$  leaving only the  $302 \text{ cm}^{-1}$  band to find. This is hidden under the  $290 \text{ cm}^{-1}$  band and is detectable as a slight broadening on its higher frequency side. A curve analysis of the spectrum showed the small intensity contribution of this peak. The resolved frequencies are presented in the table (6.12) above.

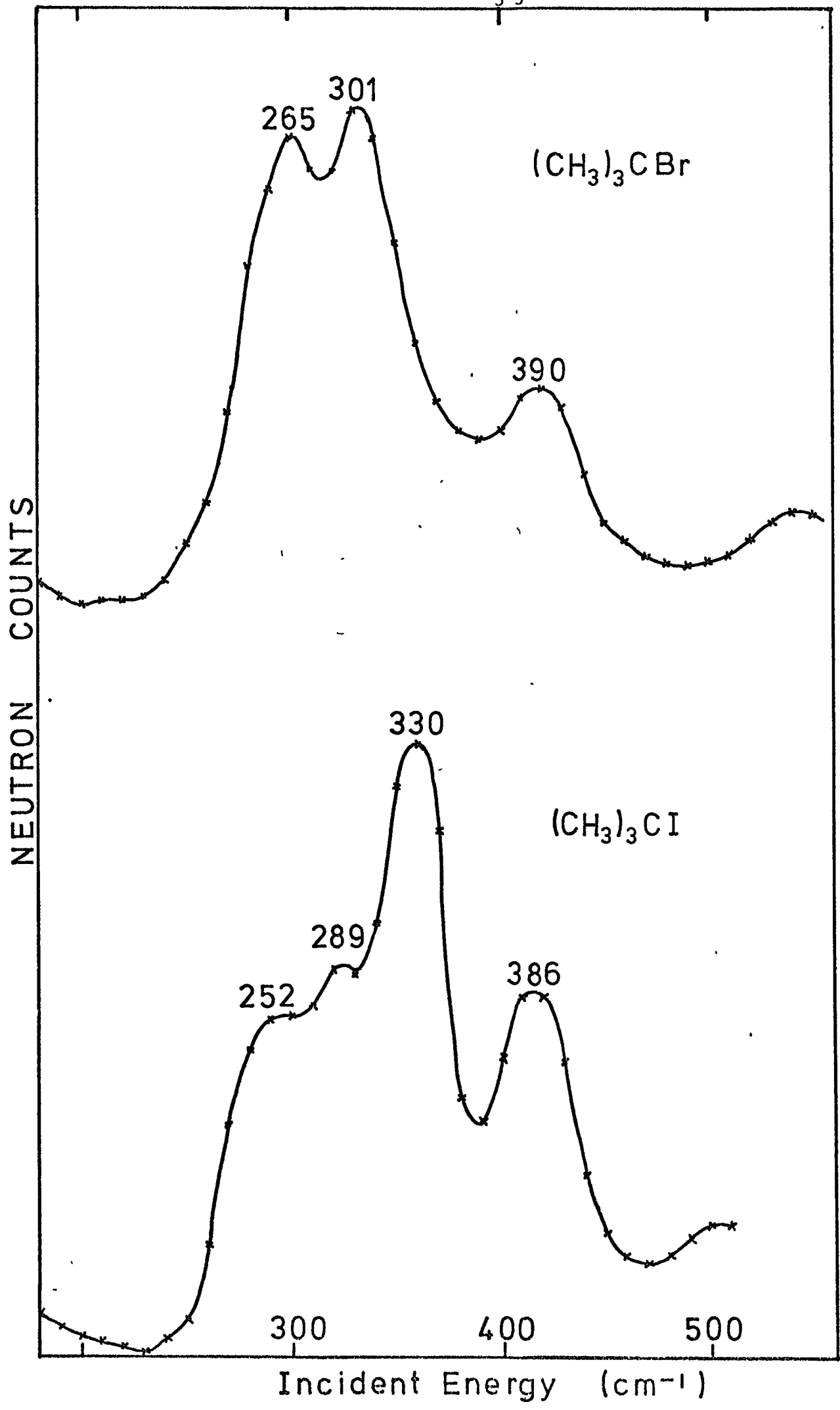
Table (6.13) Spectroscopic frequencies of  $(\text{CH}_3)_3\text{CBr}$  ( $\text{cm}^{-1}$ )

I.R. Liquid	I.R. Solid *	Raman Solid *	I.N.S. Solid	Assignment (Tentative)
517 s	{ 516 s 510 vs 501 w	{ 515 s 508 vs 501 w 404 sh 400 m	516 w	$\nu_7$ $\nu$ C-Br $A_1$
* 396 v.w	396 w	{ 397 sh	R 390 (9) R 353 (6)	$\nu_{22}$ C-C <sub>3</sub> def. E ?
{ 305 sh 300 m	{ 301 sh 296 s 287 sh	{ 300 vs 296 vvs	R 307 (17) R 294 (5)	$\nu_{24}$ ? E Torsion ?
280 w.sh	{ 281 vw 274 w	{ 274 s	R 262 (11) R 260 (9)	$\nu_{12}$ } $A_2$ Torsion $\nu_{23}$ } +C-C-Br def. E ? (not $A_2$ Torsion)
265v.w.sh	{ 270 sh 267 sh 213 <sup>+</sup>	{ 270 267		

\* Bertie and Sunder (36), + Durig (37) R = resolved by curve analyser

Once again on turning to the bromide I.N.S. spectrum (fig. 6.5 ) the bands are confused due to close proximity. Durig has assigned solid I.R. torsion bands at  $213 \text{ cm}^{-1}$  ( $A_2$ ) and  $275 \text{ (E) cm}^{-1}$  but without





deuteration studies. He assumed that the E mode was somewhere beneath the strong E band of the C-C-Br deformation ( $\nu_{23}$ ) at  $\sim 275 \text{ cm}^{-1}$ . However Bertie and Sunder (36) suggested a very weak shoulder at  $287 \text{ cm}^{-1}$  as the torsion. They give the other frequencies involved in this region as:

E	C-C-Br def.	272	
A <sub>1</sub>	C-C <sub>3</sub> def.	304	
E	C-C <sub>3</sub> def.	396	cm <sup>-1</sup>
A <sub>1</sub>	C-Br stretch	524	

The I.N.S. spectrum shows corresponding bands at 516,  $390 \text{ cm}^{-1}$ , but the remaining two modes are buried in the very strong and broad band, F.W.H.M.  $\sim 86 \text{ cm}^{-1}$  which has peaks at 265 and  $301 \text{ cm}^{-1}$ , showing a strong shoulder on its lower frequency side and a weaker broadening to higher frequencies. Durig's  $213 \text{ cm}^{-1}$  peak very clearly cannot be the A<sub>2</sub> torsion, and is only visible as a very faint broadening at the foot of the main band.

It can reasonably be said that the main band contains the equivalents of the 272 and  $304 \text{ cm}^{-1}$  bands and the two torsions. These latter two by analogy with the chloride probably have a 1:2 intensity ratio and a split of  $\sim 46 \text{ cm}^{-1}$ . Using these criteria a curve fit was attempted with reasonable success. It also became clear that there should be another weak band placed at  $\sim 353 \text{ cm}^{-1}$  between the main peaks.

Again, whether or not the curve fit is credible, one can say that if the torsion peaks make the strongest contribution to the band the upper frequency has a limit of about  $310 \text{ cm}^{-1}$  and the lower frequency a limit of about  $250 \text{ cm}^{-1}$ .

Table (6.14) Spectroscopic frequencies of  $(\text{CH}_3)_3\text{CI}$  ( $\text{cm}^{-1}$ )

I.R. Liquid	I.R. Solid	I.N.S. Solid	Assignment
489 s		479 w	$\nu_7$ $\nu$ C-I $A_1$
383* vw	390 v.w	R 386 (8)	$\nu_{22}$ $\text{CC}_3$ def. E
	348		
	332	R <u>330</u> (13)	$\nu_{24}$ E Torsion
	307 v.v.w		
	293	R <u>289</u> (7)	$\nu_{12}$ A Torsion
	275		
260 m	250 m	R 252 (4)	$\nu_{23}$ C-C-I def. E $\nu_8$ $\text{CC}_3$ def. $A_1$
~257 sh			
~250 sh			
227 *		R 234 (3)	

\* McDevitt et al (33)

R = resolved by curve analyser

The iodide I.N.S. proves quite interesting in that it leads to some conclusions which bolster the more tenuous aspects of the curve analyser assignment for the bromide.

No-one appears to have observed or assigned any torsional modes for this compound. Frequencies in the region of interest given by McDevitt et al (33) are:

E	C-C-I	def.	227	
$A_1$	C-C <sub>3</sub>	def.	259	$\text{cm}^{-1}$
E	C-C <sub>3</sub>	def.	386	
$A_1$	C-I	stretch	487	

The neutron spectrum fig. (6.5) quite clearly shows the two torsional bands at  $\sim 290$  ( $A_2$ ) and  $329$  (E)  $\text{cm}^{-1}$  i.e. between all the other frequencies, and the E mode is the most intense feature of the spectrum.

Again a curve analysis was carried out to define the peak positions a little better, the frequencies are given in table (6.14).

Two important points can immediately be made

- a) The torsional modes have increased considerably in frequency compared with the chloride, hence it is not so unreasonable that the bromide should also have a higher frequency than the chloride. (This would apply to the  $(\text{CH}_3)_2\text{CBr}_2$  case as well).
- b) The separation of the two peaks is  $\sim 41 \text{ cm}^{-1}$  not too different from the chloride ( $\sim 48 \text{ cm}^{-1}$ ). [Here one ought really to consider the difference  $(\nu_E^2 - \nu_A^2)$  rather than  $(\nu_E - \nu_A)$  - see theory chapter 1; if this difference is held as a constant the frequency separation should obviously decrease as the frequencies increase]. Hence the peak separation constraint applied in the bromide analysis would also not be too unreasonable.

The I.R. spectrum of the solid was also run at liquid nitrogen temperatures. A very thick sample was sprayed under vacuum on to the CsI plate in the cold temperature I.R. cell and a number of extremely weak features were obtained between  $250$  and  $400 \text{ cm}^{-1}$ . Two of these at  $293$  and  $332 \text{ cm}^{-1}$  roughly coincide with the neutron data but clearly a study of solid  $\text{C}_4\text{D}_9\text{I}$  would be necessary to distinguish the torsions by an I.R. method alone.



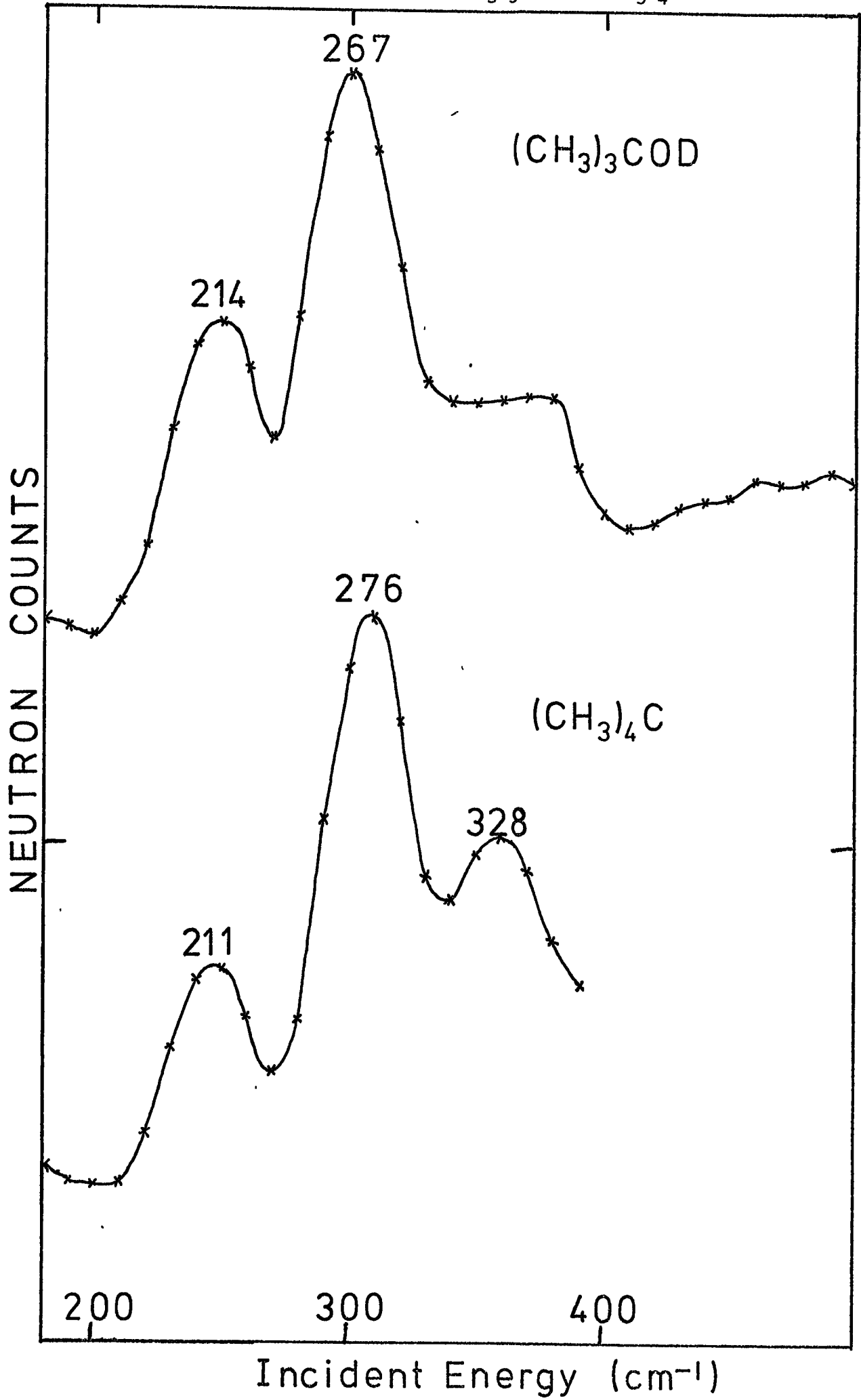
Outside the halogen series a sample of  $(\text{CH}_3)_3\text{C-OD}$  which was available was also run on Be-filter. The OD group has a mass just under that of F and also the deuterium should not interfere with the scattering significantly. Durig (38) has recently obtained I.R. spectra of solid  $\text{C}_4\text{H}_9\text{OH}$  and  $\text{C}_4\text{D}_9\text{OH}$  and assigned the torsions. The nature of the OH group introduces asymmetry which causes the former E mode to split slightly:-

t- $\text{C}_4\text{H}_9\text{OH}$	$\text{C}_4\text{D}_9\text{OH}$	
424	356	C-C <sub>3</sub> def.
361	313	} A', A'' C-C <sub>3</sub> rock
345	296	
289	213	} A', A'' CH <sub>3</sub> torsions
276	-	
235	168	A'' CH <sub>3</sub> torsion

The sample of  $\text{C}_4\text{H}_9\text{OD}$  ought to give a spectrum very similar to the undeuterated species in the I.N.S., although the small splitting of the higher frequency would not be resolved, but appear as a slight broadening. In the spectrum obtained (fig. 6.6 )

Table (6.15) Spectra of  $(\text{CH}_3)_3\text{COD}$  ( $\text{cm}^{-1}$ )

I.R. Liquid	I.N.S. Solid	Assignment
489 w brd	weak	CC <sub>3</sub> def. (A', A'') Torsions A' Torsion
437 w	broad band	
343 v.w	~ 348 m	
	<u>267</u> v.s <u>214</u> m.s	



the torsions appear at 214 and 267  $\text{cm}^{-1}$  respectively, rather more below Durig's values of 235, 282  $\text{cm}^{-1}$  than the usual shift I.R.  $\rightarrow$  I.N.S., as seen in a number of compounds, might account for. This might well indicate some degree of coupling between the -OH or -OD torsional motion with the methyl torsions. (Durig treated these separately, although he did indicate that in the case of t-butyl amine some coupling was very clearly evident.)

The 267  $\text{cm}^{-1}$  peak does in fact show a slight broadening and using the curve analyser a perfect fit was obtained using three equal intensity peaks placed at 214, 261 and 273  $\text{cm}^{-1}$ . Placing two peaks exactly on 267 give a slightly taller and narrower peak. However the barrier was determined using the average 'E' mode frequency of 267  $\text{cm}^{-1}$ .

It is also of interest that in his paper (38) Durig also looked at a number of t-butyl-X systems, where X = -SH, -NCO, -NCS,  $-\text{C} \begin{array}{l} \text{O} \\ // \\ \text{H} \end{array}$ , -O-CH<sub>3</sub> and found that in general the A' and (A', A'') modes were separated by  $\sim 50 \text{ cm}^{-1}$ , evidence which is again in favour of the rough constraint of separation used in the curve analyses.

(d) Neopentane(CH<sub>3</sub>)<sub>4</sub>C.

The case of the torsional mode frequencies of neopentane has already been solved both by I.R. (42) and I.N.S. (48, 49).

	(CH <sub>3</sub> ) <sub>4</sub> C		(CD <sub>3</sub> ) <sub>4</sub> C		
	A	F	A	F	
I.R.(42)	221	281	157	206	$\text{cm}^{-1}$
I.N.S.(49)	220	280			

The Be-filter spectrum fig. (6.6) was therefore obtained for comparison of the instrument with the other neutron technique, over the short range of the torsional vibrations, and also to observe the intensity relationship of the A and F modes.

In fact looking at the previous neutron spectrum (which used the small Q (low angle) method) shown in Rush's paper (49) but still not reported in full, their resolution appears to be greater than that of Be-filter. The Be-filter frequencies are also shifted to lower frequencies 211 and 276  $\text{cm}^{-1}$ . This may be a crystal dispersion effect since the neutrons are detected at a roughly  $90^\circ$  angle to the incident beam. The remaining band at 328  $\text{cm}^{-1}$  corresponds to a skeletal E mode seen at 335 in the Raman.

Analysis of the two torsional peaks of the beryllium filter spectrum showed a roughly 1:3 intensity ratio; % areas under peaks A:F = 27:73, a feature which is not so apparent in the previous spectrum (49).

#### Section A4. Barrier calculations.

Using the I.N.S. torsional frequencies for the  $\text{CH}_3\text{CX}_3$  compounds, barriers to internal rotation have been calculated ignoring the effects of external fields, using the tabulated Mathieu solutions. Reduced moments of inertia have been calculated using the value of  $I_{\text{CH}_3} = 3.220 \text{ \AA}^2$  used throughout the thesis and the most recent structural data for  $I_{\text{CX}_3}$ . The results are given in table (6.20) along with previously determined values.

For the two, three and four top compounds the reduced moments of inertia, (F), torsional barriers and top-top interaction terms have initially been calculated using Weiss and Leroi's S.H. formulas (see theory, chapter 1 section 4).

The moments of inertia for  $(\text{CH}_3)_2\text{CCl}_2$  and  $-\text{Br}_2$  were calculated assuming the standard methyl group geometry used throughout with all angles Td and the other bond lengths summarised by Huttner and Zeil (67) taken from the t-butyl compounds:-

	$(\text{CH}_3)_2\text{C}$	C-C	C-X	→	$I_z$	$I_x$	
Cl	1.53		1.803		210	232	
Br	1.54		1.960	$\overset{\circ}{\text{A}}$	466	513	a.m.u. $\overset{\circ}{\text{A}}^2$

For the t-butyl compounds F values have been given for the fluoride by Lide and Mann (16) and the moments of inertia for the chloride and bromide by Durig (37). F values for the -OH compound are also given by Durig (38) and these were used for the -OD case assuming only a very small change in  $I_z$ ,  $I_x$  would have occurred. The iodide  $I_z$  value was taken as the same as an old value for the bromide (66) which assumed Td angles and a C-C length of 1.54  $\overset{\circ}{\text{A}}$ ;  $I_x$  was calculated from a recent microwave study of the rotational B constant (68):

	$(\text{CH}_3)_3\text{C-}$	C-C	C-X	→	$I_z$	$I_x$	
Cl		1.53	1.803		109.5	170.5	
Br		1.54	1.960		110.2	250.5	
I		1.54	2.19		110.2	323.9	

In the case of neopentane Td angles were assumed, C-C = 1.54 Å and the standard  $I_{\text{CH}_3}$  of 3.220 a.m.u. Å<sup>2</sup>, which gave  $I = 113.42$  a.m.u. Å<sup>2</sup>. The results are given in table (6.21). The results of previous workers on (CH<sub>3</sub>)<sub>2</sub>CH<sub>2</sub> and (CH<sub>3</sub>)<sub>3</sub>CH (17,49; 79,112) are also included for comparison. The S.H. terms  $\frac{2}{9}K$  and  $\frac{2}{9}L$  are given since these are usually taken as  $\sim \bar{V}_3$  and  $\sim \bar{V}_b$  respectively assuming all the other V constants tend to zero. Some workers have tackled the problem in a slightly different way, carrying out a Mathieu solution on each frequency and then averaging to give what they call  $\bar{V}_3$ . Consequently the present results have also been treated in a similar way and the weighted average obtained. (The two frequencies have been assumed to be weighted by the coupling term  $\bar{V}_b$  as indicated by the S.H. approach). These results are presented in table (6.22).

Previous barrier determinations are given in table (6.23). These results are discussed in PART E at the end of the chapter.

Table (6.20)  $\bar{V}_3$  Barriers for  $\text{CH}_3\text{CX}_3$  Types using Mathieu Solutions,  
including previous determinations.

Compound	Study (ref.)	$I_{\text{red}}$ a.m.u. $\text{\AA}^2$	$\bar{\nu}$ $\text{cm}^{-1}$	$\bar{V}_3$ $\text{cm}^{-1}$
$\text{CH}_3\text{CF}_3$	* Present I.N.S.	3.107	208	1004 *
	I.R. Solid (23)		220	1150
	I.N.S. Gas (50)		$220 \pm 15$	1108
	Microwave gas (11)			1216
	Thermodynamic (2)			$1206 \pm 140$
	" (3)			$1136 \pm 70$
$\text{CH}_3\text{CCl}_3$	* Present I.N.S.	3.186	282	1826 *
	I.R. Solid (23)		290 ( $\text{CD}_3$ 206)	1919 (1891)
	Raman gas (27)		$2 \leftarrow 0$ 564 ( $\text{CD}_3$ $2 \leftarrow 0$ 408)	1898 (1887)
	I.N.S. Liquid (47) Solid		$297 \pm 15$	2027
	Microwave Gas (13)			$608 \pm 105$
	" (15)			1782
	Thermodynamic (4)			$944 \pm 122$
	H' N.M.R. Solid $T_1$ (55)		$E_a = 1433$ , $\bar{V}_3 = 1992$	
	" " $T_1$		$E_a = 1293$	
	" " Line (56)		$E_a = 1503 \pm 70$	
	$^{13}\text{C}$ " Shape (57)		$E_a = 1014$	
$\text{CH}_3\text{CBr}_3$	* Present I.N.S.	3.207	292 $2 \leftarrow 0$ 571	1966 *
	I.R. Solid (24)		304	2125
	Raman Gas (27)		( $2 \leftarrow 0$ ) 583	2020
$\text{CH}_3\text{CH}_3$ for comparison	I.R. Gas (111)		289	1027
	High Pressure		208 ( $\text{C}_2\text{D}_6$ )	

Table (6.21) Simple Harmonic Barrier Calculation Results  
for multiple top cases. All values in  $\text{cm}^{-1}$ .

Compound	$\bar{\nu}_A$	$\bar{\nu}_{(B,E,F)}$	$F_A$	$F_{(B,E,F)}$	$\frac{2}{9}K$	$\frac{2}{9}L$
$(\text{CH}_3)_2\text{CCl}_2$	257	290	5,287	5,332	1570	- 182
$(\text{CH}_3)_2\text{CBr}_2$ max. min.	276 265	308 297	5,257	5,277	1804 1671	- 194 - 187
$(\text{CH}_3)_3\text{CF}$	228	280	5,42	5,60	1392	- 163
$(\text{CH}_3)_3\text{CCl}$	244	292	5,285	5,368	1594	- 171
$(\text{CH}_3)_3\text{CBr}$ max. min.	264 250	310 296	5,284	5,324	1826 1657	- 180 - 171
$(\text{CH}_3)_3\text{CI}$	289	330	5,284	5,303	2107	- 175
$(\text{CH}_3)_3\text{COD}$	214	267	5,39	5,406	1282	- 169
$(\text{CH}_3)_4\text{C}$	211	276	5,439		1395	- 162
$(\text{CH}_3)_2\text{CH}_2$ <u>REF.</u> (17)	216	271	5,57	7,21	1163	- 60
(49)	234	276			1133	- 41
$(\text{CH}_3)_3\text{CH}$ (79)	237	276	5,38	5,70	1377	- 108
(112)	225	280			1367	- 160



Table (6.22) Weighted average barrier values from Mathieu solutions using the two separate torsional frequencies. All values in  $\text{cm}^{-1}$ .

Compound	Frequency	Individual Mathieu $\bar{V}_3$ Solutions	Weighted Average $\bar{V}_3$
$(\text{CH}_3)_2\text{CCl}_2$	257	1529	1718
	290	1908	
$(\text{CH}_3)_2\text{CBr}_2$	276	1762	1965
	308	2167	
$(\text{CH}_3)_3\text{CF}$	228	1195	1541
	280	1714	
$(\text{CH}_3)_3\text{CCl}$	244	1385	1742
	292	1920	
$(\text{CH}_3)_3\text{CBr}$	264	1617	1988
	310	2174	
$(\text{CH}_3)_3\text{CI}$	289	1914	2277
	330	2458	
$(\text{CH}_3)_4\text{C}$	211	1028	1537
	276	1707	
$(\text{CH}_3)_2\text{CH}_2$	234	1222	1276
	276	1330	
$(\text{CH}_3)_3\text{CH}$	237	1289	1524
	276	1642	

Table (6.23) Previous Barrier determinations.

All values in  $\text{cm}^{-1}$ .

Compound	Method	Ref.	Details
$(\text{CH}_3)_3\text{CCl}$	Solid I.R.	} 37	S.H. $\left\{ \begin{array}{l} \frac{2}{9}K = 1576 \quad \frac{2}{9}L = -154 \\ 1685 \quad -203 \\ 1363 \quad -206 \\ 1443 \quad -154 \\ 1518 \quad -158 \\ 1612 \quad -189 \end{array} \right.$
$(\text{CD}_3)_3\text{CCl}$	"		
$(\text{CH}_3)_3\text{CBr}$	"		
$(\text{CH}_3)_3\text{COH}$	"		
$(\text{CH}_3)_4\text{C}$	"		
$(\text{CD}_3)_4\text{C}$	"		
$(\text{CH}_3)_4\text{C}$	I.N.S.		
$(\text{CH}_3)_4\text{C}$	I.N.S.	49	1964
$(\text{CH}_3)_3\text{CF}$	Microwave	16	S.H. $\frac{2}{9}K = 1516 \quad \frac{2}{9}L = -247$
$(\text{CH}_3)_4\text{C}$	Thermodynamic	5	$V_3 \sim 1643 - 1748$
$(\text{CH}_3)_2\text{CCl}_2$	P.M.R. $T_1$	} 55	$E_a = 1450 \rightarrow V_3 = 1900$ = 1258 = 1300 = 1049 = ? poor fit
$(\text{CH}_3)_3\text{CCl}$			
$(\text{CH}_3)_4\text{C}$			
$(\text{CH}_3)_2\text{CCl}_2$	N.Q.R. $T_1$	} 59	$E_a = 1450$ = 1433
$(\text{CH}_3)_3\text{CCl}$			

PART B: THE SILICON SERIESSection B1. Previous Work

Although the members of this series have not been subject to quite so much scrutiny as the carbon set, there is still a wealth of literature.

A thermodynamic study by Aston et al (92) has shown the existence of two phases in  $(\text{CH}_3)_4\text{Si}$ . The  $\beta$  phase is stable over most of the solid range and would be the phase involved in the present study. The only thermodynamic barrier determination which appears to have been done is for  $(\text{CH}_3)_4\text{Si}$  (68) where  $V_3 = 489 \text{ cm}^{-1}$  was calculated.

Microwave studies have been made to the point of repetition on  $\text{CH}_3\text{SiX}_3$  (X = F, Cl, Br) and  $(\text{CH}_3)_3\text{SiCl}$  (11, 69-75). These show an increase in the distance of the methyl from the central atom i.e. C-Si  $\sim 1.86$  cf. C-C  $\sim 1.54 \text{ \AA}$  which seems to be reflected in the smaller barrier heights obtained.

In the field of I.R. and Raman, work previous to 1953 has been summarised by Tobin (64), and in the same year Smith (75) looked comprehensively at the I.R. of the methyl chloro-silanes. More recently interest has focussed on the search for the torsional bands, with Durig again very much involved. (37, 42, 43, 77-82) These have concentrated mainly on the low frequency regions and will be discussed in connection with the I.N.S. data. Normal coordinate treatments of the chloro derivatives have been carried out by Shimizu and Murata (83-85), the L matrices and P.E.D. all seem to indicate that although the low frequency vibrations are mainly composed of symmetry coordinates of skeletal or C-X types, small contributions from H active coordinates

are present. The relevant aspects will be correlated with observed neutron spectra.

I.N.S. work has been reported by Herdade (86), though this seems wrongly to have concluded that the methyls were freely rotating. Brugger et al (87) claim to have studied liquid  $(\text{CH}_3)_4\text{Si}$  by the small Q method but no report has appeared.

Activation energies for methyl rotation from N.M.R. have only been obtained for  $\text{CH}_3\text{SiCl}_3$ ,  $(\text{CH}_3)_4\text{Si}$  (56, 88, 89). Previously determined barriers are given in table (6.32) later.

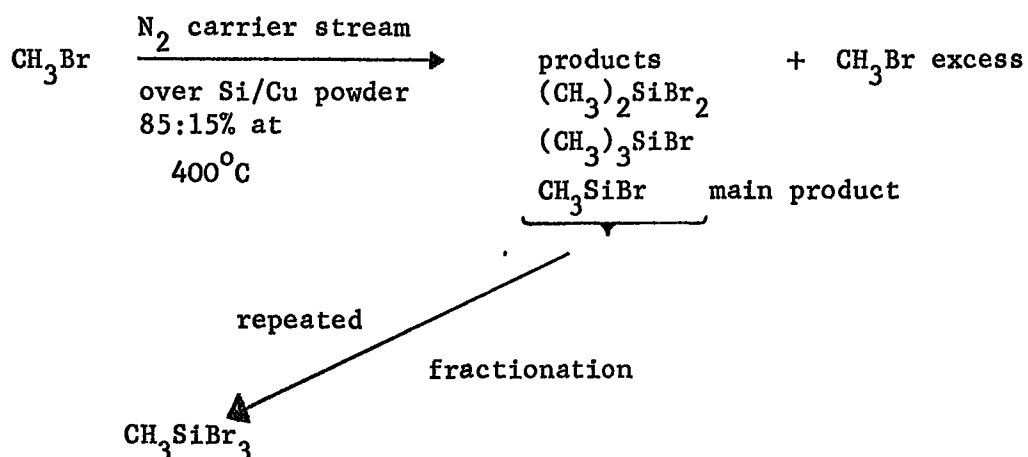
#### Section B2. Experimental.

Of the compounds studied only  $\text{CH}_3\text{SiBr}_3$  had to be prepared, the rest being obtained from commercial sources:  $\text{CH}_3\text{SiCl}_3$ ,  $(\text{CH}_3)_2\text{SiCl}_2$  and  $(\text{CH}_3)_3\text{SiCl}$  from Hopkin and Williams Ltd.  $(\text{CH}_3)_4\text{Si}$  from B.D.H. Chemicals Ltd. and  $\text{CH}_3\text{SiF}_3$  from C.P.L. Inc. College Point, N.Y.

$\text{CH}_3\text{SiF}_3$  is a gas under normal conditions and so once again had to be sealed into small tubes as a liquid under pressure. All the others are liquids but the chloro- and bromo- samples fume readily in air due to hydrolysis, producing HCl or HBr. Before sealing in Si cans these were therefore degassed and distilled several times under reduced pressure. Sample purity was checked spectroscopically as liquids, which required handling in a dry box.

The sample of  $\text{CH}_3\text{SiBr}_3$  was prepared by Dr C.J. Ludman and his assistants by a method described by Moedritzer (90) (after a rather unsuccessful attempt using the method of McCusker and Reilley (91))

summarised as follows:



A bromine analysis of the final product gave 85.06% (84.78% calculated).

All the I.N.S. spectra were obtained on the beryllium filter machine, and therefore represent the solid states.

### Section B3. Assignment and Discussion of Spectra.

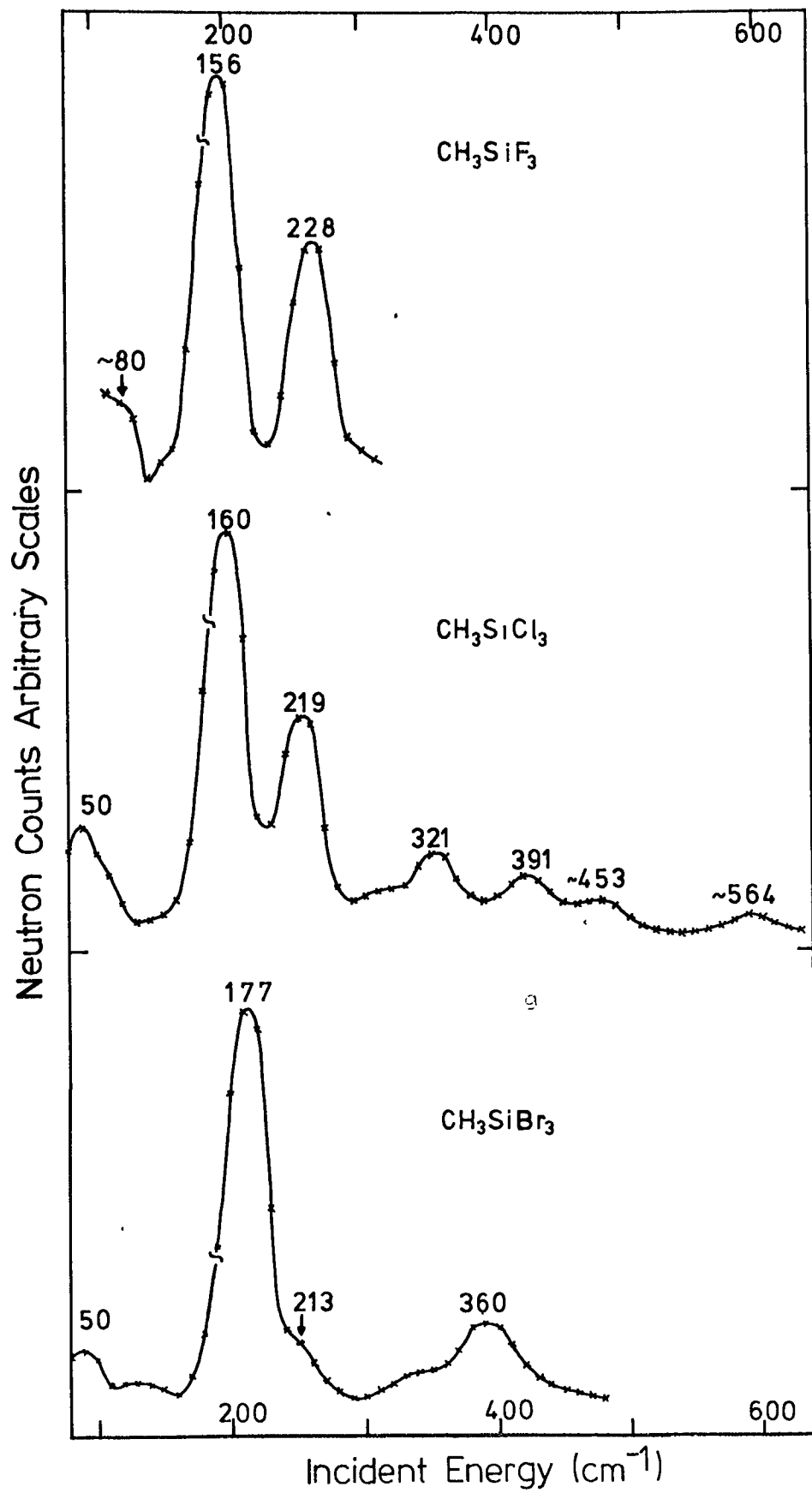
#### a) CH<sub>3</sub>SiX<sub>3</sub> types

The beryllium filter spectra of the three compounds are shown in fig. (6.8 ).

Table (6.24) Spectroscopic frequencies of CH<sub>3</sub>SiF<sub>3</sub> (cm<sup>-1</sup>)

I.R. (Gas) *	Raman (Liquid) *	I.N.S. Solid	Assignment
700 m	700 v.s		v <sub>4</sub> v Si-F A <sub>1</sub>
390 s	387 w		v <sub>5</sub> δ SiF <sub>3</sub> A <sub>1</sub>
332 s	{ 331 v.w 229 m	228 m.s	{ v <sub>11</sub> δ SiF <sub>3</sub> E v <sub>10</sub> δ SiF <sub>3</sub> E
		156 v.s	v <sub>6</sub> Torsion
		~ 80 ↓ m.w	Librations

\* Ref (77)

Fig. (6.8) Beryllium filter spectra of  $\text{CH}_3\text{SiX}_3$  types.

Collins and Nielsen (77) have reported I.R. and Raman fundamental frequencies for  $\text{CH}_3\text{SiF}_3$ ; the lowest observed was an E mode at  $229 \text{ cm}^{-1}$ , but they estimated the torsional frequency at  $\sim 156 \text{ cm}^{-1}$ . The I.N.S. spectrum confirms this; the strongest band appearing at  $156 \text{ cm}^{-1}$  well below the other fundamentals. By comparison with the  $\text{CH}_3\text{CX}_3$  compounds the moderately strong I.N.S. band at  $228 \text{ cm}^{-1}$  must again be largely due to the  $\nu_{10}$   $\text{SiF}_3$  deformation mode, though this does overlap with the  $\nu_{11}$   $\text{SiF}_3$  bending mode at  $331 \text{ cm}^{-1}$ . The low frequency for the torsion immediately indicates a much lower barrier than in  $\text{CH}_3\text{CF}_3$ , a trend which may be expected in the other Si compounds.

No-one appears to have assigned or estimated a torsional mode for  $\text{CH}_3\text{SiCl}_3$  although barriers have been obtained by other methods. The frequencies observed are given in table (6.25), with the averages of previously determined fundamental frequencies summarised by Shimizu

Table (6.25) Spectroscopic frequencies of  $\text{CH}_3\text{SiCl}_3$ . ( $\text{cm}^{-1}$ )

Fundamentals Assigned * Previously	I.N.S. Solid	Assignment
577	564 vw	$\nu_9$ $\nu$ Si-Cl
458	453 w	$\nu_4$ $\nu$ Si-Cl
	391 w	?
	321 w	Double Scatter ?
229	219 m	$\nu_5, \nu_{10}^{\delta, \rho}$ $\text{SiCl}_3$
164		$\nu_{11}^{\delta}$ $\text{SiCl}_3$
	<u>160 s</u>	$\nu_6$ Torsion
	$\sim 50$ w	Librations and Lattice Modes

\* ref. (83)

and Murata (83). The I.N.S. spectrum shows a pattern very similar to that of  $\text{CH}_3\text{CCl}_3$ . A very strong sharp peak appears at  $160\text{ cm}^{-1}$ . This could correspond with the optical band at  $164\text{ cm}^{-1}$  assigned as  $\nu_{11}(\delta\text{ SiCl}_3)$ . However, the comparison with  $\text{CH}_3\text{CCl}_3$  would rather suggest that it is the torsional band, having the greatest intensity with  $\nu_{11}$  beneath as a minor contribution. Shimizu and Murata's P.E.D. table (83) would favour this, in that the only mode which shows any strong mixing with proton motions is  $\nu_{10}, \rho\text{ SiCl}_3$ , at  $229\text{ cm}^{-1}$  (containing about 2% contribution from  $\text{CH}_3$  motions). This latter band again follows the established pattern in the I.N.S. spectrum, showing up moderately strongly at  $219\text{ cm}^{-1}$ . Hence one would feel fairly confident in assigning  $160\text{ cm}^{-1}$ , as the torsional band.

The weak broad band appearing about  $50\text{ cm}^{-1}$  can only be assigned to librational and translational modes of the whole molecule. The very weak centres at  $453$  and  $564\text{ cm}^{-1}$  have corresponding optical bands. The weak band at  $321\text{ cm}^{-1}$  could either be double scattering or possibly the torsional overtone predicted at  $\sim 308\text{ cm}^{-1}$ , but the one at  $391\text{ cm}^{-1}$  cannot be explained and may possibly be due to a decomposition product.

The I.N.S. spectrum of  $\text{CH}_3\text{SiBr}_3$  again bears a close resemblance to that of the carbon compound. A single very intense band appears at  $177\text{ cm}^{-1}$ . However, this time there is no evidence of this being composed of two strong peaks, as the F.W.H.M. is about  $38\text{ cm}^{-1}$ , but two very weak shoulders are discernible at the base. A curve analysis puts the stronger higher frequency at  $215\text{ cm}^{-1}$ . Previous spectra summarised by Tobin (64) give the frequencies of the other



Table (6.26) Spectroscopic Frequencies of  $\text{CH}_3\text{SiBr}_3$ . ( $\text{cm}^{-1}$ )

Fundamentals Previously Assigned *	I.N.S. Solid	Assignment
453		$\nu_9$ $\nu$ Si-Br
314	{ $\sim 360$ w. brd 308 v. wsh	$\nu_4$ $\nu$ Si-Br
186	213 w. sh 177 v. s	? Torsion + Libration $\nu_6$ Torsion, $\nu_{10\rho}$ $\text{SiBr}_3$
153	? v.w. sh	$\nu_5$ $\delta$ $\text{SiBr}_3$
98		$\nu_{11}$ $\delta$ $\text{SiBr}_3$
	$\sim 50$ v.w	Librations and Lattice Modes

\* ref (64).

fundamentals as listed in table (6.26). The lower shoulder most probably corresponds to the  $153 \text{ cm}^{-1}$  ( $\nu_5 \delta \text{SiBr}_3$ ) band, but the  $186 \text{ cm}^{-1}$  ( $\nu_{10\rho} \rho \text{SiBr}_3$ ) band would not fit the higher shoulder and on the previous arguments ought to be intense (c.f.  $\text{CH}_3\text{CBr}_3$ ). Consequently it must be present in the strong neutron band and accidentally degenerate with the torsion. The weak feature at  $\sim 308 \text{ cm}^{-1}$  would correspond with the optical band at  $314 \text{ cm}^{-1}$  ( $\nu_4 \nu \text{Si-Br}$ ) leaving the stronger broad band at  $\sim 355 \text{ cm}^{-1}$ . Since the torsional overtone would be predicted at  $\sim 328 \text{ cm}^{-1}$  this must either be double scattering or the overtone of  $\rho \text{SiBr}_3$ . The resolved shoulder at  $215 \text{ cm}^{-1}$  may again be a combination of the torsion with the libration about the  $C_3$  axis.

b)  $(\text{CH}_3)_2\text{SiCl}_2$ 

Durig (80) has made an I.R. study of the solid phases of all four dihalogen compounds, and claims to have observed the unresolved torsions in all except the chloride. He also studied the  $(\text{CH}_3)_2\text{SiHX}$  (X = halogen) species. A summary of torsional frequencies is given below:

X	$(\text{CH}_3)_2\text{SiX}_2$	$(\text{CH}_3)_2\text{SiHX}$	
F	156	189	
Cl	?	194	
Br	160	173	cm <sup>-1</sup>
I	170	178	
H	152		

Table (6.27) Spectroscopic Frequencies  $(\text{CH}_3)_2\text{SiCl}_2$  (cm<sup>-1</sup>)

I.R. Liquid	I.R. Solid (80)	Raman Liquid (85)	I.N.S. Solid	Assignment
{ 488m, sh				
467 s		464	463v.w	$\nu_7$ $\nu$ Si-Cl
~ 390 w			401v.w	
340 w			~ 318v.w	
	244	241		$\nu_{21}, \nu_{26}$ Skeletal rock
	231	232	222m.s	$\nu_8$ $\delta$ SiC <sub>2</sub>
	179	178		$\nu_{13}$ $\delta$ SiCl <sub>2</sub>
	166	168		$\nu_9$ $\delta$ SiCl <sub>2</sub>
			160s	$\nu_{14}, \nu_{27}$ Torsions
			~ 70v.w	} Lattice Modes
			~ 50 w	

In the silicon series, since the  $-\text{CH}_3$  groups are further from the centre than in the carbon series their interactions will also be less and so the splittings of the torsional modes ought to be less; in fact I.R. studies of  $(\text{CH}_3)_4\text{Si}$  (42) seem to indicate a splitting of  $\sim 15 \text{ cm}^{-1}$ . Hence for the dimethyl species a splitting of  $\sim 8 \text{ cm}^{-1}$  might be expected although this was not seen in the I.R. If this splitting were present, the I.N.S. torsional peak would only indicate a very slight broadening.

The beryllium filter spectrum of  $(\text{CH}_3)_2\text{SiCl}_2$  fig. (6.9) shows its most intense peak at  $160 \text{ cm}^{-1}$  with a medium band at  $222 \text{ cm}^{-1}$ . The latter would probably correlate with the optical band at  $231 \text{ cm}^{-1}$   $\nu_8$  ( $\delta \text{ SiCl}_2$  skeletal). In the region of the I.N.S. peak at  $160 \text{ cm}^{-1}$ , there are assigned fundamentals reported at  $166, 179 \text{ cm}^{-1}$   $\nu_9, \nu_{13}$   $\delta \text{ SiCl}_2$  (85). By comparison with the  $(\text{CH}_3)_2\text{CCl}_2$  case it is quite likely that these make only a small contribution and the band can be assigned to the torsions. The peak in fact has a F.W.H.M. of  $\sim 40 \text{ cm}^{-1}$  and hence any strong underlying peaks would have to be almost degenerate with the torsions. A very weak overtone or double scattering peak again occurs at about  $2 \times 160 \text{ cm}^{-1}$  and a broad band appears in the libration and lattice mode region to very low frequencies.

c)  $(\text{CH}_3)_3\text{SiCl}$

Durig has on one occasion (37) assigned the very weak torsional bands in the I.R. spectrum of solid  $(\text{CH}_3)_3\text{SiCl}$  at  $190 (\text{A}_2)$  and  $204 (\text{E}) \text{ cm}^{-1}$ .

Fig. (6.9) Beryllium filter spectra of the chloro-methylsilanes. 289.

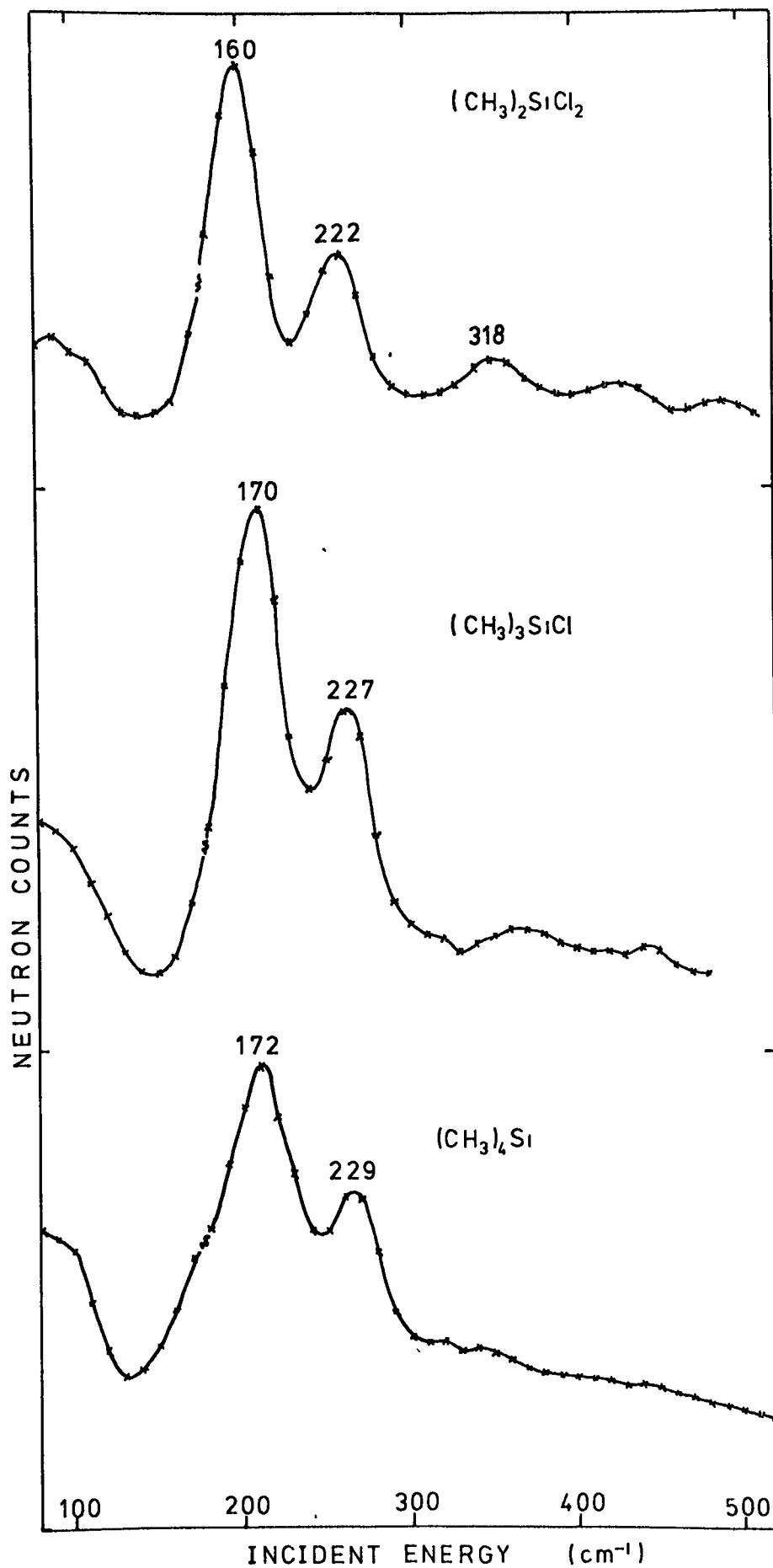


Table (6.28) Spectroscopic Frequencies  $(\text{CH}_3)_3\text{SiCl}$  ( $\text{cm}^{-1}$ )

I.R. Liquid	I.R. Solid (74)	Raman Liquid (78)	I.N.S. Solid	Resolved Curves + (Intensity)	Assignment
471s		465			$\nu_7(\text{A}_1)\text{ESi-Cl}$
			415vw		
{ 334 w 330v.w	329m		$\sim 330\text{v.w. brd}$		$\nu_{22}(\text{E})\delta \text{SiC}_3$
	244v.s	242	227m.s	227(15)	$\nu_8(\text{A}_1)\delta \text{SiC}_3$
	233m	236			
	204m				
	183s	187		{ 188(4) <u>170(19)</u> <u>157(9)</u>	$\nu_{23}(\text{E})\delta \text{SiCl} +$ Skeletal rock
			<u>170v.s</u>		$\nu_{24}(\text{E})$ Torsions
					$\nu_{12}(\text{A}_1)$

In a later paper (74) this was revised to 208 ( $\text{A}_2$ ), 233 ( $\text{E}$ )  $\text{cm}^{-1}$  (with a splitting of 25  $\text{cm}^{-1}$ ) and at 148 ( $\text{A}_2$ ), 176 ( $\text{E}$ )  $\text{cm}^{-1}$  for  $(\text{CD}_3)_2\text{SiCl}_2$ . Although these frequencies change on deuteration in the ratios of 1.40 and 1.32 respectively (values typical of torsional modes), it is difficult to see how this second very high assignment fits into the general pattern. Durig's own determination for  $(\text{CH}_3)_4\text{Si}$  puts the torsions at only  $\sim 170 \text{ cm}^{-1}$  with a splitting of only  $\sim 15 \text{ cm}^{-1}$ . Also Bürger (78) obtained a moderately strong band in the Raman at 236  $\text{cm}^{-1}$  which he assigned as  $\delta \text{SiC}_3$  (skeletal,  $\nu_8$ ).

Moving on to the present beryllium filter spectrum, fig. (6.9) this again shows two strong bands, the strongest centred at 170  $\text{cm}^{-1}$  with a moderate one at 227  $\text{cm}^{-1}$ . The latter would again correlate

with the optical band just mentioned. Another optic mode appears at  $187 \text{ cm}^{-1}$  in the Raman spectrum and  $190 \text{ cm}^{-1}$  in the I.R. spectrum, assigned as  $\nu_{23} \delta \text{ SiCl}$  which may be having some effect on the neutron band at  $170 \text{ cm}^{-1}$  which now shows a broadening F.W.H.M.  $\sim 46 \text{ cm}^{-1}$ . This band can now only be assigned as the torsion, which again by comparison with  $(\text{CH}_3)_3\text{CCl}$  would still be expected to have the most intensity. It is also worth considering that the P.E.D. calculations (85) give several % H active mode mixing in the  $242 \text{ cm}^{-1}$  band but none in the  $187 \text{ cm}^{-1}$  band. The results of a curve analysis are given in the table, this places the torsional bands at  $\sim 157, 170 \text{ cm}^{-1}$  still as the main contributors in a 1:2 ratio and a much weaker peak at  $188 \text{ cm}^{-1}$ . It is interesting to note however that the  $242 \text{ cm}^{-1}$  band is quite strong in intensity relative to the E torsion. The remaining broad, rising band at the very low frequency end appears to be increased in intensity relative to the dimethyl compound, as might be expected due to the increased number of protons. This again must contain librational and lattice modes.

d)  $(\text{CH}_3)_4\text{Si}$

The usual labelling of the modes for  $(\text{CH}_3)_4\text{M}$  compounds is given in table (6.29).

Durig's I.R. studies of this compound as the solid (42) mentioned earlier, suggests the  $A_2$  and  $F_1$  torsions are at  $163.5 \text{ cm}^{-1}$  and  $177.5 \text{ cm}^{-1}$  respectively, which would for once fit quite well with the strongest I.N.S. peak at  $172 \text{ cm}^{-1}$  table (6.30) fig. (6.9).

Table (6.29) Labelling of fundamentals for  $(\text{CH}_3)_4\text{M}$  types.

Description	$A_1$	$A_2$	E	$F_1$	$F_2$
$\nu$ C-H symmetric stretch	$\nu_1$				$\nu_{14}$
$\delta$ C-H " bend	$\nu_2$				$\nu_{16}$
$\nu$ M-C " stretch	$\nu_3$				
$\nu$ C-H asymmetric stretch			$\nu_5$	$\nu_9$	$\nu_{13}$
$\delta$ C-H " bend			$\nu_6$	$\nu_{10}$	$\nu_{15}$
$\rho$ $\text{CH}_3$ rocking			$\nu_7$	$\nu_{11}$	$\nu_{17}$
$\nu$ M-C asymmetric stretch					$\nu_{18}$
$\delta$ $\text{MC}_4$ skeletal deformation			$\nu_8$		$\nu_{19}$
TORSION		$\nu_4$		$\nu_{12}$	
Mode active in:-	Raman	-	Raman	-	Raman I.R.

Table (6.30) Spectroscopic Frequencies  $(\text{CH}_3)_4\text{Si}$  ( $\text{cm}^{-1}$ )

I.R. Solid (42)	Raman (43)	I.N.S. Solid	Curves Resolved	Assignment
		{ 308 287 $\nu_{\text{vw}}$		
239	239	229ms	232(10)	$\nu_{19}$ $F_2$ } skeletal
202	190		207 (4)	$\nu_5$ E } deformations
<u>177.5</u>		<u>172s</u>	<u>175 (15)</u>	$\nu_{12}$ $F_1$ } Torsions
<u>163.5</u>			<u>158 (5)</u>	$\nu_4$ $A_2$ }
		131w.sh	134 (6)	?
		~ 60 rising ↓		Lattice Modes

The optic skeletal deformation modes  $\nu_8$  and  $\nu_{19}$  ( $F_2$  modes) have been assigned at 202, 239  $\text{cm}^{-1}$  and a neutron band appears at 229  $\text{cm}^{-1}$ , though with a minimum at  $\sim 210 \text{ cm}^{-1}$ . The 172  $\text{cm}^{-1}$  I.N.S. band shows a considerable broadening; F.W.H.M.  $\sim 68 \text{ cm}^{-1}$ , i.e. more than would be expected for a 1:3 system with a split of about 14  $\text{cm}^{-1}$ . A curve analysis was therefore attempted with the results given in table (6.29). The only puzzling feature is the extra weak band at  $\sim 134 \text{ cm}^{-1}$ , required to fit the broadening, which has not been mentioned previously.

#### Section B4. Barrier Calculations.

Because none of the torsional mode splittings were actually resolved without the aid of the curve analyser and because they are also quite small anyway, Durig's example of taking the averaged frequency and using it in a Mathieu type solution has been followed, for the multi-top species.

Reduced Moments of inertia for  $\text{CH}_3\text{SiX}_3$  were calculated using microwave data (71, 72) and the value for  $(\text{CH}_3)_4\text{Si}$  was taken from Durig (42). Using averaged frequencies also requires an averaged reduced moment of inertia. Exactly what this ought to be for unsymmetrical species is uncertain, but values were calculated in the following manner:

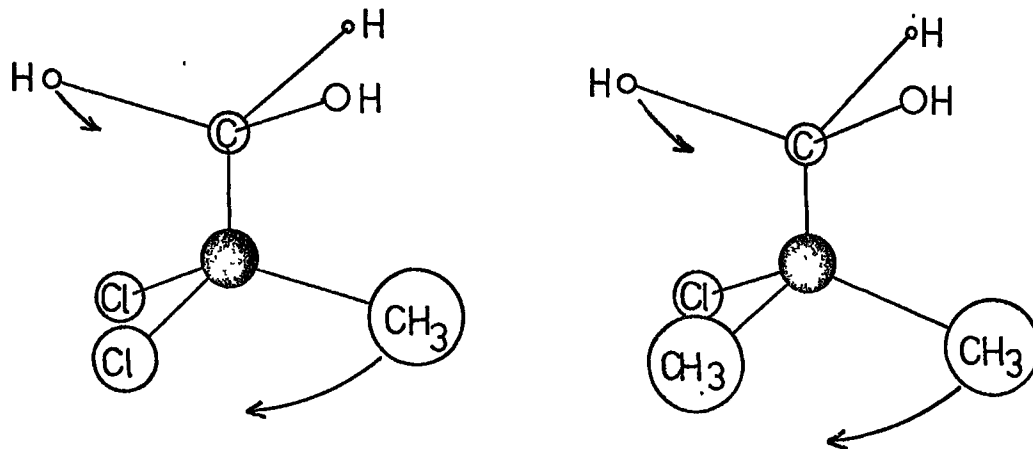


Fig. (6.10)



Td angles were assumed and simplifying the systems as shown in fig. (6.10) the moments of chlorine atoms around the axis were calculated according to the SiCl bond length and the moments of the CH<sub>3</sub> groups were calculated from the reduced moment of inertia of (CH<sub>3</sub>)<sub>4</sub>Si. The values derived expressed as the parameter F used in the Mathieu solution (see theory chapter) are given in table (6.31). Previously determined barrier values are given in table (6.32).

Table (6.31) Calculated barrier heights for methyl silicon compounds.

Compound	$\bar{\nu}_{\text{obs}}$ cm <sup>-1</sup>	F cm <sup>-1</sup>	$\Delta b_{0-1}$	S	$\bar{\nu}_{0-2}$ cm <sup>-1</sup>	Mathieu Barrier cm <sup>-1</sup>	Simple Harmonic Barrier cm <sup>-1</sup>
CH <sub>3</sub> SiF <sub>3</sub>	156	5.372	12.91	49.1	296	593	503
CH <sub>3</sub> SiCl <sub>3</sub>	160	5.276	13.48	53.5	307	635	539
CH <sub>3</sub> SiBr <sub>3</sub>	177	5.249	14.99	64.7	340	764	663
(CH <sub>3</sub> ) <sub>2</sub> SiCl <sub>2</sub>	160	5.289	13.45	53.3	307	634	538
(CH <sub>3</sub> ) <sub>3</sub> SiCl	166	5.313	13.89	56.2	318	672	576
(CH <sub>3</sub> ) <sub>4</sub> Si	171	5.372	14.15	58.0	327	701	605

These results are discussed at the end of the Chapter (PART E).

Table (6.32) Previous barrier determinations ( $\bar{V}_3$ ).

Method	Compound	Ref	Details (Values in $\text{cm}^{-1}$ )
Thermodynamic	$\text{CH}_3\text{SiF}_3$	77	$\bar{V}_3 \sim 503$
	$(\text{CH}_3)_4\text{Si}$	92	$\bar{V}_3 \sim 454$
Microwave	$\text{CH}_3\text{SiF}_3$	11,69,73	$\bar{V}_3 \sim 419, 325$
	$\text{CH}_3\text{SiCl}_3$	71	$\bar{V}_3 < 200$
	$\text{CH}_3\text{SiBr}_3$	72	$\bar{V}_3 \sim 350$
I.R. Solid	$(\text{CH}_3)_2\text{SiF}_2$		$\bar{V}_3 = 594$
	$(\text{CH}_3)_2\text{SiBr}_2$		633
	$(\text{CH}_3)_2\text{SiI}_2$	80	706
	$(\text{CH}_3)_2\text{SiH}_2$		528
	$(\text{CH}_3)_3\text{SiF}$	79	786
	$(\text{CH}_3)_3\text{SiCl}$	37,74	919, 1049
	$(\text{CH}_3)_4\text{Si}$	42	699
N.M.R. Solid	$\text{CH}_3\text{SiCl}_3$	56	$E_a = 454$ as a lower limit
	$\beta(\text{CH}_3)_4\text{Si}$	89	$E_a = 549$

PART C: GERMANIUM SPECIES.

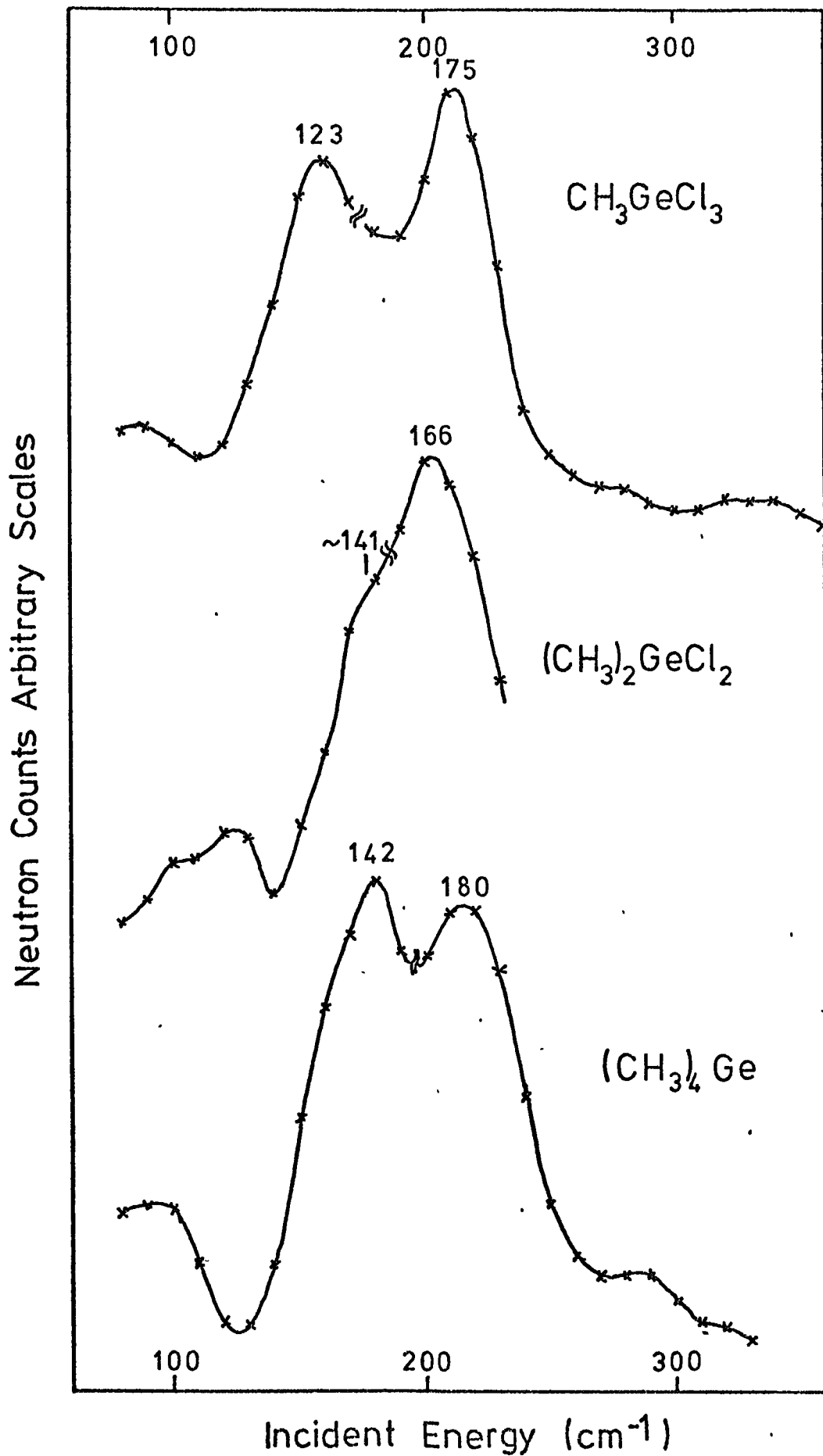
Section C1. Previous work.

Although much work has been done on a number of the methyl-halogeno-germanium compounds most of the previous work on the three compounds studied here has been spectroscopic in nature and hence this is discussed along with the new I.N.S. data. An N.M.R. study of  $(\text{CH}_3)_4\text{Ge}$  (98) has indicated a barrier to methyl rotation less than for the silicon compound, hence the torsional frequency may be expected to be lower.

Section C2. Experimental.

Unfortunately only  $\text{CH}_3\text{GeCl}_3$ ,  $(\text{CH}_3)_2\text{GeCl}_2$  and  $(\text{CH}_3)_4\text{Ge}$  could be obtained:  $\text{CH}_3\text{GeCl}_3$  and  $(\text{CH}_3)_2\text{GeCl}_2$  from ROC/RIC, Belleville, N.J., and  $(\text{CH}_3)_4\text{Ge}$  from Ventron Alfa Products, Beverly, Mass. These again are liquids which hydrolyse in air, and were therefore loaded into tubes with fitted tops, in a dry box, transferred to the vacuum line and distilled under reduced pressure. Their I.R. spectra as liquids showed no impurity peaks when compared with previous spectra (93-96, 42, 43) so pure samples were distilled into and sealed in silica liquid cans for the neutron work. Beryllium filter spectra of  $\text{CH}_3\text{GeCl}_3$  and  $(\text{CH}_3)_4\text{Ge}$  were run completely over the region of interest. Unfortunately for technical reasons the spectrum of  $(\text{CH}_3)_2\text{GeCl}_2$  had to be stopped during the run, but is included since it does cover the main peaks although no width measurement can be made. The results are shown together for convenience in fig. (6.11), with frequencies in tables (6.33 - 6.35).

Fig. (6.11) Beryllium filter spectra of the chloro-methyl-germanium types.



Section C3. Assignment and Discussion of Spectra.

A quick glance at the spectra shows a different pattern to the one observed for the carbon and silicon series.

a) CH<sub>3</sub>GeCl<sub>3</sub>.

Table (6.33) Spectroscopic Frequencies CH<sub>3</sub>GeCl<sub>3</sub> (cm<sup>-1</sup>)

I.R. Liquid (93)	Raman Liquid (96)	I.N.S. Solid	Assignment
	397		$\nu_4$ $\nu$ Ge-Cl
320 w			
268 w			? Torsion overtone
177 s	179 s	175 vs	$(\nu_5, \nu_{12}) \delta, \rho$ GeCl <sub>3</sub>
	144 s	?	$\nu_{11}$ $\delta$ GeCl <sub>3</sub>
		<u>123 s</u>	Torsion
		~ 46 w	

Durig (93) has looked at the I.R. and Raman of this species as a liquid and although the torsional fundamental was not observed he assigned a band at 268 cm<sup>-1</sup> as its first overtone. Other fundamentals in the region occur at 178 cm<sup>-1</sup> and 144 cm<sup>-1</sup> assigned as  $(\nu_5, \nu_{11}) \delta$  GeCl<sub>3</sub> and  $\nu_{12} \rho$  GeCl<sub>3</sub> (ref. 93) or with reversed descriptions of  $\nu_{11}, \nu_{12}$  (ref. 96).

The beryllium filter spectrum of the solid shows a very broad band F.W.H.M.  $\sim 81$  cm<sup>-1</sup> with two strong components showing at 123 and 175 cm<sup>-1</sup>. Although the band at 175 cm<sup>-1</sup> is the strongest, if

it were to be assigned as the torsion it would mean an increase over the barrier seen for  $\text{CH}_3\text{SiCl}_3$ , it can also clearly be correlated with the band at  $178\text{ cm}^{-1}$  in the optic spectra. The optic band at  $144\text{ cm}^{-1}$  would fit the area between the two strong I.N.S. peaks. This leaves the  $123\text{ cm}^{-1}$  with no optical counterpart which marks it as the probable torsional frequency (c.f. Durig's 134 estimate). This being the case the band at  $175\text{ cm}^{-1}$  is probably best described as  $\rho\text{ GeCl}_3$  if one follows the arguments which have been made in the carbon and silicon cases, though its much increased intensity is a puzzling feature.

b)  $(\text{CH}_3)_2\text{GeCl}_2$

Table (6.34) Spectroscopic Frequencies  $(\text{CH}_3)_2\text{GeCl}_2$  ( $\text{cm}^{-1}$ )

I.R. Liquid (96)	Raman Liquid (96)	I.N.S. Solid	Assignment
404			$\nu_{18}$ $\nu$ Ge-Cl
	387		$\nu_7$ $\nu$ Ge-Cl
	187		{ $\nu_{26}, \nu_{21}$ skeletal rock $\nu_8$ skeletal def.
	163	{ $\sim 166\text{vs}$ $\sim 141\text{s, sh}$ $\sim 80\text{ w}$	$\nu_{13}$ skeletal twist
	147		$\nu_9$ $\delta$ $\text{GeCl}_2$
			$\nu_{27}, \nu_{14}$ Torsions

On going to the dimethyl species a broad band appears in the I.N.S. spectrum peaking at  $166\text{ cm}^{-1}$ , broadening to higher frequency with a strong shoulder at  $\sim 141\text{ cm}^{-1}$ . No strong bands appear to lower frequency. Both frequencies have optical counterparts at  $163\text{ cm}^{-1}$  ( $\nu_{13}$  skeletal twist) and  $147\text{ cm}^{-1}$  ( $\nu_9$   $\text{GeCl}_2$  deformation)

and a band at  $187 \text{ cm}^{-1}$  assigned to several of the skeletal rock and deformation modes ( $\nu_{26}$ ,  $\nu_{21}$ ,  $\nu_8$ ).

The problem now remains as to where in this the torsions are placed. Since the previous patterns seem to be breaking down and fundamentals other than the torsion are becoming stronger this is difficult, but one would tend to place it nearer to the value found in  $\text{CH}_3\text{GeCl}_3$ , i.e. somewhere under the shoulder at  $\sim 141 \text{ cm}^{-1}$ .

c)  $(\text{CH}_3)_4\text{Ge}$ .

Table (6.35) Spectroscopic Frequencies  $(\text{CH}_3)_4\text{Ge}$  ( $\text{cm}^{-1}$ )

I.R. Solid (42)	Raman Liquid (95)	I.N.S. Solid	Assignment
	560		
134 v.w	189	{ 180 v.s 142 v.s	Skeletal modes Torsions
		~ 55 m.w	

The beryllium-filter spectrum shows two peaks at 142 and 180  $\text{cm}^{-1}$  on a strong broad band of F.W.H.M.  $\sim 90 \text{ cm}^{-1}$ . A band assigned as a collection of skeletal modes appears at 189  $\text{cm}^{-1}$  in the Raman spectrum (95). Durig (42) has assigned the torsion tentatively at 134  $\text{cm}^{-1}$  in the solid I.R., but does not give the other frequencies in the region, although it would seem that nothing appears at 142  $\text{cm}^{-1}$  equivalent to the strongest neutron feature. It would therefore seem most likely that this is the principal torsional band. Durig

recorded no splitting into the  $A_2$  and  $F_1$  torsional bands, but the neutron peak does show an odd shape, broadening a little to lower frequency. This could however be due to an unassigned skeletal mode.

#### Section C4. Barrier Calculations

The only structural data available on these compounds is an old electron diffraction value of Ge-C = 1.98 Å for  $(CH_3)_4Ge$  (108). However in  $CH_3GeH_3$  it has been found that Ge-C = 1.945 Å (109) and in  $GeHCl_3$ , Ge-Cl = 2.148 Å (110). These values were used in calculating the reduced moments of inertia, assuming Td angles. The barriers calculated are given in table (6.36).

Table (6.36) Calculated Barriers for the germanium species.

Compound	$I_{Red}$ (a.m.u. Å <sup>2</sup> )	$F$ (cm <sup>-1</sup> )	$\bar{\nu}_{Tor}$ (cm <sup>-1</sup> )	Mathieu $\bar{V}_3$ barrier (cm <sup>-1</sup> )	S.H. $\bar{V}_3$ barrier (cm <sup>-1</sup> )
$CH_3GeCl_3$	3.195	5.273	123	392	319
$(CH_3)_2GeCl_2$	3.193	5.277	141	505	419
$(CH_3)_4Ge$	3.157	5.337	142	504	420

Table (6.37) Previously determined barriers (values in cm<sup>-1</sup>).

Method	Compound	Torsional Frequency	Mathieu $\bar{V}_3$ barrier	Ref.
I.R.	$CH_3GeCl_3$	134	454	(93)
	$(CH_3GeI_3)$	123	384	(97)
	$(CH_3)_4Ge$	134	451	(42)
N.M.R. Solid	$(CH_3)_4Ge$	$E_a = 228$		(98)

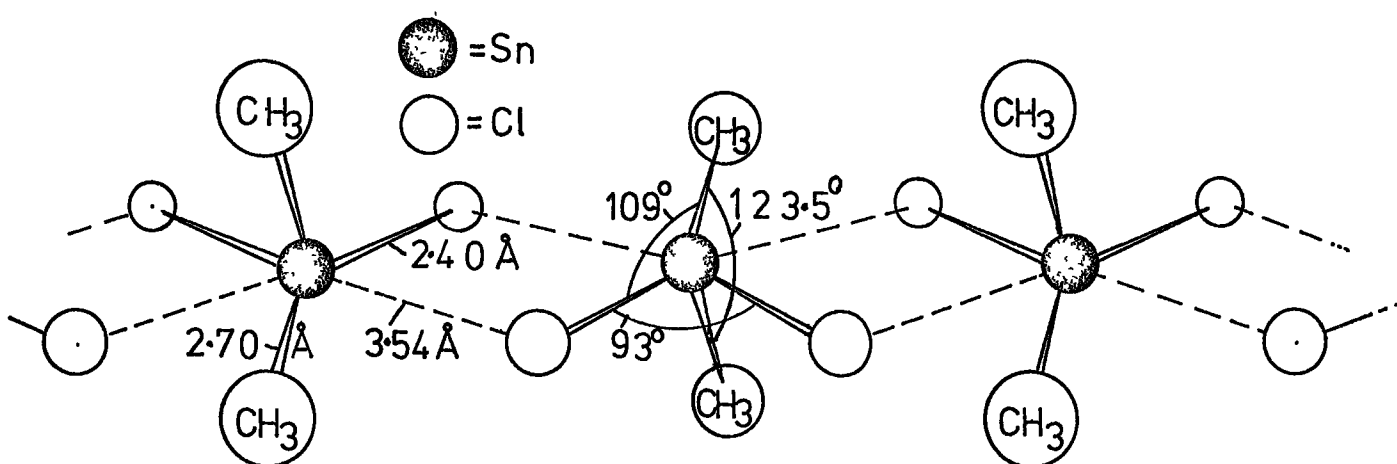


PART D. TIN SPECIES

Section D1. Previous work.

The tin compounds immediately show a difference from the carbon, silicon and germanium compounds in that the three chloro compounds are solids. Clark et al (99) have noted that nujol mulls and solutions of these compounds give different spectra; nujol mulls giving lower stretching frequencies and higher bending frequencies than the solutions, and hence it has been suggested that there may be some association in the solids.

A recent X-ray study of  $(\text{CH}_3)_2\text{SnCl}_2$  (100) has in fact shown that the solid contains chains of molecules with chlorine bridges as shown in fig. (6.12):-



This arrangement shows the tin straining towards gaining an Oh environment. Unfortunately no other X-ray work has been done on the other chloro compounds, though it would seem reasonable to assume that these follow suit to some extent.  $(\text{CH}_3)_4\text{Sn}$  with no possibility of Cl bridging is once again a liquid). This feature does introduce a further problem in that the spectra are more difficult to interpret.

Electron diffraction studies (101-103) of the vapour phases of the series  $(\text{CH}_3)_x\text{SnCl}_{4-x}$   $x = 1 \rightarrow 4$  show them to be Td coordinated. The bond length data show that substitution of chlorines has the effect of reducing the Sn-C bond length, and the Sn-Cl bond length also decreases the more chlorines there are present:-

	<u>Sn-C</u>	<u>Sn-Cl</u>	
$\text{CH}_3\text{SnCl}_3$	2.105	2.306	
$(\text{CH}_3)_2\text{SnCl}_2$	2.109	2.327	Å
$(\text{CH}_3)_3\text{SnCl}$	2.108	2.354	
$(\text{CH}_3)_4\text{Sn}$	2.134		

A number of spectroscopic studies have been undertaken (42, 43, 95, 104-107) and data from these is used in the discussion of the I.N.S. spectra.

#### Section D2. Experimental.

All four of the compounds above were obtained from commercial sources and the solids were packed in the ordinary silica cans for the neutron experiments.  $(\text{CH}_3)_4\text{Sn}$  was packed in a liquids can.  $(\text{CH}_3)_3\text{SnCl}_3$  from ROC/RIC, Belleville, N.J.;  $(\text{CH}_3)_2\text{SnCl}_2$  from Ventron Alfa Products, Beverly, Mass.;  $(\text{CH}_3)_3\text{SnCl}$  from Bristol Organics Ltd., Bristol; and  $(\text{CH}_3)_4\text{Sn}$  from K and K Labs. Inc., Plainview, N.Y.). The I.R. spectra of all the compounds showed close correspondence with those previously reported. The three chloro compounds were first run on the 6H spectrometer at room temperature, as the torsional modes were expected to be in the region of  $100 \text{ cm}^{-1}$ .

Seeing the rather poor results, a beryllium filter spectrum was also obtained for  $\text{CH}_3\text{SnCl}_3$ , as well as for solid  $(\text{CH}_3)_4\text{Sn}$  which was run only on this machine.

### Section D3. Assignment and Discussion of Spectra.

Results of all three 6H runs fig. (6.13) are rather disappointing, displaying one very broad band rising to a sharp point in the region of  $150\text{ cm}^{-1}$ , although slight variations in the band shape can be seen. All three species display I.R. and Raman fundamentals in this region. Clearly transitions from the populated higher levels of the several vibrational modes and the torsions in the region, may be adding to the complexity of the spectrum, although the Cl bridging must be remembered and may have a strong effect on the spectra.

The beryllium filter spectrum of  $\text{CH}_3\text{SnCl}_3$  fig. (6.14) shows an intense broad band (F.W.H.M.  $\sim 57\text{ cm}^{-1}$ ) rising to a peak at  $143\text{ cm}^{-1}$  with a strong shoulder at  $123\text{ cm}^{-1}$ . Both these frequencies appear to have I.R. counterparts in bands assigned as  $\delta, \rho\text{ SnCl}_3$  (106), so again there is the problem of where to place the torsion. If one agrees with the assignment made for  $\text{CH}_3\text{GeCl}_3$  in which the higher, stronger band was  $\rho\text{ GeCl}_3$ , then in this case the lower shoulder  $\sim 123\text{ cm}^{-1}$  must be assigned as the torsion with  $143\text{ cm}^{-1}$  as  $\rho\text{ SnCl}_3$ .

The Be-filter spectrum of  $(\text{CH}_3)_4\text{Sn}$  clearly shows two peaks at  $104$  and  $148\text{ cm}^{-1}$ , the higher peak showing some degree of broadening. The lowest assigned optic fundamentals are  $\nu_8, \nu_{19}$  skeletal deformations placed at  $151\text{ cm}^{-1}$ , but Durig (42) has observed a very weak feature at  $101.5\text{ cm}^{-1}$  which he assigned as the torsion. If these are the

Fig. (6.13) Time-of-flight data for the chloro-tin species.

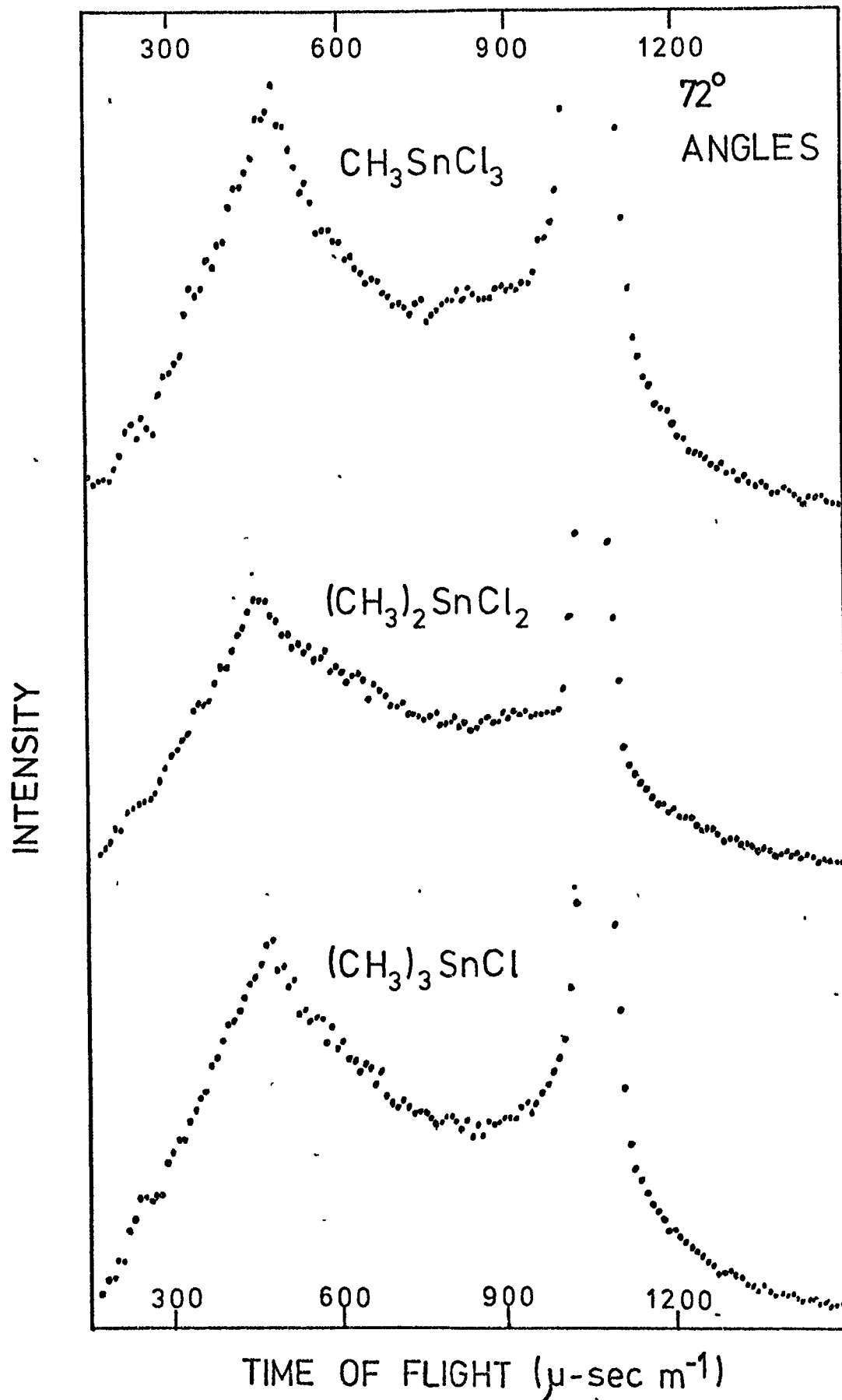
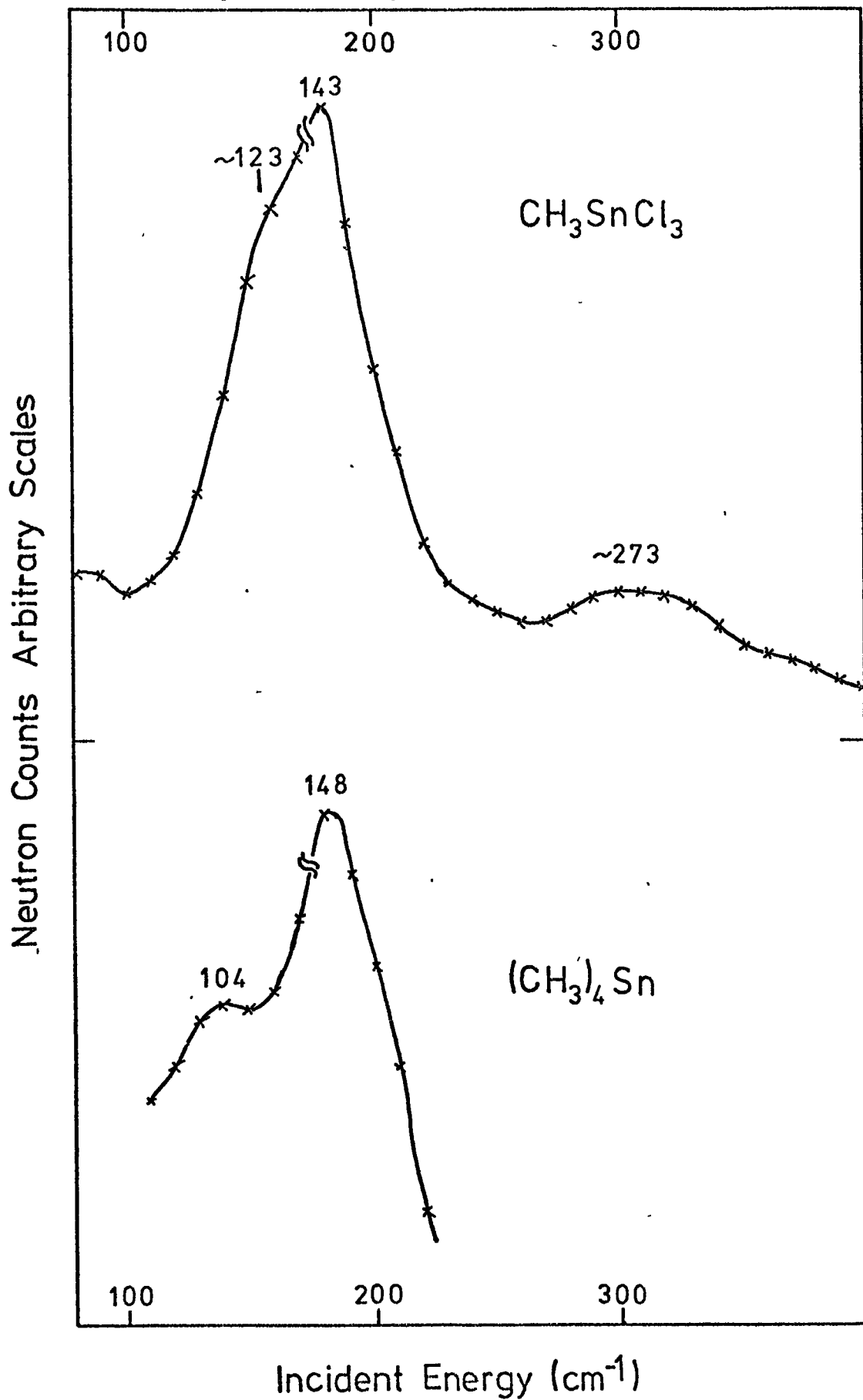


Fig. (6.14) Beryllium filter spectra.



equivalents of the I.N.S. peaks, the torsional mode, which up to now for the  $(\text{CH}_3)_4\text{M}$  series has been the strongest, is the weaker of the two peaks. The few frequencies are summarised in table (6.38).

Table (6.38) Spectroscopic frequencies  $(\text{CH}_3)_4\text{Sn}$  ( $\text{cm}^{-1}$ )

I.R. Solid (42)	Raman (104)	I.N.S. Be-filter	Assignment
	151	148 s.brd.	$\nu_{18}, \nu_{19}$ Skeletal modes
<u>101.5 w</u>		<u>104 m.sh</u>	TORSION

Returning now to the 6H spectra, for the di- and tri-methyl compounds the lower frequency side of the broad band can be seen to be increased in intensity when compared to the  $\text{CH}_3\text{SnCl}_3$  spectrum, making the spectra slightly broader in the region of  $\sim 100 \text{ cm}^{-1}$ , i.e. near the torsional frequency seen for  $(\text{CH}_3)_4\text{Sn}$ . It should be pointed out that at room temperature transitions between the populated higher levels e.g.  $1 \leftarrow 2$  will be of lower frequency than  $0 \leftarrow 1$  and hence will pull the apparent frequency of the band down. (It must be remembered that the geometry of the situations will be varying due to chlorine bridging which might be expected to affect the frequencies in different ways for the different compounds).

As can be seen the crowding of hydrogen active modes in the Ge, Sn compounds makes the assignment of a torsional frequency rather hazardous, and although reasoned assignments have been made (see table (6.39)) one ought to regard them with a deal of reserve.

Table (6.39) Spectroscopic Frequencies of the methyl chloro tin compounds ( $\text{cm}^{-1}$ )

	I.R. (106)	Raman (105)	I.N.S. 6H	I.N.S. Be-filter	Assignment
$\text{CH}_3\text{SnCl}_3$	366	363	.	273w.brd	$\nu$ Sn-Cl Overtone or Double Scatter ?
	152		sh		} $\delta, \rho$ $\text{SnCl}_3$ Torsion $\delta$ $\text{SnCl}_3$
	132	142	145 s	143v.s	
	123 m		sh	123s.sh	
		112			
$(\text{CH}_3)_2\text{SnCl}_2$		344			$\nu$ Sn-Cl
	332				} Skeletal and Sn-Cl bending modes + Torsions
	307		sh		
	158		160 vs		
	146				
		135			
129					
	124		$\sim 90$ sh		
$(\text{CH}_3)_3\text{SnCl}$	325	318			$\nu$ Sn-Cl
	145	150	sh 145 vs sh $\sim 95$ sh		} Skeletal and Sn-Cl bending modes + Torsions

#### Section D4. Barrier Calculations.

Since there is no way of telling the effect of Cl bridging on the reduced moments, apart from the fact that they cause distortion from  $T_d$  angles, these have been calculated using the electron diffraction

values for the gas phase molecules (101-103). The barriers for the  $\text{CH}_3\text{SnCl}_3$  and  $(\text{CH}_3)_4\text{Sn}$  only have been calculated, and the values for the others will likely be somewhere between.

Table (6.40) Calculated  $\bar{V}_3$  barrier parameters for  $\text{CH}_3\text{SnCl}_3$  and  $(\text{CH}_3)_4\text{Sn}$ .

	$I_{\text{red}}$	$F \text{ cm}^{-1}$	$\bar{v} \text{ cm}^{-1}$	Mathieu $\bar{V}_3 \text{ cm}^{-1}$	S.H. $\bar{V}_3 \text{ cm}^{-1}$
$\text{CH}_3\text{SnCl}_3$	3.199	5.267	123	397	319
$(\text{CH}_3)_4\text{Sn}$	3.164	5.325	104	288	226

Two previous determinations of the barrier in  $(\text{CH}_3)_4\text{Sn}$  gave the following values:

$$\text{I.R. Solid } (\text{CH}_3)_4\text{Sn} \quad \bar{v} = 101.5 \quad V_3 = 280 \text{ cm}^{-1} \quad (42)$$

$$\text{N.M.R. Solid } " \quad E_a = 161 \text{ cm}^{-1} \quad (98)$$



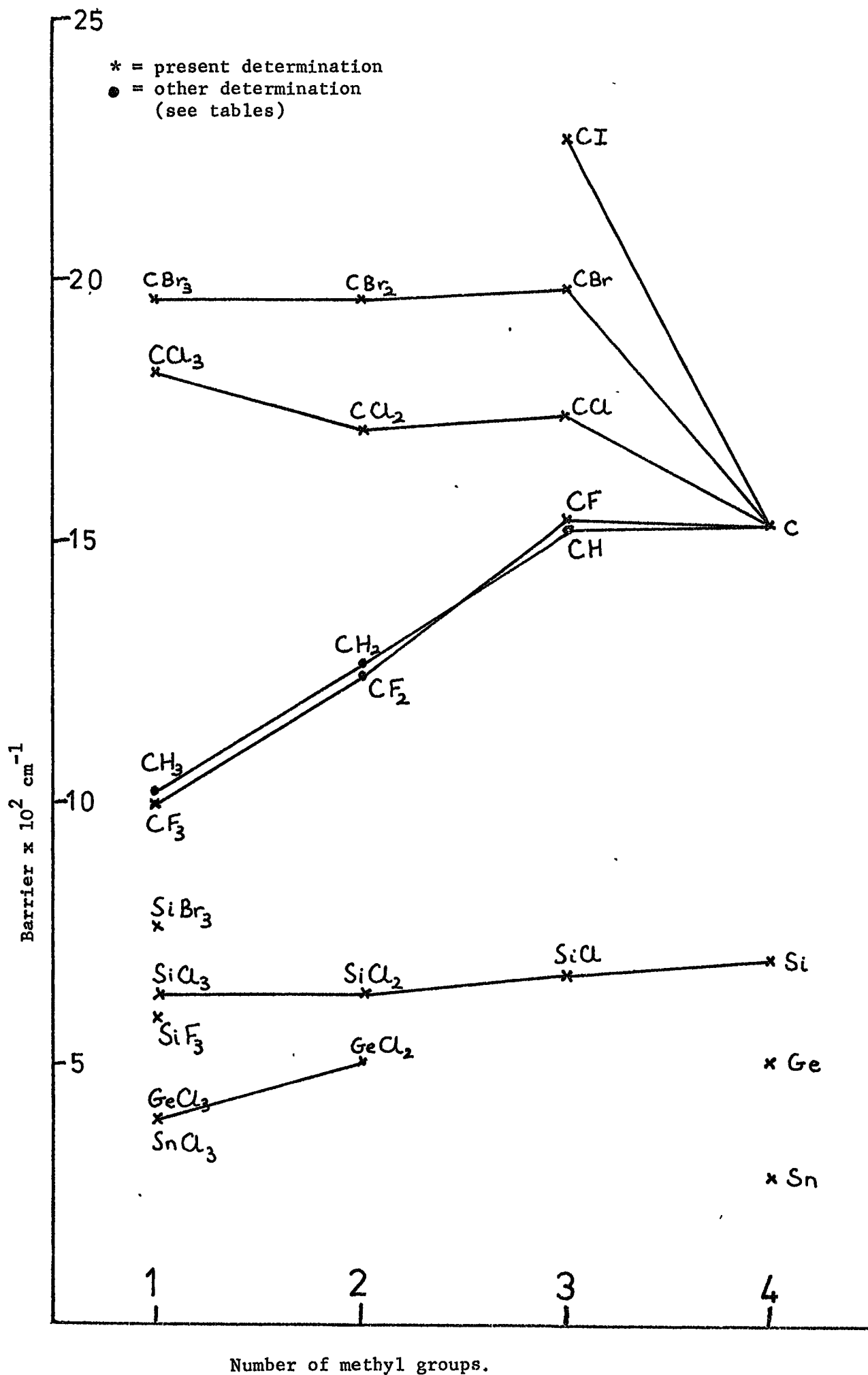
PART E: General Discussion of barrier calculations

It should be remembered before embarking on a discussion that the multiple rotor treatment is only approximate and that the values  $\frac{2}{9}K$  and  $\frac{2}{9}L$  contain a number of different potential constants, several of which have been assumed to be very small for the purpose of discussion in terms of a barrier height and an interaction term. The weighted average Mathieu barriers are also approximated values whose accuracy is not really known.

The observed torsional frequencies (and hence the barriers) obtained in the present experiment are often slightly lower frequency than in the I.R. spectra. As mentioned in Chapter 4 this may be due to dispersion in I.N.S. or to crystal size effects on the I.R. spectra. Whatever, the results in general agree reasonably with previous determinations, except for some of the early microwave and thermodynamic measurements which are probably in error due to misinterpretation.

Considering the multiple rotor systems of the carbon compounds it is very interesting to see that the results of the present investigation indicate that the coupling term is roughly constant for 2, 3 or 4 rotors at  $\sim -170 \text{ cm}^{-1}$ , which perhaps indicates that the systems do not distort much from a tetrahedral C-C-C angle. However it is worth noting that for  $(\text{CH}_3)_2\text{CH}_2$  the available data (17,49) indicates a much smaller interaction of  $\sim -60 \text{ cm}^{-1}$ . Possibly the two methyls are able to distort further away from each other allowed by the two hydrogens having small Van der Waals interaction radii. (i.e. a steric effect). (In view of this a similar effect might be seen for  $(\text{CH}_3)_2\text{CF}_2$  if coupling data were available. An uncertain I.R. assignment (32) has however given the full barrier of the order of  $\sim 1260 \text{ cm}^{-1}$ ).

Fig. (6.15 ) draws the scheme of barriers vs. the number of methyl



groups, and it appears from this that the behaviour of the hydrocarbon and fluorocarbon species is slightly different to the chloro- and bromo-species. However it is noticeable that the contribution to the total barrier from each of the groups or atoms against which the methyl rotates is very crudely additive. Consider  $\text{CH}_3\text{CH}_3$  : 1 methyl rotates against 3 hydrogens to give a barrier of  $1027 \text{ cm}^{-1}$ (111), so 1 hydrogen contributes  $342 \text{ cm}^{-1}$ . Now consider  $(\text{CH}_3)_2\text{CH}_2$  with a total barrier of  $1276 \text{ cm}^{-1}$ (49) and subtract  $2 \times 342 \rightarrow 592 \text{ cm}^{-1}$ ; the contribution of 1 methyl group to the barrier. A similar subtraction of 342 from the barrier for  $(\text{CH}_3)_3\text{CH}$  (79) gives  $2 \times 591 \text{ cm}^{-1}$  for two methyl groups. Doing exactly similar sums for the available halogen compound data gives:-

$$\text{CH}_3\text{CF}_3 \quad 1004 \div 3 = 334 \text{ cm}^{-1} \text{ for 1 F}$$

$$(\text{CH}_3)_2\text{CF}_2 \quad (32) \sim 1260 - 668 = 592 \text{ cm}^{-1} \text{ for 1 CH}_3$$

$$(\text{CH}_3)_3\text{CF} \quad 1541 - 334 = 2 \times 603 \text{ cm}^{-1} \text{ for 2 x CH}_3$$

$$\text{CH}_3\text{CCl}_3 \quad 1826 \div 3 = 609 \text{ cm}^{-1} \text{ for 1 x Cl}$$

$$(\text{CH}_3)_2\text{CCl}_2 \quad 1718 - 1218 = 500 \text{ cm}^{-1} \text{ for 1 x CH}_3$$

$$(\text{CH}_3)_3\text{CCl} \quad 1742 - 609 = 2 \times 567 \text{ cm}^{-1} \text{ for 2 x CH}_3$$

$$\text{CH}_3\text{CBr}_3 \quad 1966 \div 3 = 655 \text{ cm}^{-1} \text{ for 1 x Br}$$

$$(\text{CH}_3)_2\text{CBr}_2 \quad 1965 - 1310 = 645 \text{ cm}^{-1} \text{ for 1 x CH}_3$$

$$(\text{CH}_3)_3\text{CBr} \quad 1988 - 655 = 2 \times 667 \text{ cm}^{-1} \text{ for 2 x CH}_3$$

All the weighted Mathieu values are used above for consistency (a similar pattern occurs for the S.H. data). It can be seen that the methyl group contribution is in a very broad sense constant (varies over  $500 - 667 \text{ cm}^{-1}$ , average  $595 \text{ cm}^{-1}$ ). This would suggest for 3 methyl

groups, i.e.  $(\text{CH}_3)_4\text{C}$  a barrier of  $3 \times 595 \sim 1785 \text{ cm}^{-1}$  as apposed to  $1537 \text{ cm}^{-1}$  observed. (A weighted average barrier calculation using torsional frequencies of 220 and  $280 \text{ cm}^{-1}$  taken from previous results (49,42), shows a slightly better correspondence,  $1591 \text{ cm}^{-1}$ ).

Although this can hardly be regarded as conclusive proof of an additive effect, the simple idea is rather appealing. A similar set of calculations using some barriers tabulated by Durig (27) for the series  $\text{CH}_3\text{CH}_3 \rightarrow \text{CH}_3\text{CH}_2\text{X} \rightarrow \text{CH}_3\text{CX}_3$  (X = F, Cl, Br) also show some crude additive effects. Performing exactly the same series of calculations as above:-

$$\text{CH}_3\text{CH}_3 \quad 1027 \div 3 = 342 \text{ cm}^{-1} \text{ for } 1 \times \text{H contribution}$$

$$\text{CH}_3\text{CH}_2\text{F} \quad 1164 - 684 = 480 \text{ cm}^{-1} \quad 1 \times \text{F} \quad "$$

$$\text{CH}_3\text{CHF}_2 \quad 1111 - 342 = 2 \times 385 \text{ cm}^{-1} \quad 2 \times \text{F} \quad "$$

$$\text{CH}_3\text{CF}_3 \quad 1419 \div 3 = 473 \quad 1 \times \text{F}$$

$$\text{CH}_3\text{CH}_2\text{Cl} \quad 1300 - 684 = 616 \text{ cm}^{-1} \quad 1 \times \text{Cl}$$

$$\text{CH}_3\text{CHCl}_2 \quad 1443 - 342 = 2 \times 551 \text{ cm}^{-1} \quad 2 \times \text{Cl}$$

$$\text{CH}_3\text{CCl}_3 \quad 1887 \div 3 = 629 \text{ cm}^{-1} \quad 1 \times \text{Cl}$$

$$\text{CH}_3\text{CH}_2\text{Br} \quad 1297 - 684 = 613 \text{ cm}^{-1} \quad 1 \times \text{Br}$$

$$\text{CH}_3\text{CHBr}_2 \quad 1513 - 342 = 2 \times 586 \text{ cm}^{-1} \quad 2 \times \text{Br}$$

$$\text{CH}_3\text{CBr}_3 \quad 2020 \div 3 = 673 \text{ cm}^{-1} \quad 1 \times \text{Br}.$$

The fact that the barrier does not increase very much when the second halogen is added (decreases for fluorine) was remarked upon by Durig(27). However, these series do also seem to show a crude additivity and by using the average values for the contributions some barriers for

mixed halogen species can be predicted:-

Average contributions:    1 x F = 446  
                                   1 x Cl = 599             $\text{cm}^{-1}$   
                                   1 x Br = 624

	<u>Predictions</u>	<u>Observed (24)</u>	
$\text{CH}_3\text{CF}_2\text{Cl}$	$2 \times 446 + 599 = 1491$	1538	
$\text{CH}_3\text{CF}_2\text{Br}$	$2 \times 446 + 624 = 1516$	1573	$\text{cm}^{-1}$
$\text{CH}_3\text{CClBr}_2$	$2 \times 624 + 599 = 1847$	1817	

Although by no means perfect the predictions give the correct pattern. The observed barriers were collected by Durig from several sources; it would be interesting to obtain data for all the compounds by the same technique for a more consistent comparison.

In the case of the  $\text{CH}_3\text{CX}_3$  compounds it would be useful if the changing barriers for different substituent elements X could be related to some property of the element. By calculating the H---X internuclear distance for the eclipsed configuration and observing the difference between this and the sum of the Van der Waals radii of H and X one gains an idea of the degree of steric overlap. A plot of this vs. barrier (fig. 6.16) indicates there may be some relationship, although the fluoride appears to deviate, and there is not really enough data to say anything constructive other than that the barrier increases as the overlap increases. When a similar calculation is performed for the  $\text{CH}_3\text{SiX}_3$  compounds the H---F and H---Cl distances actually turn out to be slightly greater than the Van der Waals sum indicating that other influences must be responsible for the barrier here.

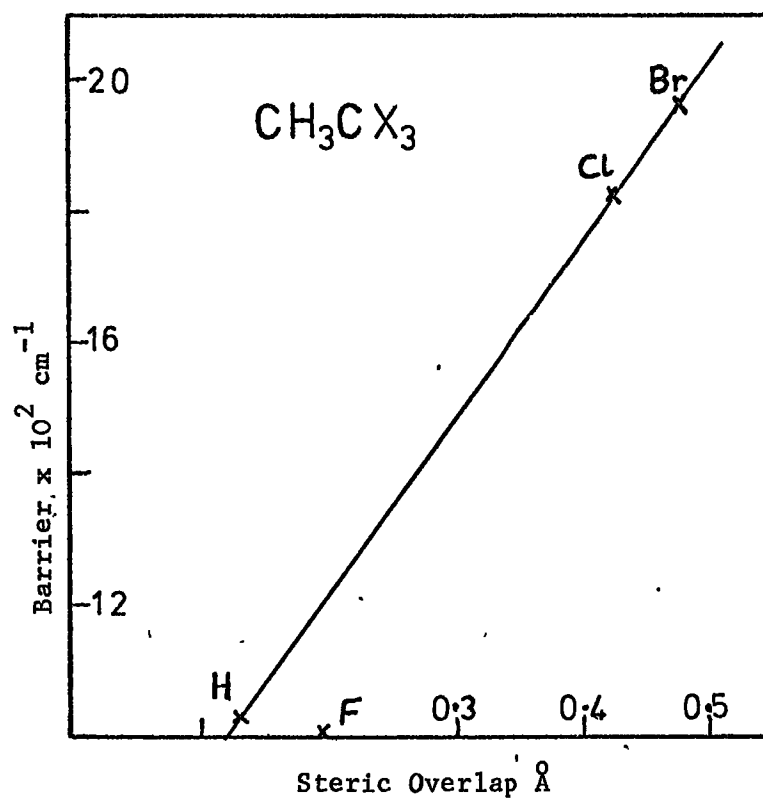


Fig. (6.16)

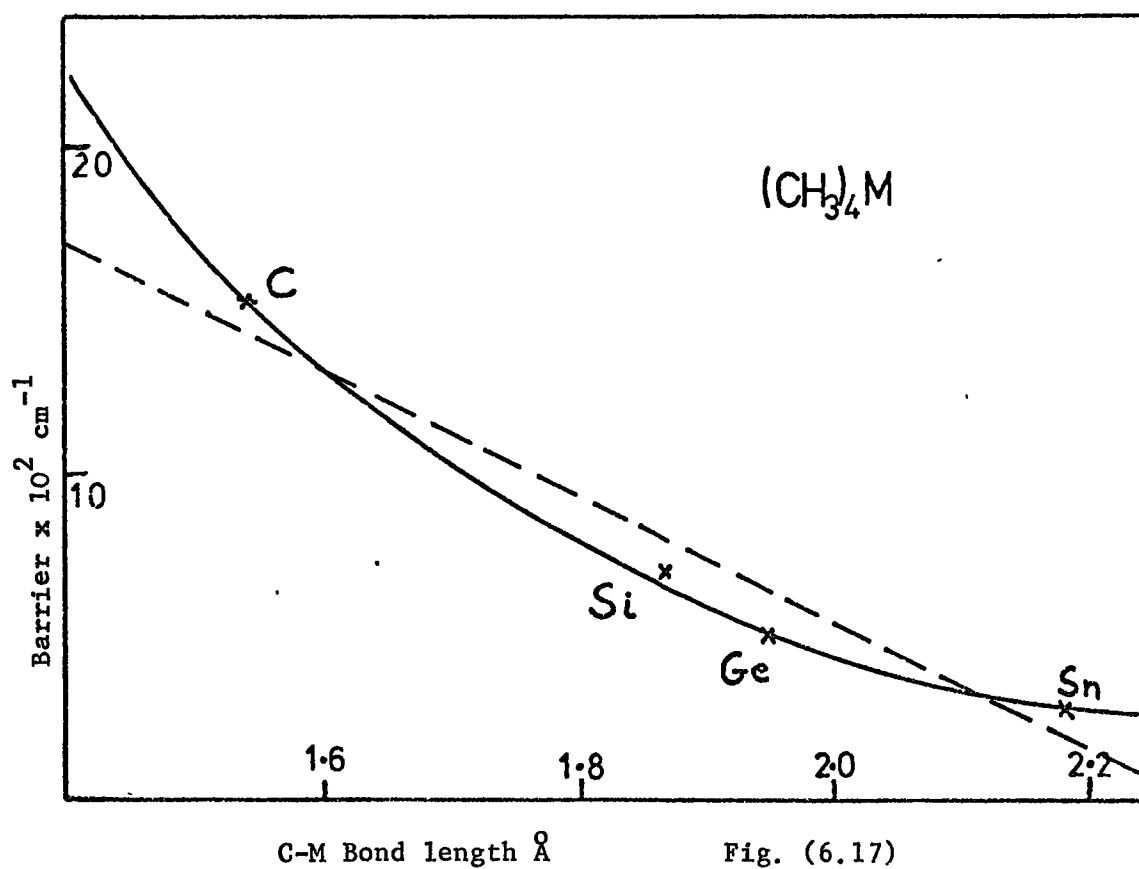


Fig. (6.17)

Returning to fig. (6. 15) it is easy to see that the silicon compounds have much lower barriers than the carbon series and that as expected the germanium and tin species fall even lower. Very little change in barrier occurs for all the series  $(\text{CH}_3)_x \text{SiCl}_{4-x}$  ( $x = 1 \rightarrow 4$ ), though the trend is to increase with the number of methyls, whereas for the chloro carbon series the overall pattern is one of decrease.

Because the tin chloro compounds probably all have chloro bridging this prevents any meaningful analysis of the barrier trends down the group IV series except for the tetramethyl cases. Here the barrier decreases going down the group and at the same time the methyl group moves further away from the central atom. Fig. (6.17) shows a plot of barrier vs. C-M distance (M = central atom).

This appears very similar to a graph obtained by Overend and Scherer (113), who calculated the C---C intermethyl repulsive force constants by a normal coordinate type analysis (also including  $\text{Pb}(\text{CH}_3)_4$ ) and plotted this against the intermethyl distance. They also suggested that the plot would best fit a relationship in which the force constant is proportional to  $(\text{C---C})^{-6.82}$ , though one would hardly feel that this is justified considering the few data points available and their deviations from the calculated relationship. Whatever, there is some clear relationship between the barrier and the C-M bond length which once again indicates a steric effect in the barrier origin.

As with the results of ab initio calculations the experimental results would tend to suggest that no one parameter can be held

responsible for the barrier; the potential arising from a complicated interaction of a number of factors, of which the proximity of the groups is an obvious and important one.

Unfortunately the determined barrier heights do not lead on to any firm conclusion about their origins other than what is already known, although a possible additive effect has been demonstrated. However the results do add to, and in some cases correct, the already existing pool of determinations. It should not be forgotten that this data (and a lot of the previous I.R. data) was obtained for the solid state, and although external effects are not likely to be large they undoubtedly still exist and may perturb any relationship patterns.



References - Chapter 6

1. L. Silver, R. Rudman, J. Phys. Chem. 74, 3134 (1970).
2. H. Russell, D.R.V. Golding, D.M. Yost, J.A.C.S. 66, 16 (1944).
3. C.A. Wulff, J. Chem. Phys. 39, 1227 (1963).
4. T.R. Rubin, B.H. Levedahl, D.M. Yost, J.A.C.S. 66, 279 (1944).
5. K.S. Pitzer, Chem. Revs. 27, 39 (1940); Disc. Farad. Soc. 10, 79 (1951).
6. A.H. Mones, B. Post, J. Chem. Phys. 20, 755 (1952).
7. R. Rudman, B. Post, Mol. Cryst. 5, 95 (1968).
8. R. Rudman, Mol. Cryst. Liq. Cryst. 6, 427 (1970).
9. L. Silver, R. Rudman, J. Chem. Phys. 57, 210 (1972).
10. J.E. Bertie, S. Sunder, Spectrochim. Acta 30A, 1373 (1974).
11. H.T. Minden, B.P. Dailey, Phys. Rev. 82, 338 (1951).
12. W.F. Edgell, G.B. Miller, J.W. Amy, J.A.C.S. 79, 2391 (1957).
13. R. Holm, M. Mitzlaff, H. Hartmann, Z. Naturforsch 23A, 307 (1968).
14. Y.S. Li, K.L. Kizer, J.R. Durig, J. Mol. Spec. 42, 430 (1972).
15. J.R. Durig, M.M. Chen, Y.S. Li, J.Mol. Struct 15, 37 (1973).
16. D.R. Lide, D.E. Mann, J. Chem. Phys. 29, 914 (1958).
17. E. Hirota, C. Matsumura, Y. Morino, Bull. Chem. Soc. Jap. 40, 1124 (1967).
18. F.L. Tobiason, R.H. Schwendeman, J. Chem. Phys. 40, 1014 (1964).
19. G. Allen, H.J. Bernstein, Can. J. Chem. 32, 1124 (1954).
20. J.C. Evans, H.J. Bernstein *ibid* 33, 1746 (1955).
21. T.R. Stengle, R.C. Taylor, J. Mol. Spec. 34, 33 (1970).

22. Many earlier works mentioned in the above paper.
23. J.R. Durig, S.M. Craven, K.K. Lau, J. Bragin, J. Chem. Phys. 54, 479 (1971).
24. J.R. Durig, S.M. Craven, C.W. Hawley, J. Bragin, J. Chem. Phys. 57, 131 (1972).
25. R. Hornischer, H. Moser, Spectrochim. Acta 28A, 81 (1972).
26. Krishnaji, R.K. Laloraya, Indian J. Pure Appl. Phys. 11, 74 (1973).
27. J.R. Durig, W.E. Bucy, C.J. Wurrey, J. Chem. Phys. 60, 3293 (1974).
28. S.G. Frankiss, D.J. Harrison, Spectrochim. Acta 31A, 29 (1975).
29. P. Klaboe, *ibid* 26A, 977 (1970).
30. J.H.S. Green, D.J. Harrison, *ibid* 27A, 1217 (1971).
31. I.L. Andresen, S.J. Cyvin, B. Larsen, O. Tørset, Acta. Chem. Scand. 25A, 473 (1971).
32. K.D. Moller, A.R. Demeo, D.R. Smith, L.H. London, J. Chem. Phys. 47, 2609 (1967).
33. N.T. McDevitt, A.L. Rozek, F.F. Bentley, A.D. Davidson, *ibid* 42, 1173 (1965).
34. J.C. Evans, G.Y.-S. Lo, J.A.C.S. 88, 2118 (1966).
35. C. Brot, B. Lassier, Spectrochim. Acta 24A, 295 (1967).
36. J.E. Bertie, S. Sunder *ibid* 30A, 1373 (1974).
37. J.R. Durig, S.M. Craven, J. Bragin *ibid* 51, 5663 (1969).
38. J.R. Durig, S.M. Craven, J. Bragin, C.W. Hawley, J.H. Mulligan, *ibid* 58, 1281 (1973).
39. C.W. Young, J.S. Koehler, D.S. McKinney, J.A.C.S. 69, 1410 (1947).
40. N. Sheppard, J. Chem. Phys. 16, 690 (1948).

41. E.R. Shull, T.S. Oakwood, D.H. Rank, *ibid* 31, 1562 (1959).
42. J.R. Durig, S.M. Craven, J. Bragin *ibid* 52, 2046 (1970).
43. A.M. Pyndyk, M.R. Aliev, V.T. Aleksanyan, *Opt. Spektrosk* 36, 676 (1974).
44. B. Lafon, J.R. Nielsen, *J. Mol. Spec.* 21, 175 (1966).
45. K. Shimizu, H. Murata, *Bull. Chem. Soc. Jap.* 30, 487 (1957).
46. J. Overend, J.R. Sherer, *J. Opt. Soc. Am.* 50, 1203 (1960).
47. J.J. Rush, *J. Chem. Phys.* 46, 2285 (1967).
48. K.A. Strong, D.M. Grant, R.M. Brugger, *Phys. Rev. Lett.* 20, 983 (1968).
49. + Unpublished results mentioned by J.J. Rush in "Study of Large Amplitude Vibrations in Molecules by Inelastic Neutron Scattering", A Reprint from 'Critical Evaluation of Chemical and Physical Structural Information' published by National Academy of Sciences, Washington D.C. 1974.
50. P.N. Brier, J.S. Higgins, *Molec. Phys.* 19, 645 (1970).
51. L.A. De Graaf, J. Sciesinski, *Physica* 48, 79 (1970).
52. J.G. Powles, H.S. Gutowsky, *J. Chem. Phys.* 21, 1695 (1953).
53. J.G. Powles, H.S. Gutowsky, *ibid* 23, 1692 (1955).
54. T.P. Das, *ibid* 27, 763 (1957).
55. E.O. Stejskal, D.E. Woessner, T.C. Farrar, H.S. Gutowsky *ibid* 31, 55 (1959).
56. H.M. McIntyre, C.S. Johnson, Jr., *ibid* 55, 345 (1971).
57. J.R. Lyerla, D.M. Grant, *J. Phys. Chem.* 76, 3213 (1972).
58. H.S. Gutowsky, D.W. McCall, *J. Chem. Phys.* 32, 548 (1960).
59. D.E. Woessner, H.S. Gutowsky, *ibid* 39, 440 (1963).

60. S. Kondo, Bull. Chem. Soc. Jap. 39, 249 (1966).
61. B.L. Barton, J. Chem. Phys. 55, 1983 (1971).
62. M.W. Thomas, Chem. Phys. Letts. 32, 271 (1975).
63. S.J. Cyvin, 'Molecular Vibrations and Mean Square Amplitudes'  
Elsevier, Amsterdam (1968) p. 79.
64. M.C. Tobin, J.A.C.S. 75, 1788 (1953).
65. K.D. Moller, H.G. Andresen, J. Chem. Phys. 37, 1800 (1962).
66. J.E. Bertie, S. Sunder, *ibid* 59, 3853 (1973).
67. W. Huttner, W. Zeil, Spectrochim. Acta 22, 1007 (1966).
68. K. Shimizu, H. Murata, J. Mol. Spec. 5, 44 (1960).
69. J. Sheridan, W. Gordy, J. Chem. Phys. 19, 965 (1951).
70. R.C. Mockler, J.H. Bailey, W. Gordy, *ibid* 21, 1710 (1953).
71. M. Mitzlaff, R. Holm, H. Hartmann, Z. Naturforsch 22A, 1415 (1967).
72. M. Mitzlaff, R. Holm, H. Hartmann, *ibid* 23A, 1819 (1968).
73. J.R. Durig, Y.S. Li, C.C. Tong, J. Mol. Struct. 14, 255 (1972).
74. J.R. Durig, R.O. Carter, Y.S. Li, J. Mol. Spec. 44, 18 (1972).
75. W. Zeil, B. Haas, Z. Naturforsch 28A, 1230 (1973).
76. A.L. Smith, J. Chem. Phys. 21, 1997 (1953).
77. R.L. Collins, J.R. Nielsen, *ibid* 23, 351 (1955).
78. H. Burger, Spectrochim. Acta 24A, 2015 (1967).
79. J.R. Durig, S.M. Craven, J. Bragin, J. Chem. Phys. 53, 38 (1970).
80. J.R. Durig, C.W. Hawley *ibid* 58, 237 (1973).
81. I.V. Shevchenko, Et al., Dokl. Akad. Nauk SSSR 184, 824 (1969).
82. S. Sportouch, C. Laioste, R. Gaufres, J. Mol. Struct 9, 119 (1971).
83. K. Shimizu, H. Murata, Bull. Chem. Soc. Jap. 32, 46 (1959).
84. K. Shimizu, H. Murata, J. Mol. Spec. 4, 201 (1960).

85. K. Shimzu, H. Murata, *ibid* 4, 214 (1960).
86. S.B. Herdade, Neutron Inelastic Scattering Proc. Symp. 4th (1968)  
2, 197.
87. R.M. Brugger, K.A. Strong, D.M. Grant *ibid* 2, 323.
88. G.W. Smith, *J. Chem. Phys.* 42, 4229 (1965).
89. S. Albert, J.A. Ripmeester, *ibid* 57, 2641 (1972).
90. K. Moedritzer, J.R. Van Wazer, *Inorg. Chem.* 5, 547 (1966).
91. P.A. McCusker, E.L. Reilly, *J.A.C.S.* 75, 1583 (1953).
92. J.G. Aston, R.M. Kennedy, G.H. Messerly, *J.A.C.S.* 63, 2343 (1941).
93. J.R. Aronson, J.R. Durig, *Spectrochim. Acta* 20, 219 (1964).
94. J.E. Griffiths, *ibid* 20, 1335 (1964).
95. H. Siebert, *Z. Anorg. Allg. Chem.* 263, 82 (1950).
96. D.F. Van de Vondel, G.P. Van der Kelen, *Bull. Soc. Chim. Belges*,  
74, 453 (1965).
97. J.R. Durig, C.F. Jumper, J.N. Willis Jr., *J. Mol. Spec.* 37, 260 (1971).
98. G.W. Smith, *J. Chem. Phys.* 42, 4229 (1965).
99. R.J.H. Clark, A.G. Davies, R.J. Puddephatt, *J.C.S.* (1968)A, 1828.
100. A.G. Davies, H.J. Milledge, D.C. Puxley, P.J. Smith *ibid* (1970)A,  
2862.
101. H. Fujii, M. Kimura, *Bull. Chem. Soc. Jap.* 44, 2643 (1971).
102. H. Fujii, M. Kimura, M. Nagashima, *ibid* 46, 3708 (1973).
103. B. Beagley, K. McAloon, J.M. Freeman, *Acta. Cryst.* 30B, 444 (1974).
104. W.F. Edgell, C.H. Ward, *J.A.C.S.* 77, 6486 (1955).
105. W.F. Edgell, C.H. Ward, *J. Mol. Spec.* 8, 343 (1962).
106. P. Taimsalu, J.L. Wood, *Spectrochim. Acta* 20, 1043 (1964).

107. Von H. Kriegsmann, S. Pauly, Z. Anorg. Allg. Chem. 330, 275 (1964).
108. L.B. Brockway, H.O. Jenkins, J.A.C.S. 58, 2036 (1936).
109. V.W. Laurie, J. Chem. Phys. 30, 1210 (1959).
110. B.P. Dailey, J.M. Mays, C.H. Townes, Phys. Rev. 76, 136 (1949).
111. S. Weiss, G.E. Leroi, J. Chem. Phys. 48, 962 (1968).
112. " " Spectrochim Acta. 25A, 1759 (1969).
113. J. Overend, J.R. Scherer, J. Opt. Soc. Am. 50, 1203 (1960).

CHAPTER 7

THE MULTI-METHYL-AMMONIUM HALIDE SALTS

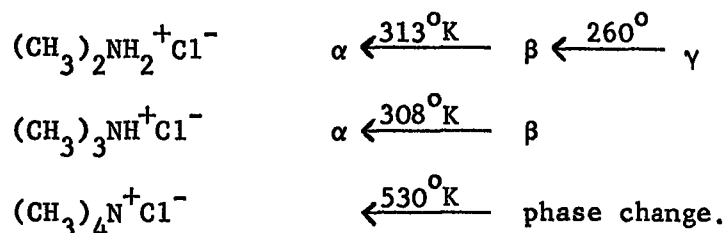
Introduction

The multi-methyl-ammonium salts present one more degree of complexity with respect to rotational barriers than the carbon group compounds just discussed. The methyl groups not only experience an internal barrier and have an interaction with each other, but also the whole ion interacts quite strongly with the lattice, especially where hydrogen bonding can occur. Although the even greater complexity of these systems means that models for the interpretation and calculation of barriers can only be quite crude, some useful and interesting information can still be extracted.

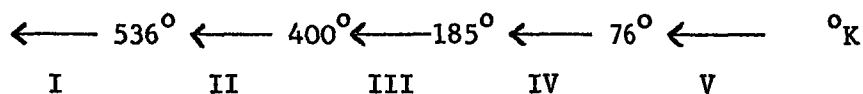
Section 1. Previous Studies

a) Phases

Stammler (1) investigated the chloride salts by differential thermal analysis down to  $-150^{\circ}\text{C}$  and discovered the following phases (using his labels)



However Andrews and Canepa (2) mention work by Gibson for a thesis (3) which indicates possibly five different phases for  $(\text{CH}_3)_4\text{N}^+\text{Cl}^-$ :-



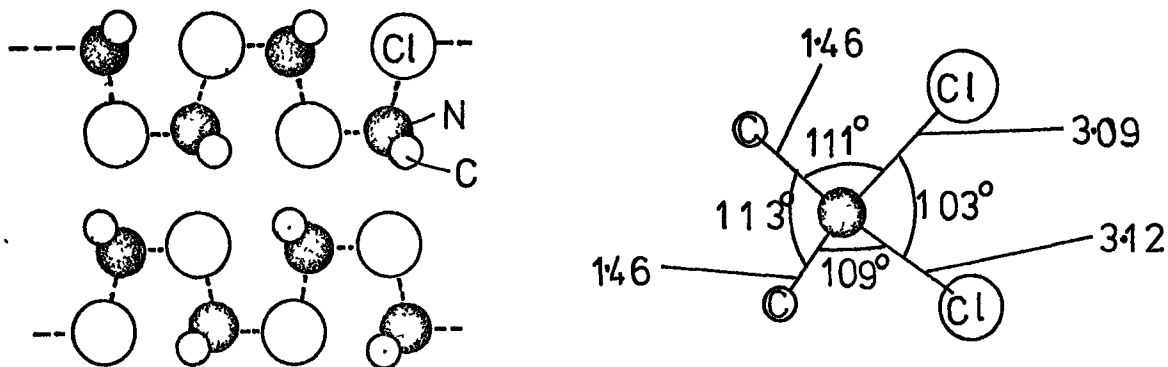
The change at  $400^{\circ}\text{K}$  was only reversible with traces of solvent present. The low temperature phases of  $(\text{CH}_3)_4\text{N}^+\text{Cl}^-$  were found earlier by Chang and Westrum (4) and an N.M.R. study (5) showed a discontinuity in  $T_1$  at  $418^{\circ}\text{K}$ ; the phase above this could be supercooled to room temperature reverting to the usual room temperature phase over a period of days. This prompted the same workers (5) to do a differential thermal analysis which showed a peak at  $\sim 434^{\circ}\text{K}$ .

#### b) Structural data

X-ray work by Lindgren et al has been undertaken on the room and higher temperature phases of  $(\text{CH}_3)_2\text{NH}_2^+\text{Cl}^-$  (6,7), and Stammer (1) obtained the cold phase powder photo but was unable to analyse it. However the room temperature structure shows up a number of important features:-

Orthorhombic      Ibam     $z = 8$   
 $a = 7.301$        $b = 14.515$        $c = 9.926 \text{ \AA}$

The ions form a distorted NaCl-type lattice, but the structure as a whole consists of infinite planar chains of Cl and N atoms linked by hydrogen bonds of lengths  $3.12$  and  $3.09 \text{ \AA}$  as shown in fig. (7.1):-





It is also interesting to note that the methyl hydrogens all point at adjacent Cl's, with a Cl---H distance of  $\sim 2.85\text{\AA}$ . The C-N-C angle is also appreciably larger than the Td angle.

Wagner in 1907 (8) observed that  $(\text{CH}_3)_3\text{NH}^+\text{Cl}^-$  was not isomorphous with the bromide and iodide salts. Mussgnug (9) who obtained X-ray powder data also showed the structural similarity of the bromide and iodide. Lindgren and Olovsson (10) undertook a single crystal study of the chloride at room temperature:-

$$\begin{array}{l} \text{Monoclinic} \quad P2_1/m \quad z = 2 \\ a = 6.088 \quad b = 7.033 \quad c = 7.031 \quad \beta = 95.73^\circ \end{array}$$

Bond lengths and angles are shown in fig. (7.2) along with those of the iodide. The structure consists of linear chains of ---Cl---HN(CH<sub>3</sub>)<sub>3</sub>---Cl---. Attention is also drawn to the decreasing N---Cl distance in the compounds:-

$\text{CH}_3\text{NH}_3^+\text{Cl}^-$	$\frac{\text{\AA}}{3.18}$	Ref. (11)
$(\text{CH}_3)_2\text{NH}_2^+\text{Cl}^-$	3.11	(6)
$(\text{CH}_3)_3\text{NH}^+\text{Cl}^-$	3.00	(10)

The iodide has been investigated by Sheldrick and Sheldrick (12)

$$\begin{array}{l} \text{Monoclinic} \quad P2_1/m \quad z = 2 \\ a = 7.13 \quad b = 8.33 \quad c = 5.62 \quad \beta = 104^\circ 48' \end{array}$$

This also has chains of --I---HN(CH<sub>3</sub>)<sub>3</sub>---I--- which appear linear.

Although the space groups are identical for the two structures the chains pack together differently resulting in quite different unit cell dimensions.

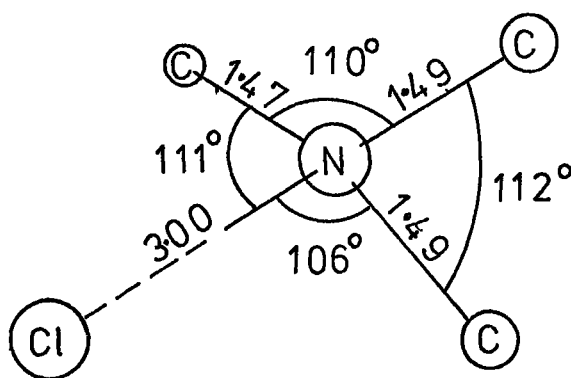


Fig. (7.2)

distances in Å

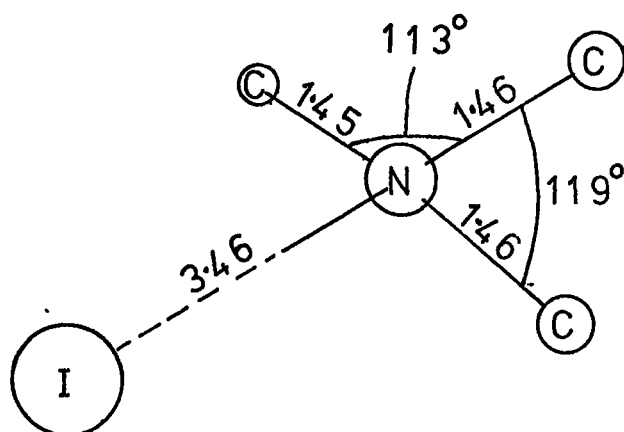


Fig. (7.3)

The  $(\text{CH}_3)_4\text{N}^+$  salts have been studied only by powder techniques, but by a number of people (1, 13-16):-

Tetragonal space groups  $P4/nmm$   $D_{4h}^7$   $Z = 2$

The values of cell parameters given by Wyckoff (15) are:-

$\text{Cl}^-$	a	7.78	
	c	5.53	
$\text{Br}^-$	a	7.76	$\text{\AA}$
	c	5.53	
$\text{I}^-$	a	7.96	
	c	5.75	

It is of interest to note that the only  $(\text{CH}_3)_4\text{N}^+$  salt so far found with a cubic cell at room temperature is with  $\text{SbCl}_6^-$  (39)

#### c) Spectroscopic Work

Edsall (17) once again pioneered the spectroscopic work with the Raman of solutions of the multi-methyl-ammonium species. The first serious studies in the I.R. appeared in 1956 (18, 19) with work on the chloride salts ranging from  $4500\text{-}500\text{cm}^{-1}$ . Ebsworth and Sheppard (20) shortly afterwards obtained the I.R. of the  $\text{I}^-$  salts, also looking at  $(\text{CH}_3)_2\text{ND}_2^+\text{I}^-$  and  $(\text{CH}_3)_3\text{ND}^+\text{I}^-$  and completed the assignments of the fundamentals. As was the case with the mono methyl-ammonium halides the N-H stretching frequencies appear much below their 'free' frequencies as a comparison with the frequencies seen for the  $\text{BCl}_4^-$ ,  $\text{BF}_4^-$  and  $\text{B}(\text{C}_6\text{H}_5)_4^-$  species shows (22, 23). This again indicates strong hydrogen bonding effects in the halides.

The N-H stretching frequency shift is also found to increase from the mono- to the trimethyl ammonium ion. Ebsworth and Sheppard (20) suggested this was perhaps due to fewer N-H's having a share in the hydrogen bonding with each anion.

$(\text{CH}_3)_4\text{N}^+\text{Cl}^-$  was first studied in detail by Möller et al (24) but Bottger and Geddes (16) in a later comprehensive study obtained the I.R. spectra of the chloride, bromide and iodide salts between  $4000\text{-}37\text{cm}^{-1}$ . They were able to correlate the band splittings with the site symmetry of the ions ( $D_{2d}$ ), and also noted the general tendency of the frequencies to increase slightly on going from  $\text{I}^- \rightarrow \text{Br}^- \rightarrow \text{Cl}^-$ . Krishnamurthy (25) recorded the Raman of the  $\text{Br}^-$  and  $\text{I}^-$  salts, and Anhouse and Tobin (26) that of the iodide. Recently Huong and Schlaak (27) have studied the I.R. and Raman of the  $(\text{CH}_3)_3\text{NH}^+$  salts and isotopic dilutions of them in the region above  $1800\text{cm}^{-1}$ .

A very recent I.R. study by Harmon et al (35) on several  $(\text{CH}_3)_4\text{N}^+$  salts put forward evidence for the existence of C-H--- $\text{X}^-$  hydrogen bonding in certain salts including the halides. The C-H stretching region of the salts with such anions as  $\text{SnCl}_6^{2-}$ ,  $\text{SnBr}_6^{2-}$  and  $(\text{C}_6\text{H}_5)_4\text{B}^-$  was found to show a sharp singlet, however for the salts,  $\text{F}^-$ ,  $\text{Cl}^-$ ,  $\text{Br}^-$ ,  $\text{I}^-$  and  $\text{ClO}_4^-$  an extra broad band appeared at lower frequencies, which in the case of the fluoride was intense and  $\sim 700\text{cm}^{-1}$  broad.

Harmon compares this with previous studies of C-H--- $\text{X}^-$  bonding and also attempts to show from available structural data that the C-H--- $\text{X}^-$  contacts are shorter than the calculated Van der Waal's

contacts e.g. :-

		<u>observed</u>	<u>V. d. W.</u>	
$\text{ClO}_4^-$	C---O	3.04	3.20	Å
$\text{I}^-$	C---I	3.79	3.96	

The fact that a sharp C-H stretching band still appeared with the broad band, was correlated to an observation by Sutor (36) for other systems that usually only one hydrogen of a methyl group will be involved in hydrogen-bonding.

Clearly such forces will have an effect on the barrier to overall rotation, and may help to explain the general increase of frequencies  $\text{I}^- \rightarrow \text{Br}^- \rightarrow \text{Cl}^-$ . Similar effects may well exist in the mono-, di- and tri-methylammonium halides but obviously cannot be detected in the I.R. on account of the much stronger broad N-H stretching bands.

#### d) N.M.R. data

Several N.M.R. studies of the motional barriers have been undertaken in recent years. Sjöblom and Tegenfeldt (28,29) studied the di- and tri-methylammonium chlorides, by line width and second moments temperature dependence, and observed changes related to the onset of methyl and whole ion rotations. Unfortunately they were only able to estimate barriers to methyl rotation:-

$$\begin{array}{l} (\text{CH}_3)_2\text{NH}_2\text{Cl} \quad E_a = 1153\text{cm}^{-1} \\ (\text{CH}_3)_3\text{NH Cl} \quad E_a = 1398\text{cm}^{-1} \end{array}$$

The study by Andrews and Canepa (2) of all three chloride salts were essentially in agreement with these, and with the numerous other

studies of the  $(\text{CH}_3)_4\text{N}^+$  salts (5, 30-34). These studies, including line width, second moment, and  $T_1$  and  $T_{1p}$  methods, seem to be generally in agreement in their derived activation energies for both methyl and whole ion reorientations. It has been noted that both values increase  $\text{I}^- \rightarrow \text{Cl}^-$ . Values of these activation energies derived by Gutowsky et al (5) from  $T_1$  and  $T_{1p}$  measurements are summarised in table (7.1) below:-

Table 7.1  $E_a$  values for  $(\text{CH}_3)_4\text{N}^+\text{X}^-$  from N.M.R. studies.  
 $\text{X} = \text{Cl}^-, \text{Br}^-, \text{I}^- (\text{cm}^{-1})$  (5)

Anion	$\text{CH}_3$ reorientation	Whole ion reorientation
$\text{Cl}^-$	2377	4546
$\text{Br}^-$	2237	4019
$\text{I}^-$	1922	3845
$\text{Cl}^- *$	2342	3076

\* = supercooled high temperature phase II

## Section 2. Experimental

Several of the salts used were available from B.D.H. laboratories, and the rest were prepared from solutions of the amines and appropriate acids. All salts were purified by recrystallisation.

Handling of the chlorides and bromides was performed in a dry box, although this precaution is perhaps not so necessary in the case of the bromides. I.R. spectra of all the compounds as nujol mulls were

obtained on the P.E. 451 spectrometer at room temperature and compared favourably with previous values (where available). Far I.R. spectra were also obtained on the F.S. 720 spectrometer at room temperature for all compounds and at liquid nitrogen temperatures for all except  $(\text{CH}_3)_4\text{N}^+ \text{Br}^-$  and  $\text{I}^-$ , since the warm and cold spectra of the chloride were found to be practically identical (even though the phases should be different).

Raman spectra were also obtained up to  $4500\text{cm}^{-1}$  in the cases which had not been previously reported, however only the low frequency spectra are reported here. The spectrum of  $(\text{CH}_3)_3\text{NH}^+\text{I}^-$  was unfortunately not obtained because of problems of decomposition in green laser light and fluorescence in red laser light.

All the I.N.S. spectra were obtained using thin samples in aluminium sachets (for which the background scattering should be very low indeed). Time-of-flight spectra at room temperature were run on 6H or 4H5 for  $(\text{CH}_3)_2\text{NH}_2^+\text{Cl}^-$ ,  $\text{Br}^-$  and  $\text{I}^-$ , and  $(\text{CH}_3)_3\text{NH}^+\text{Br}^-$  and  $\text{I}^-$ . All the salts except  $(\text{CH}_3)_4\text{N}^+\text{I}^-$  were run on the beryllium filter machine at liquid nitrogen temperatures. The 6H room temperature and beryllium filter liquid nitrogen temperature spectra of  $(\text{CH}_3)_4\text{N}^+\text{I}^-$  had been obtained previously by Dr J. Tomkinson in connection with other studies and these were kindly donated. Spectra are presented in figs.(7.4- 7.9).

### Section 3. Assignment of Spectra

Before embarking on the assignments some general comments about the phase changes can be made. The spectra of  $(\text{CH}_3)_2\text{NH}_2^+\text{Cl}^-$  at room and cold temperatures ought to be of the phases  $\beta$ , and  $\gamma$  respectively,

however very little difference could be seen in the I.R. or I.N.S. spectra, at least at frequencies below  $500\text{cm}^{-1}$ , and the same observation was found to apply to the equivalent bromide and iodide spectra.  $(\text{CH}_3)_3\text{NH}^+\text{Cl}^-$  does not change phase until above room temperature and so its 6H spectrum was not obtained, nor did the 6H and beryllium filter spectra of the bromide and iodide show any significant differences. A similar picture emerges for the two I.N.S. spectra of  $(\text{CH}_3)_4\text{N}^+\text{I}^-$ .

Hence although phase changes have been detected for some of the salts these do not appear to drastically change the low frequency spectra. (Cold temperature far I.R. values are quoted in preference since the peaks were found to have sharpened up).

Because of the relative simplicity of their spectra the  $(\text{CH}_3)_4\text{N}^+$  salts will be treated first. (The internal mode symmetry labels used assume a  $T_d$  molecular point group):-

a) The  $(\text{CH}_3)_4\text{N}^+$  salts. Frequencies are given in table (7.2).

A factor group analysis using Wyckoff's X-ray data (15) predicts for the lattice modes:-

$$\begin{aligned}
 T_{\text{Acoustic}} &= A_{2u} + E_u \\
 T_{\text{Optic}} &= \underbrace{A_{1g} + B_{1g} + 2E_g}_{\text{Raman}} + \underbrace{A_{2u} + E_u}_{\text{I.R.}} \\
 \text{Rotational} &= \underbrace{A_{2g} + E_g}_{\text{Raman}} + \underbrace{B_{1u} + E_u}_{\text{I.R.}}
 \end{aligned}$$



This gives 5 Raman and 3 I.R., but in fact fewer than this are seen. The far I.R. spectra of all three salts consist of two strong slightly broad bands, and the Raman spectrum which was obtained for the bromide shows a moderately strong low frequency peak with a lower shoulder and only 2 more weak peaks at higher frequency. Bottger and Geddes (16) saw only one Raman band for the iodide whereas Krishnamurthy (25) reports 4. The exact situation here is therefore not clear although it would appear that crystal splittings may not be great. Aside from this the most important feature is that all these observed modes are at low frequencies,  $< 120\text{cm}^{-1}$ .

The time-of-flight I.N.S. spectrum of the iodide fig.(7.4) shows an intense broad band centred at  $\sim 89\text{cm}^{-1}$  with a slight splitting giving peaks at  $\sim 83$  and  $94\text{cm}^{-1}$ , and the less well resolved aluminium 111 plane beryllium filter spectrum of the bromide also shows a moderately strong broad band below  $110\text{cm}^{-1}$ . If it is assumed once again that librational modes produce stronger I.N.S. peaks than translational modes one can assign the whole body librations to these low frequencies. (A more detailed study of this lower region may prove quite interesting but as yet has not been undertaken).

Concentrating now on the methyl torsional modes, since  $(\text{CH}_3)_4\text{N}^+$  is isoelectronic with  $(\text{CH}_3)_4\text{C}$  and its methyl groups are close to the nitrogen it ought to show a similar spectrum in the torsional mode region. But for the possibility of C-H---X<sup>-</sup> bonding one might also have expected external effects to be relatively small. The beryllium filter spectra (fig. 7.5) do in fact appear quite simple, all three salts showing three peaks in the region  $200-500\text{cm}^{-1}$ , in a

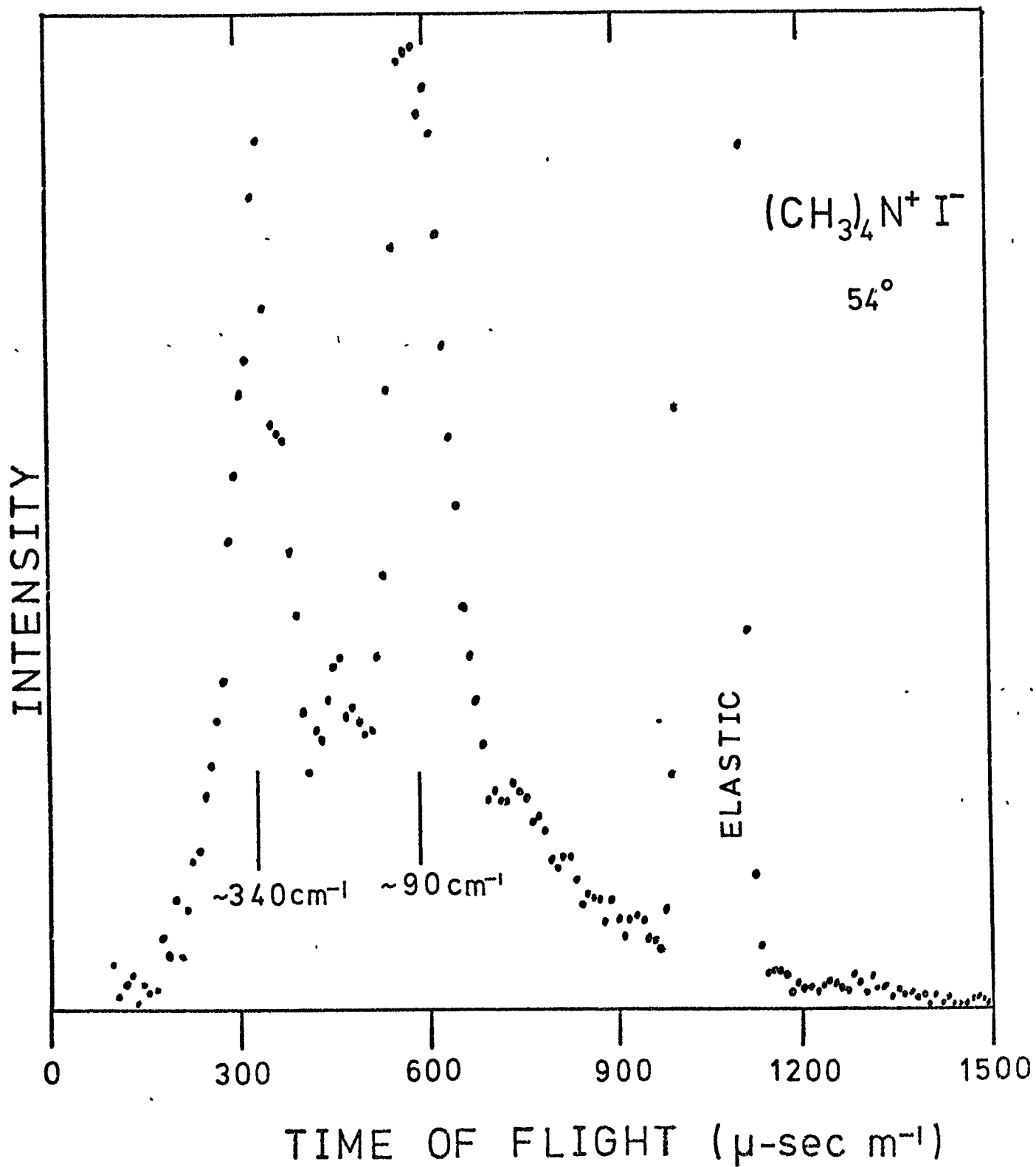
Fig. (7.4) Time-of-flight spectrum of  $(\text{CH}_3)_4\text{N}^+\text{I}^-$ .

Fig. (7.5) Beryllium filter spectra of the  $(\text{CH}_3)_4\text{N}^+$  salts, <sup>336</sup>.

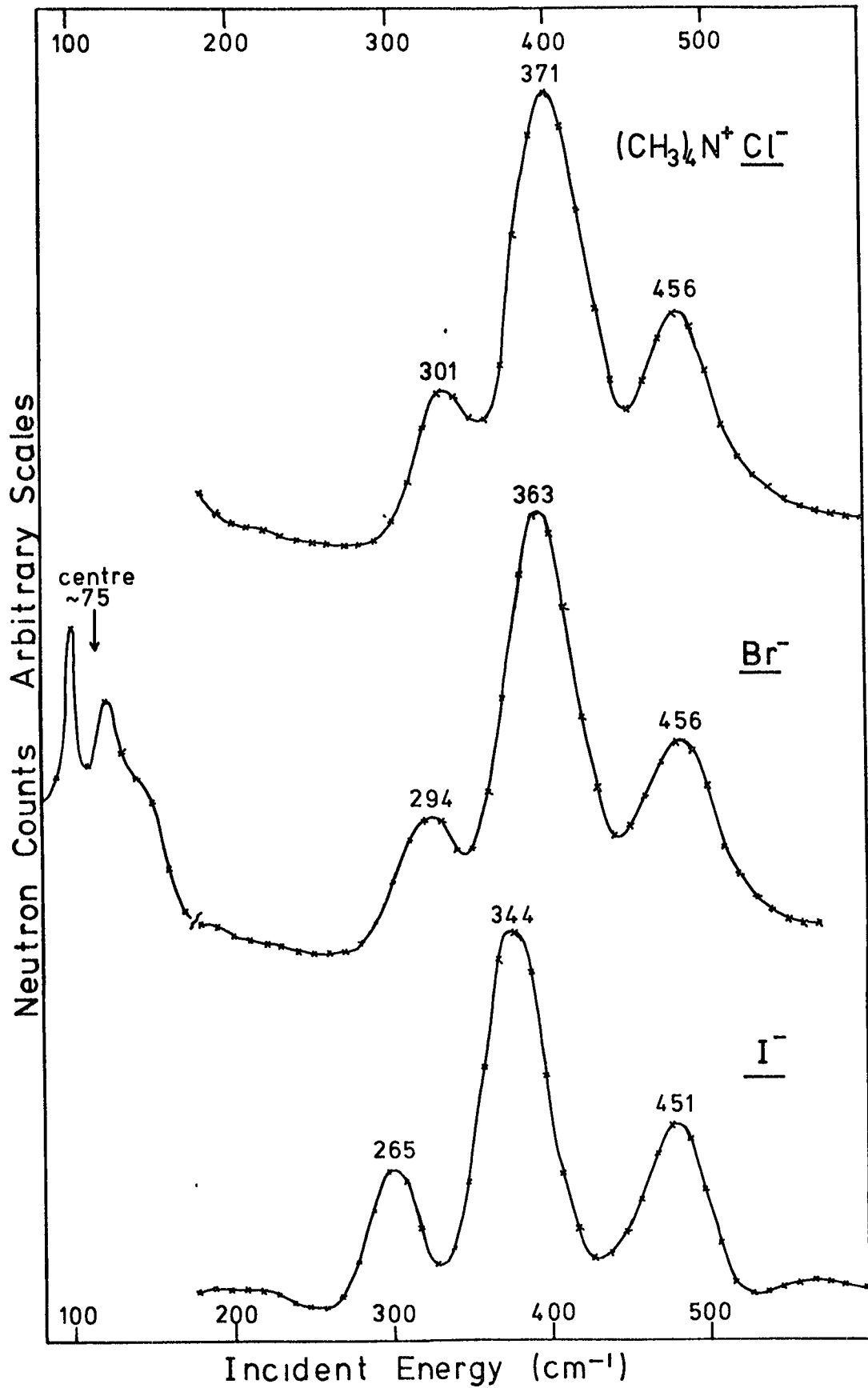


Table (7.2) Spectroscopic frequencies of the  $(\text{CH}_3)_4\text{N}^+$  Halides ( $\text{cm}^{-1}$ )

$\text{X}^-$	I.R. *	Raman †	I.N.S. (Be-filter)	Assignment
$\text{Cl}^-$	{ 473 v.w { 456 w  378 v.vw  111 vs 79 vs	455 mw  372 w	456 m.s  371 v.s  301 m.w	} $\nu_{19}(\text{F}_2) \delta \text{NC}_4$ { + $\nu_8(\text{E}) \delta \text{NC}_4$ { $\nu_{12}(\text{F}_1)$ Torsion $\nu_4(\text{A}_2)$ Torsion } Librations } Translations
$\text{Br}^-$	{ 471 vw { 455 w  361 vvw  103 vs 75 vs	462 m 455 m 385 w  109 w 78 w { 62 m.s { + sh.	456 m.s  363 v.s  294 m.w	} $\nu_{19}(\text{F}_2) \delta \text{NC}_4$ } $\nu_8(\text{E}) \delta \text{NC}_4$ } $\nu_{12}(\text{F}_1)$ Torsion } $\nu_4(\text{A}_2)$ Torsion } Librations } + Translations
$\text{I}^-$	{ 475 vw { 453 w  341 vvw  91 vs 74 vs	{ 466 m { 456 m 381 vw  120 w 100 mw 60 mw 43 w	451 m.s  344 v.s  265 m.w  { 94 } ‡ { 83 } broad band ~ 75 → 105	} $\nu_{19}(\text{F}_2) \delta \text{NC}_4$ } $\nu_8(\text{E}) \delta \text{NC}_4$ } $\nu_{12}(\text{F}_1)$ Torsion } $\nu_4(\text{A}_2)$ Torsion } Librations and } Translations

\* I.R. data of Bottger + Geddes (16)

† Raman data  $\text{Cl}^-$  Edsall (17)  
 $\text{Br}^-$  Present study  
 $\text{I}^-$  Krishnamurthy (25)

‡ 6H time-of-flight data (295°K)

similar pattern. The two lower frequencies however decrease

Cl  $\rightarrow$  Br  $\rightarrow$  I.

Two internal modes other than the torsions in this region have been characterised as  $\nu_8$  (E)  $\delta$  NC<sub>4</sub> and  $\nu_{19}$  (F<sub>2</sub>)  $\delta$  NC<sub>4</sub>.  $\nu_{19}$  does not appear to change much from salt to salt at  $\sim 455\text{cm}^{-1}$  in the I.R. and Raman. The reported Raman of the iodide (25) places  $\nu_8$  at  $\sim 380\text{cm}^{-1}$ . The Raman spectrum obtained in the present study of the bromide showed a corresponding weak peak at  $385\text{cm}^{-1}$ . Bottger and Gedes (16) did not see these frequencies in their I.R. work, but saw very weak peaks at 378, 361 and  $341\text{cm}^{-1}$  for Cl<sup>-</sup>, Br<sup>-</sup> and I<sup>-</sup> salts respectively, which they assigned as  $\nu_8$ . However on consideration of the I.N.S. spectra it would seem more probable that they saw the  $\nu_{12}$  (F<sub>1</sub>) torsional mode, and that  $\nu_8$  as seen in the Raman appears  $\sim 385\text{cm}^{-1}$ . The beryllium filter spectrum frequencies are summarised as:-

Cl	301	371	456	
Br	294	363	456	(cm <sup>-1</sup> )
I	265	344	451	
	(m)	(v.s)	(m.s)	

The  $\nu_{19}$  (F<sub>2</sub>)  $\delta$  NC<sub>4</sub> mode shows up fairly strongly as did the equivalent mode in (CH<sub>3</sub>)<sub>4</sub>C, and correlates well with the optical frequency. The two lower modes by analogy with (CH<sub>3</sub>)<sub>4</sub>C and on the basis of intensity must be assigned as the torsional modes  $\nu_4$ (A<sub>2</sub>) and  $\nu_{12}$  (F<sub>1</sub>), where  $\nu_{12}$  is the higher frequency. Their intensity ratio

is as expected 1:3, and the higher frequency corresponds fairly well with the I.R. peaks of ref (16). Raman work on  $(\text{CH}_3)_4\text{N}^+\text{MnCl}_3^-$  and  $\text{CdCl}_3^-$  by Peercy and Morosin (37) has shown the lower torsional mode at 252 and  $248\text{cm}^{-1}$  respectively, and White et al (38) have also reported the I.N.S. 6H time-of-flight spectrum of the  $\text{MnCl}_3^-$  salt which shows this frequency.

The  $\nu_8(\text{E}) \delta \text{NC}_4$  band in the I.N.S. must lie in each case under the strongest torsional band on its higher frequency side, but clearly is not very strong since the main peaks do not have any shoulders, although the iodide shows a slight broadening at its base to higher frequencies.

Attention should now be drawn to the fact that the two higher frequency I.N.S. peaks and possibly the lower one show broadening, summarised in table (7.3).

Table 7.3 Full Width at Half Maximum ( $\text{cm}^{-1}$ )

Anion	$\nu_4$	$\nu_{12}$	$\nu_{19}$
$\text{Cl}^-$	43	58	~ 58
$\text{Br}^-$	44	56	~ 56
$\text{I}^-$	40	48	50

This may in part be due to crystal splittings, but also to the effect of the external field: If the  $\text{C-H}\cdots\text{X}^-$  bonding only

affects one of the methyl protons some assymetry of the system may result, and slightly affect the shape of the torsional potential.

Barrier calculations appear in Section 4.

b) The  $(\text{CH}_3)_3\text{NH}^+$  salts.

The frequencies of this ion are labelled with symmetry species assuming a  $C_{3v}$  molecular point group. Frequencies are given in table 7.4.

Having observed the rotor coupling effect in the  $(\text{CH}_3)_4\text{N}^+$  salts, one might expect a 1:2 torsional peak ratio to be seen in the I.N.S. spectra of the  $(\text{CH}_3)_3\text{NH}^+$  salts, although odd effects due to the presence of a strong N-H--X<sup>-</sup> bond might also appear.

Beryllium filter spectra are shown in fig. (7.6). That of the chloride shows peaks at 249 and  $294\text{cm}^{-1}$  with a 1:2 intensity ratio the higher frequency being the strongest peak in the whole spectrum. No optical modes have been observed at these frequencies and the lowest internal modes, other than the torsions can be seen at 398 and  $466\text{cm}^{-1}$ . These are assigned as  $\nu_{23}(\text{E})\delta \text{NC}_3$  and  $\nu_8(\text{A}_1)\delta \text{NC}_3$  respectively. Hence it needs little argument to assign  $249\text{cm}^{-1}$  as the  $\nu_{12}(\text{A}_2)$  torsion and  $294\text{cm}^{-1}$  as the  $\nu_{24}(\text{E})$  torsion.

The beryllium filter spectra of the bromide and iodide are similar to each other but show a marked difference from that of the chloride, which must be as a consequence of the structural difference. The assignments follow along the same lines; the  $\nu_{23}(\text{E})$  and  $\nu_8(\text{A}_1)\delta \text{NC}_3$  modes (which have optical counterparts) have not changed

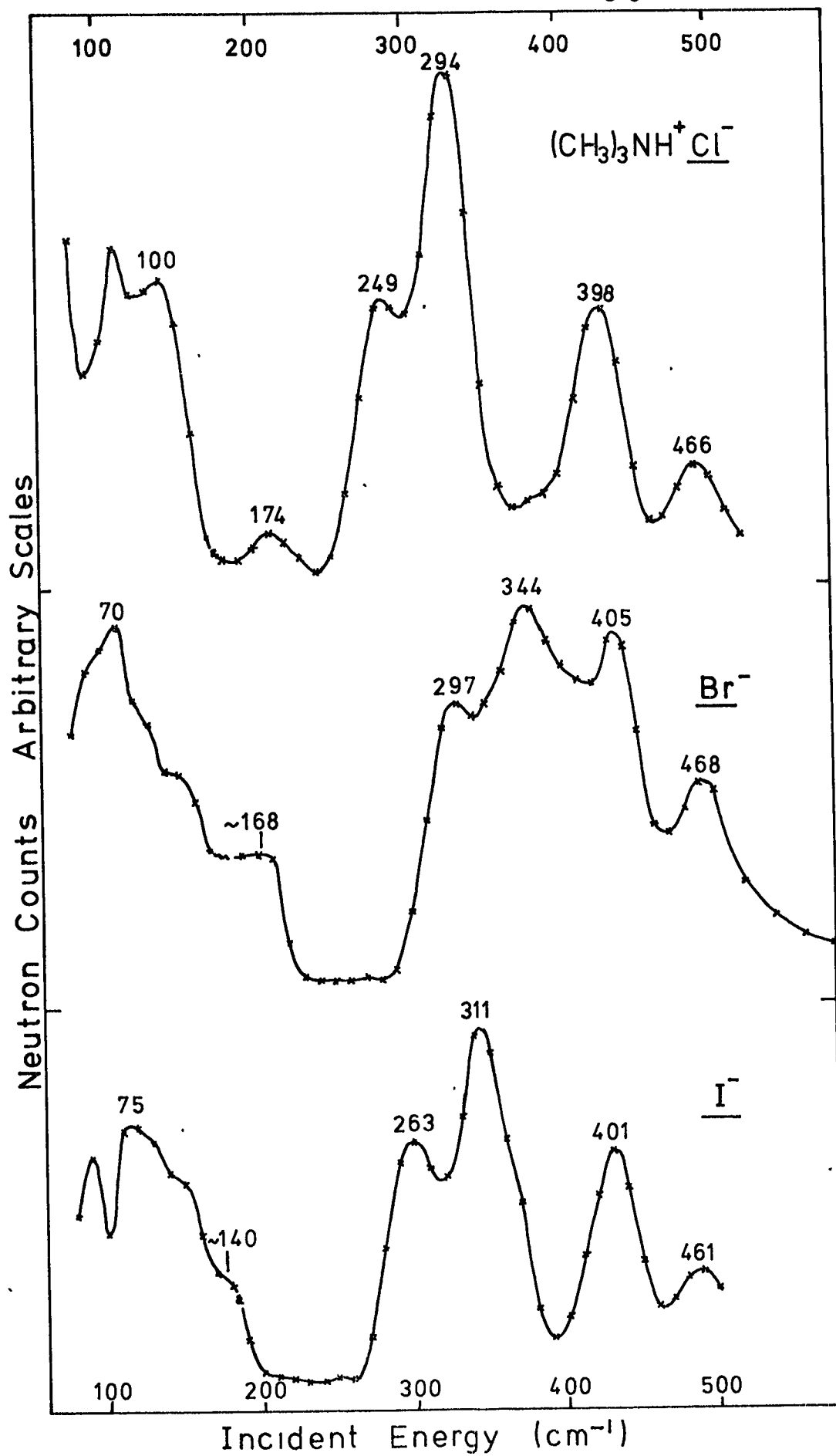
Fig. (7.6) Beryllium filter spectra of the  $(\text{CH}_3)_3\text{NH}^+$  salts.



Table (7.4) Spectroscopic frequencies of the  $(\text{CH}_3)_3\text{NH}^+$  Halides ( $\text{cm}^{-1}$ )

$\text{X}^-$	I.R. Nujol Mull	Raman Solid	I.N.S.		Assignment	
			T. of F. 295°K	Be-filter		
$\text{Cl}^-$	470 m.w	468 m		466 w	$\nu_8 (\text{A}_1)$ } $\delta \text{NC}_3$	
	409 w	{ 409 m.w 404 w.sh		398 m	$\nu_{23} (\text{E})$ }	
				294 s	$\nu_{24} (\text{E})$ }	
				249 m	$\nu_{12} (\text{A}_2)$ } Torsions	
	193 s	188 v.w		174 w		
	119 w					
	~ 72 w	101 w		~ 100 ~ 70	librations } Lattice Modes	
		61 m				
		49 s				
$\text{Br}^-$	467 v.w	471 m		468 m	$\nu_8 (\text{A}_1)$ } $\delta \text{NC}_3$	
		{ 415 m.w 409 w		405 s	$\nu_{23} (\text{E})$ }	
				344 s	$\nu_{24} (\text{E})$ }	
		321 v.w			? } Torsions	
				297 m.s	$\nu_{12} (\text{A}_2)$ }	
				sh168 m.w		
	142 s	{ 158 w 125 w	~ 140 m			
	79 s	84 w	110 v.s			
	66 m.w	85 v.s				
	53 m	~ 70 m.s				
		45 w.sh				
		43 s				
$\text{I}^-$	461 v.w	468 *		461 w	$\nu_8 (\text{A}_1)$ } $\delta \text{NC}_3$	
		406 *		401 m	$\nu_{23} (\text{E})$ }	
				311 s	$\nu_{24} (\text{E})$ }	
				263 m	$\nu_{12} (\text{A}_2)$ } Torsions	
	126 s		~ 130sh	140 w		
	103 w		105 s			
~ 74 s		80 ms				
		40 w				
					librations } Lattice Modes	

All I.R./Raman values from the present study except  
\* from Edsall (17) which are in solution.

much, appearing at 405 and 468 $\text{cm}^{-1}$  respectively for the bromide and 401 and 461 $\text{cm}^{-1}$  for the iodide. This leaves two bands in both spectra which can again be assigned as the torsional modes. The great contrast with the chloride is that these bands appear at higher frequencies:

Torsions	$A_2$	E	
$\text{Cl}^-$	249	294	
$\text{Br}^-$	297	344	$\text{cm}^{-1}$
$\text{I}^-$	263	311	

Also, whereas the chloride peaks do not show any signs of broadening the higher frequency E torsional mode in the other two salts has considerably broadened, especially in the case of the bromide, at the expense of a loss in height relative to the rest of the spectrum. In the iodide spectrum the peak at 311 $\text{cm}^{-1}$  is well resolved from the 401 $\text{cm}^{-1}$  peak and does in fact show a slight shoulder on the high frequency side.

With respect to the lattice modes at lower frequencies a factor group analysis predicts:-

$$\begin{aligned}
 T_{\text{Acoustic}} &= A_u + B_u \\
 T_{\text{Optic}} &= \underbrace{4A_g + 2B_g}_{\text{Raman}} + \underbrace{A_u + 3B_u}_{\text{I.R.}} \\
 \text{Rotational} &= \underbrace{A_g + 2B_g}_{\text{Raman}} + \underbrace{2A_u + B_u}_{\text{I.R.}}
 \end{aligned}$$

i.e. 9 Raman modes and 7 I.R. modes. The spectra are therefore likely to be quite complex, but the optical spectra obtained clearly do not resolve all the modes. See table (7.4).

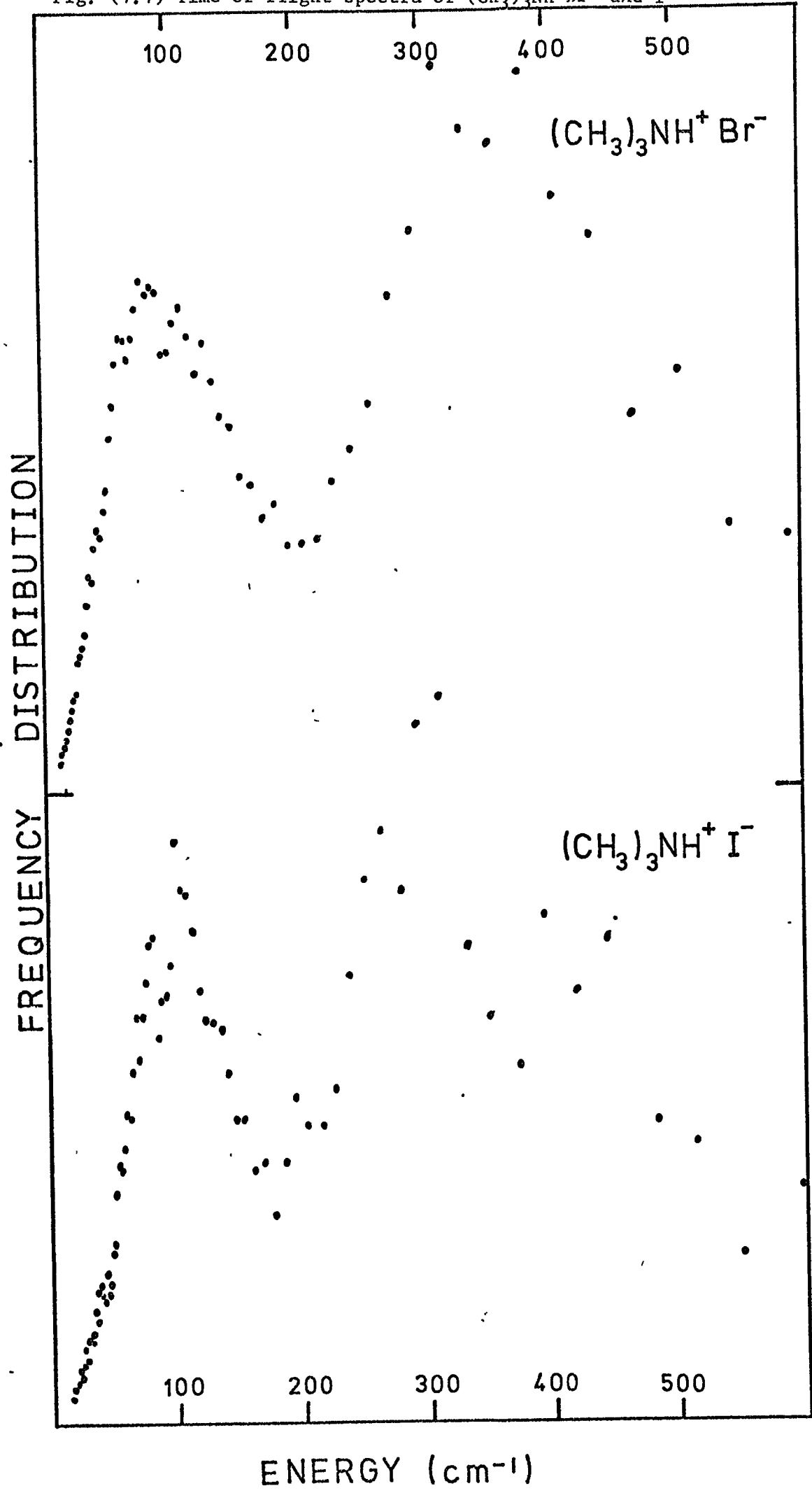
Considering the remaining low frequencies seen in the beryllium filter spectrum of the chloride a very weak peak occurs at  $174\text{cm}^{-1}$  which may correspond with the I.R./Raman band seen at 193(s) and  $188(\text{w})\text{cm}^{-1}$  respectively. This I.N.S. band might also correspond to the overtone of a moderately strong broad band centred at  $\sim 88\text{cm}^{-1}$  with peaks at  $\sim 70$  and  $100\text{cm}^{-1}$ , which must be assigned as the librational modes if similar arguments about intensity are used as before.

The remainder of the beryllium filter spectra of the bromide and iodide also show a strong broad band in the region of  $\sim 70 - 90\text{cm}^{-1}$ , the bromide also showing a well defined weak shoulder at  $\sim 168\text{cm}^{-1}$ . Assuming no phase change the time-of-flight spectra obtained for these two salts should show greater resolution, although transitions other than  $1 \rightarrow 0$ , due to thermal population of higher levels, may broaden the bands a little. The frequency distribution graphs (fig. 7.7) show a very strong broad band in the region of the torsional modes which does show some resolution in the case of the iodide, and at lower frequencies a fairly strong broad band about  $100\text{cm}^{-1}$  wide appears, on which several peaks can be seen. Both salts show two main peaks at

$\text{Br}^-$	85	110	$\text{cm}^{-1}$
$\text{I}^-$	80	105	

which again purely on the basis of intensity will tentatively be assigned as the librational modes. Disregarding site group splittings as small, one would expect an A and an E librational mode for a  $C_3$

Fig. (7.7) Time-of-flight spectra of  $(\text{CH}_3)_3\text{NH}^+ \text{Br}^-$  and  $\text{I}^-$



molecule and hence a 1:2 I.N.S. intensity ratio, whereas the two assigned peaks appear to have about the same intensity. However this might be explained by different proton amplitudes for the two modes, since for the motions around the x, and y axes (E) the methyl protons are nearer the axis than for the z axis (see fig. 7.10), and hence are likely to execute smaller movements in the oscillation.

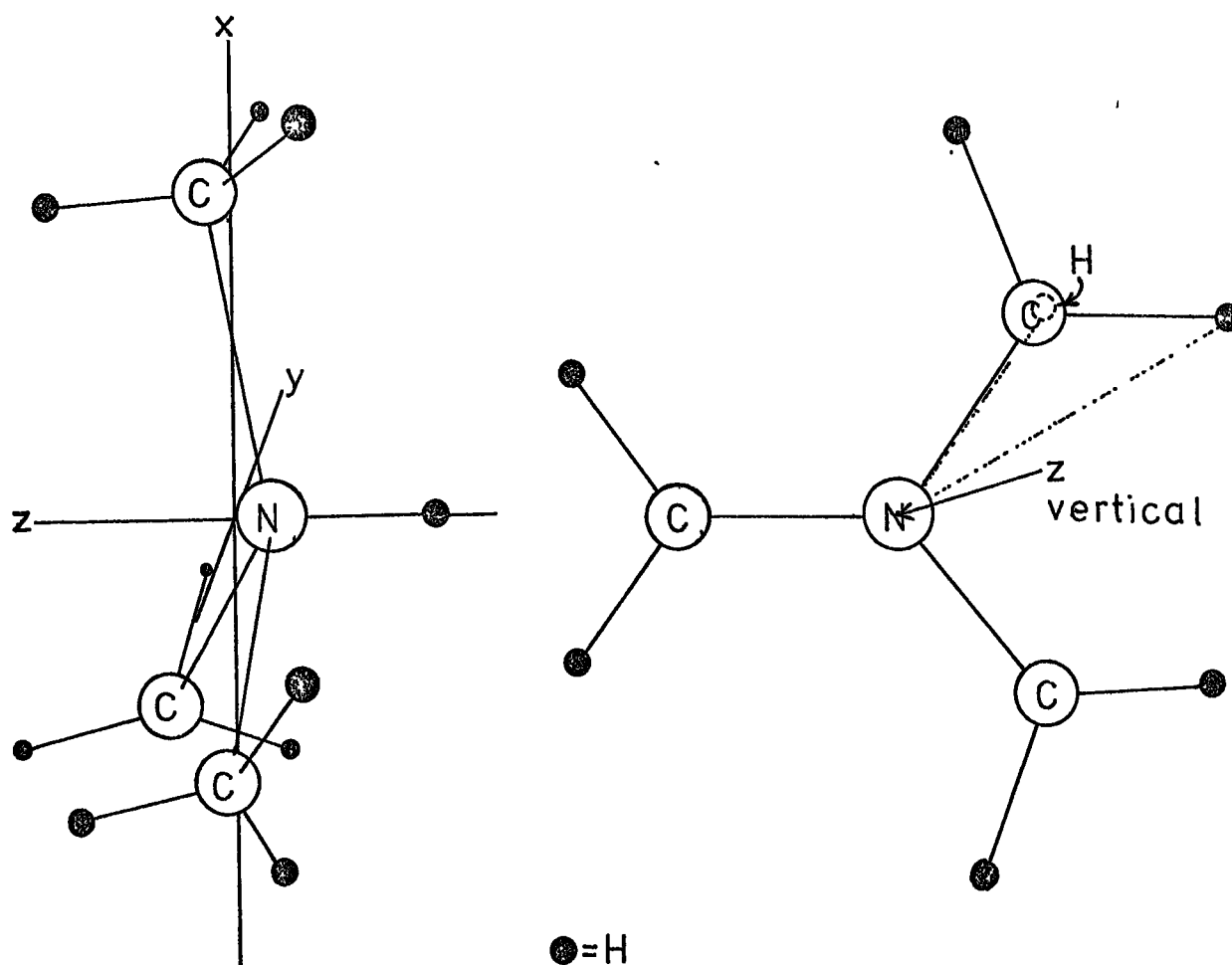


Fig. (7.10)

c) The  $(\text{CH}_3)_2\text{NH}_2^+$  salts.

The symmetry labelling used for the frequencies of this ion assumes a  $C_{2v}$  molecular point group. Frequencies are given in table(7.5).

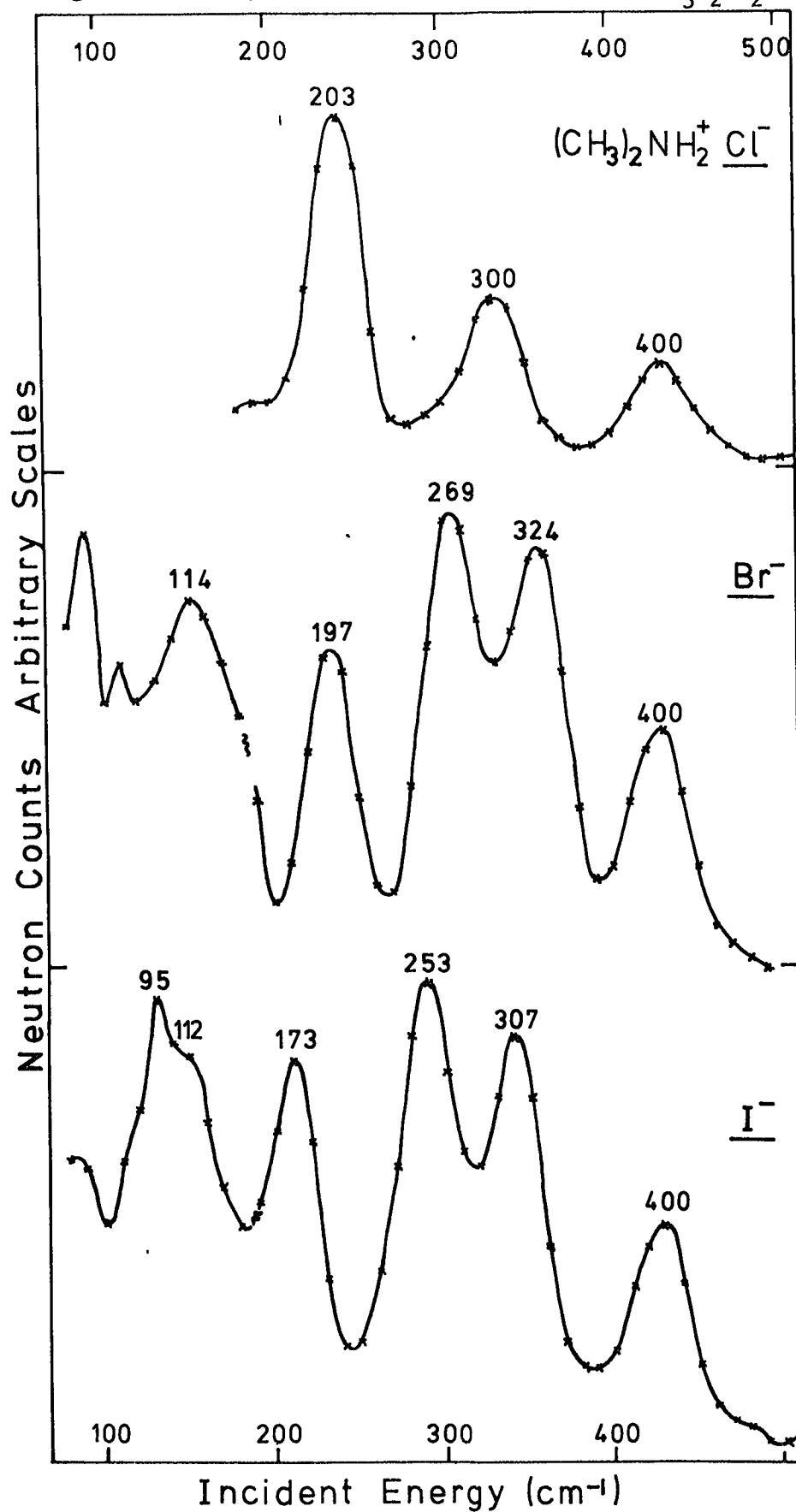
Fig. (7.8) Beryllium filter spectra of the  $(\text{CH}_3)_2\text{NH}_2^+$  salts.

Table (7.5) Spectroscopic frequencies of the  $(\text{CH}_3)_2\text{NH}_2^+$  Halides ( $\text{cm}^{-1}$ )

$\text{X}^-$	I.R. * Nujol Mull	Raman Solid	I.N.S.		Assignment	
			T. of F. †	Be-filter *		
$\text{Cl}^-$	402 w	{409 m.w 404 w.sh	~ 200 v.s	400 m.w	$\nu_9 (A_1) \delta \text{NC}_2$	
	304 m	295 v.w.brd		300 m	{ $\nu_{27} (B_2), \nu_{14} (A_2)$ Torsions + x axis ( $B_2$ ) Libration	
	209 s			203 v.s		
	170 m	167 v.w.brd		{ 110 v.s { 75 sh } broad band centred ~ 95		} y, z librations + translational modes
	115 w	110 w				
	97	94 w.sh				
		79 m				
		62 ms				
	47 s					
	30 w					
$\text{Br}^-$	~ 402 v.w	421 m.w	} broad band centered ~ 120 { 125 s { 70 m.s } 52 m 30 w	400 m	$\nu_9 (A_1) \delta \text{NC}_2$	
	~ 327 w	315 v.v.w		324 s	{ $\nu_{27} (B_2), \nu_{14} (A_2)$ Torsions	
	212 v.s			269 s		
	{145 sh			197 m.s	x axis ( $B_2$ ) libration	
	{126 m	136 m		114 m.s	y, z librations	
	{119 m.sh				+ translational modes	
	79 m	{ + sh				
	52 m	66 v.s				
		43 w.sh				
		26 v.s				
$\text{I}^-$	~ 405 v.w	408 w	} broad band centred ~ 110 { 125 m { 105 s { 90 sh { 55 m.sh { 28 w	400 m	$\nu_9 (A_1) \delta \text{NC}_2$	
	325 v.w	~ 300 v.w.brd		307 s	{ $\nu_{27} (B_2), \nu_{14} (A_2)$ Torsions	
	187 s			253 s		
				173 m.s	x axis ( $B_2$ ) libration	
	{117 m.s	117 s		~ 95 s	y, z librations	
	{104 m				+ translational modes	
		75 m				
		broad strong band				

\* = at liquid nitrogen temperatures

† = at room temperature.

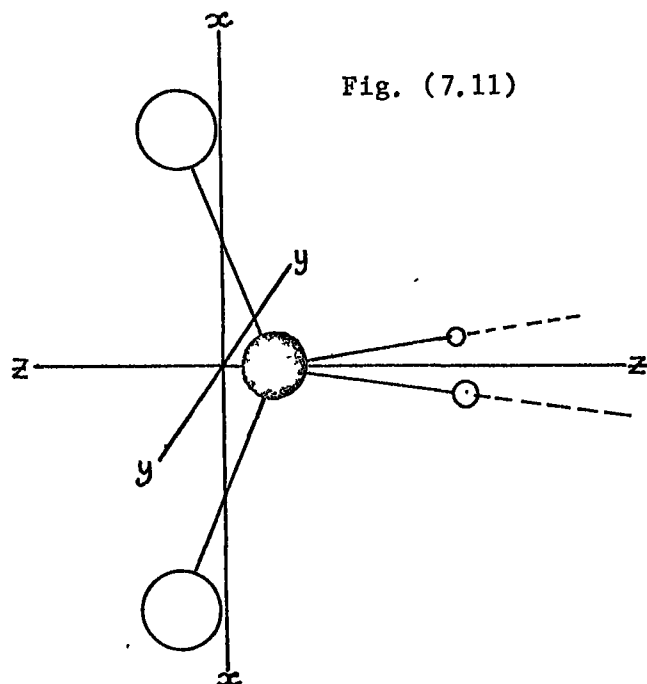
The I.N.S. spectra of these compounds again show a contrast between the chloride and the bromide and iodide (fig. 7.8 ). Following the splitting pattern seen for the carbon series and the fact that the  $(\text{CH}_3)_4\text{N}^+$  and  $(\text{CH}_3)_3\text{NH}^+$  systems give larger splittings than their carbon counterparts, one would expect to see two equally intense torsional peaks.

The beryllium filter spectra of all three salts show the low lying internal mode  $\nu_9$  ( $A_1$ )  $\delta$   $\text{NC}_2$  at  $400 \text{ cm}^{-1}$ , which is observed in the optical spectra in the same region. The bromide and iodide then also show three other strong peaks but the chloride only two:-

Cl	203 v.s		300 m
Br	197 m.s	269 s	324 s
I	173 s	253 s	307 s

The two higher peaks in the bromide and iodide spectra may be assigned as the torsional modes  $\nu_{14}$  ( $A_2$ ) and  $\nu_{27}$  ( $B_2$ ) as they lie closest together and are of similar intensity. Which way round these two should be assigned is discussed shortly. The remaining strong lower peak is at first puzzling, but a calculation of the overall rotational moments of inertia shows that one is comparatively small and hence might be expected to give a higher librational frequency than the other two, see fig. (7.11 ). So the band is probably the x axis libration, of  $B_2$  symmetry under the  $C_{2v}$  molecular point group. Since this mode will have a strong dependence on the strength of two  $\text{N-H}\cdots\text{X}^-$  bonds, one would expect the chloride to show it at even higher frequency. This points to the I.N.S. band at





$$\begin{aligned}
 & \text{(a.m.u. \AA}^2\text{)} \\
 I_x &= 16.62 \\
 I_y &= 62.54 \\
 I_z &= 54.92
 \end{aligned}$$

$203 \text{ cm}^{-1}$  since  $300 \text{ cm}^{-1}$  would seem much too drastic an increase considering that the ratio of the hydrogen bond energies found for the hydrazinium chloride and bromide is only  $\sim 11:9$ .

This leaves only the band at  $300 \text{ cm}^{-1}$  for the chloride, although two torsional frequencies are expected. A consideration of the peak intensities would suggest that the  $203 \text{ cm}^{-1}$  peak also comprises of the lower torsional frequency. Comparing the relative peak heights in the chloride and bromide spectra one sees that if the peaks corresponding to the x axis libration and the lower torsion in the bromide were to merge the pattern and resultant intensities would be similar to the chloride:-

Relative Intensities (frequency of band involved in brackets in  $\text{cm}^{-1}$ )

Cl	<u>20</u> (203)	<u>9</u> (300)
Br	<u>8</u> (197) <u>12</u> (269)	<u>11</u> (324)

The surprising aspect of this assignment is that it places the torsions at a very wide separation and yet this is the only reasonable way one can explain the disappearance of a peak. This large splitting is discussed shortly, after a consideration of the mode symmetries.

It is clear that the chloride salt torsional frequencies are again lower than for the bromide and iodide, implying that they have different structures.

Further confirmation of these assignments and the determination of the torsional mode symmetry labelling can be made by comparing the I.N.S. spectra with optical bands. The  $B_2$  torsional band should be both I.R. and Raman active, whereas the  $A_2$  band should only be Raman active, (based on  $C_{2v}$  symmetry). In fact the higher I.N.S. peaks at 300, 324 and 307  $\text{cm}^{-1}$  for chloride, bromide and iodide respectively all have counterparts in the I.R. and Raman, but the I.N.S. bands at 269 and 253  $\text{cm}^{-1}$  for the bromide and iodide respectively do not have any optical counterparts. This evidence is strongly in favour of placing the  $\nu_{27}$  ( $B_2$ ) torsion as the higher frequency and  $\nu_{14}$  ( $A_2$ ) as the lower. The x axis libration ( $B_2$ ) should also be I.R. and Raman active. I.R. peaks do appear at 209, 212 and 187  $\text{cm}^{-1}$  for the chloride, bromide and iodide respectively, slightly higher than the I.N.S. frequencies, but nothing appears in the Raman. (The absence of Raman frequencies does not imply any incorrect assignment since all the symmetry species of  $C_{2v}$  should be Raman active. The missing peaks are probably just too weak).

Returning to the bands at 203 and 300  $\text{cm}^{-1}$  in the chloride; it is now clear that the two modes involved in the 203  $\text{cm}^{-1}$  band are of  $A_2$  and  $B_2$  symmetry and therefore cannot mix, and must constitute an accidental degeneracy. (The band width F.W.H.M. is only 40  $\text{cm}^{-1}$  so the frequencies must be nearly identical).

The fact that the x axis libration and the higher frequency torsion are both  $B_2$  modes may also help to explain the large splitting between

the  $A_2$  and  $B_2$  torsions. It is quite possible for two modes of the same symmetry species to perturb each other's energy levels. Two modes which might have been expected to have about the same frequency (unperturbed) interact and 'repel' each other appearing further apart (Fermi resonance (40)). The  $B_2$  torsional mode frequency may have been raised and the  $B_2$  x-axis libration lowered.

Assuming that the same bands in the bromide and iodide represent unperturbed frequencies the x-axis libration frequency shows a trend of increasing frequency which is probably related to the strength of the two H-bonds. The chloride frequency might therefore be expected to be somewhat higher than the  $203 \text{ cm}^{-1}$  observed which is only  $6 \text{ cm}^{-1}$  higher than for the bromide, whereas bromide and iodide show a  $24 \text{ cm}^{-1}$  difference. (This argument loses a little strength when it is considered that the structures are most probably different).

It has been seen in the  $(\text{CH}_3)_4\text{N}^+$  and  $(\text{CH}_3)_3\text{NH}^+$  salts that the splitting between the torsional frequencies was fairly consistent:-

Table (7.6) Torsional Band Splittings in the multi-methylammonium salts ( $\text{cm}^{-1}$ )

	$\text{Cl}^-$	$\text{Br}^-$	$\text{I}^-$
$(\text{CH}_3)_4\text{N}^+$	70	69	79
$(\text{CH}_3)_3\text{NH}^+$	45	47	48
$(\text{CH}_3)_2\text{NH}_2^+$	(97)	55	54

This would indicate that the unperturbed splitting for  $(\text{CH}_3)_2\text{NH}_2^+\text{Cl}^-$  ought to be  $\sim 55 \text{ cm}^{-1}$ , i.e. the unperturbed higher torsional frequency should be at about  $203 + 55 \rightarrow 258 \text{ cm}^{-1}$ . This is  $42 \text{ cm}^{-1}$  below the observed frequency. Assuming now that the observed, perturbed x-axis

libration is  $42 \text{ cm}^{-1}$  below its unperturbed value places this at  $\sim 245 \text{ cm}^{-1}$ , i.e. the two unperturbed  $B_2$  mode frequencies would be only  $\sim 13 \text{ cm}^{-1}$  apart.

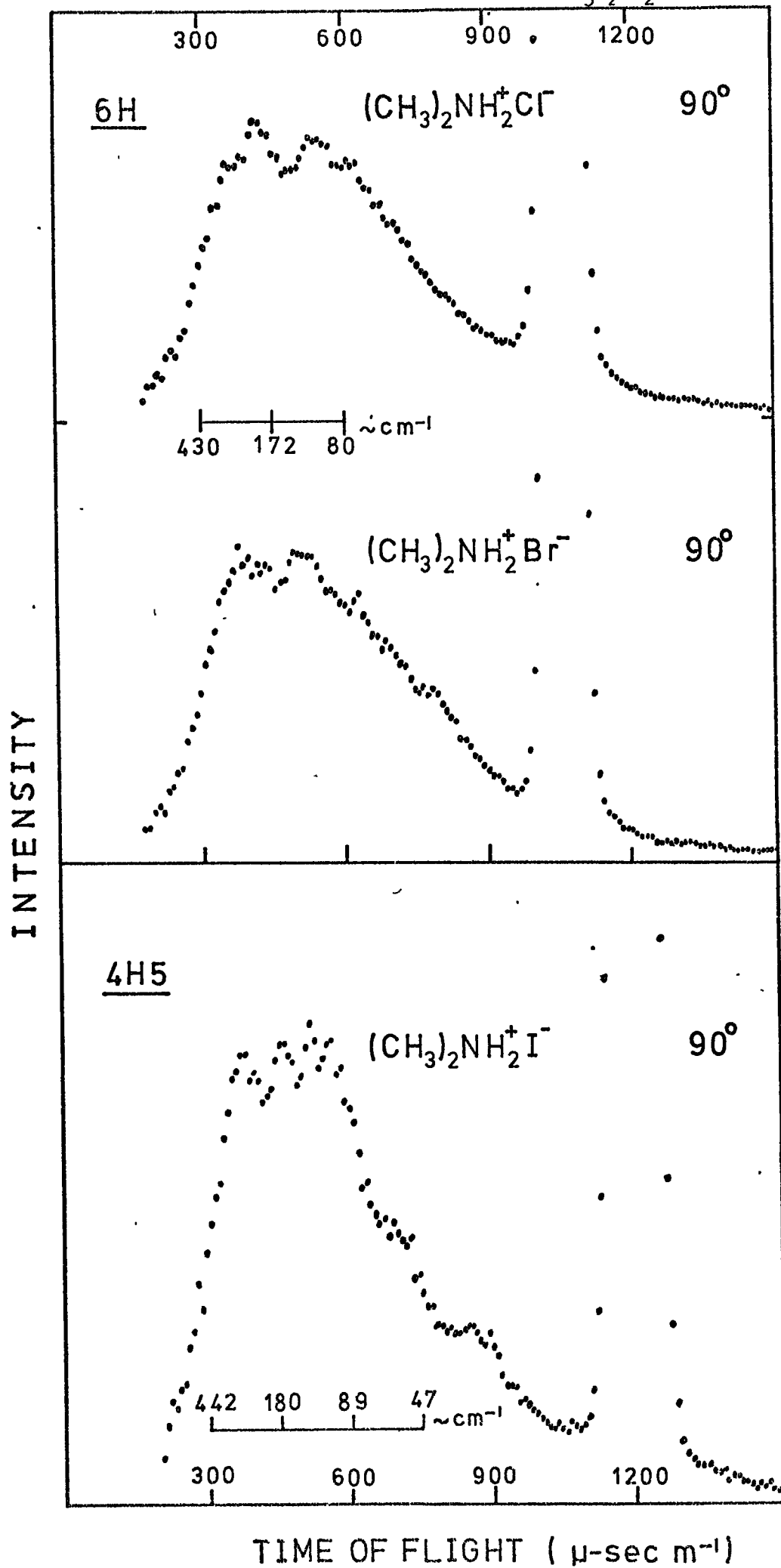
Looking now in more detail at the low frequency region of the I.N.S. spectra the libration already assigned is not broadened, from which it may be deduced that its site group splitting is small. Hence one might expect to see only two further bands for the y and z axis librations, and since their moments of inertia are similar their frequencies may also be close.

The cold temperature Aluminium 111 plane beryllium filter spectrum of the bromide and iodide show broad bands centred at  $\sim 114$  and  $100 \text{ cm}^{-1}$  respectively, which are slightly more intense than the x-axis librational band.

For a more resolved picture of this region one must now look at the time of flight room temperature spectra which, as pointed out earlier, do not appear to be very different to the cold phase. The factor group analysis for the lattice modes of the room temperature chloride is as follows:-

$$\begin{aligned}
 T_{\text{ACOUSTIC}} &= B_{1u} + B_{2u} + B_{3u} \\
 T_{\text{OPTIC}} &= \underbrace{4A_g + 4B_{1g} + 2B_{2g} + 2B_{3g}}_{\text{Raman}} + 2A_u + \underbrace{B_{1u} + 3B_{2u} + 3B_{3u}}_{\text{I.R.}} \\
 \text{ROTATIONAL (librations)} &= \underbrace{A_g + B_g + 2B_{2g} + 2B_{3g}}_{\text{Raman}} + 2A_u + \underbrace{2B_{1u} + B_{2u} + B_{3u}}_{\text{I.R.}}
 \end{aligned}$$

This predicts a multitude of bands, and in fact the I.R. and Raman spectra are quite complicated in this region. If as suggested above however the factor group splittings for the librations are small one



TIME OF FLIGHT ( $\mu\text{-sec m}^{-1}$ )

might expect to see only two bands in the I.N.S. spectra and possibly only one if they are similar in frequency. Looking at the time-of-flight spectra one would therefore tend to place the y and z librations in the strong fairly broad band which occurs, centred at  $\sim 95, 120$  and  $110 \text{ cm}^{-1}$  for the chloride, bromide and iodide respectively. Although these show finer structure on top, one would feel that a much more detailed study would be necessary to attempt a complete assignment. All three spectra show weaker bands appearing as shoulders to lower frequency which may be assigned to lattice modes.

#### Section 4. Barrier Calculations.

As pointed out at the beginning of the chapter the complexity of the situation in these salts inhibits a simple but rigorous treatment of barriers but a crude approach to interpretation can give useful information.

In all cases the S.H. treatments summarised in Chapter 1, Section (4) have first been applied on the two torsional frequencies to obtain barriers to rotation of the methyl groups and the top-top interaction terms. (Weighted averages of the barriers determined from each frequency via Mathieu eigenvalues have again also been calculated). These figures then provide a basis for discussion and further break-down.

The external librational modes have been treated separately and usually the  $(n^2 \bar{V})$  force constant parameters arising from the S.H. treatment provide most insight.

a) Moments of Inertia.

Moments of inertia were calculated from first principles using the little, available structural data. The standard methyl group geometry used throughout the thesis was again assumed, and in the cases of  $(\text{CH}_3)_4\text{N}^+$  and  $(\text{CH}_3)_3\text{NH}^+$  angles at the nitrogen were taken as tetrahedral. For  $(\text{CH}_3)_2\text{NH}_2^+$  the angle found in the X-ray structure of the chloride for C-N-C was used and the angle between the C-N-C plane and the H-N-H plane was assumed to be  $90^\circ$ . The H-N-H angle in this case was taken to be  $103^\circ$ , the same as the Cl---N---Cl angle. (Any error involved here should not be great since it involves only light atoms). The N-H bond length was taken as  $1.04 \text{ \AA}$  and C-N as  $1.46 \text{ \AA}$  for the general case. A calculation for  $(\text{CH}_3)_4\text{N}^+$  was also done assuming C-N =  $1.47 \text{ \AA}$  and found to produce a slight increase in the overall moment of inertia; however the effect of this on the reduced moment of inertia for methyl rotation was found to be very small indeed. The resulting overall moments of inertia are summarised in table (7.7) below. As before, for  $(\text{CH}_3)_2\text{NH}_2^+$  the z axis is the symmetry axis and the x axis is in the C-N-C plane. For  $(\text{CH}_3)_3\text{NH}^+$  the z axis ( $C_3$ ) is taken along the N-H bond, x and y being degenerate, as are all three axes for  $(\text{CH}_3)_4\text{N}^+$ .

Table (7.7)

Type	Overall Moment of Inertia (a.m.u. $\text{\AA}^2$ )
$(\text{CH}_3)_2\text{NH}_2^+$	$I_x = 16.62$ $I_y = 62.54$ $I_z = 54.95$
$(\text{CH}_3)_3\text{NH}^+$	$I_{x,y} = 54.86$ $I_z = 100.16$
$(\text{CH}_3)_4\text{N}^+$	$I = 103.38$ (C-N = $1.46 \text{ \AA}$ ) $I = 104.60$ (C-N = $1.47 \text{ \AA}$ )

These figures do tend to emphasise the unique small value of the x axis moment of inertia for  $(\text{CH}_3)_2\text{NH}_2^+$ .

b) Barriers to methyl rotation.

Table (7.8) gives the results of straightforward methyl torsion S.H. calculations and the weighted average Mathieu solution. The torsional frequencies observed, reduced moments of inertia and the F parameters derived from this are also included. It can be seen that using the estimated unperturbed frequency for the  $B_2$  mode of  $(\text{CH}_3)_2\text{NH}_2^+\text{Cl}^-$  the barrier is decreased, but also the interaction term reduces to a value more compatible with that of the bromide and iodide.

c) Whole body librations.

(i) Considering first the  $(\text{CH}_3)_4\text{N}^+$  salts, Gutowsky's N.M.R. results (5) for the methyl torsional barriers agree reasonably with the newly derived figures. (This is discussed in Section (5) see Table (7.12)).

Hence if one assumes the external barriers which he also obtained are equivalently good these can usefully be employed: Dufourcq and Lemenceau (31) used their external barrier N.M.R. values for the  $(\text{CH}_3)_4\text{N}^+$  salts in the simple harmonic equation,

$$\bar{\nu}_{\text{calc}}^2 = \frac{h}{8\pi^2 cI} \cdot n^2 \bar{V}$$

where  $\bar{V}$  was taken as  $E_a$ , to calculate possible librational frequencies for  $n = 3$  and  $n = 4$ . These calculated frequencies were found to lie reasonably close to the two low I.R. peaks which Bottger and Gedes (16) reported. If the same treatment is applied to Gutowsky's external barrier results (5) the correspondence is even better.



Table (7.8) Barrier calculations ( $\text{cm}^{-1}$ ) \* = estimated unperturbed value.  
K and L are used as defined in Chapter 1.

Cation	$I_{\text{red}}$ a.m.u. $\text{\AA}$	F ( $\text{cm}^{-1}$ )	Anion	Torsion $\nu$ 's ( $\text{cm}^{-1}$ )	S. H. Parameters		Mathieu Parameters	
					$2K/9$ ( $\text{cm}^{-1}$ )	$2L/9$ ( $\text{cm}^{-1}$ )	Mathieu $\bar{V}_3$ barriers	Weighted Average
$(\text{CH}_3)_4\text{N}^+$	I = 3.09	F = 5.46	$\text{Cl}^-$	A 301	2562	- 239	2009	2750
				F 371			2998	
			$\text{Br}^-$	A 294	2451	- 231	1916	2629
				F 363			2869	
$(\text{CH}_3)_3\text{NH}^+$	$I_A = 3.19$ $I_E = 2.97$	$F_A = 5.29$ $F_E = 5.68$	$\text{I}^-$	A 265	2163	- 245	1572	2340
				F 344			2592	
			$\text{Cl}^-$	A 249	1561	- 130	1440	1715
				E 294			1853	
$(\text{CH}_3)_2\text{NH}_2^+$	$I_A = 3.09$ $I_B = 2.39$	$F_A = 5.45$ $F_B = 7.06$	$\text{Br}^-$	A 297	2161	- 154	2017	2338
				E 344			2498	
			$\text{I}^-$	A 263	1746	- 146	1599	1905
				E 311			2058	
$(\text{CH}_3)_2\text{NH}_2^+$	$I_A = 3.09$ $I_B = 2.39$	$F_A = 5.45$ $F_B = 7.06$	$\text{Cl}^-$	A 203	1128	- 288	954	1267
				B 300			1581	
			$\text{Br}^-$	A 269	1564	- 88	1625	1726
				B 324			1827	
$(\text{CH}_3)_2\text{NH}_2^+$	$I_A = 3.09$ $I_B = 2.39$	$F_A = 5.45$ $F_B = 7.06$	$\text{I}^-$	A 253	1394	- 89	1447	1550
				B 307			1652	
			$\text{Cl}^-$	A 203	944	- 104	954	1073
				B 258 *			1191	

Table (7.9)

Calculated librational frequencies using Gutowsky's external barrier activation energies ( $\text{cm}^{-1}$ )

$(\text{CH}_3)_4\text{N}^+$	N.M.R. External Ea (5)	n	$\bar{\nu}_{\text{LIB}}$ Calc. from N.M.R.	I.R. $\bar{\nu}_{\text{OBS}}$ (16)
$\text{Cl}^-$	4546	3	82	79
		4	109	111
$\text{Br}^-$	4019	3	77	75
		4	102	103
$\text{I}^-$	3845	3	75	74
		4	100	91

Although this separation is somewhat artificial, in assuming the barrier is the same for a 3- or 4-fold motion if indeed both even occur, the correspondence with the two I.R. frequencies is quite striking. (It should be pointed out that the so called 3-fold potential in this case must be asymmetrical on account of the site group in the crystal). Having estimated the librational frequencies it is interesting to see that the I.N.S. spectrum of the iodide shows that the observed librations are in this same region. Using the two I.N.S. peak frequencies for the iodide at 83 and 94  $\text{cm}^{-1}$  to calculate values for  $(n^2\bar{\nu})$  and hence the possible  $\bar{\nu}_3$  and  $\bar{\nu}_4$  values gives:-

<u>I.N.S. <math>\bar{\nu}_{\text{obs}}</math> (<math>\text{cm}^{-1}</math>)</u>	<u><math>(n^2\bar{\nu})</math></u>	<u><math>(\frac{n^2\bar{\nu}}{9}) = \bar{\nu}_3 (\text{cm}^{-1})</math></u>	<u><math>(\frac{n^2\bar{\nu}}{16}) = \bar{\nu}_4 (\text{cm}^{-1})</math></u>
83	42574	<u>4730</u>	2661
94	54606	6066	<u>3413</u>

This shows that it is quite possible that the lower I.N.S. frequency is compatible with a triply hindered motion and the higher frequency with a 4-fold hindered motion, if both barriers are to have about the same value as the N.M.R. value (Figures underlined).

(ii) For the  $(\text{CH}_3)_3\text{NH}^+$  salts it has already been seen that the chloride is different. For each salt two peaks have been labelled as possible librational modes. There is now also the problem of deciding which frequency belongs to which mode since these have two different moments of inertia. Consequently  $(n^2\bar{V})$  has been calculated for each frequency using each moment of inertia in turn:-

Table (7.10) Possible  $(n^2\bar{V})$  force constants for the librational modes of the  $(\text{CH}_3)_3\text{NH}^+$  salts.

Anion	$\bar{v}_{\text{LIB}}$	$(n^2\bar{V})$ parameter using	
		$I_z$	$I_{x,y}$
$\text{Cl}^-$	70	29127 *	15953
	100	59442	32558 *
$\text{Br}^-$	85	42947 *	23523
	110	71925	39395 *
$\text{I}^-$	80	38043 *	20837
	105	65535	35895 *

It might be sensible to expect the z axis motion to be less hindered than the x,y axes motions since it does not involve any stretching of the hydrogen bond, but at the same time its moment of inertia is twice that of  $I_{x,y}$  indicating that the motion requires more room and hence may experience a greater steric force. Hence all in all

the barriers for the two modes may not be very different. Table (7.10) above shows that the barrier forces are similar when the lower frequency is taken as the z axis mode and the higher one as the x,y axes mode (the values marked with \*). This contrasts with a roughly 3:1 forces ratio if the assignments are reversed, with the z axis mode experiencing greater forces. It is interesting to note that the value of  $n^2\bar{V} = 42574$  obtained for the lower frequency of  $(\text{CH}_3)_4\text{N}^+\text{I}^-$ , which may also be a 3-fold axis motion and hence should be similar to the z axis motion of the  $(\text{CH}_3)_3\text{NH}^+$  ion, compares reasonably with the value of 38043 for the iodide.

There is one large problem involved in interpretation for these and the  $(\text{CH}_3)_2\text{NH}_2^+$  salts following; in that, as with the end-over-end motion of  $\text{CH}_3\text{NH}_3^+$ , the centre of motion may not be quite the same as the centre of mass due to the asymmetry of external forces. The calculation results presented here ignore such effects.

(iii) Fortunately, for the  $(\text{CH}_3)_2\text{NH}_2^+$  salts the x-axis libration has clearly been identified, although the exact frequency for the chloride is in question due to the possible perturbation. The calculated  $(n^2\bar{V})$  parameters using  $I_x = 16.62 \text{ a.m.u. \AA}^2$  are as follows:-

Table (7.11) x-axis Librational mode force constants  $(n^2\bar{V})$ .

Anion	$\bar{v}_x \text{ lib (cm}^{-1}\text{)}$	$(n^2\bar{V})$
$\text{Cl}^-$	(245) *	(59206)
	203	40647
$\text{Br}^-$	197	38279
$\text{I}^-$	173	29520

\* Bracketed figure = suggested unperturbed value.

These values are likely to carry a strong contribution from the two H-bonds. If the force constant contribution for such is calculated using the H-bond parameters derived from the hydrazinium salts (Chapter 3):

	$\bar{\nu}_3 (\text{cm}^{-1})$	$(n^2 \bar{\nu}_3) \times 2/3$	
Cl <sup>-</sup>	3414	20484	Force constants for 2 H-bonds
Br <sup>-</sup>	2871	17226	
I <sup>-</sup>	2181	13086	
	(predicted)		

these can be subtracted from the total (to a crude approximation) to give the contribution from the -CH<sub>3</sub> groups:

	$\bar{\nu}_{x \text{ lib}} (\text{cm}^{-1})$	$(n^2 \bar{\nu} - 2\text{H bonds})$
Cl <sup>-</sup>	(245) *	(30722)
	203	20163
Br <sup>-</sup>	197	21053
I <sup>-</sup>	173	16434

\* = estimated unperturbed frequency

Thus these external forces are slightly larger than the N-H---X<sup>-</sup> bond forces.

Both the y and z librations will also involve motion stretching the two H-bonds and moving the two methyl groups so the forces involved may not be too different to the x-mode. If one performs a calculation using  $(n^2 \bar{\nu})$  derived for the x-axis mode and the y, or z

moment of inertia the following frequencies are obtained:

	$(n^2 \bar{V})^*$	Calculated Frequencies ( $\text{cm}^{-1}$ )	
		<u>y mode</u>	<u>z mode</u>
$\text{Cl}^-$	(59206)	(126)	(135)
	40647	105	112
$\text{Br}^-$	38279	102	108
$\text{I}^-$	29520	89	95

\* values from x-axis libration calculations

These all lie within range of the peaks assigned as possible librations in the room temperature phase I.N.S. spectra.

### Section 5. Discussion.

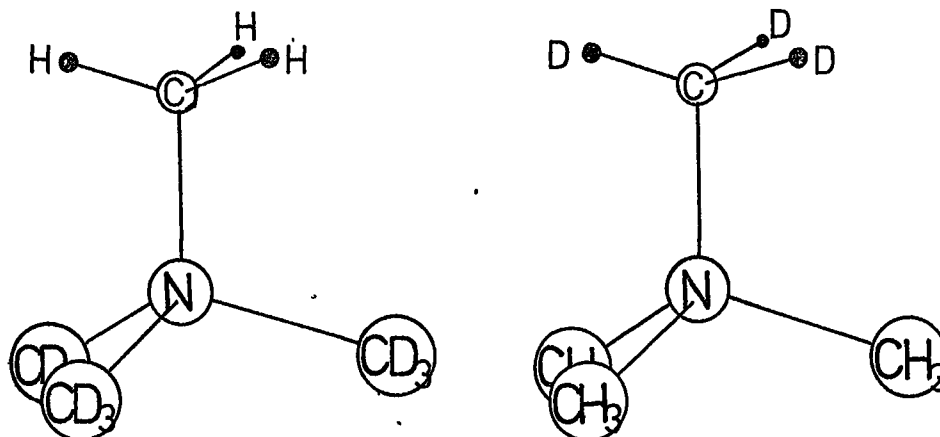
The calculations on the external librations, due to their very crudeness, cannot really form a basis for any detailed discussion, other than what has already been said in the previous section. However what they do demonstrate is that the external interactions with the methyl groups are by no means small. This may in part be due to C-H---X<sup>-</sup> hydrogen bonding although steric repulsion could be rather important in the condensed ionic lattice.

Comparing the CH<sub>3</sub> torsional barrier values for the (CH<sub>3</sub>)<sub>4</sub>N<sup>+</sup> salts with the N.M.R. activation energy data shows a reasonable correspondence as does the data for the two other chloride salts;

Table (7.12) Comparison of N.M.R. and I.N.S. data ( $\text{cm}^{-1}$ )

Ref.	Spectroscopic Barrier		N.M.R.
	S.H.	Mathieu	Activation
(CH <sub>3</sub> ) <sub>4</sub> N <sup>+</sup> (5)	Cl <sup>-</sup>	2562	2377
	Br <sup>-</sup>	2451	2237
	I <sup>-</sup>	2163	1922
(CH <sub>3</sub> ) <sub>3</sub> NH <sup>+</sup> (29)	Cl <sup>-</sup>	1561	1398
(CH <sub>3</sub> ) <sub>2</sub> NH <sub>2</sub> <sup>+</sup> (28)	Cl <sup>-</sup>	1128	1153

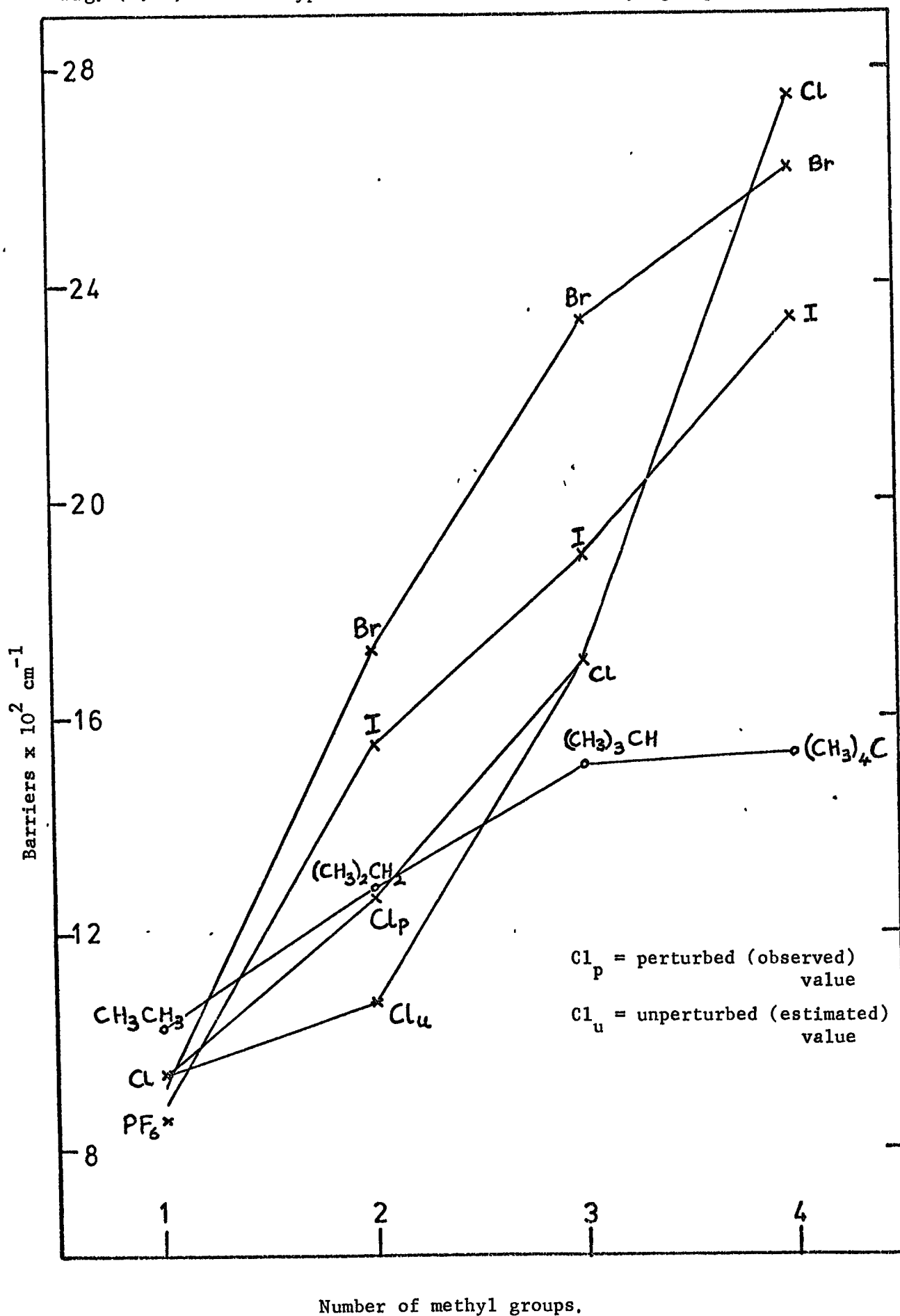
so perhaps the approximation of combining all the hindrances to motion of the  $\text{CH}_3$  groups into one barrier is not too unreasonable. (It would be very interesting to obtain data on



and then treat the data from these and the fully protonated species in a similar manner to the  $\beta\text{-CH}_3\text{NH}_3^+$  salts. This would help take into account effects due to mixing with overall rotation about one C-N axis, which has to be neglected in the present treatment). The barrier obtained in the present calculations would best be described as consisting of two effects i.e.  $(\bar{V}_3)_{\text{TOTAL}} = (\bar{V}_3)_{\text{INTERNAL}} + (\bar{V}_3)_{\text{EXTERNAL}}$ .

Fig. (7.12) shows the change of  $\text{CH}_3$  rotational barrier as the number of methyl groups increases and it is easy to see that the behaviour of  $(\text{CH}_3)_2\text{NH}_2^+$  and  $(\text{CH}_3)_3\text{NH}^+$ ,  $\text{Cl}^-$  is different to the bromides and iodides i.e. when H-bonds ( $\text{N-H}\cdots\text{X}^-$ ) are introduced. One wonders if perhaps the strength of H-bonding is more dominant than steric packing forces in determining the different crystal structures of the chlorides. It will be remembered that the I.N.S. spectrum of  $(\text{CH}_3)_3\text{NH}^+\text{Cl}^-$  showed sharp torsional peaks whereas the bromide and iodide showed considerable broadening of the E torsion which could well be due to distortions caused by crowding in the crystal packing.

Fig. (7.12) Mathieu type barrier vs. number of methyl groups.





What is also immediately apparent is that these barriers increase much more in value as more  $-\text{CH}_3$  groups are added than do the isoelectronic carbon compounds. It was seen for  $\text{CH}_3\text{NH}_3^+$  that the barrier was lower than for  $\text{CH}_3\text{CH}_3$ , which was attributed to the effects of positive charge on the nitrogen; hence one might at first expect that the barriers for the whole  $\text{N}^+$  series would be lower than the carbon series. However this should be balanced against the fact that the C-N bond distance ( $\sim 1.47\text{\AA}$ ) is somewhat shorter than the C-C bond distance ( $\sim 1.54\text{\AA}$ ). The central atom to methyl group distance was seen to be an important factor in the series of compounds with C, Si, Ge and Sn as the central atom. The barriers decreased with increasing bond length. In the  $\text{N}^+$  series as more methyl groups are added they will hinder each other more strongly than in the carbon series because they are held closer together, unless they distort away from Td symmetry (c.f. the structure of  $(\text{CH}_3)_2\text{NH}_2^+\text{Cl}^-$  which shows the C-N-C angle is  $113^\circ$ ). In fact the value of the calculated interaction term increases with the number of methyl groups, whereas in the methyl-halo-carbon series it was roughly constant. However the hydrocarbons do show the effect; certainly  $(\text{CH}_3)_2\text{CH}_2$  shows a much lower interaction term than  $(\text{CH}_3)_4\text{C}$  (recalling table 6.21) and one set of reported values for  $(\text{CH}_3)_3\text{CH}$  gives an intermediate value (the other set is not much different to  $(\text{CH}_3)_4\text{C}$ ).

$(\text{CH}_3)_4\text{N}^+$  cannot reduce interactions by distorting away from Td geometry and so this most probably indicates the interaction constant for two methyl groups at the Td angle. In the cases of  $(\text{CH}_3)_3\text{NH}^+$

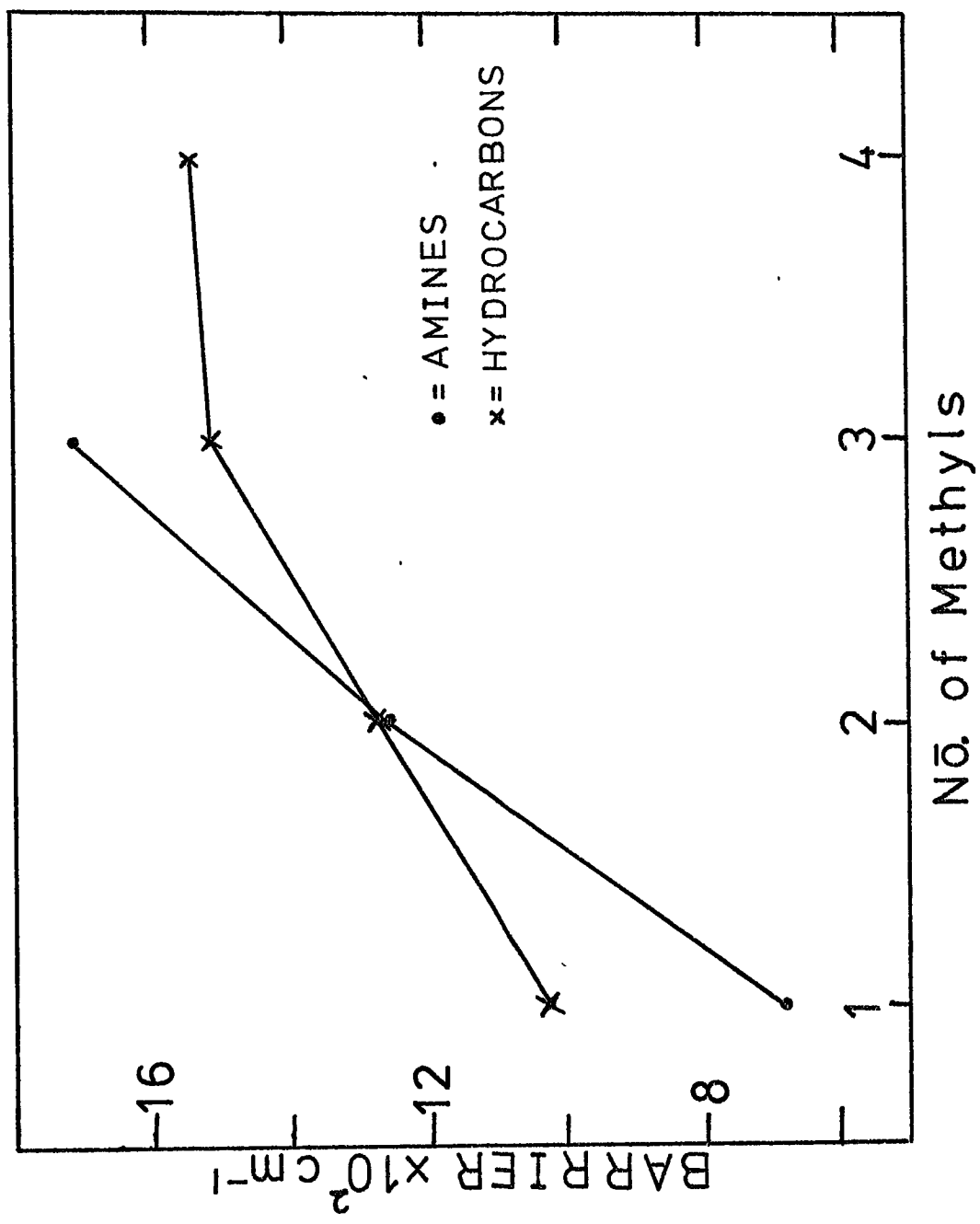
and  $(\text{CH}_3)_2\text{NH}_2^+$  the methyls can probably distort away from each other to some extent, allowed by the smaller size of the hydrogens, and therefore have lower interaction constants. A similar argument probably applies to the hydrocarbons series, although the effect may be fortified in the methylammoniums series by the positive charge on the nitrogen pulling down negative charge from the N-H's and effectively reducing the charge overlap radius of these hydrogens. Comparing the interaction terms for  $(\text{CH}_3)_4\text{C}$  and  $(\text{CH}_3)_4\text{N}^+$  of  $\sim -160$  and  $\sim -240 \text{ cm}^{-1}$  respectively shows that the interactions in the latter are larger, as would be expected since the methyls are held closer.

Further evidence showing that an increasing number of methyl groups on the nitrogen increases the internal barrier more than in the carbon series can be seen in fig. (7.13) which compares barrier values determined for the parent amines with the hydrocarbons (41-43). The values used are given below. The weighted average Mathieu value of the barrier for  $(\text{CH}_3)_3\text{N}$  was re-calculated, for consistency as opposed to using the S.H. value which was the only one reported (43).

	<u>Ref.</u>	<u><math>\bar{V}_3</math> barrier (<math>\text{cm}^{-1}</math>)</u>
$\text{CH}_3\text{NH}_2$	(41)	684
$(\text{CH}_3)_2\text{NH}$	(42)	1266
$(\text{CH}_3)_3\text{N}$	(43)	1710

No external effects will be present for these compounds but unfortunately since there is no criterion for judging the different effect of the lone pair on the barrier magnitude these cannot really

Fig. (7.13) Comparison of amines and hydrocarbons (Mathieu type barriers)



be used to estimate the barrier for the 'free' ions where the lone pair N: has been substituted by  $N^+-H$ . The barrier for  $CH_3NH_2$  of  $684\text{ cm}^{-1}$  (41) is in fact lower than that for  $CH_3NH_3^+$  in the  $PF_6^-$  salt at  $857\text{ cm}^{-1}$ , so it may at least be reasonable to say that the barriers in the parent amines are likely to be lower than for the equivalent protonated "free" ions.

All this is leading up to say that the much larger barrier observed for  $(CH_3)_4N^+$  than  $(CH_3)_4C$  is not entirely unexpected, before any external effects are also considered. It would be very interesting to find the barrier for the  $(CH_3)_4N^+ SbCl_6^-$  salt, which may give a reasonable approximation to the "free" ion since as has already been pointed out its structure is cubic and therefore probably undistorted (39) and it does not show the effects of any  $C-H---X^-$  type bonding (35). The differences between the halide salt barriers however can only be as a result of external influences. With respect to the  $(CH_3)_2NH_2^+$  and  $(CH_3)_3NH^+$  salts it has already been suggested that for the chloride the stronger  $N-H---X^-$  bonding may hold the ions in a less close packed situation than the bromide and iodide. In the  $(CH_3)_4N^+$  salts with no  $N-H---X^-$  bonds the chloride immediately falls back into what might be the expected trend. One might expect the distortions from  $T_d$  present in the crystal to produce some increase in barrier since the methyls on the same atom will be pressed closer together, i.e. a steric effect. With respect to the structures of the  $(CH_3)_4N^+$  halides it may well be that the reducing size of the anion  $I^- \rightarrow Cl^-$  is such that the rather large cation becomes the dominant structure defining the packing (i.e. the  $Cl^-$  ions effectively sit in holes left after the cations have

packed together). This would mean that  $(\text{CH}_3)_4\text{N}^+ \leftrightarrow (\text{CH}_3)_4\text{N}^+$  contacts would become more important in the external interaction barrier. Then also there is the possibility of C-H---X<sup>-</sup> bonding which would be different for each halide. If such bonding were the sole cause of the increase in barrier of  $\sim 400 \text{ cm}^{-1}$  between the I<sup>-</sup> and Cl<sup>-</sup> salts and if as is suggested by previous work this is due only to one H-bond the magnitude would be rather phenomenal, since the indicated difference for one N-H---X<sup>-</sup> bond for Cl<sup>-</sup> and I<sup>-</sup> (see Chapter 3) is itself only  $\sim 400 \text{ cm}^{-1}$ . It might perhaps indicate more than one C-H---X<sup>-</sup> bond per methyl group. However evidence from  $(\text{CH}_3)_2\text{NH}_2^+\text{Cl}^-$  might well indicate a minor role in the barrier for such bonding, in that its structure shows the methyl protons all point in the general direction of Cl<sup>-</sup> ions (6) yet the barrier for this salt is less than for the Br<sup>-</sup> and I<sup>-</sup> salts. (The N---Cl<sup>-</sup> distance would also suggest very little if any interaction). Consequently one would feel that perhaps C-H---Cl<sup>-</sup> bonding is not of any great importance in the changing magnitude of barrier heights for  $(\text{CH}_3)_4\text{N}^+\text{X}^-$  salts, but rather a steric effect of the crystal packing.

One can see that a very deep interpretation of the present results cannot really be undertaken, though some very interesting features have been observed and given possible explanations on a qualitative basis. It is worth reiterating that a number of deuteration studies would prove extremely useful in assisting interpretation, and that it would be very useful to obtain the "free ion" torsional frequencies for  $(\text{CH}_3)_4\text{N}^+$  (perhaps for the  $\text{SbCl}_6^-$  salt). This would then enable the external contribution to the barriers calculated here for the halides to be evaluated.

References - Chapter 7

1. M. Stammer, J. Inorg. Nucl. Chem. 29, 2203 (1967).
2. E.R. Andrew, P.C. Canepa, J. Mag. Res. 7, 429 (1972).
3. A.A.V. Gibson, Ph.D. Thesis, University of Natal (1971).
4. S-S. Chang, E.F. Westrum, J. Chem. Phys. 36, 2420 (1962).
5. S. Albert, H.S. Gutwosky, J.A. Ripmeester, *ibid* 56, 3672 (1972).
6. J. Lindgren, I. Olovsson, Acta. Cryst. B24, 549 (1968).
7. J. Lindgren, A. Nükhet, Acta. Chem. Scand. 26, 3043 (1972).
8. Wagner, Z. Krist. 43, 170 (1907).
9. F. Mussnug, Naturwissenschaften 29, 256 (1941).
10. J. Lindgren, I. Olovsson, Acta. Cryst. B24, 554 (1968).
  
12. G.M. and W.S. Sheldrick, *ibid* B26, 1334 (1970).
13. L. Vegard, K. Sollesnes, Philosophical Magazine, 4, 985 (1927).
14. W.H. Zachariasen, Norsk. Geol. Tidsskr, 10, 9 (1927).
15. R.W.G. Wyckoff, 'Crystal Structures' Vol 1, 2nd Edition p.107.
16. G.L. Bottger, A.L. Geddes, Spectrochim Acta 21, 1701 (1965).
17. J.T. Edsall, J. Chem. Phys. 5, 225 (1937).
18. R.A. Heacock, Leo Marion, Can. J. Chem. 34, 1782 (1956).
19. J. Bellanato, J.R. Barceló, An. Fis. Quim. B52, 469 (1956).
20. E.A.V. Ebsworth, N. Sheppard, Spectrochim. Acta. 13, 261 (1959).
21. J. Bellanato, *ibid* 16, 1344 (1960).
22. W. Kynaston et al., J.C.S. (1960) 1772.
23. R.H. Nuttall, D.W.A. Sharp, T.C. Waddington, *ibid* 4965 (1960).
24. V. Lorenzelli, K.D. Möller, Compt. Rendu. 251, 1483 (1960).

25. N. Krishnamurthy, Proc. Ind. Acad. Sci. A61, 184 (1965).
26. S.J. Anhouse, M.C. Tobin, Spectrochim. Acta. 28A, 2141 (1972).
27. P.V. Huong, H. Schlaak, Chem. Phys. Letts. 27, 111 (1974).
28. R. Sjöblom, J. Tegenfeldt Acta. Chem. Scand. 26, 3068 (1972).
29. R. Sjöblom, J. Tegenfeldt, ibid 26, 3075 (1972).
30. D.J. Blears, S.S. Danyluk, E. Bock, J. Phys. Chem. 72, 2269 (1968).
31. J. Dufourcq, B. Lemanceau, J. Chim. Phys. 67, 9 (1970).
32. S.B.W. Roeder, D.C. Douglass, J. Chem. Phys. 52, 5525 (1970).
33. M. Mahajan, B.D. Nageswara Rao, J. Phys. Chem. Solids 33, 2191 (1972).
34. M. Polak, M. Scheinblatt, J. Mag. Res. 12, 261 (1973).
35. K.M. Harmon, I. Gennick, S.L. Madeira, J. Phys. Chem. 78, 2585 (1974).
36. D.J. Sutor, Nature (London) 195, 68 (1962).
37. P.S. Peercy, D. Morosin, Phys. Letts. 36A, 409 (1971).
38. J. White, B. Lassier, C. Brot, Journal de Physique 34, 473 (1973).
39. A. Ferrari, et al., Gazzetta Chim. Ital 87, 651 (1957).
40. G. Herzberg, "Molecular Spectra and Molecular Structure II" Pg 215,  
Van Nostrand N.Y. (1956).
41. K. Tamagake, M. Tsuboi, A.Y. Hirakawa, J. Chem. Phys. 48, 5536 (1968).
42. K.D. Möller, et al., ibid 47, 2609 (1967).
43. D.R. Lide Jr., D.E. Mann ibid., 28, 572 (1958).

CHAPTER 8CONCLUSION

In this final brief chapter it is intended to draw attention to a few points of interest, to make some concluding remarks and to suggest several pieces of possible future work.

The relationship of crystal environment to the appearance of the torsion ( $\nu_6$ ) or ( $\nu_{\text{NTOR}}$ ) and the combination band; torsion +  $-\text{NH}_3$  asymmetrical bend ( $\nu_6 + \nu_9$ ) in the I.R. spectra of compounds with an  $-\text{NH}_3^+$  group is of considerable interest.

It was seen in Chapter 4 that in general the cold phases of the methylammonium halides all show a moderately strong sharp ( $\nu_6 + \nu_9$ ) band and that by subtracting  $\nu_9$  a reasonable estimate of the torsional frequency  $\nu_6$  (or  $\nu_{\text{NTOR}}$ ) can be obtained (see Table 4.7). This is usually below the observed I.R. value of the torsion ( $\nu_6$ ). The crystal field splittings for these compounds (1) also indicate that the  $-\text{NH}_3^+$  group is to some extent distorted from  $C_3$  symmetry. The calculated barriers, at least for the  $\beta$ -phases (and the amplitude calculation for the chloride) also indicate that the  $-\text{NH}_3$  group is tied down by hydrogen bonds.

Several authors have also drawn attention to a similar combination band which is a feature of the I.R. spectra of ammonium halide salts (2-4). The interesting feature of this is that it is quite sharp and moderately strong in those crystal phases which have a CsCl type lattice, in which a 3-fold axis of the ion can align with the 3-fold axis of the crystal, and all the evidence is in



favour of the ion being held by hydrogen bonds. The band in fact appears for all salts in which all four N-H bonds appear to be hydrogen bonded to the anion (4). The librational band also appears in these phases. On the other hand the NaCl type phase of  $\text{NH}_4\text{I}$  (5) shows only a weak diffuse band in the expected region of the combination, and Raman studies on single crystals (6) show that the 3-fold axis of the ion lies along a 4-fold axis of the crystal (i.e. rather similar to the  $\alpha$ ,  $\alpha'$  methylammonium halide phases). This indicates that rotation occurs about the 3-fold ion axis, along which one N-H---I<sup>-</sup> band is formed. It was also noticed in Chapter 4 that the  $\alpha$  and  $\alpha'$  methylammonium halides also show a rather broad and weak band which when  $\nu_9$  was subtracted gave frequencies in the same region as the band assigned as the torsion  $\nu_6$  (or  $\nu_{\text{NTOR}}$ ) in the I.N.S. spectra. (See table 4.8 and I.N.S. data). The torsional band in this case is not I.R. active, nor do the other I.R. bands show crystal field splitting. In these cases the barrier is small and rotation of the whole ion probably occurs, however there is still a hydrogen bonding potential. Rather interestingly the  $\text{PF}_6^-$  salt with no hydrogen bonding does not show the  $(\nu_6 + \nu_9)$  band.

Next, the  $\text{C}_6\text{H}_5\text{NH}_3^+\text{Cl}^-$  salt shows a strong, sharp  $(\nu_6 + \nu_9)$  band but no torsional band in the I.R. spectrum, whereas the cold bromide shows a weaker  $(\nu_6 + \nu_9)$  band and a torsional band which is quite strong. The chloride  $-\text{NH}_3^+$  group has a 3-fold environment and the determined barrier would indicate it is held by 3 hydrogen

bonds, whereas in the bromide only 2 hydrogen bonds are formed, although again this is probably sufficient to hold the  $-\text{NH}_3^+$  group. This rather importantly indicates that the appearance of the torsional band probably depends mainly on the degree of asymmetry of the  $-\text{NH}_3^+$  group or its immediate environment. The fact that the torsion does not appear for the chloride although its structure indicates a slight distortion of its environment may perhaps be because the  $-\text{NH}_3^+$  does not distort very much in the field and also because any distortion does not have to strain against an internal field. (The discrepancy in the structural data should also be remembered). In the methylammonium salts asymmetry is indicated for the cold phases, but not the room temperature phases, and the  $\nu_6$  band is seen, or not seen, respectively.

This being the case, one would expect that the hydrazinium halides, having symmetrical crystal structures, would not (and indeed they do not) show the torsional band equivalent to  $\nu_6$ , but the equivalent of the  $(\nu_6 + \nu_9)$  band should perhaps appear. Unfortunately it is difficult to test this on account of the predicted position of the band falling within the broad complex envelope of N-H hydrogen bonded stretching frequencies.

Sandorfy (7) used the appearance of the  $(\nu_6 + \nu_9)$  type combination band to decide on the type of structure;  $\alpha$ ,  $\beta$  or otherwise in a large number of primary amine hydrohalides; unfortunately he does not give the frequencies. This work shows that several salts give  $\beta$ -type spectra (such as the ethylammonium halides) even at room temperature, although usually these salts change to give

$\alpha$ -types at higher temperatures. Although the n-propylammonium halides have  $\alpha$ -phases (also shown by X-ray data (8)) Sandorfy (7) reports that a torsional band was seen, this would probably arise not from an  $-\text{NH}_3$  distortion but rather from the internal asymmetry, so this does not destroy the arguments above.

The I.R. spectra of some of the salts suggested by Sandorfy as having  $\beta$ -phases at room temperature were obtained during the present work and although details will not be given here it is worth listing the observed ( $\nu_6 + \nu_9$ ),  $\nu_9$  and  $\nu_6$  frequencies where observed. Several other salts with  $-\text{NH}_3$  groups were also investigated for ( $\nu_6 + \nu_9$ ). The somewhat varied collection of relevant results is given below:-

Table (8.1) The ( $\nu_6 + \nu_9$ ) type combination of several salts ( $\text{cm}^{-1}$ )

Salt	( $\nu_6 + \nu_9$ )	$\nu_9$	Calc $\nu_6$	$\nu_6$ OBS. *
$\text{C}_2\text{H}_5\text{NH}_3^+$ $\text{Cl}^-$	~ 2050	1600	~ 450	501(I.R)487(I.N.S)
$\text{C}_2\text{H}_5\text{NH}_3^+$ $\text{Br}^-$	2009	1590	419	456
$\text{C}_2\text{H}_5\text{NH}_3^+$ $\text{I}^-$	1960	1578	382	~ 404
$(\text{CH}_3)_3\text{CNH}_3^+$ $\text{Br}^-$	2028	1599	429	NOT SEEN
$(\text{CH}_3)_3\text{CNH}_3^+$ $\text{I}^-$	1972	1588	384	NOT SEEN
$^+\text{NH}_3\text{OH}$ $\text{Cl}^-$	1902	~ 1560	~ 342	338 (I.N.S)
( " ) <sub>2</sub> $\text{SO}_4^{-2}$	2020	1605	415	418
$^+\text{NH}_3\text{SO}_3^-$	~ 1800 broad	1533	267	267 (I.N.S)

\* I.R. except where indicated.

Again this shows that the torsion appears when the environment is asymmetrical and at not too different a frequency to the calculated one. It is very interesting that the tertiary-butyl ammonium salts

do not show the  $\nu_6$  (or  $\nu_{\text{NTOR}}$ ) torsional band. (Although several peaks appear in the region these do not shift sufficiently from one salt to the next and are probably internal distortion modes and torsions of the  $\text{CH}_3$  groups). This may suggest a symmetrical environment and because of this ion's similarity to  $(\text{CH}_3)_4\text{N}^+$  further studies by I.N.S. would be well worthwhile. Since the iodide also appears to be  $\beta$ -phase this could well lead to an accurate determination of a three fold hydrogen bond potential involving  $\text{N-H}\cdots\text{I}^-$ .

A small point unrelated to the discussion about  $(\nu_6 + \nu_9)$  could also be made here with respect to the estimated 3-fold barrier for  $\text{N}_2\text{H}_6^{+2}\text{I}_2$  of  $2186 \text{ cm}^{-1}$  (see discussion in Chapter 3). The  $\nu_6$  ( $\equiv \nu_{\text{NTOR}}$ ) frequencies of the  $\beta$ -ethylammonium halides would perhaps indicate that this is not too unreasonable an estimate. If one assumes that the frequency is largely the  $-\text{NH}_3$  motion once again (the true modes will be even more complex than in the  $\text{CH}_3\text{NH}_3^+$  salts due to the asymmetry of the ion and coupling effects between the  $-\text{NH}_3$  and  $\text{CH}_3$  rotors) the values of the frequency squared, which crudely speaking will be proportional to the barrier heights, are as follows:-

		$\nu_{\text{NTOR}}^2$	c.f. $\text{N}_2\text{H}_6^{+2}$ barrier $\text{cm}^{-1}$	Ratio
$\beta \text{ C}_2\text{H}_5\text{NH}_3^+$	$\text{Cl}^-$	251001	3414	73.5
	$\text{Br}^-$	207936	2871	72.4
	$\text{I}^-$	163216	2186 estimated	74.7

This shows that the estimated barrier is in the right area.

Preliminary Raman studies on the  $\beta\text{-C}_2\text{H}_5\text{NH}_3^+$  salts, together with an I.N.S. spectrum of the chloride indicate that the lower frequency

torsion-libration ( $\nu_{\text{CTOR}}$ ) band is probably Raman active. These compounds would also make a very interesting study although the spectra would be rather more complicated to interpret.

Obviously there are very many other compounds with hydrogen bonded systems which could be looked at, which might help to prove or disprove some of the conclusions just made about the structural relationship to the appearance of  $(\nu_6 + \nu_9)$  and  $\nu_6$  in the I.R.

Changing the topic now to the models used for determining barriers, it has been seen throughout that the S.H. approximation is very useful in simplifying the model and providing an insight into the motions of rotor groups, particularly for the hydrazinium and methylammonium salts, and in all cases where multiple rotor interactions occur. (The I.N.S. technique has proved rather useful with respect to the latter system in showing the degeneracies of the modes visually). It should always be remembered however that this approximation has its limits. It would be very useful to attempt to produce a more precise model for the methylammonium salts, and one which could take into account any displacement of the external fields away from the angle of  $60^\circ$  required to give the minimum potential at equilibrium (see Chapter 4). Much more suitable models for the more complex librational modes will probably take much longer to develop but would be very useful in determining the overall potential field around the ion.

A full assessment of the limitations of all the models really requires as much study as possible of a wide variety of compounds with related environments. It would for instance be interesting to look at such compounds as the salts of  $(\text{CH}_3)_3\text{N}^+-\text{NH}_3^+$  which could

be correlated with  $(\text{CH}_3)_3\text{C-NH}_3^+$  and  $(\text{CH}_3)_4\text{N}^+$ . In these systems interpretations would be made more difficult because of the combined effects of high external barriers and internal interactions. Many suggestions for further work have already been mentioned throughout the thesis, in particular the determination of the "free ion" torsional modes for species where the possibility of H-bonding has been removed, and the use of selective deuteration to observe intensity changes and frequency shifts in the I.N.S.

Another field which might prove very interesting would be an I.N.S. study of  $\text{CH}_3\text{NH}_3^+$  ions incorporated in caesium halide or other halide lattices, where the environment of the  $-\text{NH}_3^+$  group might be controlled and changed from one salt incorporation to another. Castelluci's I.R. study of  $\text{CH}_3\text{NH}_3^+$  in CsCl (9) mentioned in Chapter 4 did not observe the  $\nu_{\text{NTOR}}$  frequency, but he did estimate its value from a combination band (assumed to be  $\nu_6 + \nu_9$ ) as  $\sim 518 \text{ cm}^{-1}$ . This high frequency suggests a 3-fold environment, and the non appearance of the  $\nu_{\text{NTOR}}$  mode also suggests it is symmetrical, so perhaps the C-N axis lies on a three-fold axis of the cubic cell.

To draw the thesis to a close it should be said that the use of the expensive I.N.S. technique for observing torsional modes has been criticised in the past, since it has been found that such modes can often appear in the optical spectra under suitable conditions. One can see from the present work that this certainly is not always the case, and that on several occasions the conclusions of the I.R. spectroscopist have been proved wrong. It has also been seen that the

intensity of I.N.S. peaks is a valuable asset in assigning modes, especially where selective deuteration can be made. The use of I.N.S. and optical spectroscopy in a complimentary manner has proved to be a very useful technique for studying these molecular motions.

References - Chapter 8

1. A. Théorêt, C. Sandorfy, *Spectrochim Acta* 23A, 519 (1967).
2. E.L. Wagner, D.F. Hornig, *J. Chem. Phys.*, 18, 296, 305 (1950).
3. W. Vedder, Ph.D. Thesis, Brown University (1958).
4. T.C. Waddington, *J.C.S.* 4340 (1958).
5. R.C. Plumb, D.F. Hornig, *J. Chem. Phys.* 21, 366 (1952).
6. L.C. Mathieu, J.P. Mathieu, *J. Chim. Phys.*, 49, 226 (1952).
7. P. Chevalier, C. Sandorfy, *Symp. Molecular Structure and Spectroscopy, Tokyo* (1962).
8. M.V. King, W.N. Lipscomb, *Acta Cryst.* 3, 222, 227 (1950).
9. E. Castelluci, *J. Mol. Struct.* 23, 449 (1974).